Role of the NRF2-mediated oxidative stress response and lysosomal dysfunction in drug-induced liver injury associated with mitochondrial damage

Inauguraldissertation

zur

Erlangung der Würde eines Doktors der Philosophie

vorgelegt der

Philosophisch-Naturwissenschaftlichen Fakultät

der Universität Basel

von

Noëmi Johanna Roos

Basel, 2022

Genehmigt von der Philosophisch-Naturwissenschaftlichen Fakultät

auf Antrag von

Prof. Dr. Dr. Stephan Krähenbühl

Prof. Dr. Jörg Huwyler

Prof. Dr. Dr. Hans-Uwe Simon

Basel, den 27. April 2021

Prof. Dr. Marcel Mayor

Dekan der Philosophisch-

Naturwissenschaftlichen Fakultät

Acknowledgment

At the end of this journey, I would like to express my gratitude to everyone who has accompanied and supported me on this way.

An exceptional thank goes to Professor Stephan Krähenbühl. Thank you for offering me the opportunity to perform this thesis in your lab and for welcoming me in your group. Thank you for your guidance and scientific support. Your advices have always been an enrichment for my research and I am thankful for your trust in my work.

A special thank goes to Professor Jörg Huwyler, who not only supported me as a second supervisor, but also generously offered work space in his laboratory. Thank you for giving us a warm welcome in your group and enabling a smooth relocation to the Pharmacentre. By joining my doctoral committee as an external expert, Professor Hans-Uwe Simon supported me in the last phase of my doctoral thesis. Thank you for your time and critical assessment. Moreover, I would like to express my gratitude to Professor Alex Odermatt, who offered work space in his cell culture laboratory and warmly welcomed us in his group.

An extraordinary thank belongs to PD Dr. Jamal Bouitbir, who supported me from the first day of my thesis till the end. You always had an open ear for my sorrows. Thank you for your scientific advices, encouragements, and optimism. Furthermore, I warmly thank PD Dr. Urs Duthaler for introducing me in the world of mass spectrometry and bioanalytics. Thank you for your patience, technical and scientific support, and the good vibes you spread in our research group. Moreover, I thank Dr. Riccardo Mancuso and Dr. Gerda Sanvee for the exceptional support in my third project.

This doctoral thesis would not have been possible without the encouragement of my colleagues, friends, and family. Karolina, Gerda, Bea, Miljenko, Riccardo, Fabio, Deborah, Dino, and David – you made my time in “Lab410” extraordinary. I thank you for your scientific as well as mental support and friendship. Moreover, I thank my master student Diell Aliu for his excellent work and the fruitful scientific as well as philosophic discussions. I also thank the members of the Pharmaceutical Technology research group for welcoming us in their laboratory.

A special thank belongs to my parents. This thesis would not have been possible without the support and encouragements I received from you in the past, thank you. I also thank my grandparents and siblings for always being a resource to me. Finally, a special thank goes to my boyfriend. Thank you for your unconditional support, encouragement, and love during this intensive time.

Summary

Drug-induced liver injury is a rare, but potentially severe adverse drug reaction that is caused by various mechanisms including mitochondrial dysfunction and oxidative stress. Highly expressed in the liver, the transcription factor NRF2 stimulates the expression of phase II-detoxifying and antioxidant genes in response to electrophilic and oxidative stress. In unstressed conditions, NRF2 activation is suppressed by the cytosolic redox-sensitive protein KEAP1. As master regulator of the oxidative and electrophilic stress response, NRF2 might protect against drug-induced liver injury caused by mitochondrial damage and oxidative stress. To test this hypothesis, we assessed whether the hepatotoxic drugs benzbromarone and lapatinib, which are both associated with mitochondrial dysfunction and oxidative stress, activate the KEAP1-NRF2 pathway in HepG2 cells, a human hepatoma cell line. Moreover, lapatinib has lysosomotropic properties, which have also been described for the tyrosine kinase inhibitor imatinib. Similar to benzbromarone and lapatinib, imatinib caused severe liver injury in patients. As lipophilic weak bases, lapatinib and imatinib accumulate in acidic cellular compartments such as lysosomes. Thus, we assessed the effects of lapatinib and imatinib on lysosomal functions and related processes such as mammalian target of rapamycin complex 1 activation, lysosomal biogenesis, and autophagy in HepG2 cells.

Benzbromarone is a uricosuric drug that was withdrawn from the drug market by its manufacturer due to severe cases of liver toxicity. In our first project, benzbromarone (1-100 µM) lead to accumulation of mitochondrial superoxide radicals and cellular reactive oxygen species in HepG2 cells. The uricosuric drug caused oxidation of glutathione, the most prevalent antioxidant molecule in hepatocytes, to glutathione disulfide. Glutathione disulfide levels increased in entire HepG2 cells and especially in mitochondria. Moreover, benzbromarone increased the level of oxidized mitochondrial antioxidant protein thioredoxin 2. These findings indicate that mainly mitochondria were exposed to benzbromarone-induced oxidative stress and might have been the origin of ROS generation. Furthermore, benzbromarone activated the KEAP1-NRF2 pathway in HepG2 cells, demonstrated by nuclear accumulation of NRF2 and upregulation of several NRF2-regulated antioxidant proteins. Downregulation of KEAP1, which led to NRF2 activation, protected HepG2 cells from benzbromarone-induced ATP depletion and cell membrane permeabilization.

Approved for the treatment of human epidermal growth factor receptor 2-positive breast cancer, lapatinib received a black box warning by the U.S. Food and Drug Administration due to severe cases of hepatotoxicity in patients. We observed that lapatinib (2-20 µM) induced the generation of mitochondrial superoxide and cellular hydrogen peroxide in HepG2 cells in our second project. In this cellular system, lapatinib activated the KEAP1-NRF2 pathway at clinically relevant concentrations. Consequently, lapatinib upregulated several prototypical NRF2-regulated antioxidant genes and glutathione biosynthesis. As observed for benzbromarone, lapatinib increased the levels of glutathione disulfide, confirming that lapatinib caused oxidative stress in HepG2 cells. Co-treatment with the antioxidant N-acetylcysteine reduced the accumulation of NRF2 induced by lapatinib, indicating that reactive oxygen species were involved in the activation. N-acetylcysteine co-treatment also reduced the decrease in KEAP1 protein levels caused by lapatinib. Finally, lapatinib upregulated mitochondria-specific antioxidant genes more strongly than their cytosolic counterparts.

As lysosomotropic drugs, lapatinib and imatinib increased the lysosomal volume, raised the lysosomal pH, and showed signs of lysosomal membrane permeabilization in HepG2 cells in our third project. Both drugs disturbed the proteolytic activity of lysosomes. Moreover, imatinib reduced the activity of the mammalian target of rapamycin complex 1. This protein complex is activated on the lysosomal surface and regulates essential metabolic pathways such as protein synthesis and autophagy. Consequently, imatinib activated the transcription factor EB. This transcription factor is the master regulator of lysosomal biogenesis as well as autophagy and a substrate of the mammalian target of rapamycin complex 1. In response to imatinib, the transcription factor EB accumulated in the nucleus and upregulated the expression of lysosomal as well as autophagic genes. Inactivation of the mammalian target of rapamycin complex 1 and upregulation of autophagic genes together with the increased expression of autophagic proteins implied that imatinib induced autophagy in HepG2 cells. However, the concomitant lysosomal dysfunction caused by imatinib might impair a complete autophagic flux.

In conclusion, the hepatotoxic drugs benzbromarone and lapatinib activated the NRF2 pathway in HepG2 cells as an adaptive stress response. Activation of NRF2 protected against benzbromarone-induced hepatotoxicity. Moreover, oxidative stress was partially involved in the activation of NRF2 by lapatinib. Finally, we revealed that the impairment of lysosomal functions and related pathways might contribute to lapatinib- and imatinib-induced liver toxicity.

Table of contents

Abbreviations

A

ALP · Alkaline phosphatase

ALT · Alanine aminotransferase

APAF-1 · Apoptotic protease activating factor-1

ARE · Antioxidant response element

B

BCL-2 · B-cell lymphoma protein-2

BSEP · Bile salt export pump

C

CUL3 · Cullin 3

CYP · Cytochrome P450 enzyme

D

DILI · Drug-induced liver injury

E

ER · Endoplasmic reticulum

ETC · Electron transport chain

F

FDA · U.S. Food and Drug Administration

G

GCL · Glutamate-cysteine ligase

GPX · Glutathione peroxidase

GS · Glutathione synthetase

GSH · Glutathione

GST · Glutathione S-transferase

H

H_2O_2 · Hydrogen peroxide

HER2 · Human epidermal growth factor receptor 2

HIF-1 α · Hypoxia-inducible factor-1 α

HLA · Human leukocyte antigen

$HO^{\bullet}$ · Hydroxyl radical

HO-1 · Heme oxygenase-1

I

IMM · Inner mitochondrial membrane

IMS · Intermembrane space

K

KEAP1 · Kelch-like ECH-associated protein 1

L

LMP · Lysosomal membrane permeabilization

LSD · Lysosomal storage disease

M

MOMP · Mitochondrial outer membrane permeabilization

mtDNA · Mitochondrial DNA

mTOR · Mammalian target of rapamycin

mTORC1 · Mammalian target of rapamycin complex 1

N

NOX · NADPH oxidase

NRF2 · Nuclear factor erythroid 2-related factor 2

O

$O_2^{\bullet -}$ · Superoxide radical

OMM · Outer mitochondrial membrane

P

PHH · Primary human hepatocyte

PRX · Peroxiredoxin

R

ROS · Reactive oxygen species

S

sMAF · small MAF protein

SNP · Single nucleotide polymorphism

SOD · Superoxide dismutase

T

TK · Tyrosine kinase

TKI · Tyrosine kinases inhibitor

TR · Thioredoxin reductase

TRX · Thioredoxin

U

ULN · Upper limit of normal

Introduction

1 Drug-induced liver injury

Drug-induced liver injury (DILI) is an adverse drug reaction that is responsible for most cases of acute liver failures in the United States (1, 2). DILI is a frequent cause of drug attrition during the development and post-marketing drug withdrawal (3, 4). Elucidating the underlying mechanisms of this rare, but clinically relevant adverse drug reaction is essential for its prevention and management as well as for the development of safe drug therapies.

1.1 Classification

DILI is divided into two forms (see Figure 1): intrinsic and idiosyncratic DILI (5). Intrinsic DILI can potentially occur in any individual exposed to supratherapeutic doses of an intrinsic hepatotoxin. This form of DILI is dose-dependent, predictable, and detectable in drug development (2, 6). Moreover, it usually occurs after a relatively short latency period (hours to days). Acetaminophen (or paracetamol) is the prime example of an intrinsic hepatotoxin (7). Overdose of acetaminophen leads to accumulation of a toxic N-acetyl-p-benzoquinone imine metabolite that covalently binds to hepatic proteins (8). In contrast, idiosyncratic DILI affects only susceptible individuals and occurs under therapeutic doses usually after a longer latency period (weeks to months) (9). Due to its rarity and lack of *in vitro* as well as animal models, idiosyncratic liver injury is more difficult to detect during drug development (9). Although generally considered as dose-independent, idiosyncratic DILI occurs more often with high (≥50-100 mg/day) daily doses (10). Furthermore, idiosyncratic DILI is divided into allergic (immune-mediated) and non-allergic (non-immune-mediated or metabolic) forms (9).

DILI type	Intrinsic DILI	Idiosyncratic DILI
Predictability	Predictable	Unpredictable
Dose	Supratherapeutic	Therapeutic
Latency period	Short and consistent	Long and variable
Risk factor	Dose	Patient-specific
Mechanism	Intrinsic hepatotoxicity	Immunologic/metabolic

Figure 1: Intrinsic versus idiosyncratic drug-induced liver injury (DILI). Adapted from (11).

Systemic allergic symptoms (e.g., fever, rash, eosinophilia) occur as hypersensitivity reaction of the adaptive immune system in response to a specific drug (6). In this case, the immune system (i.e., autoreactive antibodies, T cells) causes the liver damage. Non-allergic idiosyncratic liver injury is not accompanied by allergic symptoms and has usually a longer latency period (months) than the allergic form (9)

1.2 Epidemiology

The incidences of DILI in prospective population-based studies conducted in Iceland (2010-2012) France (1997-2000), and South Korea (2005-2007) were 19.1, 13.9, and 12 cases/100'000 persons/year, respectively (12-14). Accordingly, a DILI incidence of 10-20 cases/100'000 persons/year has been estimated for Switzerland (15). Lower incidences were reported in a Swedish and an UK study, which retrospectively evaluated 2.3 and 2.4 DILI cases/100'000 persons/year (16, 17). Similarly, a population-based study conducted in the USA (2014) revealed an incidence of 2.7 DILI cases/100'000 persons/year (18). Hospitalization was required in about 12-28% of the cases (12, 13, 17). The study conducted in UK postulated an incidence of 6.7 hospitalizations/1'000'000 persons/year as a consequence of DILI (17). Moreover, 1.4% of the patients hospitalized in an Swiss University hospital developed DILI (19). The French study postulated a global DILI incidence of 8.1 cases/100'000 persons/year and provided evidence that DILI is underreported (13).

Although DILI incidences are low in the general population, drugs were the most frequent cause of acute liver failures in the USA between 1998-2013 (1, 20). While acetaminophen overdose was responsible for most of them, idiosyncratic DILI accounted for more than 10% of the cases. Excluding acetaminophen, more than half of the idiosyncratic drug-induced liver failures resulted in liver transplantation. Indeed, 15% of all liver transplantations due to acute hepatic necrosis in the USA between 1990-2002 were caused by a drug (21). Furthermore, liver toxicity was responsible for 15 (32%) of 47 drug withdrawals by the U.S. Food and Drug Administration (FDA) between 1975-2007 (4).

1.3 Clinical perspectives

Since DILI can clinically mimic any liver disease without specific biomarkers, DILI remains an exclusion diagnosis and represents an important differential diagnosis in liver disease with unclear etiology (5). Thus, clinicians use the R-value, the Hy's rule, and the Roussel Uclaf causality assessment method to diagnose and clinically manage DILI. The R value (see Figure 2) indicates the pat-

tern of liver injury and is calculated by dividing the serum alanine aminotransferase level (ALT)/upper limit of normal (ULN) by the serum alkaline phosphatase level (ALP)/ULN (5). Since liver diseases and drugs usually cause specific patterns of liver injury, the R value helps identify the causative drug and evaluate other etiologies (5). Accordingly, DILI is divided into hepatocellular (R≥5), cholestatic (R≤2), or mixed (2<R<5) forms affecting hepatocytes, the biliary system, or both structures, respectively (22). Moreover, the Hy's rule says that patients with a hepatocellular pattern combined with jaundice have an unfavorable prognosis with a mortality or transplantation risk of ≥10% (23). Other types of liver injury caused by drugs include microvesicular steatosis (e.g., amiodarone), non-alcoholic steatohepatitis (e.g., tamoxifen), vanishing bile duct syndroms (e.g., amoxicillin-clavulanic acid), or autoimmune-like hepatitis (e.g, minocycline) (2).

The Roussel Uclaf causality assessment method established by the Council for International Organizations of Medical Sciences is an instrument to systematically assess the drug causality (24, 25). Accordingly, the chronological relationship between drug exposure and occurrence of the adverse drug reaction, the presence of risk factors and alternative etiologies that could explain the liver injury (e.g., viral or autoimmune hepatitis, ischemic liver injury, alcohol consumption, cholelithiasis and biliary tract abnormalities), and previous documentation of hepatotoxicity should be evaluated (24).

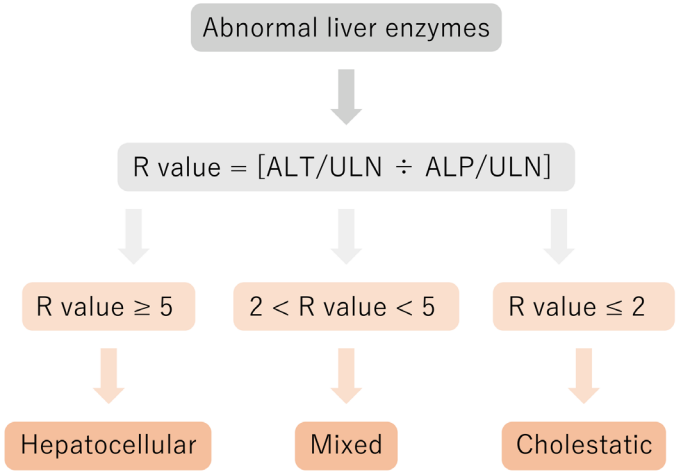

Figure 2: Pattern of liver injury. Adapted from (5).

ALT: Alanine aminotransferase, ALP: Alkaline phosphatase, ULN: Upper limit of normal

1.4 Risk factors for idiosyncratic DILI

Idiosyncratic DILI requires the presence of individual genetic, environmental, and drug-dependent risk factors (9). Age and sex are drug-specific risk factors and predispose for certain types of liver injury (26). Higher age (> 60 years) was identified as a risk factor for cholestatic liver injury, which occurred predominantly in men (27). In contrast, hepatocellular damage was more frequently observed in women and at younger age (< 60 years) (28). In addition, women are more often affected by severe forms of liver injury (i.e, fulminant hepatic failure) and drug-induced autoimmune hepatitis (20, 27, 29). In conclusion, higher age and female sex increase the susceptibility for hepatotoxicity caused by specific drugs (5, 26). Other genetic risk factors for idiosyncratic DILI are polymorphisms in drug-metabolizing, -transporting, and -detoxifying genes (30). Genetic variants of cytochrome P450 (CYP) enzymes (e.g., CYP2E1), UDP-glucuronosyltransferase, N-acetyltransferases (e.g., NAT2), ATP-binding cassette transporters, and glutathione S-transferases (GST) have been associated with an increased drug-specific DILI risk (31-35). Similarly, polymorphisms in human leukocyte antigen (HLA) genes were identified as drug-specific risk factors for hepatotoxicity (36-38). For instance, HLA polymorphisms affecting the major histocompatibility complex (MHC) increase the hepatotoxicity risk for flucloxacillin and abacavir (HLA-B*5701), ximelagatran (HLA-DRB1*07:01 and HLA-DQA1*02), and lapatinib (HLA-DQA1*02:01) (39-42).

Environmental factors such as malnutrition, alcohol consumption, or enzyme induction as well as concomitant diseases such as hepatitis C, human immune deficiency virus infection, or mitochondrial diseases increase the susceptibility to hepatotoxic drugs (43-47). For instance, pre-existing mitochondrial dysfunction significantly increases the risk for valproate-induced liver failure (48). Apart from individual risk factors, a high daily dose (≥50-100 mg/day) of a lipophilic drug (logP ≥ 3), known as the “rule-of-two”, and an extensive hepatic metabolism are risk factors for hepatotoxicity (10, 49, 50).

1.5 Mechanisms of idiosyncratic DILI

DILI is often a multifactorial disease that can result from various cellular stresses (51, 52). The actual mechanism of idiosyncratic liver injury is drug-specific and often not fully clarified. Well-characterized mechanisms of idiosyncratic DILI are the formation of reactive metabolites, recruitment of the immune system, inhibition of bile salt export pump (BSEP), and organelle (e.g., mitochondrial and endoplasmic reticulum [ER])) dysfunction (52). Reactive metabolites can covalently bind to hepatic proteins and impair their functions, causing a direct cellular damage (8, 53). Reactive metabolites formed by CYPs can also bind to ER proteins and induce an unfolded protein response, which causes oxidative stress (54). Alternatively, reactive metabolite that bind to hepatic proteins can form haptens and lead to immune-mediated hepatotoxicity (49, 55). However, according to the "danger hypothesis", haptenization and its recognition by T cells is not enough to trigger an immune reaction (51). Cellular damage with release of danger-associated molecular pattern molecules is required to activate antigen-presenting cells, which subsequently help initiating the immune response (56). Another prevalent mechanism of idiosyncratic DILI is the inhibition of BSEP (52). Drug-induced inhibition of BSEP reduces the biliary efflux of bile acids leading to hepatocellular liver injury (57). Finally, drug-induced mitochondrial and lysosomal damage can induce both apoptosis and necrosis as well as trigger the release of danger-associated molecular pattern molecules (47, 51). Mitochondrial toxicity associated with oxidative stress and lysosomal dysfunction as mechanisms of idiosyncratic DILI will be discussed in more detail in the following sections.

2 Drug-induced mitochondrial toxicity

Numerous hepatotoxic drugs withdrawn from the drug market (e.g., troglitazone, bromfenac, alpidem) or labeled with a black box warning by the FDA (e.g., lapatinib, valproic acid, tolcapone) are associated with mitochondrial dysfunction (10). These drugs can impair essential mitochondrial functions such as oxidative phosphorylation, β-oxidation, and mitochondrial DNA (mtDNA) replication (47, 58, 59). Moreover, they can cause oxidative stress, lead to permeabilization of the outer mitochondrial membrane (OMM), and induce mitochondria-dependent apoptosis (60).

2.1 Mitochondrial structure

The endosymbiotic theory proposes that mitochondria became mammalian organelles through the symbiosis between a bacterium and a host cell (61, 62). The theory bases on the fact that mitochondria contain a separate circular DNA, separate ribosomes, and an inner membrane that contains cardiolipin, a phospholipid that is typically found in bacteria (63).

Mitochondria are double-membraned organelles composed of an inner and outer membrane (see Figure 3) with different compositions and functions (64). The space between the two membranes is called intermembrane space (IMS) and has the same chemical composition as the cytosol (65). The inner mitochondrial membrane (IMM) encloses the mitochondrial matrix and is heavily invaginated (66). The invaginations increase the surface of the IMM and form sub-compartments, so called cristae, that harbor the mitochondrial electron transport chain (ETC), which will be discussed in the next section (see 2.2). The cardiolipin-rich IMM is highly impermeable to ions and molecules, but contains specific carrier proteins such as the ATP/ADP translocase, the mitochondrial pyruvate carrier, and the carnitine-acylcarnitine translocase (67). The IMM can increase its permeability through opening of the permeability transition pore, a process called mitochondrial permeability transition (68). The permeability transition pore is formed by integral membrane proteins (e.g., voltage-dependent anion channel, adenine nucleotide translocator, cyclophilin D) and resides at the contact side of the inner and outer mitochondrial membrane (69). Mitochondrial permeability transition in response to oxidative stress or Ca^{2+} leads to swelling of the mitochondrial matrix and rupture of the OMM (70, 71). This prosses can induce mitochondria-dependent apoptosis, which will be discussed in more detail in section 2.3 (68).

The IMM encloses the mitochondrial matrix, where essential metabolic processes such as β-oxidation of fatty acids and the tricarboxylic acid (TCA) cycle, also known as the citric acid or Krebs cycle, take place (72). The TCA oxidizes acetyl-CoA, derived from pyruvate, amino acid, or fatty acid

oxidation, through a series of enzyme-catalyzed chemical reactions into CO_2 and H_2O (73). The electrons gained in these oxidation reactions are transported by the electron carriers NADH and $FADH_2$ to complex I and II of the ETC, respectively. Moreover, the mitochondrial matrix contains the mtDNA, which consists of more than 16'000 base pairs and encodes 13 mitochondrial enzymes, 22 tRNAs, and 2 rRNA (74). The 13 mitochondrial encoded enzymes are subunits of the ETC enzyme complexes I, III, IV, and V (see 2.2) (75). Despite its own DNA, most mitochondrial proteins (1'000-1'500 proteins) are nucleus-encoded and have to be imported into the organelle (63). The translocase of the outer mitochondrial membrane 40 complex facilitates the transport of precursor proteins over the OMM, while the translocase of the inner membrane 23 complex catalyzes the import into the mitochondrial matrix (76). The OMM, harboring pore-forming proteins, is permeable for molecules smaller than 5'000 Da and can establishes membrane contact sites with other organelles such as the ER (64, 77).

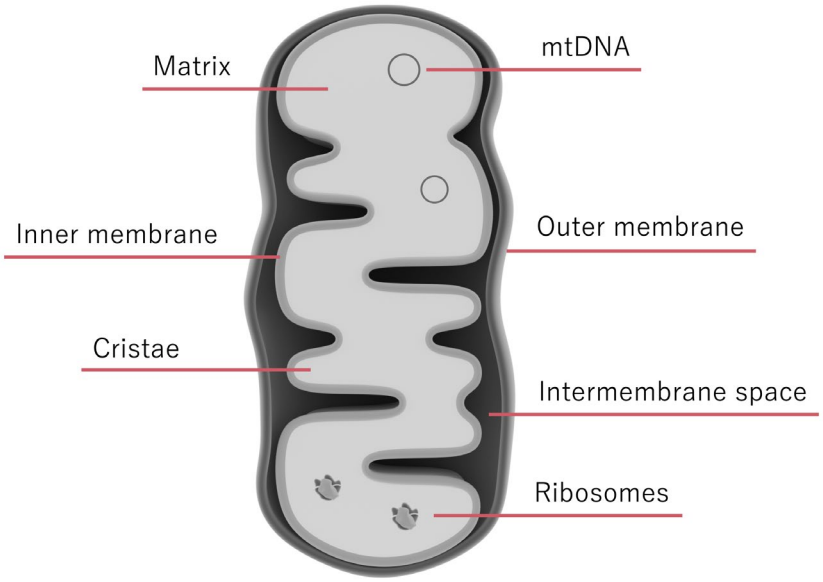

Figure 3: Mitochondrial structure. Adapted from (78).

2.2 Mitochondrial electron transport chain

The mitochondrial ETC (see Figure 4), also known as respiratory chain, consists of four membrane-embedded enzyme complexes (complex I-IV) and an F_1F_O-ATP synthase (complex V), which are assembled inside the IMM (79, 80). The ETC transfers electrons along the first four complexes to oxygen (O_2), which acts as ultimate electron acceptor, resulting in the production of H_2O (79). Since the redox potentials of the electron donors and acceptors successively increase, the electron transfer along the ETC releases energy (81). Complex I, III, and IV use the released energy to build up an

electrochemical gradient over the IMM by pumping protons from the mitochondrial matrix into the IMS (81). The energy stored in the electrochemical gradient, also known as protonmotive force, consists of an electrical (mitochondrial membrane potential, ψ) and chemical (pH) gradient (82). The protonmotive force drives the F_1F_O-ATP synthase to produce ATP, which is known as chemiosmotic coupling and produces most of the cellular ATP (72, 83). The entire process is called oxidative phosphorylation (72).

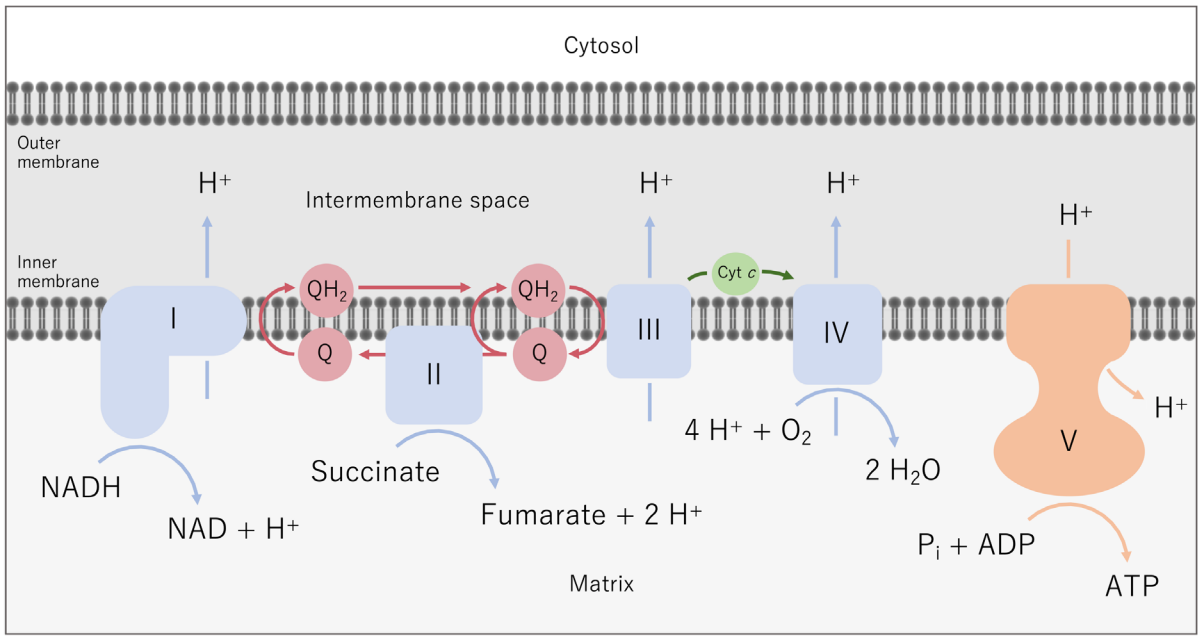

Figure 4: Mitochondrial electron transport chain. Adapted from (81).

I-V: Complexes I-V, Q: Ubiquinone, QH_2: Ubiquinol, Cyt *c*: Cytochrome *c*

The ETC enzyme complexes are composed of several subunits and contain redox cofactors that mediate the electron transfer within the complexes (80). The electron transfer between the complexes is carried out by membrane-embedded ubiquinone (coenzyme Q) and cytochrome *c*, the only soluble ETC protein (79). The first and largest complex of the ETC (complex I or NADH-ubiquinone oxidoreductase) consists of two “arms”: a hydrophobic membrane-embedded arm and a hydrophilic arm that protrudes into the mitochondrial matrix (81). Complex I receives electrons from the electron carrier NADH (72). The electrons are accepted via a flavin mononucleotide in the NADH-binding site of complex I, which feeds the electrons into a redox chain formed by seven iron-sulfur (Fe-S) clusters (81, 84). The redox chain transfers the electrons to the quinone-binding site located at the junction between the two arms. The electrons are subsequently transferred to ubiquinone (Q), generating the reduced from ubiquinol (QH_2). The electron transfer within complex I is coupled to the translocation of protons across the IMM (81).

In contrast to complex I, complex II (succinate-ubiquinone oxidoreductase) does not pump protons across the IMM (79). As succinate dehydrogenase, complex II is part of the citric acid cycle and receives electrons through the oxidation of succinate to fumarate (85). Complex II is composed of a flavin adenine dinucleotide (FAD)-binding protein and a Fe-S cluster-containing protein, which protrude into the mitochondrial matrix, as well as two hydrophobic proteins that attach the complex to the IMM (85). Complex II accepts electrons via the prosthetic group FAD, transports them through three Fe-S clusters and a heme group, before transferring them to ubiquinone (85). Thus, the electrons form both complex I and II are transferred to complex III in the form of ubiquinol (79). Complex III (ubiquinol-cytochrome *c* oxidoreductase) is a dimeric integral membrane protein with two quinone-binding sites (Q_0 and Q_1) and four prosthetic groups: the Rieske Fe-S cluster, cytochrome c_1, and two heme (b_{566} and b_{562}) groups (86). The heme groups are part of cytochrome *b*, a subunit of complex II. Complex III transports electrons from ubiquinol to cytochrome *c* and pumps protons into the IMS (86). The electron transfer within complex III occurs over a series of redox reactions known as the Q cycle (87). Ubiquinol is oxidized at the Q_0 site, while the oxidized from ubiquinone binds to the Q_1 site (81). One electron from ubiquinol is transferred to the Rieske Fe-S cluster leaving a semiquinone at the Q_0 site. This electron is further transferred to cytochrome c_1 and ultimately to cytochrome *c*. The remaining electron from the semiquinone is transferred to cytochrome b_{566}, cytochrome b_{562}, and finally to the Q_1 site ubiquinone (81). The electron moving towards the Q_1 site generates the energy for the proton translocation (88). Two Q cycles and two ubiquinol molecules are required to completely reduce the Q_1 site ubiquinone to ubiquinol, which can re-enter the cycle at the Q_0 site (81).

Cytochrome *c*, the ultimate electron acceptor of complex III, is a soluble heme-containing protein that is attached to the outer surface of the IMM by cardiolipin (89). Cytochrome *c* transfers the electrons to complex IV (cytochrome *c* oxidase), which is the last oxidase of the ETC (79). Complex IV contains four redox centers including a binuclear iron-copper cluster. Moroever, the complex contains channels for protons, O_2, and H_2O (90). Complex IV uses the electrons from cytochrome *c* to reduce molecular O_2 to two molecules of H_2O by a four electron-reduction at the binuclear iron-copper cluster (79). In parallel, complex IV pumps four protons into the IMS (91).

The protons pumped into the IMS re-enter the mitochondrial matrix through the F_1F_O-ATP synthase (79). The mitochondrial F_1F_O-ATP synthase consists of a membrane-embedded F_O region and a catalytic F_1 region that protrudes into the mitochondrial matrix (92). Translocation of protons from the IMS into the mitochondrial matrix through the F_O region induces a rotation in the F_1 region over a central rotatory stalk that connects the two regions. The F_1 region contains three nucleotide-binding

sites, which change their conformation upon rotation, and synthetize ATP. Translocation of eight protons leads to a 360° rotation of the F_1 region and produces three ATP molecules (93).

2.3 Mitochondrial regulation of apoptosis

Apoptosis is a programmed form of cell death that may occur via intrinsic or extrinsic pathway (see Figure 5) depending on the apoptotic stimulus (94). The extrinsic pathway requires binding of an extracellular ligand (e.g., Fas ligand) to the death-receptor present on the cell-surface, formation of the death-inducing signaling complex, and activation of the effector caspase-8. Caspases are cysteine proteases that cleave their substrates (e.g., other caspases, caspase-activated DNase) after an aspartate residue (95, 96). Caspases are the main executors of apoptosis and are classified as initiator (e.g., caspase-8/9) and effector (e.g., caspase-3/7) caspases (96). Initiator caspases are activated by dimerization, while effector caspases become active upon proteolytic cleavage (97).

The intrinsic pathway is initiated by mitochondria, which can release pro-apoptotic proteins (e.g., cytochrome *c,* apoptosis-inducing factor) into the cytosol upon mitochondrial outer membrane permeabilization (MOMP) (94). MOMP can be triggered by several intracellular apoptotic stimuli (e.g., DNA damage, mitochondrial damage, oxidative stress) and is regulated by members of the B-cell lymphoma protein-2 (BCL-2) family, which includes both pro- and anti-apoptotic proteins (e.g., BCL-2, BCL-X_L) (98, 99). The pro-apoptotic BCL-2 proteins are divided into BH3-only proteins (e.g., BID, BIM, PUMA, BAD, and NOXA) and proteins with several BCL-2 homology (BH) regions with effector function such as BAX and BAK (100). Intracellular apoptotic stimuli increase the concentration and/or activity of BH3-only proteins, which diminishes the effect of anti-apoptotic BCL-2 proteins and activates the pro-apoptotic effector proteins BAX and BAK (100). Activated BAX and BAK insert as oligomers into the OMM and induce MOMP through the formation of pores (101-103). The anti-apoptotic proteins BCL-2 and BCL-X_L, which reside mainly inside the OMM, sequester pro-apoptotic BCL-2 family members (e.g., BAK, BAX) and inhibit their activity (100).

Released cytochrome *c* binds to apoptotic protease activating factor-1 (APAF-1), leading to APAF-1 oligomerization and formation of the apoptosome (104). Importantly, APAF-1 oligomerization requires ATP and 2'-deoxy ATP, which makes apoptosis an ATP-dependent process (105, 106). The apoptosome recruits the initiator caspase-9 and induces its activation by dimerization. Caspase-9 subsequently activates the effector caspase-3, which in turn activates other caspases, initiating a caspase cascade (97). In addition to cytochrome *c*, mitochondria can release other pro-apoptotic proteins into the cytosol such as the apoptosis-inducing factor, which causes caspase-independent

chromatin condensation and DNA fragmentation (98). The intrinsic and extrinsic apoptosis pathways converge in the caspase-3 activation step (107). In addition, caspase-8 can activate the pro-apoptotic BH3-only protein Bid, which subsequently triggers MOMP and cytochrome *c* release (98, 108). Morphological changes and hallmarks of apoptosis resulting from caspase activation include DNA fragmentation, cleavage of nuclear lamins and cytoskeletal proteins, externalization of phosphatidylserine, and apoptotic blebbing (107, 109-111).

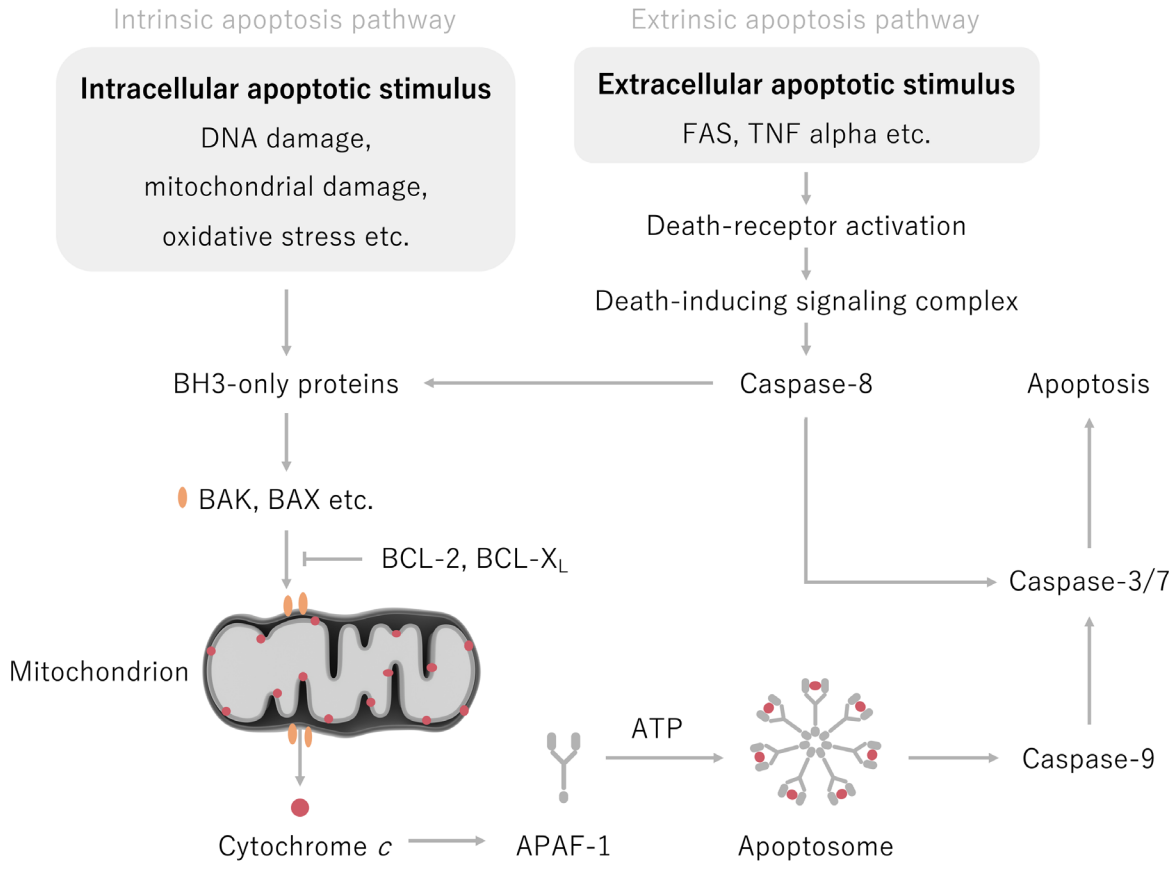

Figure 5: Extrinsic and intrinsic apoptosis pathways. Adapted from (98, 99).

3 Oxidative stress

The concept of oxidative stress was introduced in 1985 as “a disturbance in the pro-oxidant to anti-oxidant balance in favor of the former” (112). Reactive oxygen species (ROS) are prevalent pro-oxidants that derive from molecular O_2 (113). ROS are continuously produced by mitochondria and other cellular organelles and enzymes as a byproduct of aerobic life. In unstressed conditions, ROS and antioxidants form a dynamic equilibrium with balanced production and consumption. A disbalance resulting in oxidative stress leads to oxidative damage of cellular macromolecules (114). Consequently, oxidative stress can induce mitochondria-dependent apoptosis, as discussed in the previous section.

3.1 Reactive oxygen species

ROS are small-molecules with a reactive oxygen atom, which exist as both radicals and non-radicals (112, 113). Superoxide ($O_2^{\bullet -}$), hydroxyl ($HO^{\bullet}$), peroxyl ($ROO^{\bullet}$), and alkoxyl ($RO^{\bullet}$) radicals are highly reactive ROS that can directly attack cellular macromolecules (112). As non-radical ROS, hydrogen peroxide (H_2O_2), organic hydroperoxide (ROOH) and ozone (O_3) are chemically more stable and less reactive than the radical species (112). $O_2^{\bullet -}$ is generated by one-electron reduction of O_2 (see Figure 6) and is quickly dismutated to H_2O_2 by superoxide dismutases (SOD) (115).

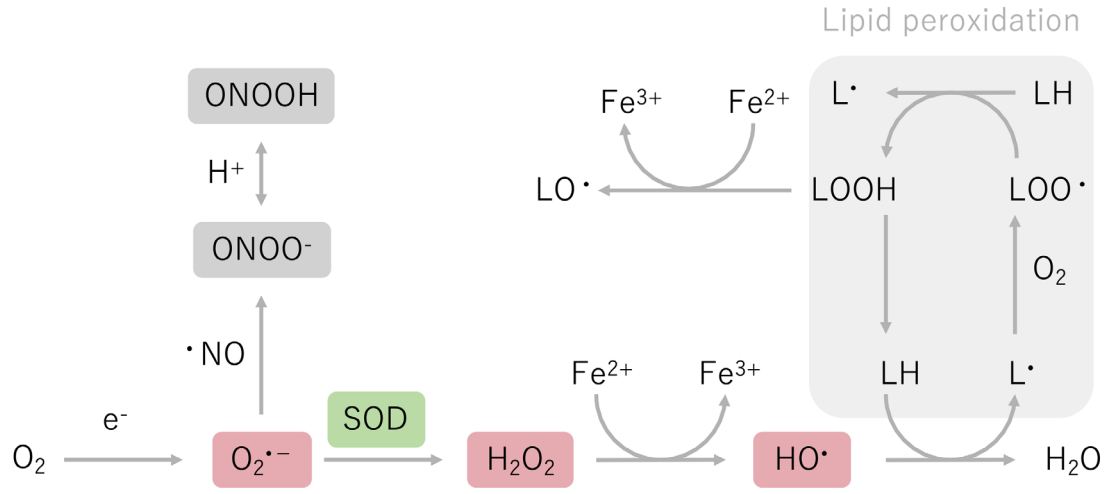

Figure 6: Formation and dynamics of reactive oxygen species (116, 117).

$O_2^{\bullet -}$: Superoxide radical, SOD: Superoxide dismutase, H_2O_2: Hydrogen peroxide, $HO^{\bullet}$: Hydroxyl radical, $^{\bullet}NO$: Nitric oxide, $ONOO^-$: Peroxynitrite anion, ONOOH: Peroxynitrous acid, LH: Unsat. lipid, $L^{\bullet}$: Unsat. lipid radical, $LOO^{\bullet}$: Lipid peroxyl radical, LOOH: Lipid hydroperoxide

Thus, the half live (10^{-6} s) and diffusion radius of $O_2^{\bullet-}$ (max. 0.5 µM) are short and intracellular concentrations reach about 10^{-11} M (112, 118). $O_2^{\bullet-}$ can oxidize Fe-S clusters and react with nitric oxide ($^{\bullet}NO$) forming the peroxynitrite ($ONOO^-$) anion (114, 119). Peroxynitrite has a half-life of about 10^{-3} s, can diffuse up to 20 µm, and reacts with carbon dioxide (CO_2) generating carbonate ($CO_3^{\bullet-}$) and nitrogen dioxide ($^{\bullet}NO_2$) radicals (118, 119). $^{\bullet}NO_2$ can nitrate proteins, DNA, and lipids. In contrast to $O_2^{\bullet-}$, H_2O_2 has a longer half live (10^{-3}-10^{-5} s) and can cross biological membranes (118). H_2O_2 can act as a physiological signaling molecule (see 3.4) at physiological concentrations of 1-100 nM (113). H_2O_2 is a two-electron oxidant with a high activation barrier that oxidizes specific protein cysteine residues and metal centers (120). In the presence of free iron, H_2O_2 is converted to $HO^{\bullet}$ by the Fenton reaction (121). Due to its high reactivity (half-life of 10^{-9} s) and lack of $HO^{\bullet}$-detoxifying enzymes, $HO^{\bullet}$ is a feared ROS (118). As an unspecific oxidant, $HO^{\bullet}$ directly attacks macromolecules with diffusion-controlled rates. For instance, $HO^{\bullet}$ can induce lipid peroxidation (see Figure 6) generating peroxyl and alkoxyl lipid radicals (116).

3.2 Mitochondrial sites of ROS production

Mitochondria are a major source of cellular ROS with eleven sites of $O_2^{\bullet-}$ and/or H_2O_2 production (122). Between 30-40% of extracellular H_2O_2 originates from mitochondria (123). As a major production site, the mitochondrial ETC generates ROS as spin-offs during oxidative phosphorylation (124). Electrons that leak from donor redox centers reduce molecular O_2 by a one- and two-electron reduction to $O_2^{\bullet-}$ and H_2O_2, respectively. Whether a site produces exclusively $O_2^{\bullet-}$ or H_2O_2 or a mixture of both species is not always clear (88). Yet, most mitochondrial ROS derive from $O_2^{\bullet-}$, which are quickly dismutated to H_2O_2 by the mitochondrial superoxide dismutase 2 (SOD2 or MnSOD) (115). Although inconsistencies exist in the literature, less than 1% of the ETC electrons leaks to O_2 (88). Complex I and complex III each contain two sites of ROS production: the flavin-binding site (I_F) and ubiquitin-binding site (I_Q) of complex I, and the Q_0 site (III_{Q0}) and Q_1 site (III_{Q1}) of complex III (122). Although the site of ROS production is tissue- and substrate-specific, I_Q and III_{Q0} are considered as the main sites of mitochondrial $O_2^{\bullet-}/H_2O_2$ production (88, 123). The I_Q site produces ROS upon reverse electron flow from ubiquinol, which is suppressed by the I_Q site inhibitor rotenone, and generates between 50-70% of mitochondrial matrix ROS (123). Semiquinones formed at III_{Q0} can reduce O_2 and produce $O_2^{\bullet-}$, especially in the presence of the III_{Q1} site inhibitor antimycin A (125). Addition of the III_{Q0} site inhibitor myxothiazol prevents ROS production at this site (88). $O_2^{\bullet-}$ produced by complex I are released into the mitochondrial matrix, while $O_2^{\bullet-}$ derived from complex III (III_{Q0}) is released to both sites of the IMM (126). The flavin-binding site of complex II (site II_F) is a

neglectable source of mitochondrial ROS in most tissues (88). Cytochrome *c* and complex IV do not remarkably contribute to mitochondrial ROS production (127).

In addition to the mitochondrial ETC, mitochondrial dehydrogenases linked to NAD (2-oxoacid dehydrogenase complexes, pyruvate dehydrogenases) or ubiquinone (dihydroorotate dehydrogenase, gycerol 3-phosphate dehydrogenase [GPDH]) contribute to mitochondrial ROS production (122). Located at the IMM, GPDH oxidizes glycerol 3-phosphate, a precursor of the phospholipid biosynthesis, to dihydroxyacetone phosphate and transfers the electrons to ubiquinone (128). From the ubiquinone-binding site, GPDH releases $O_2^{\bullet -}$ to both sites of the IMM, while NAD-linked dehydrogenase exclusively produce matrix ROS (126). Moreover, mitochondrial ROS are generated by the electron-transferring flavoprotein (ETF), the ETF-Q oxidoreductase (ETF-QOR), and external alternative NADH dehydrogenases (88, 122). ETF-QOR channels electrons from ETF and matrix dehydrogenases into the ETC via reduction of ubiquinone and produces matrix $O_2^{\bullet -}$ (129). External alternative NADH dehydrogenases, located at the outer site of the IMM, oxidize glycolysis-derived NADH and release $O_2^{\bullet -}$ into the IMS (130).

3.3 Non-mitochondrial sites of ROS production

In addition to mitochondrial enzymes, more than 40 other cellular enzymes produce $O_2^{\bullet -}$ or H_2O_2 by intention or as byproduct (113). Prominent ROS-producing enzymes are NADPH oxidases (NOX), ER and peroxisomal oxidases, CYPs, and xanthine dehydrogenases as well as xanthine oxidases (131).

NOX are transmembrane enzymes located in cell membranes as well as nuclear, ER, and mitochondrial membranes (132, 133). To date, seven NOX isoforms are known to produce $O_2^{\bullet -}$ across biological membranes (see Figure 7) by transferring electrons from NADPH to O_2 (134). Macrophages and neutrophils counteract invading micro-organisms with NOX-released $O_2^{\bullet -}$, which is a mechanism termed oxidative burst (135). In addition to phagocytes, NOX are present in various tissues and organs including liver, where they produce, together with mitochondrial enzymes, most of the cellular ROS (134, 136). Additionally, H_2O_2 is generated during oxidative protein folding by the ER oxidase ER oxidoreductin 1 (137). ER oxidoreductin 1 produces H_2O_2 during reoxidation of the thioredoxin protein disulfide isomerase, which catalyzes protein folding in its oxidized form by insertion of a disulfide bond into the target protein. Concretely, ER oxidoreductin 1 oxidizes the thioredoxin protein disulfide isomerase by a two-electron oxidation and transfers the electrons to O_2 generating H_2O_2.

As oxidative organelles, peroxisomes contain numerous oxidases (e.g., acyl-CoA oxidases, urate oxidase, D-amino acid oxidase, D-aspartate oxidase, L-pipecolate oxidase, 2-hydroxy acid oxidases, polyamine oxidase, xanthine oxidase) that generate H_2O_2 or $O_2^{\bullet -}$ during oxidative degradation of long-chain fatty acids, amino acids, or purines (138). In addition, microsomal CYPs can produce $O_2^{\bullet -}$ and H_2O_2 due to uncoupling of a catalytic cycle, leading to autooxidation of O_2 (139). Xanthine oxidase, the oxidized form of xanthine dehydrogenase, catalyzes the two last steps in purine metabolism (140). Xanthine oxidase, which is highly abundant in liver, generates H_2O_2 during oxidation of hypoxanthine and xanthine to xanthine and uric acid, respectively.

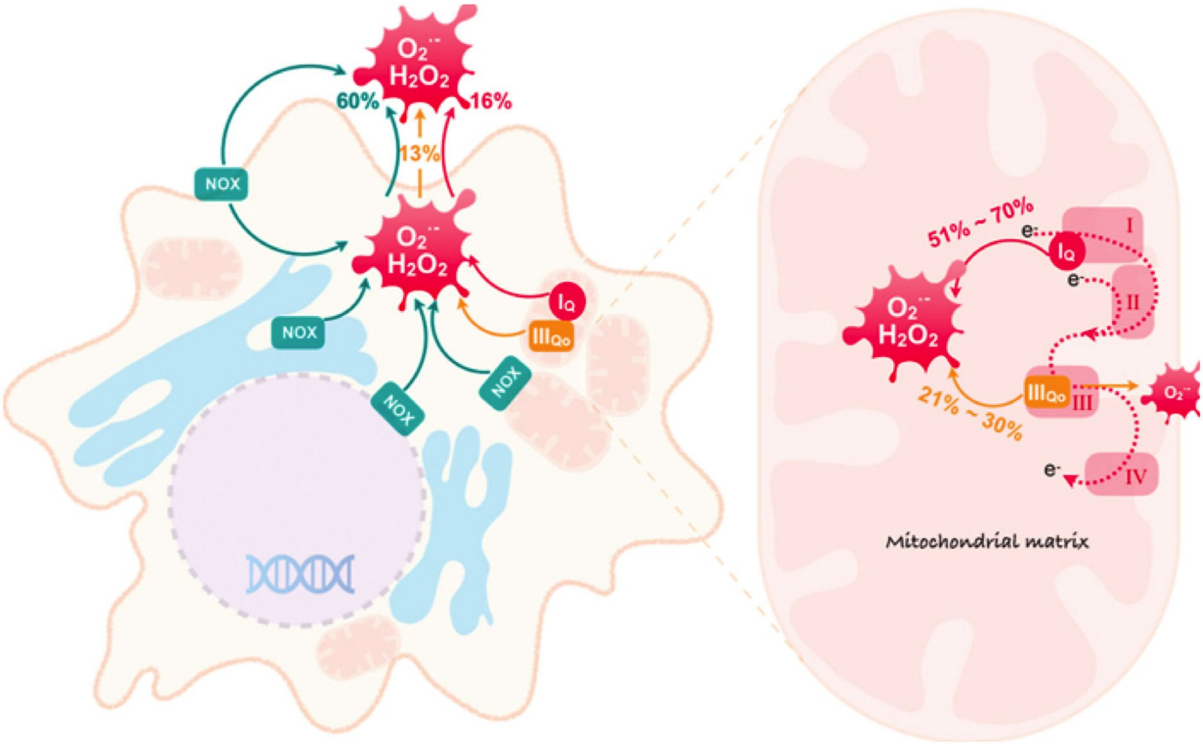

Figure 7: Cellular sites of superoxide ($O_2^{\bullet -}$) and hydrogen peroxide (H_2O_2) production (123).

NOX: NADPH oxidases produce

3.4 The role of ROS in physiology

Due to its physiochemical properties, H_2O_2 can permeate mitochondrial membranes, diffuse into the cytosol, and act as signaling molecule by oxidation of reactive cysteine residues (141). In contrast to free cysteine residues (-SH), cysteine residues that are surrounded by positively charged amino acid residues are stabilized as thiolate ($-S^-$) anions (142). They can act as nucleophiles and are readily oxidized by H_2O_2 (see Figure 8), resulting in protein sulfenylation (143). The sulfenylated proteins (-SOH) react with glutathione (-SSG) or are further oxidized to sulfinic (RSO_2H) and sulfonic (RSO_3H) species (144). While sulfenylation and glutathionylation are reversible modifications,

the oxidation to sulfinic and sulfonic species is irreversible (144). Such post-transcriptional modifications can modulated the activity of the modified enzyme (e.g., protein tyrosine phosphatases) and influence the signal transduction (142).

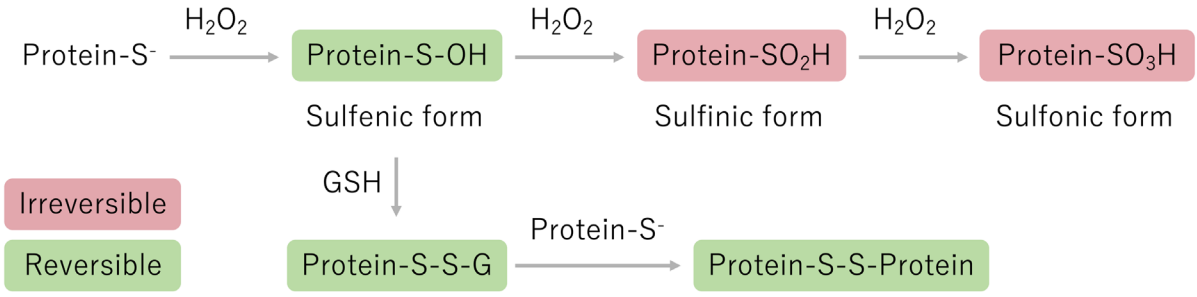

Figure 8: Hydrogen peroxide (H_2O_2)-mediated signal transduction (144).

As an important physiological function, mitochondria-derived H_2O_2 activate the hypoxia-inducible factor-1 α (HIF-1 α) in response to hypoxia (145). Under hypoxic conditions, $O_2^{\bullet -}$ is generated at the Q_0 site of complex III and released as H_2O_2 into the cytosol. Cytosolic H_2O_2 induces HIF-1 α stabilization (146). The mechanism of HIF-1 α stabilization is not fully clear, but ROS might deplete the catalytic iron of HIF-1 α's negative regulator. The stabilized transcription factor subsequently translocates into the nucleus and upregulates the expression of erythropoietin, vascular endothelial growth factor, and other hypoxia-compensating enzymes (147). In addition to HIF-1 α, also other transcription factors including p53, forkhead box protein O, NF-κB, or the nuclear factor erythroid 2-related factor 2 (NRF2) are activated by ROS (148-151).

In addition, mitochondria-derived ROS contribute to the induction of autophagy upon starvation (152). Oxidation of a reactive cysteine residue of the autophagy-related protein 4 (Cys81) stimulates autophagy by inhibiting autophagy-related protein 4-mediated delipidation of LC3-II, which is essential for autophagosome formation (152). Moreover, ROS derived from mitochondria are involved in innate immune responses such as lipopolysaccharide-induced macrophage activation, multiple Toll-like receptor-initiated pathways, or NLR family pyrin domain containing 3 (NLRP3) inflammasome activation (153-155). In addition, mitochondrial ROS can act as signaling molecules in cell differentiation (e.g., differentiation of pluripotent stem cells) (156).

3.5 The role of ROS in pathophysiology

ROS at supraphysiological levels (oxidative stress) can non-specifically oxidize cellular macromolecules (e.g., proteins, lipids, nucleic acid), which can impair their functions and potentially lead to cell death (113). Numerous pathologies such as alcohol-induced liver disease, atherosclerosis, cancer, neurodegenerative diseases, or ageing are related to oxidative stress (88).

The topology of ROS production can determine the target of cell damage and its consequences (127). Most mitochondrial ROS production sites are located in the mitochondrial matrix or at the matrix side of the IMM, releasing ROS mainly into the mitochondrial matrix (88). ROS present in the mitochondrial matrix can attack the densely packed mtDNA and oxidize its nucleobases (157). For instance, the oxidation of the nucleobase guanine at the C-8 position generates the most prevalent DNA oxidation product 8-oxo-7,8-dihydroguanine (8-oxo-G). Mitochondrial as well as nuclear DNA polymerases can misread 8-oxo-G and base-pair it with adenine instead of cytosine, leading to mutations in both mitochondrial and nuclear DNA (158, 159). Apart from being highly exposed to ROS, mtDNA is especially sensitive to oxidative damage due to the lack of histones and nucleotide excision repair mechanisms (160). Indeed, mtDNA in rat liver contained 10-fold more oxidative DNA modifications (i.e., 8-oxo-G) than nuclear DNA (161). Oxidative stress can also induce single and double stranded DNA breaks and oxidize RNA (e.g., 8-oxo-7,8-dihydroguanosine), which can induce p53-dependent cell death and reduce proteins synthesis, respectively (162, 163). Since subunits of the cytochrome *c* oxidase, ATP synthase, and cytochrome *b* are encoded by mtDNA, damaged mtDNA can lead to mitochondrial dysfunction and further amplify ROS production (74, 164).

$HO^{\bullet}$ generated by the one-electron reduction of H_2O_2 in the iron-dependent Fenton reaction can initiate non-enzymatic lipid peroxidation (116). $OH^{\bullet}$ can abstract a hydrogen atom from a polyunsaturated lipid, forming a carbon-centered lipid radical (165). The lipid radical reacts with O_2 forming a peroxyl radical, which subsequently attacks another polyunsaturated lipid, initiating a free radical chain reaction (see Figure 6). The cycle is terminated by the reaction of two peroxyl radicals or through antioxidant (e.g., vitamin E) scavenging (116). As secondary degradation products, lipid peroxidation generates reactive aldehydes such as malondialdehyde, 4-hydroxynonenal, and acrolein (116, 166). These aldehydes can covalently bind to proteins or oxidize amino acids by insertion of a carbonyl group (167). Thus, protein carbonyls are biomarkers of oxidative stress (162). Other biomarkers for lipid peroxidation are isoprostanes (e.g., F_2-isoprostanes), which are formed *in vivo* upon peroxidation of esterified arachidonic acid (162). Lipid peroxidation can damage cellular mem-

branes and induce ferroptotic cell death (168). Moreover, oxidation of cardiolipin leads to cytochrome *c* release and produces 4-hydroxynonenal, which can induce apoptosis in hepatocytes (169-172). Thus, ROS play an important role in the induction of mitochondria-dependent cell death (164). Beside protein carbonylation by lipid peroxidation degradation products, ROS can directly oxidize and cross-link proteins, which can change their structure-related functions (173). ROS can abstract hydrogen atoms from aliphatic amino acid side chains (e.g., Leu, Ile, Val, Pro.) or attack electron-rich structures such as sulfur-atoms (e.g., Cys, Met) or aromatic rings (e.g., Trp, Tyr, Phe, His). Oxidation of aliphatic side chains can generate hydroperoxides, alcohols, and carbonyls, while oxidation of electron-rich centers produces disulfides, sulfoxide, as well as hydroxylated and dimerized aromatic rings (173). $OH^{\bullet}$ can attack peptide backbones and induce their fragmentation (167). Moreover, $O_2^{\bullet -}$ can oxidize and inactivate proteins with Fe-S clusters (e.g. , aconitase, NADH dehydrogenase of complex I), releasing H_2O_2 and Fe^{2+} (174).

4 Drugs associated with mitochondrial toxicity

Our research group previously investigated mechanisms of hepatotoxicity associated with benzofuran derivatives such as benzbromarone, amiodarone, and dronedarone (175-177). All three drugs were associated with mitochondrial dysfunction in hepatocytes. Furthermore, we assessed the effects of several hepatotoxic tyrosine kinases inhibitors (TKI) including imatinib and lapatinib on mitochondrial functions in hepatocytes (178-181). The following sections give an overview of the pharmacological and toxicological properties of benzbromarone, lapatinib, and imatinib.

4.1 Benzbromarone

Benzbromarone was launched in the 1970s as uricosuric drug (Desuric®) for the treatment and prevention of hyperuricemia and gout attacks, respectively (182, 183). By inhibiting the renal urate transporter 1 and to a weaker extend the organic anion transporter 1, benzbromarone inhibits the proximal tubular reabsorption of uric acid and reduces the serum uric acid levels in hyperuricemia patients by one-fourth to one-half (184-186). The once daily administered doses range from 40-80 mg (micronized drug) to 100-200 mg (non-micronized drug) (182). After oral intake, absorbed benzbromarone is metabolized in the liver by CYPs (see Figure 9) to several hydroxylated metabolites (187, 188).

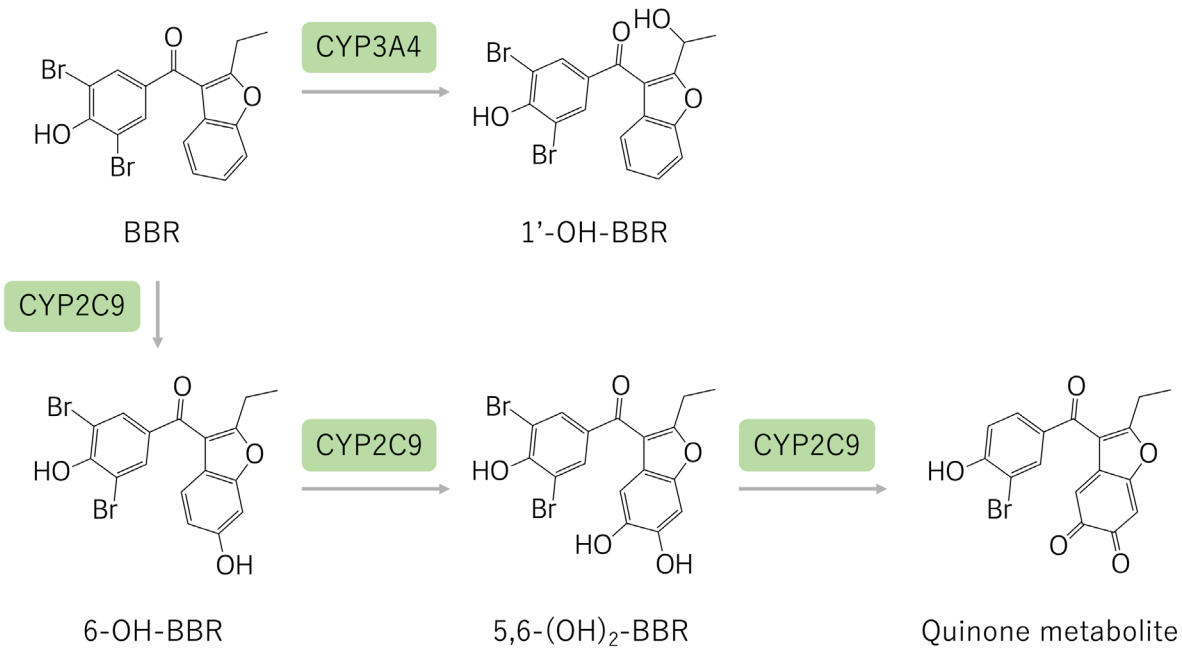

Figure 9: Main metabolic pathways of benzbromarone (BBR). Adapted from (189, 190).

The main metabolite, 6-hydroxy-benzbromarone, is generated by CYP2C9, a polymorphic enzyme, and to a lesser extent by CYP2C19 (189). Further oxidation of the active 6-hydroxy-benzbromarone metabolite results in a catechol metabolite (5,6-dihydroxy-benzbromarone) and subsequently reactive *ortho*-quinone intermediates (189). The 1'-hydroxy-benzbromarone metabolite is formed by CYP3A4 (190). Recently, several new *ipso*-substituted benzbromarone metabolites have been identified (187). Maximal benzbromarone plasma concentrations after a single therapeutic dose (100 mg) were between 4.3-13.7 µM, but increased up to 21.6 µM in CYP2C9 poor metabolizers with the *CYP2C9*3/*3* genotype (191-193). Benzbromarone and its metabolites are excreted mainly via bile and feces (188).

Benzbromarone-associated adverse drug reactions affect mainly the gastrointestinal tract (e.g., diarrhea) and are usually mild (182, 194-197). Elevation in liver enzymes was rare in clinical trials, affecting only 0.1% of the patients (186). Yet, several cases of severe benzbromarone-associated liver injury including cases with fatal outcomes occurred during the post marketing phase (198-203). As a result, the company withdrew benzbromarone from the drug market in 2003 (186). Benzbromarone-associated hepatocellular liver injury was usually associated with jaundice, occurred after several months of therapy, and presented without systemic allergic symptoms (186).

The incidence of benzbromarone-associated severe liver injury was estimated to be 1/17000 persons/year (186). Produced by alternative companies, benzbromarone it is still in clinical use in some European and Asian countries (e.g., Japan) as well as in New Zealand and Brazil, however it was never approved in the United States due to the hepatotoxicity concerns (186).

As a benzofuran derivative, benzbromarone is structurally related to benzarone, amiodarone, and dronedarone (204). All four drugs are associated with hepatotoxicity and impair mitochondrial functions in hepatocytes (175-177, 204, 205). Benzbromarone inhibited ETC enzyme complexes as well as β-oxidation, and uncouples oxidative phosphorylation in rat hepatocytes and isolated rat liver mitochondria (204). Moreover, benzbromarone was associated with ROS generation, release of cytochrome *c*, and apoptosis as well as necrosis in HepG2 cells, a human hepatoma cell line (204). The side chains of the benzofuran ring seem to be responsible for these adverse reactions (204).

4.2 Lapatinib

Lapatinib (Tykerb®, Tyverb®) is a small-molecule receptor TKI used for the treatment of advanced or metastatic breast cancer expressing the human epidermal growth factor receptor 2 (HER2) (206). As a dual inhibitor, lapatinib inhibits the intracellular tyrosine kinase (TK) domains of both epidermal growth factor receptors HER1 and HER2, the latter of which is overexpressed in many breast cancer cells and associated with an unfavorable prognosis (207, 208). Lapatinib (1250 mg/day for 14 days every 21 days) is administered orally in combination with capecitabine (Xeloda®) to patients that progressed under a previous trastuzumab (Herceptin®)-based therapy (209). Alternatively, lapatinib (1500 mg/day daily) is indicated in combination with letrozole to treat postmenopausal patients with hormone receptor- and HER2-expessing breast cancer (210). Lapatinib is metabolized in the liver via CYP3A4 as well as CYP3A5 (see Figure 10) and to a lesser extent via CYP2C8 as well as CYP2C19, to O- and N-dealkylated as well as N-hydroxylated metabolites, which are further oxidized to various metabolites (211-213).

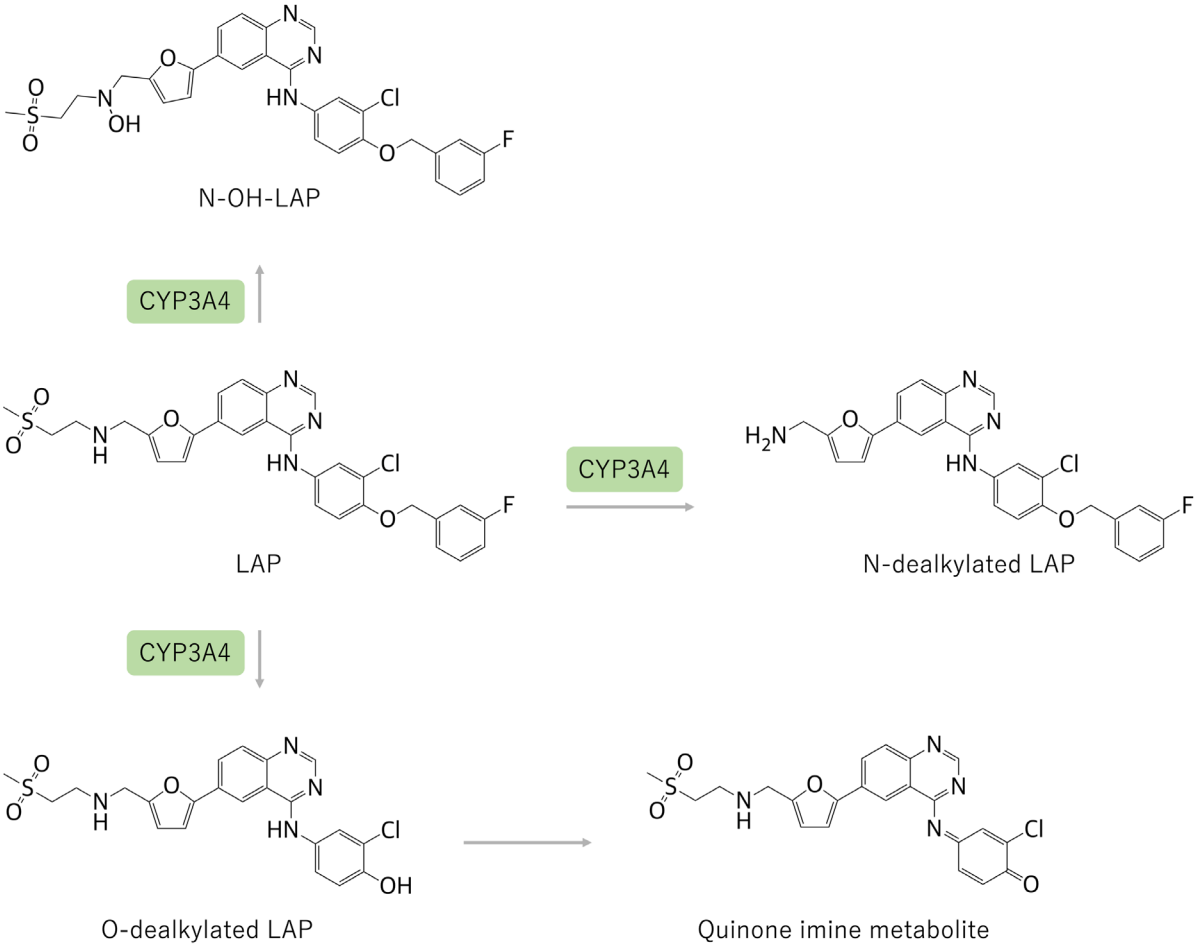

Figure 10: Main metabolic pathways of lapatinib (LAP). Adapted from (211, 212)

A therapeutic dose (1250 mg) of lapatinib in combination with capecitabine leads to a maximal plasma concentration of about 5.5 µM (4.1-7.4 µM) (214). The excretion occurs primarily in the feces (213).

At least every tenth patient that receives lapatinib and capecitabine suffers from gastrointestinal disorders, hand-foot syndrome, rash, fatigue, stomatitis, or pain in extremity (209, 215, 216). Also, mild elevated liver enzymes is a common adverse drug reaction of lapatinib combination therapy and occurs in half of the patients (217). Severe hepatotoxicity (e.g., hepatobiliary abnormalities) associated with lapatinib is rare, but well documented (218, 219). In 16 clinical trials, approximately 1.6% and 0.3% of patients who received lapatinib had severe elevations in liver enzymes (>5x ULN) and liver toxicity according to Hy's law, respectively (218). Several severe cases of lapatinib-induced liver failure including deaths prompted a black box warning by the FDA (217, 220). Lapatinib caused mainly hepatocellular injury with jaundice without allergic symptoms, which occurred within days to several months after start of the therapy (217). Lapatinib-induce hepatotoxicity might result from reactive and potentially immunogenic metabolites (211-213, 221). As mentioned above, HLA-DQA1*02:01 and HLA-DRB1*07:01 polymorphisms have been associated with an increased risk for lapatinib-induced hepatotoxicity, which might result from a delayed hypersensitivity reaction (42, 222). In addition, lapatinib and its O-dealkylated metabolite have been shown to impair mitochondrial function in hepatocytes (179, 221). Lapatinib reduced the mitochondrial membrane potential, was associated with ROS accumulation, and triggered the release of cytochrome *c* into the cytosol, inducing apoptosis in HepG2 cells (179).

4.3 Imatinib

In 2001 and 2002, imatinib (Gleevec®, Glivec®) was approved as first small-molecule TKI for the treatment of chronic myelogenous leukemia (CML) and metastatic and/or unresectable malignant gastrointestinal stromal tumors (GISTs), respectively (223, 224). Most patients with CML express the breakpoint cluster region (BCR)-Abelson (ABL) fusion protein, a non-receptor TK that results from a chromosomal translocation (225). As a constitutively activated TK, BCR-ABL causes uncontrolled cell proliferation and differentiation. Imatinib efficiently blocks the ATP-bindings site of this chimeric kinase, inhibiting its activity (226, 227). Moreover, imatinib inhibits the platelet-derived growth factor receptor (PDGFR) as well as the proto-oncogenic form of the TK c-Kit, which is found in some GISTs (224, 227). Additionally, imatinib is approved to treat patients with myeloproliferative diseases, mastocytosis, hypereosinophilic syndrome, dermatofibrosarcoma protuberans, and other imatinib-sensitive malignancies (228). Imatinib is administered in daily doses of 400-800 mg, is nearly completely adsorbed, and undergoes hepatic metabolism by CYP3A4 (see Figure 11) forming an active N-demethylated metabolite (223, 229).

Figure 11: Main metabolic pathway of imatinib (IMA). Adapted from (230).

In the steady state, a daily dose of 400 mg imatinib leads to an average maximal imatinib plasma concentration of 5.3 µM, however, clearance and plasma concentration among patients are highly variable (231). The elimination of imatinib occurs mainly in the feces (223).

The most common adverse drug reactions caused by imatinib are nausea, vomiting, diarrhea, myalgia, and edema as well as elevated liver enzymes (223, 224). Severe liver enzyme elevation occurs in about 3-6% of the patients receiving imatinib (217). The liver injuries, which represented mainly as hepatocellular necrosis or rarely cholestasis, occurred after weeks up to few months of intake, and were in some cases fatal (217, 223, 232-235).

Imatinib inhibited enzyme complexes of the ETC and reduced the mitochondrial membrane potential in HepG2 cells and isolated mouse liver mitochondria (179). Moreover, imatinib led to ROS accumulation, depleted cellular glutathione (GSH), triggered release of cytochrome *c* into the cytosol, and induced apoptosis as well as Poly ADP-ribose polymerase cleavage in HepG2 cells (179).

5 Cellular antioxidant defense: KEAP1-NRF2 pathway

Cellular ROS levels are tightly regulated by antioxidant enzymes and non-enzymatic antioxidants, forming the cellular antioxidant defense system (113). As master regulator of the oxidative stress response, NRF2 regulates together with its negative regulator Kelch-like ECH-associated protein 1 (KEAP1) the gene expression of phase II-detoxifying and antioxidant enzymes (150). The antioxidant defense system regulated by NRF2 is compartmentalized in cells and inducible in response to oxidative stress (236). The KEAP1-NRF2 pathway and its responsive antioxidant enzymes will now be discussed in more detail.

5.1 NRF2

The transcription factor NRF2 is highly expressed in various tissues and organs including muscle, kidney, lung, small intestine, stomach, and liver (237, 238). Its name derives from the homologous transcription factor nuclear factor erythroid 2 (NF-E2), which is predominantly expressed in hematopoietic cells (239, 240). NRF2 belongs to the family of cap and collar (CNC) transcription factors (named after the *Drosophila* NRF2 homolog CNC), which contain a conserved basic leucine zipper (bZIP) motif (241, 242). NRF2 contains six conserved NRF2-ECH homology (Neh) domains (see Figure 12), with ECH (erythroid cell-derived protein with CNC homology) being the chicken NRF2 homolog (243, 244).

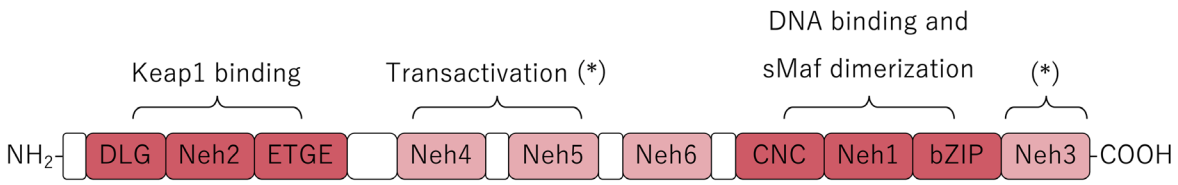

Figure 12: Domain structure of NRF2. Adapted from (150).

Neh 1-6: NRF2-ECH homology domains 1-6, CNC: Cap and collar, bZIP: Basic leucine zipper

Neh1 contains the conserved CNC-bZIP motif, which is required for heterodimerization with small MAF (sMAF) proteins (i.e, MAFF, MAFG and MAFK) (245). Heterodimerization with sMAFs increases the DNA binding affinity of CNC transcription factors and is therefore indispensable for NRF2's transcriptional activity (246-248). The amino-terminal Neh2 domain comprises seven lysine residues for ubiquitination and two KEAP1-binding motifs, ETGE and DLG (243, 249). ETGE has a high binding affinity towards KEAP1, while DLG binds with a lower affinity to KEAP1 (250). DLG brings the lysine residues in an optimal position for ubiquitination. Neh3 , Neh4, and Neh5 act as

transactivation domains (150). Neh6 is a serine-rich domain that is phosphorylated by glycogen synthase kinase 3 (GSK-3) promoting NRF2 degradation (251).

NRF2-sMAF heterodimers bind as *trans*-acting factors to specific *cis*-regulatory DNA elements, known as antioxidant response elements (AREs) or electrophile-responsive element (EpRE) (242, 252, 253). The core ARE/EpRE sequence is 5'-TGACNNNGC-3' and is present in the promotor region of NRF2-regulated genes. The activity of NRF2 is regulated at the post-transcriptional level (see Figure 14) by its negative regulator KEAP1 (243).

5.2 KEAP1

KEAP1 is a cysteine-rich cytoplasmic protein that represses the activity of NRF2 under unstressed conditions (243, 254). KEAP1 owes its name to the *Drosophila* actin-binding protein Kelch (255). KEAP1 (see Figure 13) contains a double glycine repeat module, a bric à brac (BTB) domain, and an intervening region (IVR) (150). The double glycine repeat or Kelch module interacts both with the KEAP1-binding motifs of NRF2 (ETGE and DLG) and cytoplasmic actin filaments (256).

Figure 13: Domain structure of KEAP1. Adapted from (150).

BTB: Bric à brac domain, IVR: Intervening region, DGR: Double glycine repeats, CUL3: Cullin 3

KEAP1 acts thereby as a cytoplasmic anchor that retains NRF2 in the cytoplasm (243). The BTB domain, a conserved 100-residue protein motif with a dimerization domain, enables KEAP1 homodimerization (257, 258). Moreover, a hydrophobic groove between the BTB domain and IVR qualifies KEAP1 to act as an adaptor for Cullin 3 (CUL3)-based E3 ubiquitin ligases (259-261). KEAP1 forms together with CUL3 and RING-box protein 1 (RBX1) a functional E3 ubiquitin ligase complex that recruits an E2 ubiquitin-conjugating enzyme, which continuously polyubiquitinates NRF2. Ubiquitinated NRF2 undergoes proteasomal degradation (262). Thus, NRF2 has a short half-life (less than 20 min) and low basal activity despite its continuous synthesis.

Beside recruiting CUL3-based E3 ubiquitin ligases and regulating NRF2 activity through proteasomal degradation, KEAP1 senses oxidative and electrophilic stress through reactive cysteine residues (150). Modification of these residues by electrophiles or ROS induces a conformational change in KEAP1. According to the "hinge-and-latch" binding model, the low affinity DLG motif ("latch") subsequently dissociates from KEAP1, which brings NRF2 in a less favorable position for

ubiquitination (263). In parallel, the high affinity ETGE motif (“hinge”) remains bound to KEAP1, which enables newly synthetized NRF2 to directly translocate in the nucleus (250). KEAP1 functions thereby as nuclear floodgate (150). Similarly, the "cyclic sequential attachment and regeneration model of KEAP1-mediated degradation of NRF2" proposes that inactivated KEAP1 remains occupied with undegraded NRF2, enabling newly synthetized NRF2 to directly translocate to the nucleus (264, 265). In both models, the proteasomal degradation of NRF2 is impaired.

So far, four cysteine sensors in KEAP1 have been identified: Cys151, Cys273, Cys288, and a fourth sensor formed by several redundant cysteine residues (Cys226, Cys613, Cys622/Cys624) (266-268). Cys151 is located in the BTB domain, while Cys273, Cys288, Cys226 are part of the IVR (264). Cys613, Cys622, and Cys624 are localized in the C-terminal domain of KEAP1. Most of these residues are surrounded by basic amino acids that stabilize the thiolate anion. As a ROS sensor, the cysteines of the fourth sensor are able to form disulfide bridges in response to H_2O_2 in any combination (268). Hence, this “fail-safe” mechanism can sense oxidative stress even if one residue is inactivated (268).

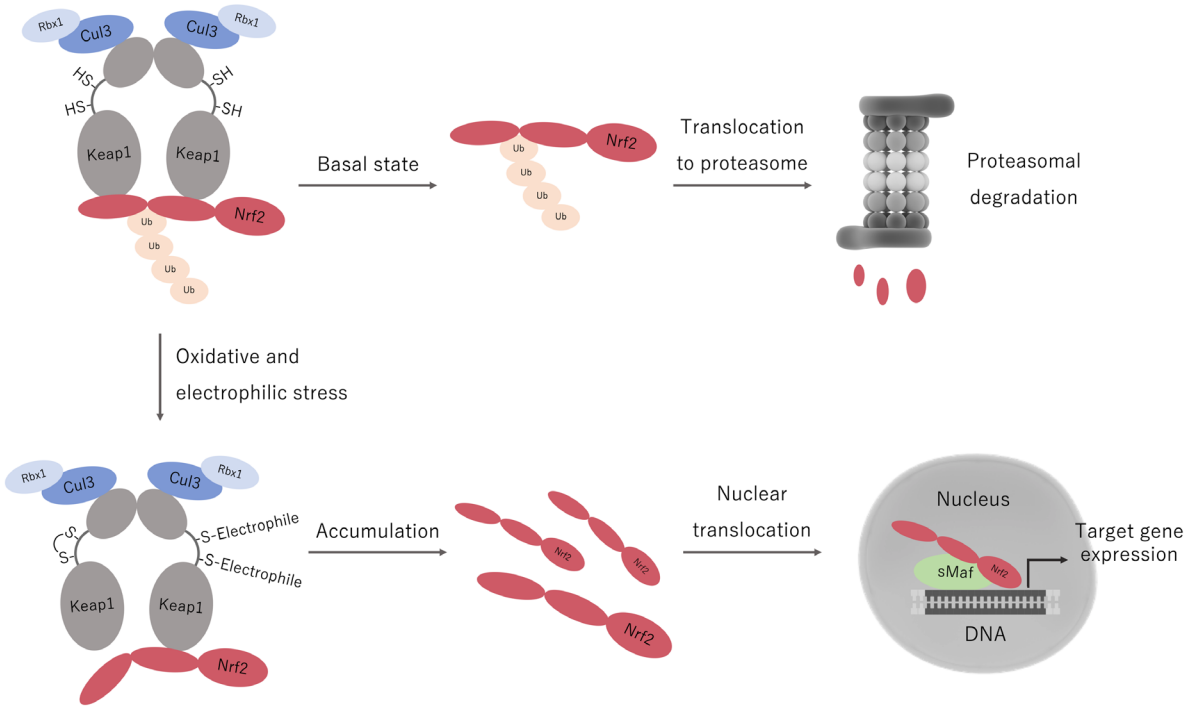

Figure 14: The KEAP1-NRF2 pathway. Adapted from (150)

CUL3: Cullin 3, RBX1: RING-box protein 1, Ub: Ubiquitin, sMAF: Small MAF protein

5.3 Classes of NRF2-inducers

ROS (e.g., H_2O_2) and numerous structurally diverse compounds such as substituted phenols, coumarins, indoles, and sulfur compounds (phase II inducers) can disturb KEAP1-mediated NRF2 ubiquitination and induce NRF2 activation (269). A common characteristic of these inducers is their ability to oxidize, reduce, or alkylate reactive KEAP1's cysteine residues. NRF2-inducers are divided into six classes according to their sensor preference (264). Class I are Cys151-preferring inducers (e.g., diethyl maleate, *tert*-butylhydroquinone, sulforaphane) (270). The class II inducer 15d-PGJ_2 preferentially modifies Cys288, while class III inducers (e.g., 4-hydroxynonenal) can bind to any of the three cysteines Cys151, Cys273, and Cys288 (267). Class IV inducers (e.g., H_2O_2, Cd^{2+}) act over the ROS sensor, while the sensor of class V inducers (e.g., prostaglandin A_2) is not yet identified. In addition, protein-protein interaction inhibitors or class VI inducers (e.g., p62) inactivate KEAP1 by competitively binding to its NRF2-binding site (271). Protein-protein interaction inhibitors such as p62 activates NRF2 through the "hinge-and-latch" mechanism, indicating that different inducers might activate NRF2 through different mechanisms (264).

5.4 NRF2-regulated cytoprotective enzymes

NRF2 regulates the gene expression of numerous phase II-detoxifying as well as antioxidant and antioxidant-generating enzymes (236, 242). NRF2 regulates the expression of the GSH-biosynthetic enzymes glutamate-cysteine ligase (GCL) and GSH synthetase (GS) (238). Moreover, NRF2 controls the expression of the GSH-dependent enzymes GSH reductases, GSH peroxidases (GPX) and GST (272). GCL and GS sequentially catalyze the biosynthesis of GSH (273). GSH (y-glutamyl-cysteinyl-glycine), a tripeptide-like molecule composed of glutamate, cysteine, and glycine, is the most abundant antioxidant molecule in cells (273). GCL catalyzes the first and rate-limiting step of GSH biosynthesis, the ligation of cysteine and glutamate to y-glutamyl-cysteine. The bond between glutamate and cysteine occurs over the y-carboxyl group of glutamate, which can only be hydrolyzed by the y-glutamyl transpeptidase (274). The GS ligates y-glutamyl-cysteine to glycine. Hepatocytes belong to the GSH-richest cells of the human body, containing GSH in the millimolar range (5-10 mM) (273). Hepatic GSH is also exported into the plasma and bile. Mitochondria contain a separate GSH pool, which has to be imported from the cytosol and accounts for 10-15% of the cellular pool (275). GSH serves as reductant to detoxify H_2O_2, reduces disulfide bonds, and protects thiol groups from oxidation (273). Moreover, GSH serves as cysteine reservoir and detoxifies electrophiles trough conjugation. GSH conjugation reactions are catalyzed by GSTs (276). GPXs (see Figure 15) reduce H_2O_2 to H_2O using GSH as reducing agent (277). This reaction is especially important

in hepatic mitochondria that lack the H_2O_2-reducing enzyme catalase. GPX1 is a soluble peroxidase located in the cytosol and mitochondrial matrix, while GPX4 adheres to cell membranes and uniquely reduces lipid hydroperoxides (278, 279). By serving as reducing agents, two molecules of GSH undergo oxidation to glutathione disulfide (GSSG). Therefore, the ratio of GSSG to GSH represents an indicator for oxidative stress (280). GSH reductases (GR) subsequently regenerates GSH from GSSG using NADPH as reducing agent (280).

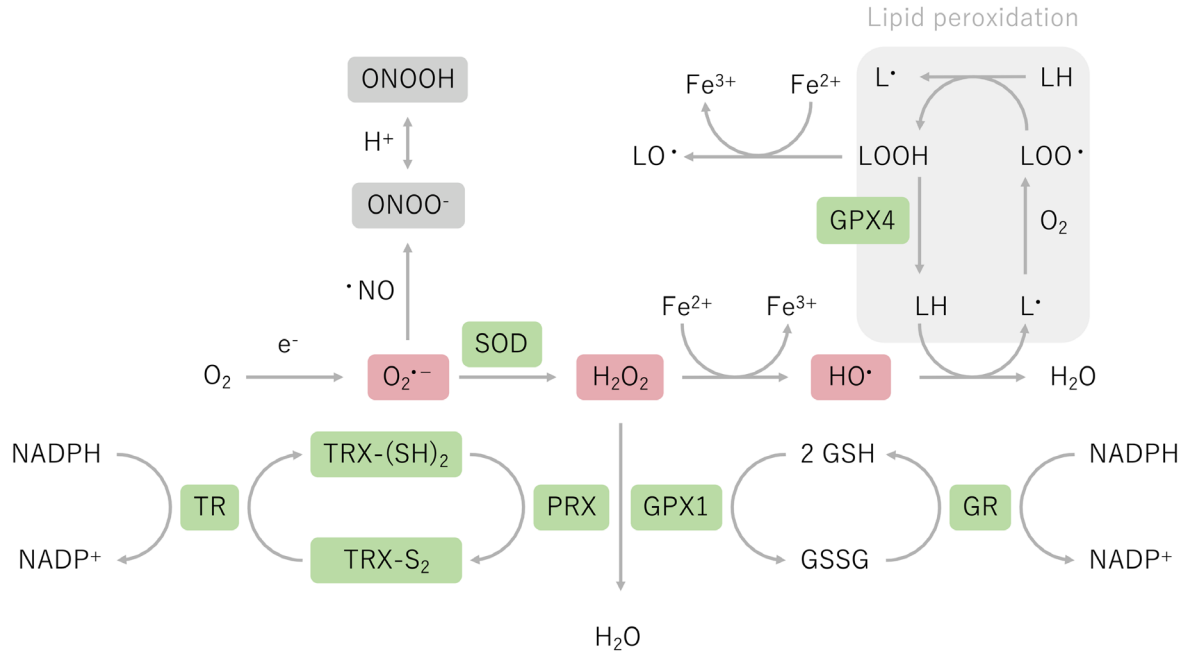

Figure 15: Network of antioxidant enzymes regulated by NRF2 (116, 281).
SOD: Superoxide dismutase, GSH: Glutathione, GSSG: GSH disulfide, GPX: GSH peroxidase, GR: GSSG reductase, PRX: Peroxiredoxin: TRX: Thioredoxin, TR: TRX reductase

In addition to genes involved in GSH homeostasis, NRF2 regulates the gene expression of peroxiredoxins (PRX), thioredoxins (TRX), and thioredoxin reductases (TR) (282). PRXs are thiol-dependent peroxidases that reduce organic hydroperoxides and H_2O_2 to alcohols and H_2O, respectively (283, 284). To date, six mammalian PRX isoforms containing catalytic cysteine residues are identified (285). PRX3 and PRX5 are mitochondrial PRXs that detoxify matrix peroxides (286). PRXs receive electrons from the TRX system formed by TRX, TR, and NADPH (287). TRXs are small proteins (about 12 kDa) containing two cysteine residues in their catalytic site, which participate in redox reactions (288). TRXs reduce protein disulfide bonds using their catalytic dithol as electron donor. Consequently, TRXs' catalytic dithiol is oxidized to a disulfide bond. TR maintain TRXs in their reduce forms by NADPH-dependent reduction of oxidized TRX. The mitochondrial matrix contains a separate TRX system formed by TRX2 and TR2, while TRX1 and TR1 are found in the cytosol (289).

In addition, NRF2 regulates the gene expression of heme oxygenase-1 (HO-1) (236). HO-1 catalyzes the degradation of oxidant heme to biliverdin, mono oxide, and Fe^{2+} (290). Moreover, NRF2 can induce the gene expression of SODs and catalase (291). As previously described, SODs dismutate superoxide radicals to H_2O_2 and O_2 (115). NRF2 can induce both the mitochondrial form (SOD2 or MnSOD), which is exclusively located in the mitochondrial matrix, and the cytosolic form (SOD1 or CuSOD), which is also present in the mitochondrial IMS (291-293). Catalase is the most abundant H_2O_2-detoxifying enzyme in mammalian peroxisomes (138). Cytosolic catalase reduces two H_2O_2 molecules to H_2O and O_2. In contrast, mitochondria do not contain catalases, except in heart, and relay on alternative H_2O_2-detoxifying enzyme (294). Another prominent NRF2-regulated enzyme is the phase II-detoxifying enzyme NAD(P)H-quinone oxidoreductase 1 (NQO1) (242). NQO1 reduces ROS-generating quinones to quinols using both NADH and NADPH as reducing agents. In addition, NRF2 regulates many other genes involved in antioxidant defense and redox signaling such as p62, sulfiredoxins, or glucose-6-phosphate dehydrogenase (295).

6 Drug-induced lysosomal toxicity

Lysosomes coordinate important cellular functions such as cell metabolism and intracellular quality control by degradation of damaged or unnecessary material (296). Therefore, functional lysosomes are crucial for cellular homeostasis. Thus, lysosomal accumulation of weak basic drugs (pK_a between 6 and 10) by proton trapping (see Figure 16), a phenomenon known as lysosomotropism, can impair lysosomal functions and contribute to the cytotoxicity of these drugs (297, 298).

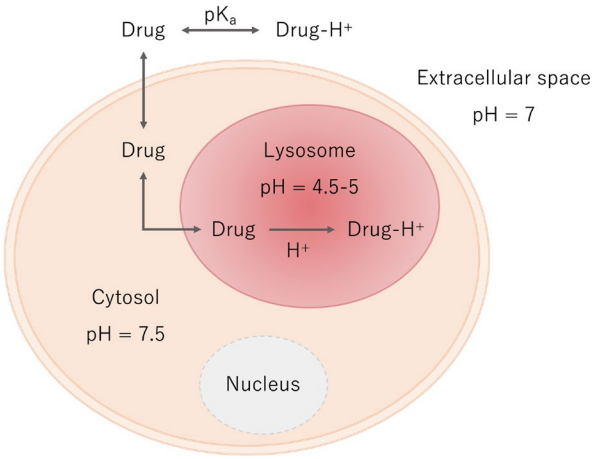

Figure 16: Lysosomal accumulation of lysosomotropic drugs. Adapted from (299).

6.1 Lysosomal structure

Lysosomes were discovered in 1955 by Christiane de Duve in the course of a rat liver fractionation (300). Containing various acid hydrolases that degrade diverse substrates, the newly discovered organelle was named “digestive body” (301). Lysosomes are membrane-enclosed organelles with acidic lumens (pH 4.5-5) containing more than 60 acid hydrolases (302). The lysosomal lumen is acidified by the membrane-associated vacuolar-type H^+-ATPase (V-ATPase), which continuously pumps H^+ inside the lysosomal lumen (303). The V-ATPase is composed of a membrane-embedded H^+-pumping V_0 subunit and a cytosolic V_1 unit, which hydrolyses ATP (304). In order to dissipate the electrical gradient created by the V-ATPase, the translocation of H^+ is accompanied by the transport of counterions across the lysosomal membrane (305). Proposed counterions are Cl^-, imported into lysosomes by a 2 Cl^-/H^+ antiporter, and K^+ or Ca^{2+}, exported from lysosomes by cationic channels (e.g., TRPML1, TPC2). In addition to V-ATPases and ion channels or transporters, the lysosomal membrane contains highly glycosylated transmembrane proteins, the lysosome-associated membrane proteins (LAMPs) (306). The glycosylated luminal parts of the LAMPs form a glycocalyx at the inner side of the lysosomal membrane, which protects the lysosomal membrane from

self-digestion by lysosomal hydrolases (307). Lysosomes contain many different hydrolytic enzymes such as proteases, lipases, nucleases, glycosidases, phospholipases, or phosphatases (308). They are produced in the trans-Golgi network and delivered to lysosomes via endosomes (309). Lysosomal proteases, the cathepsins, are divided into aspartic (e.g., cathepsin D), cysteine (e.g., cathepsin B, H, and L), and serine proteases (e.g., cathepsin A, G) and fulfill diverse functions including peptide digestion and antigen processing (310, 311).

6.2 Lysosomal functions

As digestive organelles, lysosomes degrade and recycle intracellular and extracellular material through autophagy and endocytosis, respectively (306). Endocytosed extracellular materials (e.g., pathogens) are delivered to lysosomes via endosomes (312). Intracellular materials such as unfolded proteins, lipid droplets, or damaged organelles are sequestered into double-membraned vesicles called autophagosomes, which fuse with lysosomes to autolysosomes (313). This process, known as macroautophagy, represents a major intracellular degradation pathway and quality control (314).

Beside the digestive functions, lysosomes are involved in the regulation of cell metabolism (306). The lysosomal surface serves as a platform for AMP-activated protein kinase (AMPK) and mammalian target of rapamycin complex 1 (mTORC1) activation (315). mTORC1 is a protein complex composed of raptor, MLST8, PRAS40, deptor, and the serine/threonine protein kinase mammalian target of rapamycin (mTOR). mTORC1 is recruited from the cellular endomembrane system (e.g., ER, Golgi, endosomes) to the lysosomal surface in response to amino acids (316). The availability of amino acids is sensed in the lysosomal lumen by the lysosomal amino acid transporter SLC38A9, which interacts with the lysosome-anchored Ragulator-RAG GTPase protein complex (317). The complex contains small RAG GTPases (RAGA, RAGB, RAGC, RAGD) that form heterodimers (RAGA or RAGB with RAGC or RAGD) (318). By extruding essential amino acids (e.g., arginine and leucine) from the lysosomal lumen into the cytosol via an “inside-out-mechanism”, SLC38A9 activates the Ragulator complex together with the V-ATPase (319). The Ragulator subsequently activates the RAG GTPases, which recruit mTORC1 to the lysosomal surface (316). Rheb, a small GTPase present on the lysosomal surface, subsequently activates mTORC1 in response to growth factors and ATP (315, 318). Growth factors (e.g., insulin) activate mTORC1 via the phosphatidylinositol 3-kinases (PI3K)-Akt pathway by inactivating Rheb’s inhibitor, the tuberous sclerosis complex 1/2 (TSC1/2) (320). AMPK is activated by glucose deprivation and inactivates mTORC1 by both

inhibition of raptor and activation of TSC1/2 (67). mTORC1 regulates anabolic (e.g., protein synthesis) and catabolic processes (e.g., autophagy, lysosomal biogenesis) by phosphorylation of other proteins including transcription factors (321). For instance, mTORC1 regulates the activity of the transcription factor EB (TFEB), which controls lysosomal biogenesis (see Figure 17) and autophagy (322, 323). TFEB belongs to the microphthalmia-transcription factor E (MiT/TFE) family, a subfamily of the basic helix-loop-helix transcription factor family (324). In normal conditions, phosphorylation of TFEB by mTORC1 stimulates its binding to cytosolic 14-3-3 proteins, retaining TFEB inside the cytoplasm (325, 326). Inactivation of mTORC1 upon starvation or lysosomal stress (e.g., lysosomal enlargement/storage) dephosphorylates TFEB and induces its translocation into the nucleus. TFEB-target genes, numerous lysosomal and autophagic genes, contain a 10- base pairs (GTCACGTGAC) sequence in their promotor, known as the coordinated lysosomal expression and regulation (CLEAR) element (327). Nuclear TFEB binds to CLEAR elements and promotes the transcription of these genes. In addition to cellular clearance and regulation of cell metabolism, lysosomes store Ca^{2+}, repair cell membranes, and regulate cell death (296, 328).

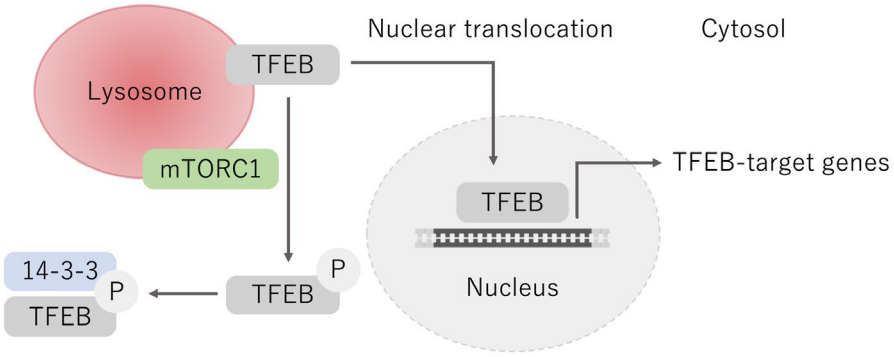

Figure 17: Regulation of lysosomal biogenesis. Adapted from (297).

TFEB: Transcription factor EB, mTORC1: Mammalian target of rapamycin complex 1

6.3 Lysosomal regulation of apoptosis

Several stressors such as photodamage, apoptotic effector proteins (e.g., BAX, BAK), sphingosines, and lysosomotropic drugs can induce lysosomal membrane permeabilization (LMP), which results in the release of lysosomal content into the cytoplasm (329, 330). Moreover, as an iron-rich organelle without antioxidant enzymes, the lysosomal membrane is prone to lipid peroxidation in the presence of H_2O_2 (331). Excessive LMP can lead to a massive release of lysosomal enzymes, acidification of the cytoplasm, and eventually induce necrosis by uncontrolled hydrolysis of cytoplasmic components (297). Selective release of specific cathepsins that remain active at neutral pH (e.g., cathepsin B, D, L) can cleave and activate the pro-apoptotic BH3-only protein BID to truncated BID (tBID) (332). tBID subsequently activates pro-apoptotic effector proteins (e.g., BAX, BAK), which can induce mitochondrial membrane permeabilization and cytochrome *c* release (333, 334). Alternatively, cathepsins can degrade the anti-apoptotic BCL-2 protein or directly activate BAX (335). Damaged lysosomes are therefore immediately repaired by the endosomal sorting complex required for transport (ESCRT) machinery or ubiquitinated and subsequently degraded via lysophagy, a selective form of autophagy (336).

7 Aims of the thesis

Idiosyncratic DILI is caused by various mechanisms including mitochondrial dysfunction and oxidative stress. Thus, the aim of the present thesis was to study the role of the NRF2-mediated oxidative stress response in DILI caused by mitochondrial toxicants. We evaluated the consequences of drug-induced mitochondrial oxidative stress on the mitochondrial and cellular antioxidant defense. Moreover, we studied the role of lysosomes in DILI caused by lysosomotropic TKIs.

7.1 Paper I

The aim of the first project was to investigate the consequences of benzbromarone-induced oxidative stress on (i) the KEAP1-NRF2 pathway in HepG2 cells. More specifically, we studied the effects of benzbromarone-induced oxidative stress on (ii) NRF2-regulated antioxidant proteins and (iii) on the cellular as well as mitochondrial GSH pool, identifying markers of mitochondrial and cellular oxidative damage. Finally, we sought to answer the question whether an impaired NRF2-mediated oxidative stress response represents a risk factor for benzbromarone-induced hepatotoxicity.

7.2 Paper II

In the second project, we aimed to evaluated the effects of lapatinib on (i) the KEAP1-NRF2 pathway and (ii) the involvement of oxidative stress in its activation. Thereby, we intended to investigate the mechanism of NRF2 activation by lapatinib. Moreover, we assessed the consequences of lapatinib on (iii) NRF2-regulated genes and proteins as well as on (iv) the cellular GSH pool.

7.3 Paper III

The overall goal of this project was to elucidate whether the lysosomotropic properties of imatinib and lapatinib contribute to their hepatotoxic effects. Therefore, we evaluate the effects of lapatinib and imatinib on (i) lysosomal morphology and (ii) lysosomal functions such as proteolytic activity and mTORC1 activation. Moreover, we elucidated the effects of imatinib on (iii) the lysosomal stress response regulated by TFEB. Finally, we assessed the effects of imatinib on (iv) autophagy in HepG2 cells.

Results

1 Paper I

The uricosuric benzbromarone disturbs the mitochondrial redox homeostasis and activates the NRF2 signaling pathway in HepG2 cells

Noëmi Johanna Roos[1,2,3], Urs Duthaler[1,2], Jamal Bouitbir[1,2,3], and Stephan Krähenbühl[1,2,3]

[1]Division of Clinical Pharmacology & Toxicology, University Hospital, Basel, Switzerland

[2]Department of Biomedicine, University of Basel, Switzerland

[3]Swiss Centre for Applied Human Toxicology (SCAHT), Basel, Switzerland

Published in Free Radic Biol Med. 2020 May 20;152:216-226.

Free Radical Biology and Medicine 152 (2020) 216–226

Contents lists available at ScienceDirect

Free Radical Biology and Medicine

journal homepage: www.elsevier.com/locate/freeradbiomed

Original article

The uricosuric benzbromarone disturbs the mitochondrial redox homeostasis and activates the NRF2 signaling pathway in HepG2 cells

Noëmi Johanna Roos[a,b,c], Urs Duthaler[a,b], Jamal Bouitbir[a,b,c], Stephan Krähenbühl[a,b,c,*]

[a] Division of Clinical Pharmacology & Toxicology, University Hospital of Basel, Switzerland
[b] Department of Biomedicine, University of Basel, Switzerland
[c] Swiss Centre for Applied Human Toxicology (SCAHT), Basel, Switzerland

ARTICLE INFO

Keywords:
Benzbromarone
HepG2 cells
Mitochondria
Reactive oxygen species
NRF2
Glutathione
Thioredoxin

ABSTRACT

The uricosuric benzbromarone is a mitochondrial toxicant associated with severe liver injury in patients treated with this drug. Since dysfunctional mitochondria can increase mitochondrial superoxide ($O_2^{\bullet -}$) production, we investigated the consequences of benzbromarone-induced mitochondrial oxidative stress on the hepatic antioxidative defense system. We exposed HepG2 cells (a human hepatocellular carcinoma cell line) to increasing concentrations of benzbromarone (1-100 μM) for different durations (2-24 h), and investigated markers of antioxidative defense and oxidative damage. At high concentrations (≥50 μM), benzbromarone caused accumulation of mitochondrial superoxide ($O_2^{\bullet -}$) and cellular reactive oxygen species (ROS). At concentrations > 50 μM, benzbromarone increased the mitochondrial and cellular GSSG/GSH ratio and increased the oxidized portion of the mitochondrial thioredoxin 2. Benzbromarone stabilized the transcription factor NRF2 and caused its translocation into the nucleus. Consequently, the expression of the NRF2-regulated antioxidative proteins superoxide dismutase 1 (SOD1) and 2 (SOD2), glutathione peroxidase 1 (GPX1) and 4 (GPX4), as well as thioredoxin 1 (TRX1) and 2 (TRX2) increased. Finally, upregulation of NRF2 by siRNA-mediated knock-down of KEAP1 partially protected HepG2 cells from benzbromarone-induced membrane damage and ATP depletion. In conclusion, benzbromarone increased mitochondrial $O_2^{\bullet -}$ accumulation and activates the NRF2 signaling pathway in HepG2 cells, thereby strengthening the cytosolic and mitochondrial antioxidative defense. Impaired antioxidative defense may represent a risk factor for benzbromarone-induced hepatotoxicity.

1. Introduction

Benzbromarone is an uricosuric that has been used for several decades in Europe and South East Asia to treat hyperuricemia and gout [1]. Benzbromarone inhibits the proximal tubular reabsorption of uric acid and thereby lowers the serum uric acid concentration. As a benzofuran derivative, benzbromarone shows no structural similarity with uric acid, however, shares structural similarities with the antiarrhythmics amiodarone and dronedarone [2]. Similar to amiodarone and dronedarone, benzbromarone is associated with a risk for liver injury [2,3]. The reported hepatic injuries range from mild elevation of serum transaminases, which is mostly reversible, to potentially fatal acute liver failure [3]. As a consequence, benzbromarone was withdrawn from the drug market in many countries; however, it can still be prescribed to patients in Germany, Netherlands, Spain, and Japan [4].

The exact mechanisms of benzbromarone-associated hepatotoxicity are still unknown. We have shown in a previous study performed in rat liver mitochondria and isolated rat hepatocytes that the hepatotoxicity of benzbromarone is related to mitochondrial dysfunction [2]. Later, we showed that benzbromarone impairs the activity of enzyme complexes of the electron transport chain and of mitochondrial ß-oxidation in HepG2 cells, a human cell line derived from a patient with hepatocellular carcinoma [5]. Furthermore, benzbromarone disturbs the mitochondrial network, and causes both apoptosis and necrosis in HepG2 cells [5].

As a consequence of the inhibition of the enzyme complexes of the electron transport chain, HepG2 cells exposed to benzbromarone exhibit accumulation of mitochondrial reactive oxygen species (ROS), which derive mainly from superoxide radicals ($O_2^{\bullet -}$). ROS can damage DNA bases, modify proteins, and oxidize membrane lipids, and consequently cause cell death [6,7]. The nuclear factor erythroid 2-related factor 2 (NRF2), a basic-leucine zipper transcription factor, regulates

* Corresponding author. Clinical Pharmacology & Toxicology, University Hospital, 4031, Basel, Switzerland.
E-mail address: stephan.kraehenbuehl@usb.ch (S. Krähenbühl).

https://doi.org/10.1016/j.freeradbiomed.2020.03.009
Received 22 January 2020; Received in revised form 8 March 2020; Accepted 12 March 2020
Available online 17 March 2020
0891-5849/

the expression of diverse antioxidative genes, and plays therefore a central role in the defense against oxidative stress [8]. Under physiological conditions, NRF2 is trapped in the cytoplasm by its repressor Kelch-like ECH-associated protein 1 (KEAP1), a redox-sensitive protein. KEAP1 functions as an adapter for Cullin 3-based E3 ligase, which enables ubiquitination and subsequent degradation of NRF2 [9,10]. Upon exposure to ROS, reactive cysteine residues of KEAP1 are oxidized, and KEAP1 is unable to target NRF2 for proteasomal degradation [11]. The cellular NRF2 content increases and NRF2 translocates into the nucleus where it binds to antioxidant response elements (ARE) located in the upstream promoter region of the respective target genes, such as superoxide dismutases (SODs) [12], glutathione (GSH)-dependent glutathione peroxidase 1 (GPX1) and glutamate-cysteine ligase (GCL) [13]. Superoxide dismutases (SODs) transform $O_2^{\bullet -}$ to hydrogen peroxide (H_2O_2), a less reactive, but membrane-permeable ROS [14]. GPX1 subsequently detoxifies H_2O_2 to H_2O [15]. GSH, the most prevalent antioxidative molecule in hepatocytes, reacts either directly with ROS or serves as an electron donor for ROS-detoxifying proteins such as GPX1 [16]. In these processes, two molecules of GSH undergo oxidation to glutathione disulfide (GSSG). Thus, the ratio of GSSG to GSH (GSSG/GSH) increases with increasing oxidative stress [17,18]. GSH is compartmentalized in hepatocytes, whereby mitochondria contain their own pool [19]. Thus, hepatocytes and their mitochondria possess an own antioxidative defense system to detoxify ROS [20]. To date, the consequences of benzbromarone-induced oxidative stress on the mitochondrial antioxidative defense system and on the NRF2 signaling pathway including downstream target antioxidative proteins are still unknown.

Based on these considerations, the aim of the present study was to investigate the consequences of benzbromarone-induced mitochondrial oxidative stress on the mitochondrial and cellular antioxidative defense capacity in HepG2 cells. We investigated the effect of benzbromarone on the accumulation of mitochondrial and cellular ROS, on the mitochondrial and cellular GSH pools, and on the expression of thioredoxins and the redox state of the mitochondrial thioredoxin 2 (TRX2). Since NRF2 plays a central role in protecting hepatocytes against drug-induced oxidative stress, we also investigated whether benzbromarone activates the NRF2 signaling pathway and whether changes in the protein expression of NRF2 alters the cytotoxic characteristics of benzbromarone.

2. Materials and methods

2.1. Reagents

We purchased the cell culture medium, supplements, and the transfection reagent from Thermo Fisher Scientific (Basel, Switzerland). The chemicals, including benzbromarone, were obtained from Sigma-Aldrich (Buchs, Switzerland), if not indicated otherwise. For LC-MS/MS measurements, we used solvents of HPLC grade from Merck (Darmstadt, Germany). Internal standards and reference substances were purchased from Toronto Research Chemicals (Ontario, Canada), antibodies for Western blotting either from Abcam (Cambridge, UK) or Santa Cruz Biotechnology (Heidelberg, Germany). The siRNA for transfection were also obtained from Santa Cruz Biotechnology.

2.2. Cell culture

We cultured the human hepatoma cell line HepG2 in Dulbecco's modified eagle medium (1.0 g/L D-glucose, 4 mM L-glutamine, 1 mM sodium pyruvate) supplemented with 10% (v/v) inactivated fetal bovine serum, 10 mM HEPES buffer (pH 7.4), 2 mM GlutaMAX, 1% (v/v) MEM non-essential amino acids solution (100x), and 100 U/mL penicillin/streptomycin. The cells were kept at 37 °C in a humidified 5% CO_2 cell culture incubator and passaged using TrypLE express enzyme. The cell number was determined using a Neubauer hemocytometer, and the cell viability was checked using the trypan blue exclusion method.

2.3. Treatment of HepG2 cells with benzbromarone

We exposed HepG2 cells (90% confluency) to increasing benzbromarone concentrations in the range of 1–100 μM for different durations (2, 4, 6, 24, and 48 h). Benzbromarone stock solutions (1000x) were prepared in dimethyl sulfoxide (DMSO) and stored at -20 °C. Thus, we used 0.1% (v/v) DMSO as a negative control.

2.4. Cellular ROS accumulation

Cellular ROS accumulation was measured in benzbromarone-exposed HepG2 cells using dihydrorhodamine 123 (Sigma-Aldrich, Buchs, Switzerland) as molecular probe. Dihydrorhodamine 123 is oxidized by ROS, including H_2O_2, to rhodamine 123, a highly fluorescent oxidation product. Thus, we incubated benzbromarone-exposed HepG2 cells with 1 μM dihydrorhodamine 123 in PBS for 15 min at room temperature protected from light. As positive control, we exposed HepG2 cells to 50 μM menadione, a redox cycler [21]. We stopped the oxidation reaction by adding 100 μL ice-cold phosphate-buffered saline (PBS) to the cells and measured the fluorescence of rhodamine 123 ($\lambda_{excitation}$ = 500 nm, $\lambda_{emission}$ = 536 nm) with a microplate reader (Infinite 200 PRO, Tecan Group, Männedorf, Switzerland). After the measurement, we lysed the cells using radio-immunoprecipitation assay buffer (RIPA buffer). We determined the protein concentration by performing a bicinchoninic acid assay using bovine serum albumin (BSA) as protein standard (Pierce BCA Protein Assay Kit, Thermo Fisher Scientific, Waltham, USA), and measured the absorbance with a microplate reader (Infinite 200 PRO, Tecan Group, Männedorf, Switzerland). The measured fluorescence was normalized to the protein concentration.

2.5. Mitochondrial $O_2^{\bullet -}$ accumulation

We measured mitochondrial $O_2^{\bullet -}$ accumulation in benzbromarone-exposed HepG2 cells using MitoSOX red (Thermo Fisher Scientific, Basel, Switzerland) as molecular probe. MitoSOX red accumulates in mitochondria, where it is oxidized by mitochondrial $O_2^{\bullet -}$ to a highly fluorescent oxidation product after its binding to nucleic acids. Thus, we incubated benzbromarone-exposed HepG2 cells with 2.5 μM MitoSOX red in PBS for 10 min at 37 °C protected from light. As a positive control, we exposed HepG2 cells to 25 μM amiodarone, which is a well-known inhibitor of the mitochondrial electron transport chain [22]. The fluorescence ($\lambda_{excitation}$ = 510 nm, $\lambda_{emission}$ = 580 nm) was measured using a microplate reader. After the measurement, we lysed the cells using RIPA buffer, and determined the protein concentration. The measured fluorescence was normalized to the protein concentration.

2.6. Mitochondrial isolation from HepG2 cells by magnetic separation

Mitochondria were isolated from HepG2 cells using the human mitochondria isolation kit (Miltenyi Biotec, Solothurn, Switzerland) according to the manufacturer's protocol. The isolation is based on magnetic separation [23]. Briefly, we harvested, washed and lysed 40 × 10^6 HepG2 cells, and homogenized them with a dounce homogenizer applying 90 strokes. We magnetically labelled the mitochondria by incubating the cell homogenate for 1 h with superparamagnetic microbeads conjugated to anti-TOM22 (translocase of outer mitochondrial membrane) antibodies. After the incubation, we applied the cell homogenate stepwise on pre-rinsed LS columns (Miltenyi Biotec, Solothurn, Switzerland) placed in the magnetic field of a MACS separator (Miltenyi Biotec, Solothurn, Switzerland). Pre-separation filters were used to remove cell aggregates. The magnetic field retained the labelled mitochondria in the columns, while the rest of the cell

homogenate ran through. After several washing steps, we removed the columns from the separator and placed them in new Eppendorf tubes. We flushed out the mitochondria by gently pushing a plunger into the column loaded with separation buffer. The mitochondrial pellet was obtained after centrifugation at 13'000 g for 2 min at 4 °C using a microcentrifuge (centrifuge 5415 R; Eppendorf, Schönenbuch, Switzerland).

2.7. Mitochondrial isolation from HepG2 cells by differential centrifugation

Alternatively, we isolated mitochondria from HepG2 cells by differential centrifugation according to the protocol of Kappler and coworkers [24]. Briefly, we collected 10×10^6 HepG2 cells in a falcon tube by centrifugation at 500g for 5 min, washed the cell pellet with ice-cold PBS, and resuspended it in 20 mL ice-cold STE buffer (250 mM sucrose, 5 mM Tris, 2 mM EGTA; pH 7.4) containing 0.5% bovine serum albumin (BSA). We homogenized the cells with a dounce homogenizer by applying 15 strokes, and centrifuged the homogenate at 1000 g for 10 min at 4 °C. The supernatant was transferred into a new falcon tube by filtering through a double gauze (250 μM mesh size). The pellet, which possibly contains still unbroken cells, was resuspended in 15 mL STE buffer containing 0.5% BSA, homogenized again by applying 15 strokes, and centrifuged using an ultracentrifuge (Beckman Avant J-25 centrifuge, Beckman Instruments, California, USA) at 1000 g for 10 min at 4 °C. We centrifuged the combined supernatants at 10'400 g for 10 min at 4 °C, and obtained a crude mitochondria pellet, which we resuspended in 5 mL STE buffer containing 0.5% BSA. After centrifugation at 10'400 g for 10 min at 4 °C, we resuspended the pelleted mitochondria in 100 μL STE buffer, and centrifuged at 16'000 g for 2 min at 4 °C. We finally resuspended the mitochondria in 100 μL RIPA buffer, and stored the lysates at -80 °C until western blot analysis.

2.8. Cellular and mitochondrial GSH and GSSG content

We analyzed GSH and GSSG by liquid chromatography tandem mass spectrometry (LC-MS/MS) in benzbromarone-exposed HepG2 cells and mitochondria isolated from benzbromarone-exposed HepG2 cells. As positive control, we exposed HepG2 cells to 100 μM L-buthionine sulfoximine (BSO), which inhibits the GSH biosynthesis [19]. GSH ammonium salt-d_5 (3.2 mM, in DMSO) and GSSG-$^{13}C_4$,$^{15}N_2$ (1 mM, in H_2O) were used as internal standards. We alkylated the thiol group of GSH and GSH ammonium salt-d_5 with N-ethylmaleimide (NEM) forming GS-NEM and GS-NEM-d_5 to prevent auto-oxidation of the thiol group during the sample preparation [25].

Briefly, 5×10^5 HepG2 cells were harvested after having been exposed to benzbromarone, washed, and the cell pellet was immediately incubated with 250 μL alkylating solution (50 mM NEM in PBS) for 30 min on ice. During the washing step, we took an aliquot to determine the protein concentration of our samples. In addition, we measured the protein concentration of the isolated mitochondrial pellet. An amount of approximately 0.4 mg mitochondria were afterwards incubated in 100 μL alkylating solution. The samples were extracted in a ratio of 1:4 (v/v) with internal standard solution, which consisted of 1 μM GSSG-$^{13}C_4$,$^{15}N_2$ and 400 nM GS-NEM-d_5 in methanol. We kept the extracts for 30 min at -20 °C to ensure protein precipitation. After centrifugation at 3500g for 10 min at 4 °C, we transferred 250 μL supernatant into a LC-MS/MS tube. Calibration lines of GS-NEM (250–0.25 μM) and GSSG (25–0.025 μM) were prepared in alkylating solution and extracted as described above for the cell samples.

An aliquot of 10 μL was injected into the LC-MS/MS system consisting of a Shimadzu HPLC (Kyoto, Japan) coupled to an API 4000 QTrap tandem mass spectrometer (ABSciex, Concord, Canada). The system was operated with Analyst 1.6.2 software (AB Sciex, Concord, Canada). GS-NEM and GSSG were separated on a Symmetry C18 column (3.5 μm, 100 Å, 4.6 mm × 75 mm; Waters, Eschborn, Germany) at a flow rate of 0.7 mL/min and a temperature of 45 °C. We used H_2O (phase A) and acetonitrile (phase B) both supplemented with 0.1% formic acid as mobile phases. We loaded the samples onto the analytical column using 7% mobile phase B and diluted it inline via a t-union with mobile phase A during the first 0.5 min of each run. Within the next 1.5 min, we linearly increased the gradient to 95% mobile phase B. We flushed the column with 95% mobile phase B for 1.5 min, and finally reconditioned the system with 7% mobile phase B for 1 min. The retention times of GSSG and GS-NEM were 1.74 min and 2.14 min, respectively. The analytes were positively charged by electro spray ionization and analyzed using scheduled multiple reaction monitoring. We applied an ion spray voltage of 5500 V, and set the probe temperature at 700 °C. We used the following mass transitions: 433.1 → 304.0 *m/z* for GS-NEM; 438.1 → 304.1 *m/z* for GS-NEM-d_5; 613.2 → 355.2, 483.9, 231.0 *m/z* for GSSG; and 619.2 → 361.0, 490.0, 230.8 for GSSG-$^{13}C_4$$^{15}N_2$.

The measured GS-NEM and GSSG concentrations were normalized to the protein concentration of each sample. Finally, we calculated the ratio of GSSG to GSH (GSSG/GSH).

2.9. Mitochondrial TRX2 redox state

We performed a redox western blot of mitochondrial protein TRX2 to determine its redox state according to the protocol of Go and Jones [26]. Reduced TRX2 was separated from oxidized TRX2 by non-reducing PAGE. The separation based on the size difference (1 kDa) between the oxidized and reduced form after derivatization of reduced TRX2 with 4-acetamido-4'-maleimidylstilbene-2,2'-disulfonic acid (AMS). AMS, a molecule of 500 Da, reacts with the two thiol groups in the active site of reduced TRX2. Briefly, benzbromarone-exposed HepG2 cells, seeded in a 6-well plate (2×10^5 cells/well), were washed with PBS, lysed with ice-cold 10% (m/v) trichloroacetic acid, and scraped from the plate using a cell scraper. The cell lysates were transferred into new Eppendorf tubes, and incubated for 30 min on ice. We obtained a protein pellet after centrifugation at 12'000 g for 5 min at 4 °C. We washed the pellet with 100% acetone, and solved the proteins in 50 μL derivatization buffer (15 mM AMS, 50 mM Tris·Cl, 0.1% SDS; pH 8.0) using a Bioruptor Pico sonication device (Diagenode SA, Seraing, Belgium). The proteins were derivatized for 3 h at room temperature in the dark. We loaded 10 μg protein mixed with 5 μL non-reducing sample loading buffer on a 15% polyacrylamide separating gel and performed western blotting as described below. As a primary antibody, we used the anti-thioredoxin 2 antibody from Abcam (ab185544) diluted 1:10'000 in 5% non-fat milk in PBS plus 0.1% Tween (PBST).

2.10. Cytoplasmic and nuclear protein extraction

We used a nuclear and cytoplasmic extraction kit (NE-PER Nuclear and Cytoplasmic Extraction Reagents, Thermo Fisher Scientific, Basel, Switzerland) to obtain nuclear and cytoplasmic protein fractions from benzbromarone-exposed HepG2 cells. According to the manufacturer's protocol, we incubated the cells with ice-cold cytoplasmic extraction reagent I for 10 min on ice. The buffer volumes were chosen according to the cell pellet size. We added ice-cold cytoplasmic extraction reagent II, vortexed the sample for 5 s, and incubated for another minute on ice. After centrifugation at 16'000 g for 5 min, we obtained the cytoplasmic protein fraction (supernatant). The pellet was further incubated in ice-cold nuclear extraction reagent for 40 min on ice with occasional vortexing. After centrifugation at 16'000 g for 10 min, we obtained the nuclear protein fraction (supernatant). The protein fractions were stored at -80 °C until western blot analysis.

2.11. Western blotting

We prepared protein samples from HepG2 cells and isolated mitochondria using RIPA buffer as lysis buffers. After determining the protein concentration of each sample, we prepared denatured and

reduced protein samples. Thus, we used sodium dodecyl sulfate (SDS) as denaturing detergent, and boiled the samples at 95 °C for 5 min. We loaded 20 µg protein on a NuPage 4-12% Bis-Tris Gel (Thermo Fisher Scientific, Basel, Switzerland), and separated the proteins by one dimensional gel electrophoresis according to their molecular weight. NuPAGE LDS sample buffer was used as loading buffer and PageRuler prestained protein ladder as molecular weight marker, both purchased from Thermo Fisher Scientific (Basel, Switzerland). The proteins were transferred on a nitrocellulose membrane (Trans-Blot Turbo Mini Nitrocellulose Transfer Packs; Bio-Rad Laboratories, Cressier, Switzerland) by a Trans-blot turbo transfer system (Bio-Rad Laboratories, Cressier, Switzerland). To prevent non-specific background binding of the antibodies, we blocked the membrane for 1 h with 5% non-fat milk in PBST under constant shaking. The membrane was incubated overnight in primary antibody diluted in 5% non-fat milk in PBST at 4 °C. The following primary antibodies and dilutions were used: NRF2 (1:10'000, ab62352), SOD1 (1:5000, ab51254), SOD2 (1:5000, ab74231), GPX1 (1:1000, ab108427), GPX4 (1:1000, ab125066), TRX1 (1:10'000, ab109385), TOMM20 (translocase of outer mitochondrial membrane 20; 1:1000, ab78547), KDEL (ER specific sequence K-D-E-L; 1:10'000, ab176333), LAMP1 (lysosome-associated membrane protein 1; 1:200, sc-17768). Antibodies against glyceraldehyde-3-phosphate dehydrogenase (GAPDH; 1:1000, sc-365062) and Lamin B1 (1:500, ab8982) were used as loading controls.

After washing and incubating for 1 h with the corresponding horseradish peroxidase-conjugated secondary antibody (m-IgGK BP-HRP, 1:2000, sc-516102; mouse anti-rabbit IgG-HRP, 1:2000, sc-2357), we detected the protein bands using an ECL detection kit (Clarity Western ECL Substrate; Bio-Rad Laboratories, Cressier, Switzerland) and Fusion pulse 6 (Witec AG, Switzerland) as imaging system. The protein bands were visualized and quantified using Evolution-Capt software (Witec AG, Switzerland).

2.12. siRNA transfection

We transfected HepG2 cells with NRF2 siRNA (30 nM, sc-37030) and KEAP1 siRNA (10 nM, sc-43878) to downregulate the protein expression of NRF2 and KEAP1, respectively. We performed a reverse transfection using Lipofectamine RNAiMAX as transfection reagent. A non-targeting CTRL siRNA-A (10 nM, sc-37007) was used as negative control. Briefly, we prepared siRNA-Lipofectamine RNAiMAX complexes by diluting the siRNA in Opti-MEM reduced serum medium followed by the addition of Lipofectamine RNAiMAX. We gently mixed the preparation, and incubated for 20 min at room temperature. Subsequently, we transferred the siRNA-Lipofectamine RNAiMAX complexes to a 96-well plate (20 µL/well), and added 7500 HepG2 cells/well diluted in 100 µL of antibiotics-free growth medium. The cells were incubated for 48 h at 37 °C in a in a 5% CO_2 incubator.

2.13. Membrane toxicity

We assessed the cell membrane integrity of benzbromarone-treated HepG2 cells using the ToxiLight assay from Lonza (Basel, Switzerland). The assay measures the release of the intracellular enzyme adenylate kinase (AK) into the cell culture medium upon cell membrane damage. We treated siRNA-transfected HepG2 cells, seeded in a 96-well plate, with increasing concentrations of benzbromarone (10-100 µM) for 24 h. Triton X 0.1% was applied as positive control. We combined 20 µL of the cell culture medium with 50 µL of AK detection solution in an opaque 96-well plate, incubated for 5 min, and measured the luminescence using a microplate reader.

2.14. Cellular ATP content

We measured the intracellular ATP content as a marker of cell viability in benzbromarone-treated HepG2 cells using the CellTiter-Glo luminescent cell viability assay from Lonza (Basel, Switzerland). Briefly, we added CellTiter-Glo reagent directly to the cells seeded in a 96-well plate using an equal volume as the cell culture medium. Cell lysis was induced by shaking the plate for 2 min on an orbital shaker. After incubation at room temperature for 10 min, we recorded the luminescence using a microplate reader.

2.15. Statistical analysis

The data are presented as the mean ± standard error of the mean (SEM) of at least three independent experiments. We performed one-way ANOVA statistical analysis or 2 way ANOVA with Dunnett's multiple comparison test using GraphPad prism version 8.2.1 (Graph Pad Software, San Diego, USA). Significant values, indicated in the figures with a star, were reached with a p-value < 0.05 compared to the negative control. We used an unpaired *t*-test with a p-value < 0.05 to statistically compare the effect of each positive control to the corresponding negative control.

3. Results

3.1. Exposure to benzbromarone increased mainly mitochondrial superoxide in HepG2 cells

First, we exposed HepG2 cells to increasing concentrations of benzbromarone (1-100 µM) for 2 h, 6 h, and 24 h. We measured total cellular ROS and mitochondria-specific $O_2^{\bullet -}$ accumulation (Fig. 1). As expected, cellular ROS accumulated significantly in HepG2 cells exposed to the positive control menadione for 2 h (100 µM), 6 h (100 µM), and 24 h (50 µM) (Fig. 1A, 1B, and 1C). Moreover, HepG2 cells exposed to the positive control amiodarone for 2 h (50 µM), 6 h (50 µM), and 24 h (25 µM) revealed a significant mitochondrial $O_2^{\bullet -}$ accumulation (Fig. 1D, 1E, and 1F). Exposure to increasing concentrations of benzbromarone for 2 h caused a decrease in cellular ROS accumulation starting to be significant at 20 µM (Fig. 1A), and caused a significant increase in mitochondrial $O_2^{\bullet -}$ accumulation at 100 µM (Fig. 1D). Exposure for 6 h did not affect cellular and mitochondrial ROS accumulation (Fig. 1B and 1E). After exposure for 24 h, 50 µM and 100 µM benzbromarone showed a trend to increase cellular ROS in HepG2 without reaching significance (Fig. 1C). Similarly, after exposure for 24 h, benzbromarone showed a clear concentration-dependent trend to increase mitochondrial $O_2^{\bullet -}$ accumulation in HepG2 cells starting at 5 µM and reaching significance at 100 µM (Fig. 1F).

Overall, benzbromarone caused a time- and concentration-dependent accumulation of cellular ROS and mitochondrial $O_2^{\bullet -}$ in HepG2 cells, whereby the accumulation of mitochondrial $O_2^{\bullet -}$ was more pronounced than the accumulation of cellular ROS.

3.2. Benzbromarone caused mainly oxidation of mitochondrial GSH in HepG2 cells

We measured GSH and GSSG levels in HepG2 cells and mitochondria isolated from HepG2 cells after exposure to benzbromarone for 24 h as representatives of the antioxidative system. We isolated mitochondria from cells by two different approaches (MACS technology vs differential centrifugation), and tested the purity of the isolated mitochondria by western blot. Mitochondria obtained by MACS technology showed less lysosomal, ER, and cytosolic contaminations compared to mitochondria obtained by differential centrifugation (Suppl. Fig. 1). We isolated approximately 0.5 mg mitochondrial protein per 40×10^6 HepG2 cells.

The positive control BSO significantly decreased GSH in cells by ~76% and isolated mitochondria by ~65%, when applied for 24 h at a concentration of 100 µM (Fig. 2A and 2D, respectively). Benzbromarone at 100 µM increased both GSH (~1.4-fold) and GSSG (~2.0-fold) in entire HepG2 cells (Fig. 2A and 2B, respectively). The cellular

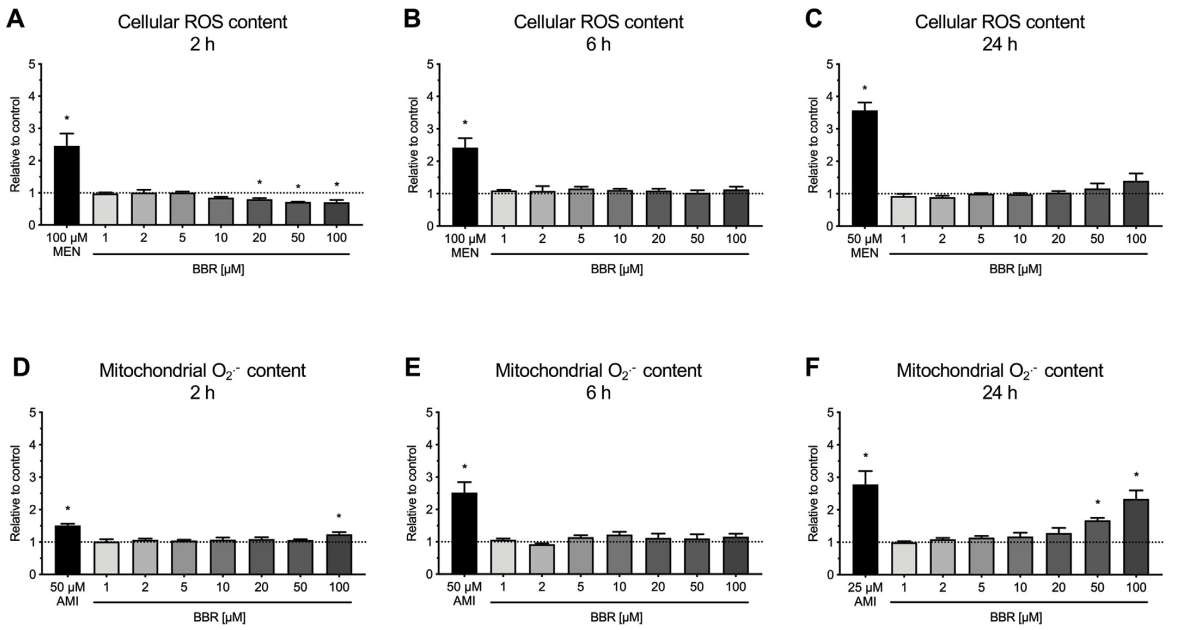

Fig. 1. Accumulation of cellular ROS and mitochondrial superoxide in HepG2 cells. Cellular ROS accumulation in HepG2 cells relative to the negative control (0.1% DMSO) after exposure to benzbromarone for 2 h **(A)**, 6 h **(B)**, and 24 h **(C)**. Benzbromarone concentrations were in the range of 1-100 µM. The ROS accumulation is shown as fold increase relative to the negative control (0.1% DMSO, represented by the grid line). Mitochondrial superoxide accumulation in HepG2 cells relative to the negative control (0.1% DMSO) after exposure to benzbromarone for 2 h **(D)**, 6 h **(E)**, and 24 h **(F)**. The superoxide accumulation is shown as fold increase relative to the negative control (0.1% DMSO, represented by the grid line). Data are the mean ± SEM of at least three independent experiments. *$p < 0.05$ versus negative control.

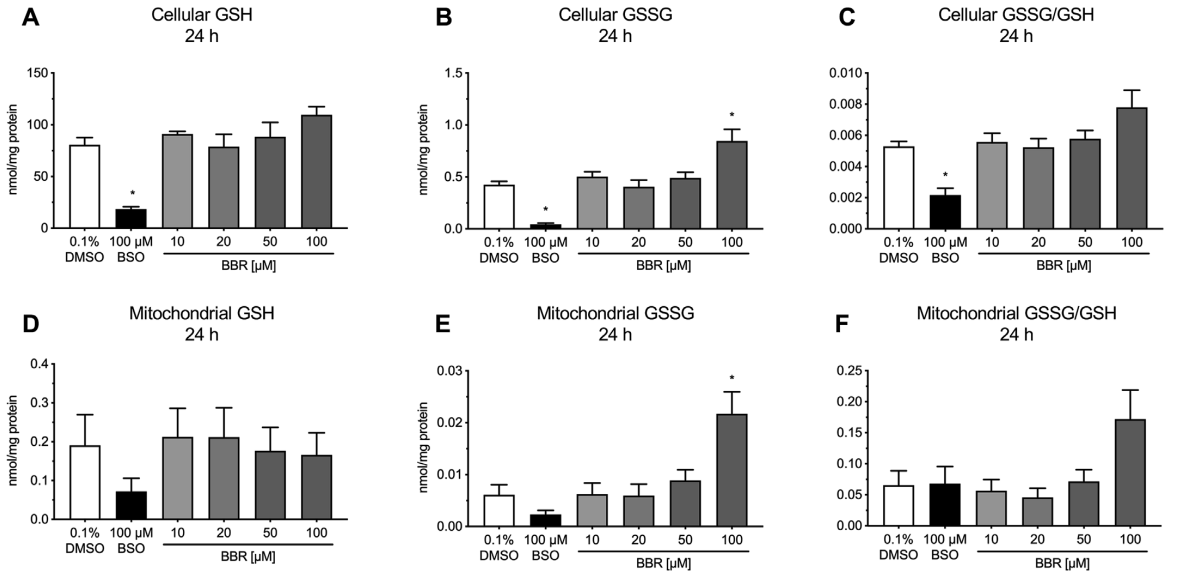

Fig. 2. Levels of GSH and GSSG, and ratio of GSSG to GSH (GSSG/GSH) in HepG2 cells and isolated mitochondria. Levels of GSH **(A)** and GSSG **(B)**, and GSSG/GSH ratio **(C)** in HepG2 cells exposed to benzbromarone for 24 h using concentrations in the range of 10-100 µM. Levels of GSH **(D)** and GSSG **(E)**, and GSSG/GSH ratio **(F)** in mitochondria isolated from HepG2 cells exposed to benzbromarone for 24 h using concentrations in the range of 10-100 µM. GSH and GSSG concentrations in HepG2 cells and isolated mitochondria were measured by LC-MS/MS analysis, and normalized to the protein concentration. We used 0.1% DMSO as a negative control. Data are the mean ± SEM of at least three independent experiments. *$p < 0.05$ versus negative control.

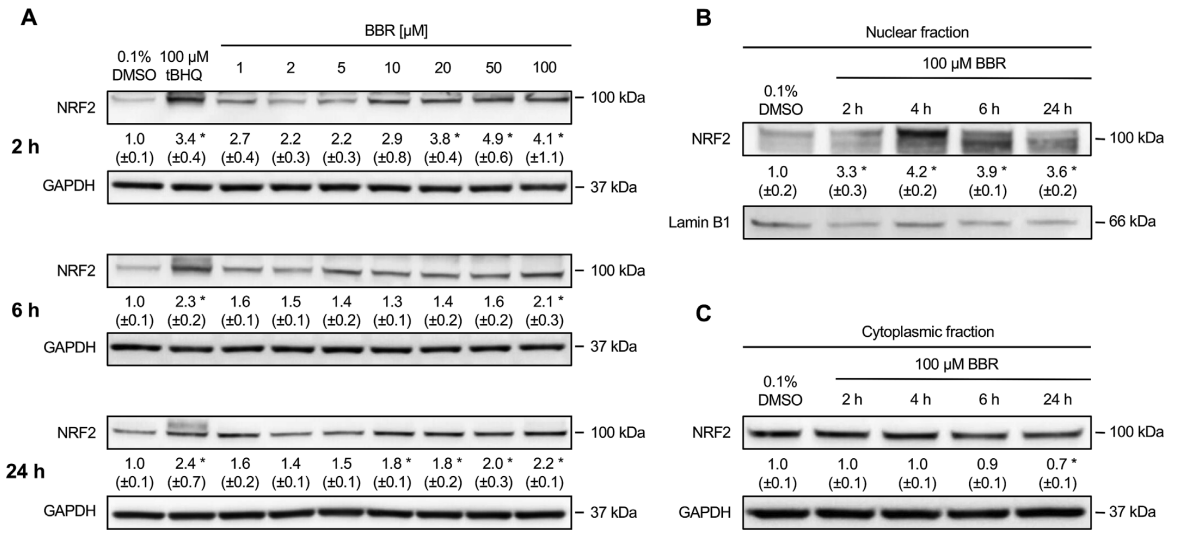

Fig. 3. Protein expression of NRF2 in HepG2 cells. (A) Representative western blot of NRF2 after exposure to benzbromarone for 2 h, 6 h, and 24 h, respectively. We used 100 μM tert-butylhydroquinone (tBHQ) as positive control to stabilize NRF2. GAPDH served as loading control. **(B)** Representative western blot of NRF2 protein expression in nuclear fraction of HepG2 cells. **(C)** Representative western blot of NRF2 protein expression in cytoplasmic fraction of HepG2 cells. The cells were exposed to 100 μM benzbromarone for 2 h, 4 h, 6 h, and 24 h, respectively. Lamin B1 (nuclear fraction) and GAPDH (cytoplasmic fraction) served as loading controls. Data are the mean ± SEM of at least three independent experiments. *p < 0.05 versus negative control.

GSSG/GSH ratio increased (~1.5-fold), without reaching significance (Fig. 2C). Benzbromarone showed a trend to decrease the mitochondrial GSH level at 50 μM and at 100 μM, but without reaching significance (Fig. 2D). Mitochondrial GSSG, however, was significantly increased (~3.5-fold) at a concentration of 100 μM benzbromarone (Fig. 2E), leading to an increased (~2.6-fold) mitochondrial GSSG/GSH ratio at this concentration (Fig. 2F). Furthermore, the GSSG/GSH ratio in mitochondria was approximately 10 times higher than in entire cells (Fig. 2C and 2F).

3.3. Benzbromarone activated the NRF2 signaling pathway in HepG2 cells

The NRF2 signaling pathway is the major regulator of cytoprotective responses to ROS. Thus, we determined the protein expression of NRF2 in HepG2 cells after exposure to increasing concentrations of benzbromarone (1-100 μM) for 2 h, 6 h and 24 h. As expected, 100 μM tert-butylhydroquinone (tBHQ), an established NRF2 inducer, increased the protein expression of NRF2 more than 2-fold after 6 h and 24 h of exposure, and more than 3-fold after exposure for 2 h compared to the negative control (Fig. 3A). Benzbromarone caused a concentration-dependent increase in NRF2 protein expression in HepG2 cells exposed for 2 h (Fig. 3A), starting already at 1 μM, the lowest concentration studied (2.7-fold increase) and starting to be significant at 20 μM. Similarly, benzbromarone increased NRF2 protein expression in HepG2 cells exposed for 6 h and 24 h at any concentration studied (Fig. 3A). Significant effects were observed after 6 h of exposure for 100 μM, and starting at 10 μM after an exposure for 24 h (Fig. 3A). Our data are compatible with a rapid stimulation of NRF2 protein expression by benzbromarone, which slowly declined over 24 h despite the presence of benzbromarone.

NRF2 is a transcription factor, which has to reach the nucleus in order to be active. We therefore investigated the translocation of NRF2 into the nucleus caused by benzbromarone at different time points. After having exposed HepG2 cells to 100 μM benzbromarone for 2 h, 4 h, 6 h, and 24 h, we prepared nuclear and cytoplasmic fractions, and determined the protein expression of NRF2 in each fraction. NRF2 accumulated significantly (> 3.0-fold) in the nuclear fraction after exposure to 100 μM benzbromarone at any time point compared to the negative control (Fig. 3B). In parallel, the expression of NRF2 in the cytoplasm was stable over the exposure period except for the 24 h time point, at which NRF2 expression was lower compared to the control (Fig. 3C).

3.4. Benbromarone increased the expression of NRF2-regulated antioxidative proteins in HepG2 cells

To examine the effects of benzbromarone on the expression of antioxidative proteins that are stimulated by NRF2, we analyzed their expression by western blot in HepG2 cells exposed to benzbromarone for 2 h, 6 h, and 24 h. We observed that benzbromarone exposure increased the protein expression of antioxidative proteins, including SOD1, SOD2, GPX1 and GPX4 in a concentration-dependent manner at any time point studied (Fig. 4 and Suppl. Fig. 2, respectively). The most pronounced effects were observed for SOD2 and GPX1, which showed the largest increase in protein expression already after 2 h of exposure with benzbromarone (Fig. 4A). For all proteins studied, the effect lasted for 24 h (Fig. 4 and Suppl. Fig. 2). For SOD2, the increase in protein expression started already at a benzbromarone concentration of 1 μM (Fig. 4 and Suppl. Fig. 2).

3.5. Benzbromarone increased the ratio of oxidized to reduced TRX2 in HepG2 cells

Thioredoxins are key actors for ROS scavenging and participate in redox-regulatory processes of cells [27]. We first quantified the total protein expression of TRX1 (cytosolic) and TRX2 (mitochondrial) in HepG2 cells exposed for 24 h to different benzbromarone concentrations (Fig. 5A). Benzbromarone caused an increase in the protein expression of TRX1 and TRX2, which was numerically present already at 1 μM, but reached significance at 5 μM for TRX1 and at 50 μM for TRX2.

Since TRX2 is located in the mitochondrial matrix and benzbromarone caused an increase in mitochondrial $O_2^{\bullet -}$ accumulation, we determined the redox state of TRX2 after exposure of HepG2 cells to different concentrations of benzbromarone for 24 h (Fig. 5B).

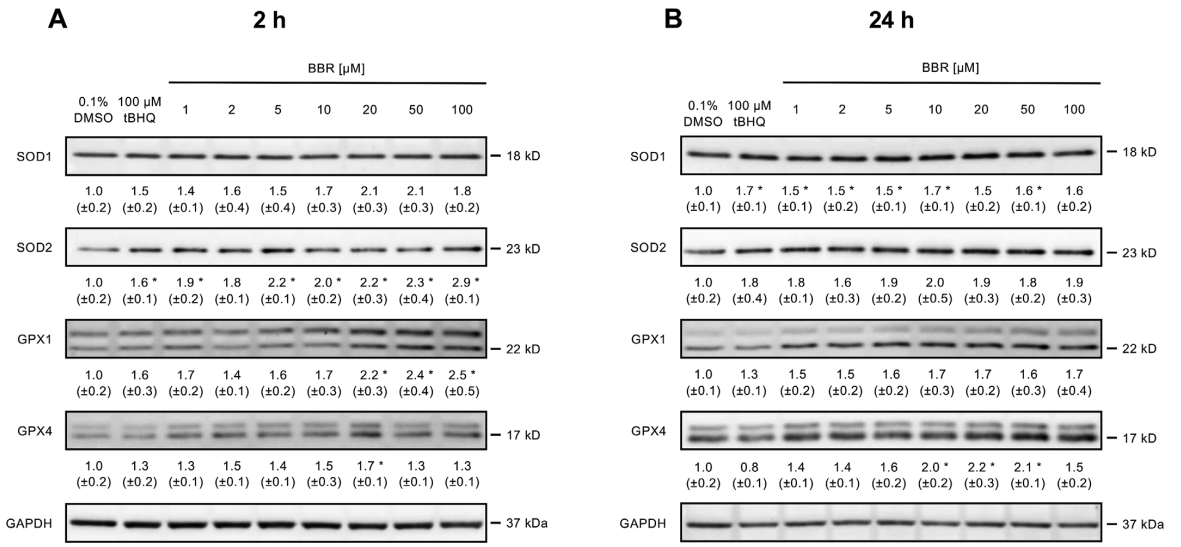

Fig. 4. Protein expression of NRF2-regulated antioxidative proteins in HepG2 cells. Representative western blots of SOD1, SOD2, GPX1, and GPX4 in HepG2 cells. The cells were exposed to 1-100 μM benzbromarone for 2 h **(A)** and 24 h **(B)**, respectively. For cells exposed for 6 h, see Suppl. Fig. 2. We used 100 μM tert-butylhydroquinone (tBHQ) as a positive control. GAPDH served as loading control. Data are the mean ± SEM of at least three independent experiments. *p < 0.05 versus negative control.

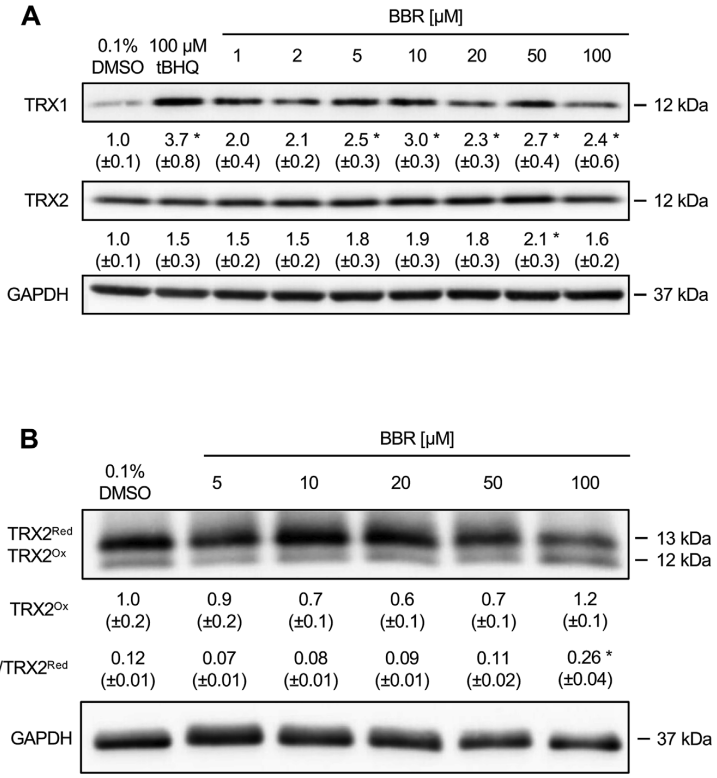

Fig. 5. Protein expression of thioredoxin (TRX) 1 and 2 in HepG2 cells. **(A)** Representative western blots of TRX1 and TRX2 after exposure to benzbromarone for 24 h using concentrations in the range of 1-100 μM. **(B)** Representative redox western blot of TRX2 after exposure to benzbromarone for 24 h using concentrations in the range of 5-100 μM. The reduced form of TRX2 ($TRX2^{red}$) is separated from the oxidized form ($TRX2^{ox}$) upon derivatization. We used 0.1% DMSO as negative control. Data are the mean ± SEM of at least three independent experiments. *p < 0.05 versus negative control.

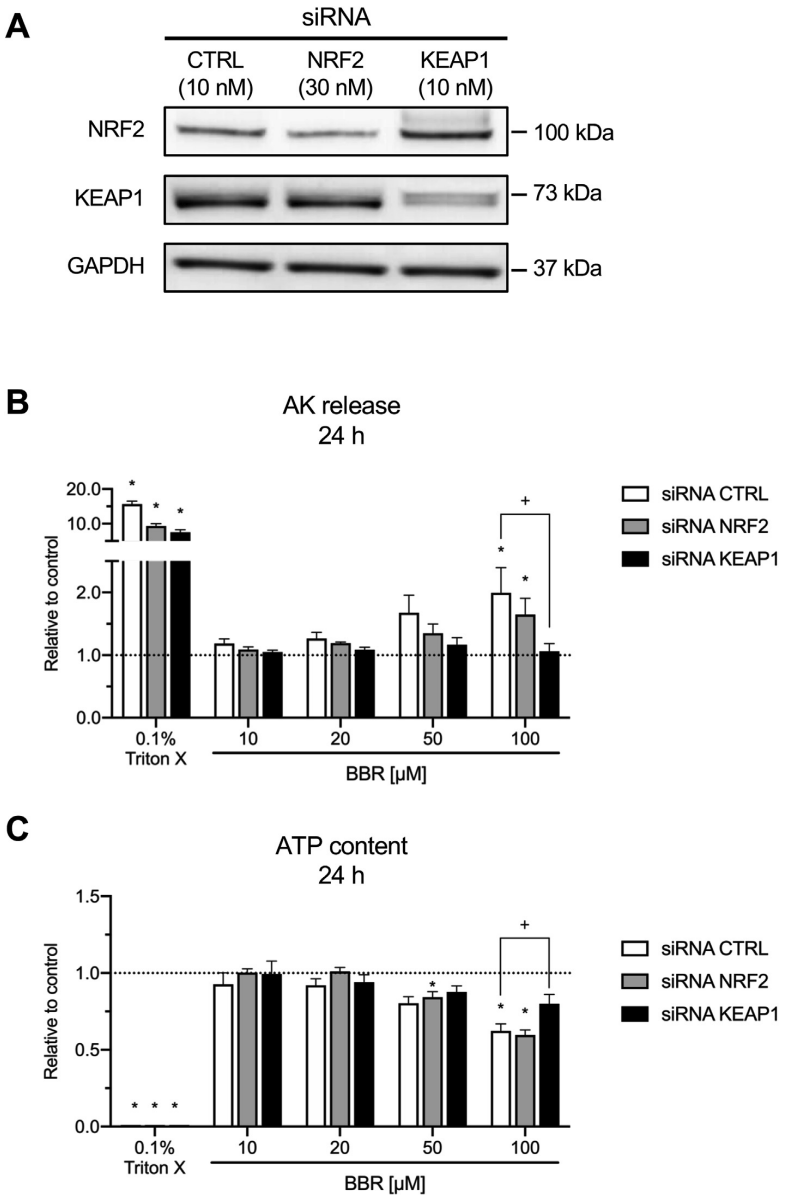

Fig. 6. AK release and ATP content in siRNA-transfected HepG2 cells. (A) Protein expression of NRF2 and KEAP1 in siRNA-transfected-HepG2 cells. Representative western blots of NRF2 and KEAP1 in HepG2 cells, which were incubated for 48 h with siRNA NRF2 (30 nM), siRNA KEAP1 (10 nM) or siRNA CTRL (10 nM). GAPDH served as loading control. **(B)** Adenylate kinase (AK) release (cell membrane integrity marker) and **(C)** cellular ATP content (cell viability marker) in HepG2 cells with decreased (siRNA NRF2), increased (siRNA KEAP1), or basal (siRNA CTRL) protein expression of NRF2, which were exposed for 24 h to increasing concentration of benzbromarone (10-100 µM). Data are shown as fold increase relative to the negative control (0.1% DMSO, represented by the grid line). Data are the mean ± SEM of three independent experiments. *p < 0.05 versus negative control of the same siRNA transfection group. $^{+}$p < 0.05 versus siRNA of the same benzbromarone treatment group.

Benzbromarone significantly increased the ratio of oxidized TRX2 to reduced TRX2 ($TRX2^{ox}/TRX2^{red}$) at a concentration of 100 µM. We also found a trend to an increased expression of the oxidized TRX2 form related to GAPDH at 100 µM benzbromarone (Fig. 5B).

3.5.1. Upregulation of NRF2 by siRNA knockdown of KEAP1 reduced membrane toxicity and ATP depletion upon benzbromarone exposure in HepG2 cells

To investigate whether NRF2 is involved in benzbromarone-induced hepatotoxicity, we used NRF2 siRNA to downregulate NRF2, and KEAP1 siRNA to upregulate NRF2 in HepG2 cells. We measured the release of AK (a marker for cell membrane integrity) and the cellular ATP content (a marker for cell viability) in benzbromarone-treated HepG2 cells, which had a reduced (siRNA NRF2), increased (siRNA KEAP1), or basal (siRNA CTRL) NRF2 protein expression (Fig. 6A). As expected, the positive control 0.1% Triton X showed an increase of AK release in the cell supernatant (Fig. 6B) and a decrease in the ATP content (Fig. 6C). Benzbromarone caused a concentration-dependent membrane damage (Fig. 6B) and ATP depletion (Fig. 6C) in HepG2 cells with basal (siRNA CTRL) and decreased (siRNA NRF2) NRF2 expression, starting at 50 µM and reaching significance at 100 µM (Fig. 6C). We did not observe these effects in HepG2 cells with an increased expression of NRF2 (siRNA KEAP1). AK release was significantly lower in siRNA KEAP1 cells compared to siRNA CTRL cells, when exposed to 100 µM benzbromarone, supporting a protective effect of NRF2 (Fig. 6B). Moreover, cellular ATP depletion was significantly less pronounced in siRNA KEAP1 cells compared to control cells (siRNA CTRL)

(Fig. 6C).

4. Discussion

The present study provides the first evidence that *in vitro* benzbromarone exposure increases preferentially the mitochondrial $O_2^{\bullet -}$ content and activates the NRF2 signaling pathway in HepG2 cells. The nuclear translocation of NRF2 resulted in upregulation of NRF2-regulated proteins, including the antioxidative proteins SOD1, SOD2, GPX1, GPX4, TRX1 and TRX2. This was not sufficient, however, to avoid mitochondrial $O_2^{\bullet -}$ accumulation and cell damage at the highest benzbromarone concentrations. By increasing NRF2 abundance through KEAP1 knockdown, membrane toxicity and ATP depletion following exposure to benzbromarone for 24 h could be mitigated.

In our previous studies, we showed that benzbromarone inhibits the activity of enzyme complexes of the mitochondrial electron transport chain [2,5]. More precisely, in HepG2 cells exposed to 50 μM benzbromarone for 24 h, the activity of all complexes of the electron transport chain was decreased with a more pronounced drop in the activity of complex I and II [2,5]. The mitochondrial ROS production is closely connected to the activity of the electron transport chain [2,28]. Complex I and III of the electron transport chain are considered as the main site of ROS production and the inhibition of one or both of these enzyme complexes is associated with increased mitochondrial production of $O_2^{\bullet -}$ [29,30]. Taking into account the established toxicity of benzbromarone on the electron transport chain, we determined the mitochondrial superoxide accumulation in HepG2 cells exposed to increasing concentrations of benzbromarone. As expected, we observed a concentration- and time-dependent accumulation of superoxide (Fig. 1). Mitochondrial $O_2^{\bullet -}$ accumulation was more pronounced than ROS accumulation in entire cells, suggesting that the primary oxidative event caused by benzbromarone was in the mitochondria.

The KEAP1-NRF2 signaling pathway is an important system located in the cytoplasm to protect cells from oxidative stress [10]. In the absence of an oxidative burst, KEAP1 traps NRF2, facilitating its ubiquitination and degradation by the 26S proteasome in order to maintain NRF2 at a constant low level. When ROS accumulate in the cytoplasm, KEAP1 is oxidized and dissociates from NRF2, which translocates into nucleus, where it combines with small MAF proteins and binds to the response elements of genes involved in antioxidative defense. Since the effect of benzbromarone on the NRF2 signaling pathway was so far unknown, we investigated the effect of benzbromarone on NRF2 protein expression and function. First, we found that the expression of NRF2 increased already after 2 h of benzbromarone exposure, which was surprising taking into account that a mitochondrial and cellular increase in ROS could only be demonstrated after 24 h of exposure. A possible explanation for this apparent discrepancy is that although mitochondrial production of $O_2^{\bullet -}$ and export of H_2O_2 into the cytoplasm increase rapidly after exposure to benzbromarone, accumulation occurs late due to sufficient antioxidative defense mechanisms. Second, we determined nuclear translocation of NRF2 by western blot analysis, and observed a significant time-dependent accumulation upon benzbromarone exposure, directly demonstrating that benzbromarone stimulates the NRF2 signaling pathway. Although it is well-established that ROS induce NRF2 activation, recent data support that alternative pathways independent of ROS can also be operative [31]. We can speculate that benzbromarone has been metabolized to electrophilic compounds that could bind covalently to cysteine residues of KEAP1, which would liberate and stabilize NRF2. In support of this hypothesis, the formation of electrophilic metabolites from benzbromarone such as 2,6-dibromohydroquinone has been reported [32,33]. This mechanism has been described for phenolic NRF2 activators such as honokiol and chlorogenic acid [34–36]. In addition, cysteine adducts of benzbromarone were found in hepatic proteins obtained from livers of benzbromarone-treated mice, demonstrating the ability of electrophilic benzbromarone metabolites to interact with sulfhydryl groups of cellular proteins [37].

In order to counteract the accumulation of ROS, thioredoxins play an important role in most cells. These small proteins are involved in the reduction of protein disulfide bridges, and therefore essential to maintain cellular proteins in their functional form in the case of oxidative stress [27]. We observed a concentration-dependent increase in the abundance of the mitochondrial (TRX2) and the cytosolic form (TRX1) of thioredoxin as well as an increase in the oxidized portion of TRX2 at the highest concentration studied (Fig. 5). Thioredoxins also belong to the NRF2-regulated genes, which might explain the observed increase [8]. This result again illustrates that benzbromarone caused oxidative stress, which most probably originated in mitochondria and then spread into the cytoplasm.

In addition to the thioredoxins, GSH is a prominent cellular antioxidative that protects against oxidative stress by scavenging reactive oxygen species [38]. Depletion of reduced GSH and/or increased GSSG, which results in a shift in the cellular GSSG/GSH redox balance, are considered indicative for oxidative stress [39]. In this study, benzbromarone caused an increase in GSSG and in the GSSG/GSH ratio in both cytoplasm and mitochondria, whereby the effect in mitochondria was more accentuated than in the cytoplasm (Fig. 2). Importantly, mitochondria are equipped with their own pool of glutathione, since GSH is synthesized in the cytoplasm and has to be transported into mitochondria [38]. Interestingly, beside the increase in GSSG in the cytoplasm and in mitochondria, which is explained by the oxidative effect of benzbromarone, there was a trend for an increase in the cytoplasm and for a decrease in the mitochondrial GSH pool at high benzbromarone concentrations. In the cytoplasm, these findings may reflect increased GSH synthesis due to activation of NRF2 [8] and in the mitochondria the oxidation of GSH to GSSG. As reported recently, GSSG is an oxidant itself and its accumulation in conditions with mitochondrial oxidative stress could itself cause oxidative damage [40]. The uncontrolled generation of GSSG during oxidative stress has been shown to contribute to mitochondrial dysfunction by glutathionylation of proteins [41].

Our study shows that NRF2 can rapidly be activated by a mitochondrial toxicant that primarily increases mitochondrial $O_2^{\bullet -}$ production and accumulation. Since $O_2^{\bullet -}$ cannot pass the inner mitochondrial membrane, the transmission of the oxidative burst from the mitochondria to the cytoplasm is achieved by H_2O_2, which is uncharged and is produced by SOD2 in the mitochondrial matrix. Our study shows that NRF2 activation leads rapidly to the upregulation of cytosolic and mitochondrial proteins that efficiently limit the accumulation of ROS in mitochondria and in the cytoplasm. When the antioxidative defense becomes overwhelmed, as illustrated by ROS accumulation (Fig. 1), mitochondrial oxidative stress can induce mitochondrial swelling due to the formation of the mitochondrial membrane permeability transition pore, which is associated with apoptosis and/or necrosis [40,42]. In our previous study, we showed that 100 μM benzbromarone was associated with increased apoptosis and also necrosis [22], which is compatible with the current results. Mitochondrial ROS accumulation is therefore a possible mechanism for hepatocyte death associated with benzbromarone exposure.

Considering the central role of NRF2 for the antioxidative defense in the presence of benzbromarone, we hypothesized that increased expression of NRF2 could be protective and decreased expression of NRF2 could be associated with increased toxicity of benzbromarone. Accordingly, we directly downregulated NRF2 and indirectly upregulated NRF2 by downregulation of KEAP1 in HepG2 cells, and exposed the cells to benzbromarone for 24 h. We found that membrane toxicity was significantly decreased in HepG2 cells with NRF2 accumulation exposed to 100 μM benzbromarone compared to control cells. In addition, cellular ATP depletion was significantly less marked in HepG2 cells with NRF2 accumulation compared to control cells, supporting the protective effect of NRF2. Benzbromarone associated severe liver injury is an idiosyncratic reaction, it is observed in patients treated with

therapeutic doses and is rare, indicating that affected patients have to have risk factors rendering them more susceptible to benzbromarone associated hepatotoxicity. Our study suggests that impaired function of NRF2 may be one these susceptibility factors.

Maximal plasma concentrations reported in humans after a single, therapeutic dose (100 mg) of benzbromarone are in a range of 5 to 10 μM [43–45]. The concentrations in the liver are not known, but may be higher after oral ingestion. It is important to note that patients with a 5 to 10-fold reduced clearance have been described, who may reach considerably higher steady state concentrations [44–46]. Several primary metabolites have been described; one of them is 6-hydroxybenzbromarone (hydroxylation of position 6 of the benzofurane ring), formed by CYP2C9. CYP2C9 is a polymorphic enzyme and subjects with the *3/*3 genotype have a reduced function of CYP2C9. Indeed, Uchida et al. [44] described a patient with this genotype with a very low benzbromarone clearance. The CYP2C9 *3/3* genotype may therefore be a risk factor for benzbromarone hepatotoxicity, which is in agreement with the clinical observation that hepatotoxicity with benzbromarone is rare.

In conclusion, the mitochondrial toxicant benzbromarone causes a rapid increase in cytoplasmic and mitochondrial antioxidative defense mechanisms, which prevent ROS accumulation at low benzbromarone concentrations. Increased expression of NRF2 mitigates hepatocellular toxicity of benzbromarone, illustrating the important role of NRF2 as a regulator of antioxidative defense.

Financial support

The study was supported by a grant from the Swiss National Science Foundation to S. K. (SNF 31003A_156270).

Author contribution

N.R. conducted the experiments, interpreted data, prepared figures and helped in writing the manuscript.

J.B. and U.D. designed the study, supervised the lab work and helped in writing the manuscript.

J.B. and S.K. helped in designing the study, discussed and helped in the interpretation of the data and prepared the final version of the manuscript.

Declaration of competing interest

None of the authors reports a conflict of interest regarding this study.

Appendix A. Supplementary data

Supplementary data to this article can be found online at https://doi.org/10.1016/j.freeradbiomed.2020.03.009.

References

[1] R.C. Heel, R.N. Brogden, T.M. Speight, G.S. Avery, Benzbromarone: a review of its pharmacological properties and therapeutic use in gout and hyperuricaemia, Drugs 14 (5) (1977) 349–366.
[2] P. Kaufmann, M. Torok, A. Hanni, P. Roberts, R. Gasser, S. Krahenbuhl, Mechanisms of benzarone and benzbromarone-induced hepatic toxicity, Hepatology 41 (4) (2005) 925–935.
[3] M.M. van der Klauw, P.M. Houtman, B.H. Stricker, P. Spoelstra, Hepatic injury caused by benzbromarone, J. Hepatol. 20 (3) (1994) 376–379.
[4] M.H. Lee, G.G. Graham, K.M. Williams, R.O. Day, A benefit-risk assessment of benzbromarone in the treatment of gout. Was its withdrawal from the market in the best interest of patients? Drug Saf. 31 (8) (2008) 643–665.
[5] A. Felser, P.W. Lindinger, D. Schnell, D.V. Kratschmar, A. Odermatt, S. Mies, P. Jeno, S. Krahenbuhl, Hepatocellular toxicity of benzbromarone: effects on mitochondrial function and structure, Toxicology 324 (2014) 136–146.
[6] S. Dey, M. Guha, A. Alam, M. Goyal, S. Bindu, C. Pal, P. Maity, K. Mitra, U. Bandyopadhyay, Malarial infection develops mitochondrial pathology and mitochondrial oxidative stress to promote hepatocyte apoptosis, Free Radic. Biol. Med. 46 (2) (2009) 271–281.
[7] M. Ott, V. Gogvadze, S. Orrenius, B. Zhivotovsky, Mitochondria, oxidative stress and cell death, Apoptosis 12 (5) (2007) 913–922.
[8] Q. Ma, Role of nrf2 in oxidative stress and toxicity, Annu. Rev. Pharmacol. Toxicol. 53 (2013) 401–426.
[9] A. Kobayashi, M.I. Kang, H. Okawa, M. Ohtsuji, Y. Zenke, T. Chiba, K. Igarashi, M. Yamamoto, Oxidative stress sensor Keap1 functions as an adaptor for Cul3-based E3 ligase to regulate proteasomal degradation of Nrf2, Mol. Cell Biol. 24 (16) (2004) 7130–7139.
[10] M. Yamamoto, T.W. Kensler, H. Motohashi, The KEAP1-NRF2 system: a thiol-based sensor-effector apparatus for maintaining redox homeostasis, Physiol. Rev. 98 (3) (2018) 1169–1203.
[11] A.T. Dinkova-Kostova, W.D. Holtzclaw, R.N. Cole, K. Itoh, N. Wakabayashi, Y. Katoh, M. Yamamoto, P. Talalay, Direct evidence that sulfhydryl groups of Keap1 are the sensors regulating induction of phase 2 enzymes that protect against carcinogens and oxidants, Proc. Natl. Acad. Sci. U. S. A. 99 (18) (2002) 11908–11913.
[12] S.A. Reisman, R.L. Yeager, M. Yamamoto, C.D. Klaassen, Increased Nrf2 activation in livers from Keap1-knockdown mice increases expression of cytoprotective genes that detoxify electrophiles more than those that detoxify reactive oxygen species, Toxicol. Sci. 108 (1) (2009) 35–47.
[13] K. Itoh, T. Chiba, S. Takahashi, T. Ishii, K. Igarashi, Y. Katoh, T. Oyake, N. Hayashi, K. Satoh, I. Hatayama, M. Yamamoto, Y. Nabeshima, An Nrf2/small Maf heterodimer mediates the induction of phase II detoxifying enzyme genes through antioxidant response elements, Biochem. Biophys. Res. Commun. 236 (2) (1997) 313–322.
[14] Y. Sheng, I.A. Abreu, D.E. Cabelli, M.J. Maroney, A.F. Miller, M. Teixeira, J.S. Valentine, Superoxide dismutases and superoxide reductases, Chem. Rev. 114 (7) (2014) 3854–3918.
[15] R. Brigelius-Flohe, M. Maiorino, Glutathione peroxidases, Biochim. Biophys. Acta 1830 (5) (2013) 3289–3303.
[16] N. Kaplowitz, T.Y. Aw, M. Ookhtens, The regulation of hepatic glutathione, Annu. Rev. Pharmacol. Toxicol. 25 (1985) 715–744.
[17] L. Cao, D. Waldon, Y. Teffera, J. Roberts, M. Wells, M. Langley, Z. Zhao, Ratios of biliary glutathione disulfide (GSSG) to glutathione (GSH): a potential index to screen drug-induced hepatic oxidative stress in rats and mice, Anal. Bioanal. Chem. 405 (8) (2013) 2635–2642.
[18] D. Han, N. Hanawa, B. Saberi, N. Kaplowitz, Mechanisms of liver injury. III. Role of glutathione redox status in liver injury, Am. J. Physiol. Gastrointest. Liver Physiol. 291 (1) (2006) G1–G7.
[19] O.W. Griffith, A. Meister, Origin and turnover of mitochondrial glutathione, Proc. Natl. Acad. Sci. U. S. A. 82 (14) (1985) 4668–4672.
[20] L. Slade, J. Chalker, N. Kuksal, A. Young, D. Gardiner, R.J. Mailloux, Examination of the superoxide/hydrogen peroxide forming and quenching potential of mouse liver mitochondria, Biochim. Biophys. Acta Gen. Subj. 1861 (8) (2017) 1960–1969.
[21] L. Deferme, J.J. Briede, S.M. Claessen, D.G. Jennen, R. Cavill, J.C. Kleinjans, Time series analysis of oxidative stress response patterns in HepG2: a toxicogenomics approach, Toxicology 306 (2013) 24–34.
[22] A. Felser, K. Blum, P.W. Lindinger, J. Bouitbir, S. Krahenbuhl, Mechanisms of hepatocellular toxicity associated with dronedarone–a comparison to amiodarone, Toxicol. Sci. 131 (2) (2013) 480–490.
[23] H.T. Hornig-Do, G. Gunther, M. Bust, P. Lehnartz, A. Bosio, R.J. Wiesner, Isolation of functional pure mitochondria by superparamagnetic microbeads, Anal. Biochem. 389 (1) (2009) 1–5.
[24] L. Kappler, J. Li, H.U. Haring, C. Weigert, R. Lehmann, G. Xu, M. Hoene, Purity matters: a workflow for the valid high-resolution lipid profiling of mitochondria from cell culture samples, Sci. Rep. 6 (2016) 21107.
[25] D. Giustarini, I. Dalle-Donne, A. Milzani, P. Fanti, R. Rossi, Analysis of GSH and GSSG after derivatization with N-ethylmaleimide, Nat. Protoc. 8 (9) (2013) 1660–1669.
[26] Y.M. Go, D.P. Jones, Thioredoxin redox western analysis, Chapter 17, Curr. Protoc. Toxicol. (2009) Unit17 12.
[27] A. Holmgren, Thioredoxin, Annu. Rev. Biochem. 54 (1985) 237–271.
[28] R.S. Balaban, S. Nemoto, T. Finkel, Mitochondria, oxidants, and aging, Cell 120 (4) (2005) 483–495.
[29] M.D. Brand, The sites and topology of mitochondrial superoxide production, Exp. Gerontol. 45 (7–8) (2010) 466–472.
[30] M.D. Brand, Mitochondrial generation of superoxide and hydrogen peroxide as the source of mitochondrial redox signaling, Free Radic. Biol. Med. 100 (2016) 14–31.
[31] N. Robledinos-Anton, R. Fernandez-Gines, G. Manda, A. Cuadrado, Activators and inhibitors of NRF2: a review of their potential for clinical development, Oxid. Med. Cell Longev. (2019) 9372182 2019.
[32] M.G. McDonald, A.E. Rettie, Sequential metabolism and bioactivation of the hepatotoxin benzbromarone: formation of glutathione adducts from a catechol intermediate, Chem. Res. Toxicol. 20 (12) (2007) 1833–1842.
[33] T. Ohe, R. Umezawa, Y. Kitagawara, D. Yasuda, K. Takahashi, S. Nakamura, A. Abe, S. Sekine, K. Ito, K. Okunushi, H. Morio, T. Furihata, N. Anzai, T. Mashino, Synthesis of novel benzbromarone derivatives designed to avoid metabolic activation, Bioorg. Med. Chem. Lett 28 (23–24) (2018) 3708–3711.
[34] J. Yao, S. Peng, J. Xu, J. Fang, Reversing ROS-mediated neurotoxicity by chlorogenic acid involves its direct antioxidant activity and activation of Nrf2-ARE signaling pathway, Biofactors 45 (4) (2019) 616–626.
[35] Y. Hou, S. Peng, X. Li, J. Yao, J. Xu, J. Fang, Honokiol alleviates oxidative stress-induced neurotoxicity via activation of Nrf2, ACS Chem. Neurosci. 9 (12) (2018) 3108–3116.
[36] H. Erlank, A. Elmann, R. Kohen, J. Kanner, Polyphenols activate Nrf2 in astrocytes

via H2O2, semiquinones, and quinones, Free Radic. Biol. Med. 51 (12) (2011) 2319–2327.
[37] H. Wang, Y. Feng, Q. Wang, X. Guo, W. Huang, Y. Peng, J. Zheng, Cysteine-based protein adduction by epoxide-derived metabolite(s) of benzbromarone, Chem. Res. Toxicol. 29 (12) (2016) 2145–2152.
[38] G. Calabrese, B. Morgan, J. Riemer, Mitochondrial glutathione: regulation and functions, Antioxidants Redox Signal. 27 (15) (2017) 1162–1177.
[39] J.B. Owen, D.A. Butterfield, Measurement of oxidized/reduced glutathione ratio, Methods Mol. Biol. 648 (2010) 269–277.
[40] M. Carraro, P. Bernardi, Calcium and reactive oxygen species in regulation of the mitochondrial permeability transition and of programmed cell death in yeast, Cell Calcium 60 (2) (2016) 102–107.
[41] V. Ribas, C. Garcia-Ruiz, J.C. Fernandez-Checa, Glutathione and mitochondria, Front. Pharmacol. 5 (2014) 151.
[42] B. Antonsson, Mitochondria and the Bcl-2 family proteins in apoptosis signaling pathways, Mol. Cell. Biochem. 256–257 (1–2) (2004) 141–155.
[43] H. Ferber, H. Vergin, G. Hitzenberger, Pharmacokinetics and biotransformation of benzbromarone in man, Eur. J. Clin. Pharmacol. 19 (6) (1981) 431–435.
[44] S. Uchida, K. Shimada, S. Misaka, H. Imai, Y. Katoh, N. Inui, K. Takeuchi, T. Ishizaki, S. Yamada, K. Ohashi, N. Namiki, H. Watanabe, Benzbromarone pharmacokinetics and pharmacodynamics in different cytochrome P450 2C9 genotypes, Drug Metabol. Pharmacokinet. 25 (6) (2010) 605–610.
[45] I. Walter-Sack, J.X. de Vries, A. Ittensohn, E. Weber, Rapid and slow benzbromarone elimination phenotypes in man: benzbromarone and metabolite profiles, Eur. J. Clin. Pharmacol. 39 (6) (1990) 577–581.
[46] I. Walter-Sack, U. Gresser, M. Adjan, I. Kamilli, A. Ittensohn, J.X. de Vries, E. Weber, N. Zollner, Variation of benzbromarone elimination in man–a population study, Eur. J. Clin. Pharmacol. 39 (2) (1990) 173–176.

2 Paper II

Lapatinib activates the Kelch-like ECH-associated protein 1-nuclear factor erythroid 2-related factor 2 pathway in HepG2 cells

Noëmi Johanna Roos[1,2,3], Diell Aliu[1,2], Jamal Bouitbir[1,2,3], and Stephan Krähenbühl[1,2,3]

[1]Division of Clinical Pharmacology & Toxicology, University Hospital, Basel, Switzerland

[2]Department of Biomedicine, University of Basel, Switzerland

[3]Swiss Centre for Applied Human Toxicology (SCAHT), Basel, Switzerland

Published in Front Pharmacol. 2020 Jun 30;11:944.

frontiers in Pharmacology

ORIGINAL RESEARCH
published: 30 June 2020
doi: 10.3389/fphar.2020.00944

Lapatinib Activates the Kelch-Like ECH-Associated Protein 1-Nuclear Factor Erythroid 2-Related Factor 2 Pathway in HepG2 Cells

Noëmi Johanna Roos[1,2,3], *Diell Aliu*[1,2], *Jamal Bouitbir*[1,2,3] *and Stephan Krähenbühl*[1,2,3]*

[1] Division of Clinical Pharmacology & Toxicology, University Hospital, Basel, Switzerland, [2] Department of Biomedicine, University of Basel, Basel, Switzerland, [3] Swiss Centre for Applied Human Toxicology (SCAHT), Basel, Switzerland

The receptor tyrosine kinase inhibitor lapatinib, indicated to treat patients with HER2-positive breast cancer in combination with capecitabine, can cause severe hepatotoxicity. Lapatinib is further associated with mitochondrial toxicity and accumulation of reactive oxygen species. The effect of lapatinib on the Kelch-like ECH-associated protein 1 (Keap1)-nuclear factor erythroid 2-related factor 2 (Nrf2) pathway, the major cellular defense pathway against oxidative stress, has so far not been studied in detail. In the present study, we show that lapatinib (2–20 μM) activates the Keap1-Nrf2 pathway in HepG2 cells, a hepatocellular carcinoma-derived cell line, in a concentration-dependent manner upon 24 h of treatment. Lapatinib stabilized the transcription factor Nrf2 at concentrations ≥5 μM and caused its nuclear translocation. Well-established Nrf2 regulated genes (*Nqo1*, *Gsta1*, *Gclc*, and *Gclm*) were upregulated at lapatinib concentrations ≥10 μM. Furthermore, cellular and mitochondrial glutathione (GSH) levels increased starting at 10 μM lapatinib. As a marker of oxidative stress, cellular GSSG significantly increased at 10 and 20 μM lapatinib. Furthermore, the gene expression of mitochondrial *Glrx2* and *SOD2* were increased upon lapatinib treatment, which was also observed for the mitochondrial SOD2 protein content. In conclusion, lapatinib treatment for 24 h activated the Keap1-Nrf2 pathway in HepG2 cells starting at 10 μM, which is a clinically relevant concentration. As a consequence, treatment with lapatinib increased the mRNA and protein expression of antioxidative and other cytoprotective genes and induced GSH synthesis, but these measures could not completely block the oxidative stress associated with lapatinib.

Keywords: lapatinib, HepG2 cells, mitochondria, reactive oxygen species, Nrf2, Keap1, glutathione

OPEN ACCESS

Edited by:
Stefan Schildknecht,
University of Konstanz, Germany

Reviewed by:
Chong-Kuei Lii,
China Medical University, Taiwan
HawWen Chen,
China Medical University, Taiwan
Albena Todorova Dinkova-Kostova,
University of Dundee, United Kingdom

***Correspondence:**
Stephan Krähenbühl
stephan.kraehenbuehl@usb.ch

Specialty section:
This article was submitted to Predictive Toxicology, a section of the journal Frontiers in Pharmacology

Received: *21 March 2020*
Accepted: *10 June 2020*
Published: *30 June 2020*

Citation:
Roos NJ, Aliu D, Bouitbir J and Krähenbühl S (2020) Lapatinib Activates the Kelch-Like ECH-Associated Protein 1-Nuclear Factor Erythroid 2-Related Factor 2 Pathway in HepG2 Cells. Front. Pharmacol. 11:944. doi: 10.3389/fphar.2020.00944

INTRODUCTION

Receptor tyrosine kinases (TK) are transmembrane proteins that regulate important cellular pathways such as differentiation, proliferation, and apoptosis by phosphorylation of tyrosine residues (Yarden and Sliwkowski, 2001; Krause and Van Etten, 2005). Constantly activated or overexpressed TK can cause uncontrolled cell growth and are found in many tumor cells. Inhibitors

of receptor tyrosine kinases (TKI), a class of small-molecule drugs, are efficient targeted anticancer drugs with a higher clinical benefit than non-targeted chemotherapeutic drugs (Amir et al., 2011).

Lapatinib is a TKI that is used in combination with capecitabine to treat patients with advanced or metastatic HER2-positive breast cancer (Moy et al., 2007). The TK HER2 (human epidermal growth factor receptor 2, also known as ErbB2) is overexpressed in up to 25% of invasive or metastatic breast cancers, and is associated with an unfavorable prognosis (Slamon et al., 1987). Lapatinib inhibits the intracellular TK domain of both HER1 (also known as epidermal growth factor receptor [EGFR] or ErbB1) and HER2. The most common adverse reactions of lapatinib therapy are diarrhea, nausea, rash, palmar-plantar erythrodysesthesia, and fatigue (Chu et al., 2007; Ryan et al., 2008). Furthermore, acute liver injury has been reported, a rare, but serious and potentially fatal adverse drug reaction prompting a FDA black-box warning in 2008 (Gomez et al., 2008). Lapatinib-induced liver injuries range from asymptomatic transaminase elevation, which affects approximately half of the patients treated with lapatinib in combination with capecitabine, to fatal cases of liver failure (Peroukides et al., 2011; Baselga et al., 2012; Azim et al., 2013). One possible explanation for lapatinib's hepatotoxicity is mitochondrial dysfunction, as we have shown in our previous study (Paech et al., 2017). We found that lapatinib impairs mitochondrial function in a hepatocellular carcinoma-derived cell line (HepG2), which was accompanied by accumulation of reactive oxygen species (ROS) and release of cytochrome c from mitochondria into the cytosol inducing apoptosis. Dysfunctional mitochondria can generate ROS, mainly in the form of superoxide radicals ($O_2^{\bullet-}$) (Brand, 2010; Brand, 2016). Mitochondrial (SOD2) and cytosolic (SOD1) superoxide dismutase convert mitochondrial $O_2^{\bullet-}$ to H_2O_2, which is further detoxified to H_2O and O_2 by several antioxidative enzymes including glutathione-dependent hydrogen peroxidase (Balaban et al., 2005). An effective antioxidative defense is essential, since excess ROS can modify DNA bases, induce lipid peroxidation, and oxidize cellular proteins (Ott et al., 2007).

The nuclear factor erythroid 2-related factor 2 (Nrf2), a basic-leucine zipper transcription factor, and its negative regulator Kelch-like ECH-associated protein 1 (Keap1) form an inducible pathway for the defense against oxidative stress (Itoh et al., 1999; Yamamoto et al., 2018). Stimulated by ROS and electrophiles, Nrf2 induces the transcription of genes important for antioxidative defense and for phase II (conjugation) reactions (Reisman et al., 2009). Under unstressed conditions, Nrf2 is captured in the cytosol by Keap1, a cysteine-rich protein. Keap1 associates with Cullin 3 and RING-box protein to form a ubiquitin E3 ligase complex, which continuously ubiquitinates newly synthesized Nrf2 (Kobayashi et al., 2004). Ubiquitinated Nrf2 is efficiently degraded by the 26S proteasome, leading to low cellular Nrf2 levels under unstressed conditions. Specific cysteine residues of Keap1 can be oxidized and alkylated by H_2O_2 and electrophiles, respectively, leading to Keap1 inactivation (Suzuki et al., 2019). As a result, Keap1-dependent ubiquitination of Nrf2 decreases, Nrf2 is stabilized and translocates into the nucleus. Once in the nucleus, Nrf2 binds to antioxidant response elements located in the upstream promoter region of target genes and induces their transcription. Nrf2 regulates the transcription of genes involved in detoxification reactions (NADPH quinone oxidoreductase 1 [*Nqo1*], glutathione S-transferases [*Gst*]), glutathione (GSH) biosynthesis (glutamate-cysteine ligase [*Gclc*, *Gclm*]), and ROS elimination such as *SOD1* and *SOD2* (Reisman et al., 2009).

In the present study, we investigated the effect of lapatinib on the Keap1-Nrf2 pathway and its downstream effects. Specifically, we evaluated whether lapatinib stabilizes Nrf2 in a ROS-dependent fashion, studied the nuclear translocation of Nrf2 and determined the mRNA and protein expression of Nrf2-regulated genes.

MATERIAL AND METHODS

Reagents

The cell culture medium and supplements were purchased from Thermo Fisher Scientific (Basel, Switzerland). Lapatinib (SRP01210) was obtained from Sequoia research products (Pangbourne, United Kingdom). The other chemicals were purchased from Sigma-Aldrich (Buchs, Switzerland), if not indicated otherwise. For the LC-MS/MS measurements, we used HPLC grade solvents from Merck (Darmstadt, Germany), while the internal standards and the reference substances were obtained from Toronto Research Chemicals (Ontario, Canada). For western blotting, we used antibodies from Abcam (Cambridge, United Kingdom) and Santa Cruz Biotechnology (Heidelberg, Germany). The qPCR primers were produced by Microsynth (Balgach, Switzerland).

Cell Culture

We cultured the human hepatocellular carcinoma cell line HepG2 in Dulbecco's modified eagle medium (1.0 g/L D-glucose, 4 mM L-glutamine, 1 mM sodium pyruvate) supplemented with 10% (v/v) inactivated fetal bovine serum, 10 mM HEPES buffer (pH 7.4), 2 mM GlutaMAX, 1% (v/v) MEM non-essential amino acids solution (100x), and 100 U/ml penicillin/streptomycin. The cells were kept at 37°C in a humidified 5% CO_2 cell culture incubator and passaged using TrypLE express enzyme (Thermo Fisher Scientific, Basel, Switzerland). We used the trypan blue exclusion method and the EVE automatic cell counter (NanoEnTek, Seoul, Korea) to determine the number of cells and their viability.

Treatment of HepG2 Cells With Lapatinib

We treated HepG2 cells with 2, 5, 10, and 20 μM lapatinib for 2, 6, or 24 h. The stock solutions (1,000X) were prepared in dimethyl sulfoxide (DMSO) and stored at −20°C. Accordingly, we used 0.1% (v/v) DMSO as a negative control treatment.

Membrane Toxicity

We used the ToxiLight bioassay kit from Lonza (Basel, Switzerland) to assess the cell membrane integrity of lapatinib-treated HepG2 cells. The assay measures the release of the

intracellular enzyme adenylate kinase (AK) into the surrounding cell culture medium upon loss of cell membrane integrity. Released AK converts ADP, present in the detection reagent, to ATP, which creates a luminescent signal in the presence of luciferase. Briefly, we seeded HepG2 cells in a 96-well plate (10,000 cells/well). After lapatinib-treatment, we transferred 20 µl of cell culture medium from the treated HepG2 cells to an opaque-walled 96-well plate. After adding the AK detection reagent (50 µl/well), we incubated the plate for 5 min at room temperature, and recorded the luminescence using a microplate reader (Infinite 200 PRO, Tecan Group, Männedorf, Switzerland). As a positive control, we treated the cells with 0.1% (v/v) Triton X to induce cell lysis. Data were normalized to the ctrl. The AK release increased ~11.0-fold upon Triton X treatment compared to the negative control.

Cellular ATP Content

We used the CellTiter-Glo luminescent cell viability assay (Promega, Dübendorf, Switzerland) to measure the cellular ATP content in lapatinib-treated HepG2 cells. After induction of cell lysis, the luciferase present in the CellTiter-Glo reagent generates a luminescent signal proportional to the ATP content. After lapatinib-treatment, we added an equal volume of CellTiter-Glo reagent directly to the lapatinib-treated HepG2 cells seeded in a white-walled 96-well plate (10,000 cells/well). The plate was placed on an orbital shaker for 2 min (600 rpm), incubated for further 8 min at room temperature, and the luminescence was recorded using the microplate reader. Data were normalized to control incubations containing 0.1% (v/v) DMSO. We used 0.1% (v/v) Triton X as a positive control, which caused a complete loss of viable cells (~100% ATP depletion).

Mitochondrial Membrane Potential

We used the JC-1 mitochondrial membrane potential assay kit (ab113850, Abcam, Cambridge, United Kingdom) to determine the mitochondrial membrane potential ($\Delta\psi_M$) in lapatinib-treated HepG2 cells. Attracted by a high $\Delta\psi_M$, the cationic dye JC-1 (tetraethylbenzimidazolylcarbocyanine iodide) accumulates within polarized mitochondria, where it forms red fluorescent aggregates at high concentrations. Upon $\Delta\psi_M$ dissipation, JC-1 stops accumulating within mitochondria, and the JC-1 molecules, present as monomers at low concentration, emit green fluorescence. We performed the assay according to the manufacturer's protocol. Briefly, HepG2 cells were seeded in a black-walled 96-well plate (15,000 cells/well) and covered with 100 µl of treatment solution. Thirty minutes before completed lapatinib-treatment, we added 2X JC-1 solution (40 µM) to each well (100 µl/well) and incubated for 30 min at 37°C protected from light. The cells were washed twice with pre-warmed 1X dilution buffer (100 µl/well). The last wash was left on the cells, and the fluorescence of both aggregates ($\lambda_{excitation}$ = 475 nm, $\lambda_{emission}$ = 590 nm) and monomers ($\lambda_{excitation}$ = 475 nm, $\lambda_{emission}$ = 530 nm) was measured using the microplate reader. We formed the ratio between the aggregate and monomer fluorescence (JC-1 ratio), which decreases upon $\Delta\psi_M$ depolarization, and calculated the fold-change relative to the negative control. Both JC-1 staining and final measurement were performed in the presence of lapatinib. Therefore, we spiked both staining solution and dilution buffer with the corresponding concentration of lapatinib. As a positive control, we treated the cells for 2 h with the ionophore uncoupler FCCP (carbonyl cyanide 4-(trifluoromethoxy) phenylhydrazone, 50 µM), which decreased the JC-1 ratio to ~38% of the control (DMSO 0.1%) levels.

Mitochondrial $O_2^{\bullet-}$ Accumulation

We used MitoSOX red (Thermo Fisher Scientific, Basel, Switzerland) to determine the accumulation of mitochondrial $O_2^{\bullet-}$ in lapatinib-treated HepG2 cells. MitoSOX red accumulates in mitochondria and is selectively oxidized by mitochondrial $O_2^{\bullet-}$ to a highly fluorescent oxidation product. We incubated lapatinib-treated HepG2 cells seeded in a black-walled 96-well plate (25,000 cells/well) with MitoSOX red (2.5 µM in PBS) for 10 min at 37°C under light protection. We recorded the fluorescence ($\lambda_{excitation}$ = 510 nm, $\lambda_{emission}$ = 580 nm) using the microplate reader, and subsequently lysed the cells with radioimmunoprecipitation assay (RIPA) buffer. The protein concentration was determined using a bicinchoninic acid assay with serum albumin as protein standard (Pierce BCA Protein Assay Kit, Thermo Fisher Scientific, Waltham, USA). Finally, we normalized the measured fluorescence to the protein concentration. As a positive control, we exposed HepG2 cells to amiodarone (25 µM for 24 h and 50 µM for 2 h or 6 h of exposure), a $O_2^{\bullet-}$-generating mitochondrial toxicant (Felser et al., 2013). Amiodarone caused a ~1.5–2.4-fold increase of mitochondrial $O_2^{\bullet-}$ accumulation.

Cellular H_2O_2 Accumulation

We used the ROS-Glo H_2O_2 assay from Promega (Dübendorf, Switzerland) to measure the accumulation of H_2O_2 in lapatinib-treated HepG2 cells. The cellular H_2O_2 reacts directly with the H_2O_2 substrate, a luciferin derivative present in the H_2O_2 substrate solution, generating a luciferin precursor. The precursor is converted to luciferin upon addition of the ROS-Glo detection solution. Subsequently, the luciferase present in the luciferin detection solution generates a luminescent signal proportional to cellular H_2O_2 levels. HepG2 cells were seeded in a transparent 96-well plate (10,000 cells/well) and covered with treatment solution (80 µl/well). Six hours before the lapatinib-treatment was completed, we added H_2O_2 substrate solution to each well (20 µl/well), and incubated the plate for 6 h at 37°C. When the treatment with lapatinib was shorter than 6 h, the H_2O_2 substrate solution was added together with the treatment. After the incubation, we transferred 50 µl of supernatant from each well to a new white-walled plate and added ROS-Glo detection solution (50 µl/well). After incubation for 20 min at room temperature, we recorded the luminescence using the microplate reader. After the measurement, we lysed the cells with RIPA buffer and determined the protein concentration. Finally, the luminescent signal was normalized to the protein concentration. As a positive control, we treated the cells with menadione (50 µM), a H_2O_2-generating redox cycler (Deferme et al., 2013). The cellular H_2O_2 increased ~13.0–30.0-fold upon menadione treatment.

Western Blotting

We assessed the expression of cellular proteins in lapatinib-treated HepG2 cells by western blotting. Briefly, we prepared protein lysates from lapatinib-treated HepG2 cells seeded in a six-well plate (2 x 10^6 cells/well). RIPA buffer was used as lysis buffer. We determined the protein concentration of each sample, and prepared denatured and reduced protein samples by adding sodium dodecyl sulfate (SDS) and by boiling the samples at 95°C for 5 min. To separate the proteins according to their molecular weight, we loaded the protein samples (20 µg protein) on a NuPage 4–12% Bis-Tris Gel (Thermo Fisher Scientific, Basel, Switzerland), and ran a one-dimensional gel electrophoresis. NuPAGE LDS sample buffer was used as a loading buffer and PageRuler prestained protein ladder as a molecular weight marker, both purchased from Thermo Fisher Scientific (Basel, Switzerland). We used an eBlot L1 wet protein transfer system (Genescript, Piscataway, USA) and the eBlot L1 transfer sandwich (Genescript, Piscataway, USA) to transfer the separated proteins on a 0.2 µm nitrocellulose membrane (Bio-Rad, Cressier, Switzerland). To prevent non-specific background binding of the antibodies, we blocked the membrane for 1 h with 5% (w/v) non-fat milk in PBS containing 0.1% (v/v) Tween 20 (PBST) under constant shaking. The membrane was incubated overnight with primary antibody diluted in 5% (w/v) non-fat milk in PBST at 4°C. The following primary antibodies and dilutions were used: Nrf2 (1:10,000, ab62352), Keap1 (1:2,000, ab119403), SOD1 (1:5,000, ab51254), and SOD2 (1:5,000, ab74231). Antibodies against glyceraldehyde-3-phosphate dehydrogenase (GAPDH; 1:1,000, sc-365062) and Lamin B1 (1:1,000, ab229025) were used as loading controls.

After washing and incubating for 1 h with the corresponding horseradish peroxidase-conjugated secondary antibody (m-IgGK BP-HRP, 1:2,000, sc-516102; mouse anti-rabbit IgG-HRP, 1:2,000, sc-2357), we detected the protein bands using an ECL detection kit (Clarity Western ECL Substrate; Bio-Rad Laboratories, Cressier, Switzerland) and Fusion pulse 6 (Witec AG, Switzerland) as imaging system. The protein bands were visualized and quantified using the Evolution Capture software (Witec AG, Switzerland).

Cytoplasmic and Nuclear Protein Extraction

We used the nuclear and cytoplasmic extraction kit (NE-PER Nuclear and Cytoplasmic Extraction Reagents, Thermo Fisher Scientific, Basel, Switzerland) to obtain nuclear and cytoplasmic protein fractions from lapatinib-treated HepG2 cells seeded in a six-well plate (500,000 cells/well). The cells were harvested, washed, and incubated in ice-cold cytoplasmic extraction reagent I. The buffer volumes were chosen according to the pellet size according to the manufacturer's protocol. After incubating 10 min on ice, we added ice-cold cytoplasmic extraction reagent II to each sample, vortexed for 5 s, and incubated for 1 min on ice. We subsequently centrifuged the sample at 16,000 g for 5 min and obtained the cytoplasmic protein fraction (supernatant). The remaining pellet was further incubated in ice-cold nuclear extraction reagent on ice for 40 min with vortexing every 10 min. After centrifugation at 16,000 g for 10 min, we obtained the nuclear protein fraction (supernatant). The fractions were stored at −80°C until western blot analysis.

Real-Time PCR

We extracted and purified RNA from lapatinib-treated HepG2 cells seeded in a six-well plate (2 x 10^6 cells/well) using QIAshredders and the RNeasy mini kit (Qiagen, Hombrechtikon, Switzerland). Both extraction and purification were performed according to the manufacturer's instruction. We determined the purity and RNA concentration of each extract using the NanoDrop One (Thermo Fisher Scientific, Basel, Switzerland). Then, we synthetized complementary DNA from 1 µg RNA using the Omniscript system (Qiagen, Hombrechtikon, Switzerland). SYBR green (Roche Diagnostics, Rotkreuz, Switzerland) and specific forward and reverse primers (**Table 1**; Microsynth, Balgach, Switzerland) were used to amplify the DNA templates.

The real-time PCR was performed with three independent replicates on an ABI PRISM 7700 sequence detector (PE Biosystems, Switzerland) using the ViiA7 software (Life Technologies, Switzerland). We applied the comparative C_t method ($\Delta\Delta C_t$) to determine relative gene expression levels after normalizing to the housekeeping gene (*GAPDH*).

Mitochondrial Isolation From HepG2 Cells by Magnetic Separation

Mitochondria were isolated from HepG2 cells using the human mitochondria isolation kit from Miltenyi Biotec (Solothurn, Switzerland). The isolation, which is based on magnetic separation using microbeads, was performed according to the manufacturer's protocol (Hornig-Do et al., 2009). In brief, we harvested, washed, and lysed 40 x 10^6 HepG2 cells, and homogenized them with a Dounce homogenizer applying 90 strokes. The mitochondria were magnetically labeled by incubating the cell homogenate for 1 h with superparamagnetic microbeads conjugated to anti-TOM22 (translocase of outer mitochondrial membrane) antibodies. After the incubation, we applied the cell homogenate stepwise on pre-rinsed LS columns (Miltenyi Biotec, Solothurn, Switzerland) placed in the magnetic field of a MACS separator (Miltenyi Biotec, Solothurn, Switzerland). Pre-separation filters (30 µm) were used to remove cell aggregates. The magnetic field retains the labeled mitochondria in the columns, while the rest of the cell homogenate runs through. After three washing steps, we removed the columns from the separator and placed them in new microcentrifuges tubes. We flushed out the mitochondria by gently pushing a plunger into the column loaded with separation buffer. The mitochondrial pellet was obtained after centrifugation at 13,000 g for 2 min at 4°C using a microcentrifuge (Eppendorf Centrifuge 5415 R, Eppendorf, Schönenbuch, Switzerland).

Cellular and Mitochondrial GSH and GSSG Content

We analyzed GSH and GSSG by liquid chromatography tandem mass spectrometry (LC-MS/MS) in lapatinib-treated HepG2 cells. GSH was also measured in mitochondria isolated from

TABLE 1 | Specific forward and reverse primers used for real-time PCR.

Gene	Direction	Sequence (5′-3′)
Nqo1	Forward	5′-ATGGAAGAAACGCCTGGAGA-3′
	Reverse	5′-TGGTTGTCAGTTGGGATGGA-3′
Gsta1	Forward	5′-GAAGCCTCCCATGGATGAGA-3′
	Reverse	5′-AGCTTCACAACAGGCACAAT-3′
Gclc	Forward	5′-CATTGATTGTCGCTGGGGAG-3′
	Reverse	5′-CTGGGCCAGGAGATGATCAA-3′′
Gclm	Forward	5′-TGTATCAGTGGGCACAGGTA-3′
	Reverse	5′-GTGCGCTTGAATGTCAGGAA-3′
Glrx1	Forward	5′-CAGCCACCAACCACACTAAC-3′
	Reverse	5′-TGGTTACTGCAGAGCTCCAA-3′
Glrx2	Forward	5′-TCTGGGATGGAGAGCAATACA-3′
	Reverse	5′-TTCAAGCAGGTCCAGTTCCA-3′
SOD1	Forward	5′-TGTTGGAGACTTGGGCAATG-3′
	Reverse	5′-CAATGATGCAATGGTCTCCTGA-3′
SOD2	Forward	5′-TTTAGTCCCTGGTGTTCCCC-3′
	Reverse	5′-CTTCACCGAAAACTCCAGGC-3′
Nrf2	Forward	5′-TGAGCCCAGTATCAGCAACA-3′
	Reverse	5′-AGTGAAATGCCGGAGTCAGA-3′
GAPDH	Forward	5′-AGGTCGGAGTCAACGGATTT-3′
	Reverse	5′-TGACAAGCTTCCCGTTCTCA-3′

lapatinib-exposed HepG2 cells, while mitochondrial GSSG could not be analyzed due to stability problems during the measurement. As positive control, we treated HepG2 cells with 100 µM L-buthionine sulfoximine (BSO), which inhibits the GSH biosynthesis (Griffith and Meister, 1985). Upon 24 h-treatment, BSO reduced the cellular and mitochondrial GSH to ~9.0% and ~43.0% of the control levels, respectively. GSH ammonium salt-d_5 (~10 mM, in H_2O) and GSSG-$^{13}C_4$,$^{15}N_2$ (1 mM, in H_2O) were used as internal standards. To prevent auto-oxidation of GSH and GSH ammonium salt-d_5 during the sample preparation, we alkylated the thiol group with N-ethylmaleimide (NEM) forming GS-NEM and GS-NEM-d_5 (Giustarini et al., 2013).

Briefly, 1 x 10^6 lapatinib-treated HepG2 cells seeded in a six-well plate (1 x 10^6/well) were harvested, washed, and immediately incubated in 250 µl alkylating solution (50 mM NEM in PBS) for 30 min on ice. During the washing step, we took an aliquot to determine the protein concentration of our samples. The same was done with the isolated mitochondrial pellet. Approximately 0.4 mg mitochondria were afterwards incubated in 100 µl alkylating solution. Both mitochondrial and cellular samples were extracted in a ratio of 1:4 (v/v) with internal standard solution, which consisted of 500 nM GSSG-$^{13}C_4$,$^{15}N_2$ and 500 nM GS-NEM-d_5 in methanol. We kept the extracts at −20°C for 30 min to ensure protein precipitation. After centrifugation at 3,500 g for 10 min at 4°C, we transferred 250 µl of supernatant into a LC-MS/MS tube. Calibration lines of GS-NEM (250–0.25 µM) and GSSG (25–0.025 µM) were prepared in alkylating solution and extracted as described above.

An aliquot of 10 µl was injected into the LC-MS/MS system consisting of a Shimadzu HPLC (Kyoto, Japan) coupled to an API 4000 QTrap tandem mass spectrometer (ABSciex, Concord, Canada). The system was operated with the Analyst 1.6.2 software (AB Sciex, Concord, Canada). GS-NEM and GSSG were separated on a Symmetry C18 column (3.5 µm 100 Å, 4.6 mm x 75 mm; Waters, Eschborn, Germany) at a flow rate of 0.7 ml/min and a temperature of 45°C. We used H_2O (phase A) and acetonitrile (phase B) both supplemented with 0.1% (v/v) propionic acid as mobile phases. We loaded the samples onto the analytical column using 7% mobile phase B and diluted it inline *via* a t-union with mobile phase A during the first 0.5 min of each run. Within the next 1.5 min, we linearly increased the gradient to 95% mobile phase B. We flushed the column with 95% mobile phase B for 1.5 min, and finally reconditioned the system with 7% mobile phase B for 1 min. The retention times of GSSG and GS-NEM were 2.00 min and 2.21 min, respectively. The analytes were positively charged by electro spray ionization and analyzed using scheduled multiple reaction monitoring. We applied an ion spray voltage of 5,500 V, and set the probe temperature at 700°C. The following mass transitions were used: 433.1 → 304.0 m/z for GS-NEM, 438.1 → 304.0 m/z for GS-NEM-d_5, 613.1 → 355.0, 484.0, 231.1 m/z for GSSG, and 619.1 → 361.0, 490.0, 231.0 for GSSG-$^{13}C_4{}^{15}N_2$. Finally, the amount of GS-NEM and GSSG was normalized to the protein content of each sample.

Statistical Analysis

The data are presented as the mean ± standard error of the mean (SEM) of at least three independent experiments. We performed one-way ANOVA statistical analysis with Dunnett's multiple comparison test using GraphPad prism version 8.2.1 (GraphPad Software, San Diego, USA). Significant values, indicated in the figures with an asterisk (*), were reached with a p-value <0.05 compared to control values (ctrl). We additionally performed two-way ANOVA statistical analysis followed by Sidak's multiple comparison test, whereby significant differences between groups (p-value <0.05) were indicated with hashtags (#).

RESULTS

Membrane Toxicity, ATP Content, and Mitochondrial Membrane Potential in HepG2 Cells

To confirm the findings of our previous study (Paech et al., 2017), we determined the release of AK, a marker for plasma membrane damage, into the surrounding cell culture medium from HepG2 cells treated with lapatinib for 2, 6, or 24 h (**Figure 1A**). The plasma membrane remained intact up to 6 h of lapatinib treatment. After 24 h of treatment, lapatinib started to damage the plasma membrane at 10 µM and caused a significant membrane damage at 20 µM. As a marker of cell viability, we measured the cellular ATP content in lapatinib-treated HepG2 cells (**Figure 1B**). While the cell viability was not diminished after 2 h of lapatinib treatment at any concentration, the cellular ATP level started to decrease after 6 h of treatment with 20 µM lapatinib (~17% ATP depletion). After 24 h, lapatinib significantly reduced the cell viability at 10 µM (~22% ATP depletion) and 20 µM (~76% ATP depletion).

ATP depletion could result from an impaired function of mitochondria, which could be reflected by a reduced $\Delta\psi_M$. We therefore measured the $\Delta\psi M$ (represented by the JC-1 ratio), a

marker of mitochondrial function, in HepG2 cells treated with lapatinib for 2, 6, or 24 h (**Figure 1C**). The JC-1 ratio started to decrease at 10 μM lapatinib and was significantly reduced at this concentration after 24 h of treatment. A concentration of 20 μM lapatinib caused a significant JC-1 ratio reduction already after 6 h of exposure.

Mitochondrial and Cellular ROS Accumulation

The drop in the $\Delta\psi_M$ indicated mitochondrial dysfunction, possibly due to impaired function of the mitochondrial electron transport chain (Paech et al., 2017), which can be associated with increased generation of mitochondrial superoxide ($O_2^{\bullet-}$) radicals (Brand, 2010; Brand, 2016). Mitochondrial $O_2^{\bullet-}$ can spread into the cytosol once it is converted to H_2O_2. Thus, we measured the accumulation of mitochondrial $O_2^{\bullet-}$ (**Figure 2A**) and cellular H_2O_2 (**Figure 2B**) in lapatinib-treated HepG2 cells. After 2 h of treatment, mitochondrial $O_2^{\bullet-}$ accumulated at 10 and 20 μM without reaching significance. Upon lapatinib-treatment for 6 and 24 h, the mitochondrial $O_2^{\bullet-}$ started to accumulate at 5 μM with a significant accumulation at both 10 and 20 μM. Cellular H_2O_2 started to accumulate upon 24 h-treatment at 10 μM, reaching significance at 20 μM. Overall, the effects were concentration- and time-dependent, and mitochondrial $O_2^{\bullet-}$ started to accumulate at a lower lapatinib concentration than cellular H_2O_2.

Activation of the Keap1-Nrf2 Pathway

Accumulation of ROS can activate the Keap1-Nrf2 pathway, a major cytoprotective pathway against oxidative stress (Yamamoto et al., 2018). Concretely, H_2O_2 can induce disulfide bond formation between specific cysteine residues of Keap1 leading to Nrf2 stabilization (Suzuki et al., 2019). Thus, we assessed the cellular protein levels of Nrf2 in HepG2 cells treated with lapatinib for 2, 6, or 24 h (**Figures 3A, B**). No changes in the cellular protein levels were observed after 2 and 6 h of treatment. Nrf2 protein levels started to increase in HepG2 cells upon 24 h-treatment with 5 μM lapatinib and accumulated significantly upon treatment with 10 and 20 μM lapatinib (**Figures 3A, B**). Thus, lapatinib significantly increased the cellular protein levels of Nrf2 in a concentration-dependent manner, indicating Nrf2 stabilization. As shown in **Supplementary Figure 1**, lapatinib led to a numerical increase in Nrf2 mRNA expression, suggesting that increased Nrf2 gene transcription could contribute to the observed rise in the cellular Nrf2 protein content. In parallel, the cellular protein level of Keap1 (**Figures 3A, C**), which negatively regulates Nrf2, decreased in a concentration-dependent manner starting at 20 μM (after 6 h) and 5 μM lapatinib (after 24 h). Upon 24 h-treatment with 20 μM lapatinib, the Keap1 protein level was significantly reduced in HepG2 cells (**Figures 3A, C**).

After stabilization, the transcription factor Nrf2 translocates into the nucleus, where it binds to specific DNA promotors, the antioxidative response elements (Yamamoto et al., 2018). Therefore, we assessed the nuclear translocation of Nrf2 upon lapatinib-treatment (**Figures 4A, B**). We determined the protein levels of Nrf2 in the nuclear and cytoplasmic fraction extracted from HepG2 cells treated with 10 and 20 μM lapatinib (**Figure 4A**). Nrf2 protein levels significantly increased in both fractions in a concentration-dependent manner, whereby the accumulation in the nuclear fraction was significantly more pronounced (**Figure 4B**), indicating nuclear translocation of Nrf2.

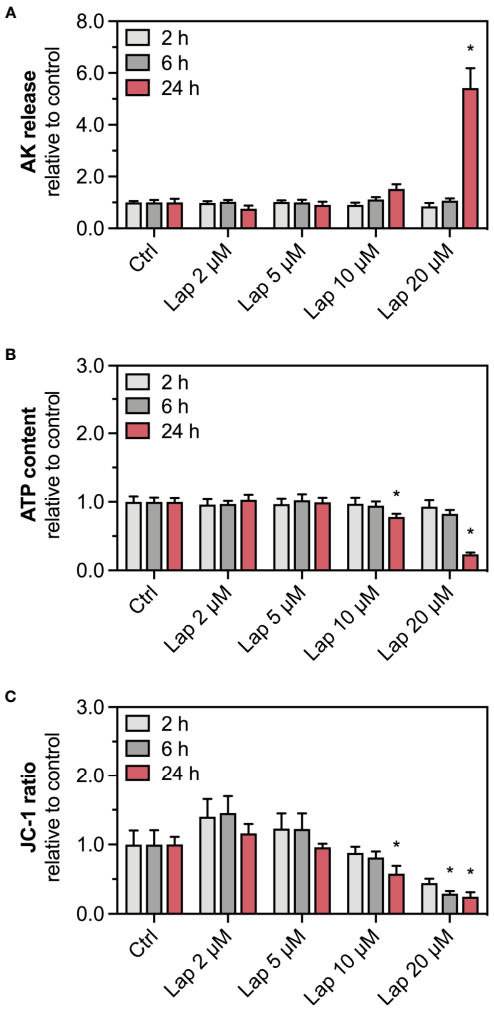

FIGURE 1 | AK release, ATP content, and mitochondrial membrane potential in HepG2 cells. **(A)** Adenylate kinase (AK) release (cell membrane integrity marker), **(B)** cellular ATP content (cell viability marker), and **(C)** mitochondrial membrane potential ($\Delta\psi_M$) represented by the JC-1 ratio in HepG2 cells after treatment with 2–20 μM lapatinib (Lap) for 2, 6, and 24 h. The JC-1 ratio represents the ratio between JC-1 aggregates fluorescence (high $\Delta\psi_M$) to the fluorescence of JC-1 monomers (low $\Delta\psi_M$). Data are shown as fold increase relative to the negative control (0.1% DMSO, ctrl), and are the mean ± SEM of three independent replicates. *$p < 0.05$ versus negative control.

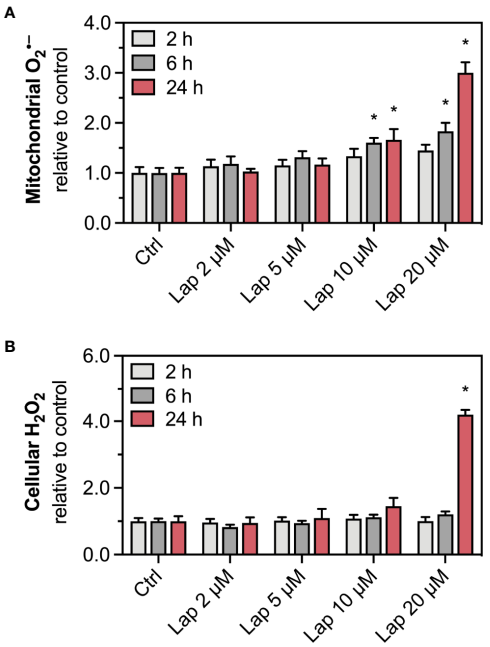

FIGURE 2 | Accumulation of mitochondrial superoxide and cellular H_2O_2 in HepG2 cells. **(A)** Mitochondrial superoxide and **(B)** cellular H_2O_2 accumulation in HepG2 cells after treatment with 2–20 µM lapatinib (Lap) for 2, 6, and 24 h. Data are shown as fold increase relative to the negative control (0.1% DMSO, Ctrl), and are the mean ± SEM of at least three independent replicates. *$p < 0.05$ versus negative control.

mRNA Expression of Nrf2-Regulated Genes

Once accumulated in the nucleus, Nrf2 induces the transcription of several genes involved in cellular antioxidative defense and cell protection mechanisms. We assessed the mRNA expression of *Nqo1* and *Gsta1*, two well-established Nrf2-regulated genes, in HepG2 cells upon lapatinib-treatment (**Figure 4C**). After 24 h of exposure, lapatinib induced the transcription of both genes in a concentration-dependent manner starting at 5 µM and reaching statistical significance at 10 and 20 µM for both genes. No such increase in mRNA expression of these genes was observed at 2 and 6 h of exposure to lapatinib (**Supplementary Figures 2A, B**).

Involvement of ROS in the Activation of the Keap1-Nrf2 Pathway

Since we observed accumulation of ROS upon lapatinib treatment, we assessed whether ROS accumulation is responsible for the activation of the Keap1-Nrf2 pathway induced by lapatinib. Thus, we used N-acetyl cysteine (NAC, 2 mM), a widely used antioxidant, to scavenge lapatinib-induced H_2O_2-accumulation after 24 h of treatment (**Figure 5A**). Co-treatment with NAC significantly reduced H_2O_2 accumulation at 10 and 20 µM lapatinib, qualifying NAC as an efficient ROS scavenger in our system. Co-treatment with NAC diminished the Nrf2 stabilization at the protein level at 10 and 20 µM after 24 h of treatment (**Figure 5B**). At 20 µM, the cellular Nrf2 content was significantly lower with a NAC co-treatment (**Figure 5C**). Nevertheless, the Nrf2 protein level increased at 10 and 20 µM lapatinib in the presence of NAC, suggesting that also activation mechanisms other than ROS accumulation are involved in the Nrf2 stabilization. The negative regulator Keap1 was less decreased in the presence of NAC at 10 µM lapatinib than in incubations without NAC (**Figures 5B, D**), suggesting that exposure to lapatinib could be associated with Keap1 oxidation.

mRNA Expression of GSH-Related Genes and Levels of GSH and GSSG in HepG2 Cells and Isolated Mitochondria

The product of the *Gsta1* gene detoxifies electrophiles through conjugation with glutathione (GSH), the most prevalent antioxidative molecule in hepatocytes (Griffith and Meister, 1985). The first step of the GSH synthesis is catalyzed by the glutamate-cysteine ligase (Gcl), which consists of a catalytic (Gclc) and a modifying subunit (Gclm). Since expression of both subunits is regulated by Nrf2, we measured the mRNA expression of *Gclc* and *Gclm* in lapatinib-treated HepG2 cells after 24 h (**Figure 6A**) and observed a concentration-dependent increase starting at 10 and 5 µM, respectively. The expression of both genes was significantly upregulated at 20 µM. We also measured the mRNA expression of glutaredoxin 1 (*Glrx1*) and 2 (*Glrx2*), which use GSH as a co-factor to reduce protein disulfides (**Figure 6B**). Interestingly, the transcription of the mainly cytosolic *Glrx1* was not significantly affected by lapatinib treatment at any concentration, while the expression of the mitochondrial *Glrx2* was significantly induced at 10 and 20 µM.

Lapatinb induced the transcription of *Gcl*, which encodes for the rate-limiting enzyme of GSH synthesis. GSH can directly detoxify ROS whereby being oxidized to GSSG. Thus, we measured GSH and its oxidized form GSSG in HepG2 cells treated with 10 and 20 µM lapatinib (**Figures 6C, D**). In HepG2 cells, we observed increased GSH levels at both concentrations (**Figure 6C**), and also significantly increased GSSG levels (**Figure 6D**). Since the GSH pool is compartmentalized within cells, we measured GSH specifically in mitochondria isolated from lapatinib-treated HepG2 cells (**Figure 6E**). Similar to the cellular GSH pool, also the mitochondrial GSH pool increased at both lapatinib concentrations investigated. The mitochondrial GSSG pool could not be analyzed due to stability issues during the measurement.

mRNA and Protein Expression of Antioxidative Proteins

Nrf2 also regulates the transcription of the antioxidative genes *SOD1* and *SOD2*, whose protein products are particularly important to detoxify mitochondrial $O_2^{\bullet-}$ accumulated upon lapatinib-treatment. We measured the mRNA and protein expression of both superoxide dismutases in HepG2 cells after lapatinib-treatment for 2, 6, and 24 h. Regarding SOD1, neither mRNA (**Figure 7A** and **Supplementary Figure 3D**) nor protein

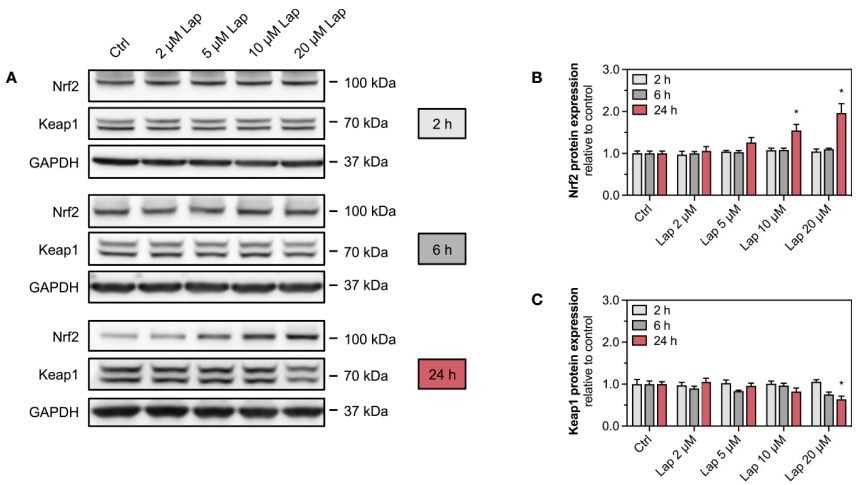

FIGURE 3 | Protein expression of Nrf2 and Keap1 in HepG2 cells. **(A)** Representative western blot and quantification of **(B)** Nrf2 and **(C)** Keap1 protein expression in HepG2 cells after treatment with 2–20 µM lapatinib (Lap) for 2, 6, and 24 h. GAPDH represents the loading control. Data are shown as fold increase relative to the negative control (0.1% DMSO, Ctrl), and are the mean ± SEM of at least three independent replicates. *p < 0.05 versus negative control.

expression (**Figures 7B, C** and **Supplementary Figure 3B**) were affected by lapatinib. In contrast, mRNA and protein expression of SOD2, an enzyme uniquely located in the mitochondrial matrix, significantly increased in a concentration-dependent manner at 10 and 20 µM lapatinib after 24 h of exposure (**Figures 7A–C**). In comparison, at 2 and 6 h of exposure to lapatinib, no such increase in SOD2 mRNA or protein expression was observed (**Supplementary Figures 3A, C, D**).

DISCUSSION

The present study provides evidence that the mitochondrial toxicant lapatinib activates the Keap1-Nrf2 signaling pathway in HepG2 cells. The nuclear translocation of Nrf2 induced the transcription of typically Nrf2-regulated genes including *Nqo1*, *Gsta1*, *Gclc*, and *Gclm*. Consequently, activation of the Nrf2 pathway resulted in increased cellular and mitochondrial GSH levels. Furthermore, lapatinib upregulated the gene expression of *Glrx2* and *SOD2*, which encode for mitochondrial antioxidative proteins. Activation of the Keap1-Nrf2 pathway, however, was not sufficient to avoid mitochondrial $O_2^{\bullet-}$ and cellular H_2O_2 accumulation, GSSG formation, cell membrane damage, and ATP depletion upon 24 h-treatment with 10 and 20 µM lapatinib.

In our previous study, we showed that mitochondrial impairment is involved in the hepatotoxicity of lapatinib (Paech et al., 2017). In agreement with this earlier study, in the current study, we found a concentration-dependent membrane damage and

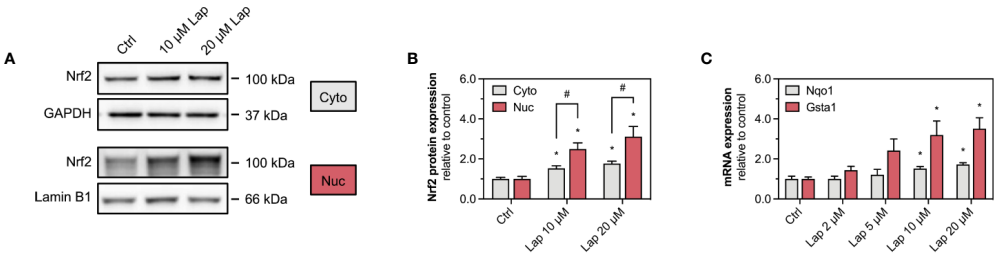

FIGURE 4 | Activation of Keap1-Nrf2 pathway in HepG2 cells. **(A)** Representative western blots and **(B)** quantification of Nrf2 in nuclear (nuc) and cytoplasmic (cyto) fraction of HepG2 cells after 24 h-treatment with 10 and 20 µM lapatinib (Lap). Lamin B1 (nuclear fraction) and GAPDH (cytoplasmic fraction) represent the loading controls. **(C)** mRNA expression of the Nrf2-regulated genes *Nqo1* and *Gsta1* in HepG2 cells after treatment with 2–20 µM lapatinib (Lap) for 24 h. Data are shown as fold increase relative to the negative control (0.1% DMSO, Ctrl), and are the mean ± SEM of at least three independent replicates. *p < 0.05 versus negative control, #p < 0.05 versus the same concentration of lapatinib of the other experimental group.

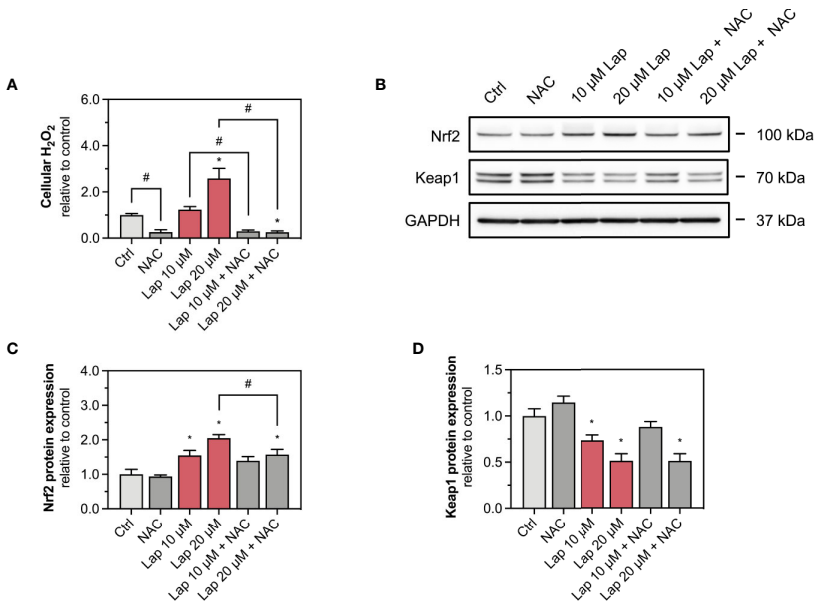

FIGURE 5 | Involvement of ROS in the activation of the Keap1-Nrf2 pathway. **(A)** Cellular H_2O_2 accumulation in HepG2 cells after treatment with 10 and 20 µM lapatinib (Lap) with or without N-acetyl cysteine (NAC, 2 mM) for 24 h. **(B)** Representative western blot and quantification of **(C)** Nrf2 and **(D)** Keap1 protein expression in HepG2 cells after treatment with 10 and 20 µM lapatinib (Lap) with or without N-acetyl cysteine (NAC, 2 mM) for 24 h. Data are shown as fold increase relative to the negative control (0.1% DMSO, Ctrl), and are the mean ± SEM of at least three independent replicates. *$p < 0.05$ versus negative control, #$p < 0.05$ versus the same concentration of lapatinib of the other experimental group.

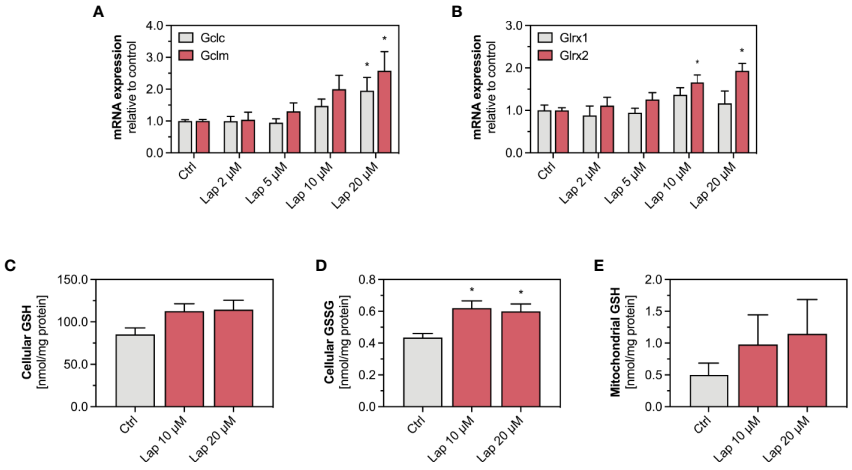

FIGURE 6 | mRNA expression of GSH-related genes and levels of GSH and GSSG in HepG2 cells and isolated mitochondria. **(A)** mRNA expression of the Nrf2-regulated genes *Gclc* and *Gclm* as well as **(B)** *Glrx1* and *Glrx2* in HepG2 cells after treatment with 2–20 µM lapatinib (Lap) for 24 h. Data are shown as fold increase relative to the negative control (0.1% DMSO, Ctrl), and are the mean ± SEM of three independent replicates. *$p < 0.05$ versus negative control. Levels of **(C)** GSH and **(D)** GSSG in HepG2 cells after treatment with 2–20 µM lapatinib (Lap) for 24 h. **(E)** GSH levels in mitochondria isolated from HepG2 cells after treatment with 2–20 µM lapatinib (Lap) for 24. Data are the mean ± SEM of four independent experiments. *$p < 0.05$ versus negative control.

reduced ATP pool in HepG2 cells after 24 h of treatment with lapatinib. We also observed that lapatinib dissipated the $\Delta\psi_M$ after 24 h of treatment, which was 24 h earlier than observed in our previous study. A decrease in $\Delta\psi_M$ could result from an inhibition of the mitochondrial electron transport chain and/or uncoupling of oxidative phosphorylation. In addition, we observed a concentration-dependent accumulation of mitochondrial $O_2^{\bullet-}$ and accumulation of cellular H_2O_2 upon lapatinib-treatment, indicating that this drug causes oxidative stress. Taking into account that lapatinib is a mitochondrial toxicant, we can assume that ROS is generated first within mitochondria as $O_2^{\bullet-}$, which is converted by SOD2 to H_2O_2. H_2O_2 can leave the mitochondria and accumulate in the cytoplasm, as observed in the current study. This sequence of events fits well with the findings in the current study, since we observed mitochondrial superoxide accumulation after 6 h and cellular H_2O_2 accumulation after 24 h of incubation with lapatinib. Inhibition of mainly complex I and III of the mitochondrial electron transport chain can stimulate the generation of mitochondrial $O_2^{\bullet-}$ (Brand, 2010). However, in our previous study, lapatinib did not impair oxygen consumption by HepG2 cells, suggesting that lapatinib does not impair the mitochondrial electron transport chain (Paech et al., 2017). Importantly, mitochondria can produce ROS not only in the electron transport chain, but also at other sites such as for instance by the reaction of mitochondrial NADPH oxidase, monoaminoxidase, and/or α-glycerophosphate dehydrogenase (Zorov et al., 2014), with which lapatinib may interfere and induce mitochondrial ROS production.

Oxidative stress can inactivate Keap1 and increase its ubiquitination, resulting in decreased levels of Keap1, which is associated with decreased degradation and therefore increased cytoplasmic levels of Nrf2 (Zhang et al., 2005; Roos et al., 2020). Nrf2 stabilization, nuclear translocation, and upregulated transcriptional Nrf2 activity demonstrated the activation of this pathway by lapatinib in the current study. In addition, we assume that the observed rise in the cellular and mitochondrial GSH pools results from increased Nrf2 activity. Upregulation of GSH synthesis strengthens the cellular antioxidative capacity, which seems to be required since GSSG, the oxidized form of GSH, accumulated significantly in HepG2 cells.

In order to show the relationship between ROS accumulation and the Nrf2 activation, we co-treated HepG2 cells with lapatinib and the ROS scavenger N-acetyl cysteine (NAC). The co-exposure with NAC prevented lapatinib-associated ROS accumulation. Interestingly, in the presence of NAC, the Nrf2 accumulation was less pronounced when cells were exposed to lapatinib. This suggests that ROS accumulation upon lapatinib treatment can participate in the activation of the Keap1-Nrf2 pathway. The current study does not show, however, that activation of Nrf2 diminishes the toxicity of lapatinib. We have shown that in a recent publication for the mitochondrial toxicant benzbromarone, which was less toxic after stimulating the expression of Nrf2 by Keap1 knock-down (Roos et al., 2020).

Although ROS accumulation is a well-established mechanism of Keap1-Nrf2 pathway activation, we cannot exclude that lapatinib itself or reactive lapatinib metabolites contributed to the activation.

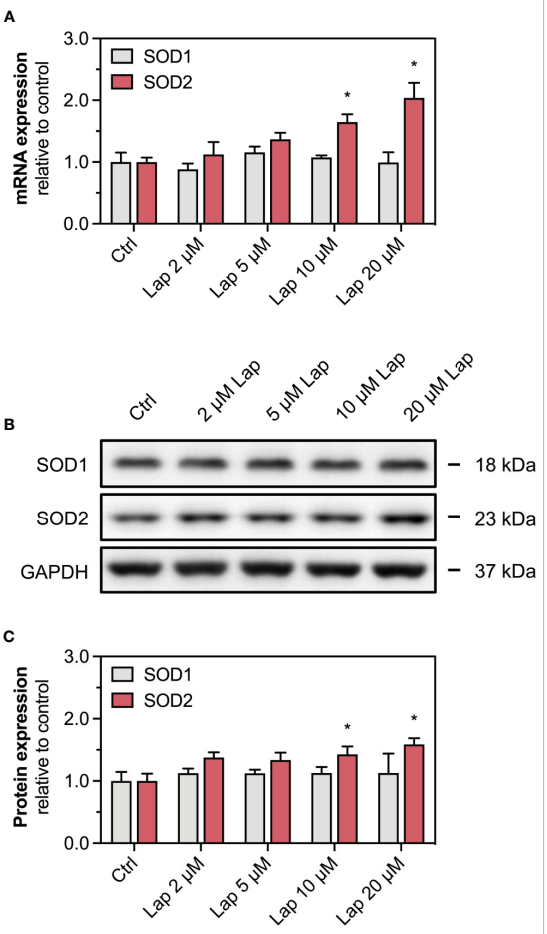

FIGURE 7 | mRNA and protein expression of cytosolic SOD1 and mitochondrial SOD2. **(A)** mRNA expression of *SOD1* and *SOD2* in HepG2 cells after treatment with 2–20 µM lapatinib (Lap) for 24 h. **(B)** Representative western blot and **(C)** quantification of SOD1 and SOD2 in HepG2 cells after treatment with 2–20 µM lapatinib (Lap) for 24 h. GAPDH represents the loading control. Data are shown as fold increase relative to the negative control (0.1% DMSO, Ctrl), and are the mean ± SEM of three independent replicates. *$p < 0.05$ versus negative control.

Lapatinib is metabolized in the liver by cytochrome P450 enzymes, mainly by CYP3A4/5, to mostly pharmacologically inactive metabolites (Teng et al., 2010). HepG2 cells have only low levels of drug-metabolizing enzymes (Gerets et al., 2012; Berger et al., 2016). Thus, the formation of reactive metabolites in our cell system by cytochrome P450 enzymes is unlikely. Reactive metabolites could, however, be formed also upon oxidation by ROS. Oxidative cleavage of lapatinib's fluorobenzyl group (O-dealkylation) and/or oxidation of lapatinib's benzene rings could

generate phenolic metabolites that could covalently bind to cysteine residues of Keap1 and subsequently stabilize Nrf2 (Teng et al., 2010; Castellino et al., 2012). This mechanism has been described for phenolic compounds that activate Nrf2 (Erlank et al., 2011). Furthermore, O-dealkylated lapatinib could be converted to a quinone imine reactive metabolite that forms GSH-adducts, demonstrating its ability to bind to cysteine residues (Hardy et al., 2014). This could, together with cellular accumulation of ROS, explain the need for increased GSH synthesis upon lapatinib treatment. Furthermore, covalent binding of reactive metabolites to cellular proteins can form haptens that could be phagocytosed by macrophages following hepatocyte breakdown and be presented on their surface by HLA proteins, which could activate T-cells. Indeed, HLA-DQA1*02:01 and DRB1*07:01 have been identified as risk factors for hepatotoxicity in patients treated with lapatinib (Spraggs et al., 2011; Spraggs et al., 2018). This mechanism cannot explain the observed hepatocellular toxicity in the current study, however, since no macrophages and T-cells were present in our assays.

Our results are in apparent contradiction to those reported by Eno et al. (2016). Eno et al. showed that 10 μM lapatinib for 24 h did neither impair oxygen consumption, nor activate the Keap1-Nrf2 pathway in HepG2 cells. Impairment of the cellular oxygen consumption and Nrf2 activation was only seen after transfection of HepG2 cells with CYP3A4, suggesting that a lapatinib metabolite was responsible for these findings. Indeed, O-dealkylated lapatinib reduced oxygen consumption and induced Nrf2 activation also in wild type HepG2 cells. In the current study, we started to see significant effects on mitochondrial function and Nrf2 activation at 10 μM lapatinib with more accentuated toxicity at 20 μM. Looking at the results on the NAD(P)H concentration in the publication of Eno et al. (Eno et al., 2016), it is clear that a numerical reduction without reaching statistical significance was already seen at 10 μM lapatinib. The difference in the findings of the two studies may therefore result mostly from the fact that we systematically studied lapatinib also at a concentration of 20 μM. Relevant CYP3A4 expression by the HepG2 cells can be excluded as shown in a previous publication by us (Berger et al., 2016).

In the current study, lapatinib started to activate the Nrf2 pathway at 5 μM with a significant effect at 10 and 20 μM, respectively. The maximal plasma concentrations after oral ingestion of a daily dose lapatinib (1,250 mg) combined with capecitabine are between 4.1–7.4 μM (Chu et al., 2007). Since lapatinib undergoes an extensive first-pass metabolism in the liver, the hepatic lapatinib concentrations are likely to be higher. Furthermore, the simultaneous intake of a fatty meal increased the bioavailability of lapatinib up to 4.3-fold (Koch et al., 2007; Koch et al., 2009). Also, the concomitant administration of 3A4-inhibitors such as ketoconazole increases the maximal plasma concentrations of lapatinib, a CYP3A4-substrate, up to 3.6-fold. (Medina and Goodin, 2008). Thus, we can conclude that the concentrations needed to activate the Keap1-Nrf2 pathway in our *in vitro* investigations can be reached in the liver of patients treated with this drug.

In conclusion, the mitochondrial toxicant lapatinib stabilized the transcription factor Nrf2 in HepG2 cells in a concentration-dependent manner, leading to the induction of important antioxidative and cell-protective Nrf2-regulated genes and upregulation of GSH synthesis. Beside the role of Nrf2 as a nuclear transcription factor, cellular Nrf2 accumulation can also be regarded as a marker of oxidative stress. The study illustrates that the hepatocellular toxicity of lapatinib is accompanied by activation of the Keap1-Nrf2 pathway. Beside the proposed immunological mechanism, mitochondrial toxicity with increased $O_2^{\bullet -}$ production is an additional toxicological mechanism associated with liver injury of lapatinib.

DATA AVAILABILITY STATEMENT

All datasets for this study are included in the figshare repository: https://doi.org/10.6084/m9.figshare.12034608.v1.

AUTHOR CONTRIBUTIONS

NR and DA conducted the experiments, interpreted data, prepared figures and helped writing the manuscript. JB helped designing the study, supervised the lab work and helped in writing the manuscript. SK helped in designing the study, discussed and helped in the interpretation of the data and prepared the final version of the manuscript.

FUNDING

The study was supported by a grant from the Swiss National Science Foundation to SK (SNF 31003A_156270).

SUPPLEMENTARY MATERIAL

The Supplementary Material for this article can be found online at: https://www.frontiersin.org/articles/10.3389/fphar.2020.00944/full#supplementary-material

SUPPLEMENTARY FIGURE 1 | mRNA expression of Nrf2 gene. **(A)** mRNA expression of the *Nrf2* gene in HepG2 cells after treatment with 2–20 μM lapatinib (Lap) for 24 h. Data are shown as fold increase relative to the negative control (0.1% DMSO, Ctrl), and are the mean ± SEM of three independent replicates. *p < 0.05 versus negative control.

SUPPLEMENTARY FIGURE 2 | mRNA expression of Nqo1 and Gsta1 gene. mRNA expression of **(A)** Nqo1 and **(B)** Gsta1 in HepG2 cells after treatment with 2–20 μM lapatinib (Lap) for 2 and 6 h. Data are shown as fold increase relative to the negative control (0.1% DMSO, Ctrl), and are the mean ± SEM of three independent replicates. *p < 0.05 versus negative control.

SUPPLEMENTARY FIGURE 3 | mRNA and protein expression of cytosolic SOD1 and mitochondrial SOD2. **(A)** mRNA expression of SOD2 after treatment with 2–20 μM lapatinib (Lap) for 2 and 6 h. **(B)** Representative western blot and quantification of **(C)** SOD1 and **(D)** SOD2 in HepG2 cells after treatment with 2–20 μM lapatinib (Lap) for 2 and 6 h. GAPDH represents the loading control. Data are shown as fold increase relative to the negative control (0.1% DMSO, Ctrl), and are the mean ± SEM of three independent replicates. *p < 0.05 versus negative control.

REFERENCES

Amir, E., Seruga, B., Martinez-Lopez, J., Kwong, R., Pandiella, A., Tannock, I. F., et al. (2011). Oncogenic targets, magnitude of benefit, and market pricing of antineoplastic drugs. *J. Clin. Oncol.* 29, 2543–2549. doi: 10.1200/JCO.2011.35.2393

Azim, H. A.Jr., Agbor-Tarh, D., Bradbury, I., Dinh, P., Baselga, J., Di Cosimo, S., et al. (2013). Pattern of rash, diarrhea, and hepatic toxicities secondary to lapatinib and their association with age and response to neoadjuvant therapy: analysis from the NeoALTTO trial. *J. Clin. Oncol.* 31, 4504–4511. doi: 10.1200/JCO.2013.50.9448

Balaban, R. S., Nemoto, S., and Finkel, T. (2005). Mitochondria, oxidants, and aging. *Cell* 120, 483–495. doi: 10.1016/j.cell.2005.02.001

Baselga, J., Bradbury, I., Eidtmann, H., Di Cosimo, S., De Azambuja, E., Aura, C., et al. (2012). Lapatinib with trastuzumab for HER2-positive early breast cancer (NeoALTTO): a randomised, open-label, multicentre, phase 3 trial. *Lancet* 379, 633–640. doi: 10.1016/S0140-6736(11)61847-3

Berger, B., Donzelli, M., Maseneni, S., Boess, F., Roth, A., Krahenbuhl, S., et al. (2016). Comparison of Liver Cell Models Using the Basel Phenotyping Cocktail. *Front. Pharmacol.* 7, 443. doi: 10.3389/fphar.2016.00443

Brand, M. D. (2010). The sites and topology of mitochondrial superoxide production. *Exp. Gerontol.* 45, 466–472. doi: 10.1016/j.exger.2010.01.003

Brand, M. D. (2016). Mitochondrial generation of superoxide and hydrogen peroxide as the source of mitochondrial redox signaling. *Free Radic. Biol. Med.* 100, 14–31. doi: 10.1016/j.freeradbiomed.2016.04.001

Castellino, S., O'mara, M., Koch, K., Borts, D. J., Bowers, G. D., and Maclauchlin, C. (2012). Human metabolism of lapatinib, a dual kinase inhibitor: implications for hepatotoxicity. *Drug Metab. Dispos.* 40, 139–150. doi: 10.1124/dmd.111.040949

Chu, Q. S., Schwartz, G., De Bono, J., Smith, D. A., Koch, K. M., Versola, M. J., et al. (2007). Phase I and pharmacokinetic study of lapatinib in combination with capecitabine in patients with advanced solid malignancies. *J. Clin. Oncol.* 25, 3753–3758. doi: 10.1200/JCO.2007.11.1765

Deferme, L., Briede, J. J., Claessen, S. M., Jennen, D. G., Cavill, R., and Kleinjans, J. C. (2013). Time series analysis of oxidative stress response patterns in HepG2: a toxicogenomics approach. *Toxicology* 306, 24–34. doi: 10.1016/j.tox.2013.02.001

Eno, M. R., El-Gendy Bel, D., and Cameron, M. D. (2016). P450 3A-Catalyzed O-Dealkylation of Lapatinib Induces Mitochondrial Stress and Activates Nrf2. *Chem. Res. Toxicol.* 29, 784–796. doi: 10.1021/acs.chemrestox.5b00524

Erlank, H., Elmann, A., Kohen, R., and Kanner, J. (2011). Polyphenols activate Nrf2 in astrocytes via H2O2, semiquinones, and quinones. *Free Radic. Biol. Med.* 51, 2319–2327. doi: 10.1016/j.freeradbiomed.2011.09.033

Felser, A., Blum, K., Lindinger, P. W., Bouitbir, J., and Krahenbuhl, S. (2013). Mechanisms of hepatocellular toxicity associated with dronedarone–a comparison to amiodarone. *Toxicol. Sci.* 131, 480–490. doi: 10.1093/toxsci/kfs298

Gerets, H. H., Tilmant, K., Gerin, B., Chanteux, H., Depelchin, B. O., Dhalluin, S., et al. (2012). Characterization of primary human hepatocytes, HepG2 cells, and HepaRG cells at the mRNA level and CYP activity in response to inducers and their predictivity for the detection of human hepatotoxins. *Cell Biol. Toxicol.* 28, 69–87. doi: 10.1007/s10565-011-9208-4

Giustarini, D., Dalle-Donne, I., Milzani, A., Fanti, P., and Rossi, R. (2013). Analysis of GSH and GSSG after derivatization with N-ethylmaleimide. *Nat. Protoc.* 8, 1660–1669. doi: 10.1038/nprot.2013.095

Gomez, H. L., Doval, D. C., Chavez, M. A., Ang, P. C., Aziz, Z., Nag, S., et al. (2008). Efficacy and safety of lapatinib as first-line therapy for ErbB2-amplified locally advanced or metastatic breast cancer. *J. Clin. Oncol.* 26, 2999–3005. doi: 10.1200/JCO.2007.14.0590

Griffith, O. W., and Meister, A. (1985). Origin and turnover of mitochondrial glutathione. *Proc. Natl. Acad. Sci. U. S. A* 82, 4668–4672. doi: 10.1073/pnas.82.14.4668

Hardy, K. D., Wahlin, M. D., Papageorgiou, I., Unadkat, J. D., Rettie, A. E., and Nelson, S. D. (2014). Studies on the role of metabolic activation in tyrosine kinase inhibitor-dependent hepatotoxicity: induction of CYP3A4 enhances the cytotoxicity of lapatinib in HepaRG cells. *Drug Metab. Dispos.* 42, 162–171. doi: 10.1124/dmd.113.054817

Hornig-Do, H. T., Gunther, G., Bust, M., Lehnartz, P., Bosio, A., and Wiesner, R. J. (2009). Isolation of functional pure mitochondria by superparamagnetic microbeads. *Anal. Biochem.* 389, 1–5. doi: 10.1016/j.ab.2009.02.040

Itoh, K., Wakabayashi, N., Katoh, Y., Ishii, T., Igarashi, K., Engel, J. D., et al. (1999). Keap1 represses nuclear activation of antioxidant responsive elements by Nrf2 through binding to the amino-terminal Neh2 domain. *Genes Dev.* 13, 76–86. doi: 10.1101/gad.13.1.76

Kobayashi, A., Kang, M. I., Okawa, H., Ohtsuji, M., Zenke, Y., Chiba, T., et al. (2004). Oxidative stress sensor Keap1 functions as an adaptor for Cul3-based E3 ligase to regulate proteasomal degradation of Nrf2. *Mol. Cell Biol.* 24, 7130–7139. doi: 10.1128/MCB.24.16.7130-7139.2004

Koch, K. M., Beelen, A. P., Ho, P. T., and Roychowdhury, D. F. (2007). The value of label recommendations: how to dose lapatinib. *J. Clin. Oncol.* 25, 5331–5332. doi: 10.1200/JCO.2007.13.8644

Koch, K. M., Reddy, N. J., Cohen, R. B., Lewis, N. L., Whitehead, B., Mackay, K., et al. (2009). Effects of food on the relative bioavailability of lapatinib in cancer patients. *J. Clin. Oncol.* 27, 1191–1196. doi: 10.1200/JCO.2008.18.3285

Krause, D. S., and Van Etten, R. A. (2005). Tyrosine kinases as targets for cancer therapy. *N. Engl. J. Med.* 353, 172–187. doi: 10.1056/NEJMra044389

Medina, P. J., and Goodin, S. (2008). Lapatinib: a dual inhibitor of human epidermal growth factor receptor tyrosine kinases. *Clin. Ther.* 30, 1426–1447. doi: 10.1016/j.clinthera.2008.08.008

Moy, B., Kirkpatrick, P., Kar, S., and Goss, P. (2007). Lapatinib. *Nat. Rev. Drug Discovery* 6, 431–432. doi: 10.1038/nrd2332

Ott, M., Gogvadze, V., Orrenius, S., and Zhivotovsky, B. (2007). Mitochondria, oxidative stress and cell death. *Apoptosis* 12, 913–922. doi: 10.1007/s10495-007-0756-2

Paech, F., Bouitbir, J., and Krahenbuhl, S. (2017). Hepatocellular Toxicity Associated with Tyrosine Kinase Inhibitors: Mitochondrial Damage and Inhibition of Glycolysis. *Front. Pharmacol.* 8, 367. doi: 10.3389/fphar.2017.00367

Peroukides, S., Makatsoris, T., Koutras, A., Tsamandas, A., Onyenadum, A., Labropoulou-Karatza, C., et al. (2011). Lapatinib-induced hepatitis: a case report. *World J. Gastroenterol.* 17, 2349–2352. doi: 10.3748/wjg.v17.i18.2349

Reisman, S. A., Yeager, R. L., Yamamoto, M., and Klaassen, C. D. (2009). Increased Nrf2 activation in livers from Keap1-knockdown mice increases expression of cytoprotective genes that detoxify electrophiles more than those that detoxify reactive oxygen species. *Toxicol. Sci.* 108, 35–47. doi: 10.1093/toxsci/kfn267

Roos, N. J., Duthaler, U., Bouitbir, J., and Krahenbuhl, S. (2020). The uricosuric benzbromarone disturbs the mitochondrial redox homeostasis and activates the NRF2 signaling pathway in HepG2 cells. *Free Radic. Biol. Med.* 152, 216–226. doi: 10.1016/j.freeradbiomed.2020.03.009

Ryan, Q., Ibrahim, A., Cohen, M. H., Johnson, J., Ko, C. W., Sridhara, R., et al. (2008). FDA drug approval summary: lapatinib in combination with capecitabine for previously treated metastatic breast cancer that overexpresses HER-2. *Oncologist* 13, 1114–1119. doi: 10.1634/theoncologist.2008-0816

Slamon, D. J., Clark, G. M., Wong, S. G., Levin, W. J., Ullrich, A., and Mcguire, W. L. (1987). Human breast cancer: correlation of relapse and survival with amplification of the HER-2/neu oncogene. *Science* 235, 177–182. doi: 10.1126/science.3798106

Spraggs, C. F., Budde, L. R., Briley, L. P., Bing, N., Cox, C. J., King, K. S., et al. (2011). HLA-DQA1*02:01 is a major risk factor for lapatinib-induced hepatotoxicity in women with advanced breast cancer. *J. Clin. Oncol.* 29, 667–673. doi: 10.1200/JCO.2010.31.3197

Spraggs, C. F., Parham, L. R., Briley, L. P., Warren, L., Williams, L. S., Fraser, D. J., et al. (2018). Characterisation of the HLA-DRB1*07:01 biomarker for lapatinib-induced liver toxicity during treatment of early-stage breast cancer patients with lapatinib in combination with trastuzumab and/or taxanes. *Pharmacogenom. J.* 18, 480–486. doi: 10.1038/tpj.2017.39

Suzuki, T., Muramatsu, A., Saito, R., Iso, T., Shibata, T., Kuwata, K., et al. (2019). Molecular Mechanism of Cellular Oxidative Stress Sensing by Keap1. *Cell Rep.* 28, 746–758 e744. doi: 10.1016/j.celrep.2019.06.047

Teng, W. C., Oh, J. W., New, L. S., Wahlin, M. D., Nelson, S. D., Ho, H. K., et al. (2010). Mechanism-based inactivation of cytochrome P450 3A4 by lapatinib. *Mol. Pharmacol.* 78, 693–703. doi: 10.1124/mol.110.065839

Yamamoto, M., Kensler, T. W., and Motohashi, H. (2018). The KEAP1-NRF2 System: a Thiol-Based Sensor-Effector Apparatus for Maintaining Redox Homeostasis. *Physiol. Rev.* 98, 1169–1203. doi: 10.1152/physrev.00023.2017

Yarden, Y., and Sliwkowski, M. X. (2001). Untangling the ErbB signalling network. *Nat. Rev. Mol. Cell Biol.* 2, 127–137. doi: 10.1038/35052073

Zhang, D. D., Lo, S. C., Sun, Z., Habib, G. M., Lieberman, M. W., and Hannink, M. (2005). Ubiquitination of Keap1, a BTB-Kelch substrate adaptor protein for Cul3, targets Keap1 for degradation by a proteasome-independent pathway. *J. Biol. Chem.* 280, 30091–30099. doi: 10.1074/jbc.M501279200

Zorov, D. B., Juhaszova, M., and Sollott, S. J. (2014). Mitochondrial reactive oxygen species (ROS) and ROS-induced ROS release. *Physiol. Rev.* 94, 909–950. doi: 10.1152/physrev.00026.2013

Conflict of Interest: The authors declare that the research was conducted in the absence of any commercial or financial relationships that could be construed as a potential conflict of interest.

3 Paper III

Imatinib disturbs lysosomal function and morphology and impairs the activity of mTORC1 in human hepatocyte cell lines

Noëmi Johanna Roos[1,2,#], Riccardo Vincenzo Mancuso[1,3,#],
Gerda Mawududzi Sanvee[1,2], Jamal Bouitbir[4], and Stephan Krähenbühl[1]

[#]contributed equally to the work

[1]Division of Clinical Pharmacology & Toxicology, University Hospital of Basel, Switzerland
[2]Division of Pharmaceutical Technology, [3]Molecular Pharmacy, and
[4]Molecular and Systems Toxicology,
Department of Pharmaceutical Sciences, University of Basel, Switzerland

Published in Food Chem Toxicol. 2022 Feb 16;162:112869.

Food and Chemical Toxicology 162 (2022) 112869

Contents lists available at ScienceDirect

Food and Chemical Toxicology

journal homepage: www.elsevier.com/locate/foodchemtox

Imatinib disturbs lysosomal function and morphology and impairs the activity of mTORC1 in human hepatocyte cell lines

Noëmi Johanna Roos [a,b,1], Riccardo Vincenzo Mancuso [a,c,1], Gerda Mawududzi Sanvee [a,b], Jamal Bouitbir [d], Stephan Krähenbühl [a,*]

[a] Division of Clinical Pharmacology & Toxicology, University Hospital of Basel, Switzerland
[b] Division of Pharmaceutical Technology, Department of Pharmaceutical Sciences, University of Basel, Switzerland
[c] Division of Molecular Pharmacy, Department of Pharmaceutical Sciences, University of Basel, Switzerland
[d] Division of Molecular and Systems Toxicology, Department of Pharmaceutical Sciences, University of Basel, Switzerland

ARTICLE INFO

Handling editor. Dr. Jose Luis Domingo

Keywords:
Tyrosine kinase inhibitors (TKI)
Hepatotoxicity
HepG2 cells
mTORC1
TFEB
Autophagy

ABSTRACT

The tyrosine kinase inhibitors (TKIs) imatinib and lapatinib are associated with severe hepatotoxicity, whose mechanisms are currently under investigation. As amphiphilic drugs, imatinib and lapatinib enrich in lysosomes. In the present study, we investigated their effects on lysosomal morphology and function in HepG2 and HuH-7 cells and explored possible links between lysosomal dysfunction and hepatotoxicity. Both TKIs increased the lysosomal volume time and concentration-dependently in HepG2 and HuH-7 cells. In HepG2 cells, lapatinib and imatinib raised the lysosomal pH and destabilized the lysosomal membrane, thereby impairing lysosomal proteolytic activity such as cathepsin B processing. Imatinib activated the transcription factor EB (TFEB), a regulator of lysosomal biogenesis and function, as demonstrated by nuclear TFEB accumulation and increased expression of TFEB-target genes. Because of lysosomal dysfunction, imatinib impaired mTORC1 activation, a protein complex activated on the lysosomal surface, which explained TFEB activation. HepG2 cells treated with imatinib showed increased levels of MAP1LC3A/B-II and of ATG13 (S318) phosphorylation, indicating induction of autophagy due to TFEB activation. Finally, imatinib induced apoptosis in HepG2 cells in a time and concentration-dependent manner, explained by lysosomal and mitochondrial toxicity. Our findings provide a new lysosome-centered mechanism for imatinib-induced hepatotoxicity that could be extended to other lysosomotropic drugs.

1. Introduction

Tyrosine kinases (TKs) are transmembranous or cytosolic proteins that phosphorylate intracellular protein tyrosine residues after having been activated by binding of their ligands. Activated TKs initiate intracellular signaling pathways that regulate fundamental processes such as cell differentiation, proliferation, and apoptosis (Krause and Van Etten, 2005). Permanently activated TKs can lead to uncontrolled cell growth and cancer. Small-molecule drugs that specifically inhibit oncogenic TKs, classified as tyrosine kinase inhibitors (TKIs), are therefore efficacious anticancer drugs (Huang et al., 2020).

Imatinib mesylate, the first approved TKI, inhibits the breakpoint cluster region protein-Abelson tyrosine kinase (BCR-ABL) fusion protein by competitively binding to the ATP-binding site of the protein (Goldman and Melo, 2001). Furthermore, imatinib is an inhibitor of the oncogenic platelet-derived growth factor receptor, stem cell factor, and c-Kit. Imatinib is indicated to treat patients with BCR-ABL positive chronic myelogenous leukemia (CML) and acute lymphoblastic leukemia, gastrointestinal stromal tumors, mastocytosis, and other tumors caused by imatinib-sensitive TK (Peng et al., 2005). The most frequent adverse effects of imatinib are edema, myalgias, and gastrointestinal irritations (Druker et al., 2001). In addition, imatinib is associated with liver injury, which is in most cases asymptomatic and transient (Peng et al., 2005). However, severe cases of liver injury leading to liver transplantation or death have also been reported in patients treated with imatinib (Lin et al., 2003).

Lapatinib, a TKI that inhibits the erb-b2 receptor tyrosine kinase 2 (ERBB2), is approved for the treatment of advanced or metastatic ERBB2-positive breast cancer (Moy et al., 2007). Common adverse

* Corresponding author. Clinical Pharmacology & Toxicology University Hospital, 4031, Basel, Switzerland.
E-mail address: stephan.kraehenbuehl@usb.ch (S. Krähenbühl).
[1] contributed equally to this work.

https://doi.org/10.1016/j.fct.2022.112869
Received 24 October 2021; Received in revised form 20 December 2021; Accepted 12 February 2022
Available online 16 February 2022

List of abbreviations

TKI	Tyrosine kinase inhibitor
TK	Tyrosine kinase
CML	Chronic myelogenous leukemia
LTDR	LysoTracker Deep Red
AO	Acridine orange
DQ-BSA	De-quenched bovine serum albumin
mTOR	Mechanistic target of rapamycin kinase
CTSB	Cathepsin B
TFEB	Transcription factor EB
mTORC1/2	Mechanistic target of rapamycin kinase complex 1/2
AKT1	AKT serine/threonine kinase 1
GSK3B	Glycogen synthase kinase 3 beta
MAPK1/3	Mitogen-activated protein kinase 1/3
ULK1	Unc-51 like autophagy activating kinase 1
RPS6	Ribosomal protein S6
EIF4EBP1	Eukaryotic translation initiation factor 4E binding protein 1
TSC1/2	TSC complex
PRKAA	Protein kinase AMP-activated catalytic subunit alpha 1 and 2
SQSTM1	Sequestosome 1
ATG13	Autophagy related protein 13
MAP1LC3A/B	Microtubule associated protein 1 light chain 3 alpha/beta
LMP	Lysosomal membrane permeabilization

reactions associated with lapatinib include gastrointestinal irritations, rash, palmar-plantar erythrodysesthesia, and fatigue (Ryan et al., 2008). In 2008, the U.S. Food and Drug Administration prompted a black box warning due to severe cases of acute liver toxicity caused by lapatinib, including cases with fatal outcome (Azim et al., 2013).

We have previously reported that imatinib and lapatinib are mitochondrial toxicants, which may partially explain hepatotoxicity associated with these drugs (Paech et al., 2017). In a more recent study, we observed that the hepatotoxic multi-kinase inhibitors ponatinib, regorafenib and sorafenib rapidly increased the number and size of lysosomes in HepG2 cells, a hepatocyte-derived immortalized cell line (Paech et al., 2018). Due to their physicochemical properties (lipophilic compounds with a nitrogen atom that can be protonated), several TKIs including lapatinib and imatinib have been reported to accumulate in lysosomes (Burger et al., 2015; Fu et al., 2014; Nadanaciva et al., 2011). Since lysosomal drug accumulation can disturb the lysosomal function and cause cytotoxicity (Boya et al., 2003a, 2003b), we hypothesized that lysosomal accumulation of TKIs may represent an additional mechanism of hepatotoxicity. Based on these considerations, we decided to study the effect of lapatinib and imatinib on lysosome morphology and function as well as the relation to cytotoxicity in HepG2 cells.

2. Materials and methods

2.1. Reagents

Cell culture media (DMEM, low glucose, pyruvate, 31885023; DPBS, no calcium, no magnesium, 14190094), supplements (fetal bovine serum, 10500064; HEPES, 15630056; GlutaMAX, 35050038; MEM non-essential amino acids solution, 11140035; penicillin-streptomycin 10'000 U/mL, 15140122), and TrypLE express enzyme (12605010) were purchased from Thermo Fisher Scientific. Imatinib mesylate (SRP00530i) and lapatinib (SRP01210l) were obtained from Sequoia Research Products. Bafilomycin A1 (1334) and chloroquine diphosphate (4109) were purchased from Bio-Techne, while amiodarone hydrochloride (A8423), staurosporine (S5921), doxorubicin hydrochloride (D1515), and PIPES (P6757), BSA (A7906) and Tween 20 (93773) were ordered from Sigma-Aldrich. The antibodies were obtained from the companies listed in Table S1. Microsynth produced the primers listed in Table S2. The reagents used for transmission electron microscopy (paraformaldehyde, 15710; glutaraldehyde, 16310; osmium tetroxide, 19100; uranyl acetate, 22400; acetone, 15056; Epon812 resin, 14120) were ordered from Electron Microscopy Sciences.

2.2. Cell culture

HepG2 cells (ATCC, HB-8065), a human hepatoma cell line, were cultured in DMEM (1.0 g/L D-glucose, 4 mM L-glutamine, 1 mM sodium pyruvate) supplemented with 10% (v/v) inactivated FBS, 10 mM HEPES buffer (pH 7.4), 2 mM GlutaMAX, 1% (v/v) MEM non-essential amino acids solution (100x), and 100 U/mL penicillin/streptomycin. We grew the cells in a humidified 5% CO_2 cell culture incubator (Heracell 150i, Thermo Fisher Scientific, Basel, Switzerland) at 37 °C and passaged them using TrypLE express enzyme. We subcultured the cells in a ratio of 1:5 and did not exceed a passage number of 30. Both cell number and cell viability were determined by trypan blue exclusion using the EVE automatic cell counter (NanoEnTek, Seoul, Korea).

HuH-7 cells (RCB1366, RIKEN Cell Bank), a human hepatoma cell line, were cultured at 37 °C in a humidified 5% CO_2 cell culture incubator. The cells were kept in DMEM High Glucose 4.5 g/L (BioConcept, 1–26F03-I) supplemented with 10% fetal bovine serum (Thermo Fisher Scientific, 10500064) and 1% penicillin-streptomycin (10'000 μg/mL; Thermo Fisher Scientific, 15140122). We subcultured the cells in a ratio of 1:5 when they reached 70% confluency and did not exceed a passage number of 30.

2.3. Drug treatment

We treated HepG2 cells (80% confluency) with imatinib mesylate (5–50 μM) and lapatinib (2–20 μM) for 0.5, 6, and 24 h. The drug stock solutions (1'000x) were prepared in DMSO (Sigma-Aldrich, 472301) and stored at -20 °C. The DMSO concentration in the incubations did not exceed 0.1%. Negative control incubations (Ctrl) contained 0.1% (v/v) DMSO in the respective incubation buffer.

2.4. Flow cytometry with LTDR

We assessed the volume of the lysosomal compartment in imatinib- and lapatinib-treated HepG2 cells using LysoTracker Deep Red (LTDR, Thermo Fisher Scientific, L12492). LTDR is a fluorescent dye ($\lambda_{ex./em.}$ = 647/668 nm) that accumulates in lysosomes. We seeded HepG2 cells in a 24-well plate (150'000 cells/well) and treated them with imatinib and lapatinib for 0.5 h, 6 h, and 24 h. Amiodarone (50 μM), an amphiphilic drug that enlarges the lysosomal compartment, was used as a positive control (Funk and Krise, 2012). After the treatment, we harvested the cells using TrypLE express enzyme, transferred them into a clear V-bottom 96-well plate (Sigma-Aldrich, CLS3897-100 EA), and pelleted

the cells by centrifugation (400 *g*, 5 min). We resuspended the cell pellet in LTDR solution (1 nM, 200 μL/well) prepared in pre-warmed (37 °C) cell culture medium and incubated for 5 min (37 °C, protected from light). Afterward, the cells were pelleted again by centrifugation (400 *g*, 5 min) and resuspended in pre-warmed (37 °C) cell culture medium. The cells were subsequently analyzed with a CytoFLEX flow cytometer (Beckman Coulter, Indianapolis, IN, USA). For the flow cytometry gating strategy, singlets were first identified by a forward scatter area (FSC-A) and forward scatter height (FSC-H) gate, and then by an FSC-A and side scatter area (SSC-A) gate. The fluorescence of 10'000 HepG2 cells from five independent replicates for each condition was quantified using the FL-5-A channel and analyzed with the FlowJo software (Tree Star, Ashland, OR, USA).

2.5. Fluorescence microscopy with LTDR

We assessed the lysosomal morphology with a fluorescence microscope using LTDR and Hoechst 33342 (Sigma-Aldrich, 14533) as lysosomal and nuclear staining, respectively. In brief, HepG2 cells were grown into a six channel (18'000 cells/channel) ibiTreat μ-Slide VI 0.4 (ibidi, 80606) and treated with imatinib (10 μM) and lapatinib (5 μM) for 24 h. We stained the cells with 100 μL/channel LTDR (100 nM) and Hoechst 33342 (1 μM) dissolved in cell culture medium (1 h, 37 °C, protected from light). Then, we washed and covered the cells with cell culture medium and acquired microscopic pictures with an Olympus IX83 microscope (Olympus, Tokyo, Japan).

2.6. Acridine orange redistribution

We assessed the redistribution of acridine orange (AO) hydrochloride (Bio-Techne, 5092) as a measure of lysosomal pH and stability (Palmgren, 1991). AO exhibits red and green fluorescence when located in acidic compartments (e.g., lysosomes) and cytosol, respectively. An increased ratio of AO green-to-red indicates a loss of lysosomal pH gradient and/or decreased lysosomal stability (Yoshimori et al., 1991). HepG2 cells seeded in a black-walled 96-well plate (25'000 cells/well) were incubated with AO (5 μM) diluted in cell culture medium (15 min, 37 °C, protected from light). Afterward, the cells were washed with medium and treated with imatinib and lapatinib for 6 h or 24 h. As lysosomal pH-raising drugs, bafilomycin A1 (0.1 μM) and chloroquine (30 μM) were used as positive controls (Poole and Ohkuma, 1981; Yoshimori et al., 1991). After the treatment, we covered the cells with PBS and measured the red ($\lambda_{ex./em.}$ = 460⁄650 nm) and green ($\lambda_{ex./em.}$ = 495⁄530 nm) fluorescence using a microplate reader (Infinite 200 PRO, Tecan Group, Männedorf, Switzerland). After the measurement, we lysed the cells with radioimmunoprecipitation (RIPA) buffer (60 μL/well) and determined the protein concentration of each well using the Pierce BCA Protein Assay Kit (Thermo Fisher Scientific, 23225). The fluorescence intensities were normalized to the protein concentration and the ratio green-to-red AO fluorescence was calculated. We run the experiment with at least three independent replicates for each condition.

2.7. Flow cytometry with DQ-BSA

We investigated the lysosomal proteolytic activity of imatinib- and lapatinib-treated HepG2 cells using de-quenched green bovine serum albumin (DQ-BSA, Thermo Fisher Scientific, D12050) (Klionsky et al., 2016; Reis et al., 1998). DQ Green BSA consists of BSA conjugated to self-quenched Bodipy FL dye. After endocytosis and lysosomal accumulation, DQ Green BSA is degraded by lysosomal proteases releasing fluorescent ($\lambda_{ex./em.}$ = 505⁄515 nm) BSA-fragments (Fig. S7). HepG2 cells were seeded in a 24-well plate (150'000 cells/well) and treated with imatinib and lapatinib for 6 h and 24 h. Four hours before the treatment was completed, we pulsed the cells for 2 h with DQ Green BSA (100 μg/mL), which was followed by a 2 h-chase period. Both pulse and chase were conducted in the presence of the drug. Finally, the cells were harvested using TrypLE express enzyme, transferred to a V-bottom 96-well plate, and pelleted by centrifugation (400 *g*, 5 min). We resuspended the cells in pre-warmed (37 °C) cell culture medium and analyze them with the CytoFLEX flow cytometer. Singlets were gated as described above. The fluorescence of 10'000 HepG2 cells was quantified using the FL-1-A channel and analyzed with the FlowJo software. We run the experiment with five independent replicates for each condition.

2.8. Western blotting

Protein expression in imatinib-treated HepG2 cells was assessed by Western blotting as described before (Roos et al., 2020). In brief, we loaded denatured and reduced protein samples (10–20 μg protein) on a NuPage 4–12% Bis-Tris Gel (Thermo Fisher Scientific, NP0335BOX) and ran a one-dimensional gel electrophoresis. We used NuPAGE LDS sample buffer (Thermo Fisher Scientific, NP0007) and PageRuler prestained protein ladder (Thermo Fisher Scientific, 26617) as loading buffer and molecular weight marker, respectively. The separated proteins were transferred on a 0.2 μm nitrocellulose membrane (Bio-Rad, 1620112) using the eBlot L1 transfer sandwich (GenScript, L00724) and wet protein transfer system (GenScript, Piscataway, NJ, USA). The membrane was blocked under constant orbital shaking (1 h, at room temperature) with 5% (w/v) non-fat dried milk or BSA (as recommended by the manufacturer) in PBS containing 0.1% (v/v) Tween 20 (PBST). Subsequently, the membrane was incubated with the primary antibody diluted in 5% (w/v) non-fat dried milk or BSA in PBST under constant shaking (overnight, at 4 °C). To assess the protein phosphorylation, we used PhosphoSafe Extraction Buffer (Merck, 71296) and 5% (w/v) BSA in PBS containing 0.1% (v/v) Tween 20 as blocking buffer. The primary antibodies and dilutions are listed in Table S1. Glyceraldehyde-3-phosphate dehydrogenase (GAPDH) and Lamin B1 served as cytoplasmic and nuclear loading control, respectively. We run the experiments with at least three independent replicates for each condition.

2.9. Cytoplasmic and nuclear protein extraction

We used the NE-PER Nuclear and Cytoplasmic Extraction Reagents (Thermo Fisher Scientific, 78833) to obtain nuclear and cytoplasmic protein fractions from imatinib-treated HepG2 cells seeded in a 6-well plate (500'000 cells/well). The buffer volumes were chosen according to the pellet size as recommended by the manufacturer's protocol. We first harvested the cells covered with ice-cold cytoplasmic extraction reagent I with a cell scraper, transferred them to a 2 mL-Eppendorf tube, and vortexed each lysate for 15 s. After incubation on ice for 10 min, we added ice-cold cytoplasmic extraction reagent II, vortexed for 5 s, and incubated for 1 min on ice. We subsequently centrifuged the sample (5 min, 16'000 *g*) and obtained the cytoplasmic protein fraction (supernatant). The remaining pellet was further incubated for 40 min on ice in ice-cold nuclear extraction reagent (vortexing every 10 min). After centrifugation (16'000 *g*, 10 min), we obtained the nuclear protein fraction (supernatant). We run the experiment with three independent replicates for each condition and stored the fractions at -80 °C until analysis.

2.10. Quantitative PCR

We run a quantitative PCR to assess the mRNA expression of TFEB-regulated genes in HepG2 cells treated with imatinib for 6 h or 24 h. In brief, we first extracted and purified RNA from imatinib-treated HepG2 cells seeded in a 6-well plate (2×10^6 cells/well) using QIAshredders (Qiagen, 79656) and the Rneasy mini kit (Qiagen, 74104). We determined the purity and concentration of each RNA extract using the NanoDrop One (Thermo Fisher Scientific, Basel, Switzerland) and synthetized complementary DNA of 1 μg RNA with the Omniscript system (Qiagen, 205113). Specific DNA templates were amplified using specific

forward and reverse primers (listed in Table S2) and detected using a DNA double-strand-binding fluorescent dye (FastStart Universal SYBR Green Master, Sigma-Aldrich, 4913914001). We run the qPCR on an ABI PRISM 7700 sequence detector (PE Biosystems, Switzerland) equipped with the ViiA7 software (Life Technologies, Switzerland). We run the experiment with four independent replicates and applied the comparative Ct method (ΔΔCt) to determine the relative mRNA expression normalized to *GAPDH*.

2.11. mTOR/FKBP12 kinase activity in a cell-free assay

The mTOR/FKBP12 Human PIKK Kinase Enzymatic Radiometric Assay (14-769FKKP10) was performed by Eurofins Cerep SA according to their online protocol. In brief, human mTOR/FKBP12 was incubated with 50 mM HEPES (pH 7.5), 1 mM EGTA, 0.01% Tween 20, 2 mg/mL mTOR substrate (C-terminal fragment of p70S6K), 10 μM FKBP12, 3 mM $MnCl_2$, and 10 μM [gamma-33P]-ATP. PI-103, an ATP-competitive mTOR inhibitor, was used as control inhibitor and added to the blank. The reaction was initiated by adding the Mn/ATP mix. After incubation (40 min, room temperature), the reaction was stopped with phosphoric acid to a concentration of 0.5%. Then, 10 μL of the reaction mixture was spotted onto a P30 filter mat and washed four times for 4 min with 0.425% phosphoric acid as well as once with methanol. The sample was dried and subjected to scintillation counting. Eight concentrations in the range of 0.5–100 μM imatinib were tested in triplicates. The counts of the blank containing PI-103 were set as zero, representing full mTOR inhibition. After subtracting the blank, the counts were related to the control, which was considered as 100% active.

2.12. Transmission electron microscopy

We fixed 5 Mio imatinib-treated HepG2 cells (confluency less than 70%) with 1:1 (v/v) cell culture medium/2x fixative mixture (4% paraformaldehyde, 5% glutaraldehyde, in 0.1 M PIPES buffer, pH 7.0, 37 °C) at room temperature. After 20 min, we replaced the medium/2x fixative mixture with fresh 1x fixative mixture (2% paraformaldehyde, 2.5% glutaraldehyde, in 0.1 M PIPES buffer, pH 7.0) and harvested the cells with a cell scraper. The cells were subsequently pelleted (500 *g*, 5 min) and fixed again in fresh 1x fixative mixture (15 min, room temperature). We carefully dislodged the pellet from the tube and continued the fixation (45 min, 4 °C). Then, the cells were pelleted (500 *g*, 5 min), washed three times with 0.1 M PIPES buffer (pH 7.0), and embedded in low-melting point agarose (Sigma-Aldrich, A2576). From the cell-containing solid agarose plug, 1- to 2-mm cubes were trimmed, washed with PBS (10 min), and post-fixed in 1% buffered osmium tetroxide (1h, 4 °C). After rinsing with distilled water, the cubes were stained in aqueous uranyl acetate (1h, 4 °C, protected from light) and subsequently dehydrated in an ethanol (v/v) series (30, 50, 75, 95, and 100%). After three changes of absolute ethanol, the cubes were washed in acetone and embedded in a mixture of resin/acetone followed by pure Epon 812 resin (48 h, 60 °C). Semi-thin sections were cut from the hardened epoxy resin block using a glass knife followed by thinning with a diamond knife. Finally, the thin sections were placed on copper grids, impregnated with uranyl acetate and lead citrate, and analyzed using a FEI Tecnai T12 Transmission Electron Microscope (FEI Technologies Inc., OR, USA) operating at 80 kV. Images were recorded using a CCD Veleta digital camera.

2.13. Annexin V/propidium iodide staining

We used the annexin V Alexa Fluor 488 and propidium iodide (PI) kit (V13245) from Thermo Fisher Scientific to assess the number of apoptotic, necrotic, and viable HepG2 cells after exposure to imatinib. We treated HepG2 cells seeded in a 24-well plate (200'000 cells/well) with imatinib for 6 h and 24 h. Staurosporine (200 nM) and doxorubicin (0.5 μM) were used as positive controls for apoptosis and necrosis, respectively. After the treatment, we harvested the cells with TrypLE express enzyme, transferred them to a V-well plate, and centrifuged the cells (400 *g*, 5 min). The cell pellet was resuspended in 1X annexin-binding buffer (50 μL/well) containing Alexa Fluor 488 annexin V (5 μL/100 μL) as well as PI (0.1 μg/100 μL) and subsequently incubated for 30 min (4 °C, protected from light). HepG2 cells were analyzed with a CytoFLEX flow cytometer. For the flow cytometry gating strategy, singlets were first identified by an FSC-A and an FSC-H gate, and then 10'000 cells per sample were counted in an FSC-A and an SSC-A gate. Apoptotic cells showed green fluorescence (measured in FL-1-A:FITC channel), necrotic cells showed both green and red fluorescence (measured in FL-1-A:FITC and FL-3-A:PC5.5, respectively), while viable cells were not fluorescent. Results were analyzed using the FlowJo software. We run the experiment with four independent replicates.

2.14. Statistical analysis

Experimental data are presented as the mean ± SEM. The number of independent replicates for each experiment is indicated in the respective material and method section. We performed an ANOVA with Dunnett's multiple comparison test using GraphPad prism version 8.2.1 (GraphPad Software, San Diego, USA). Significant values (p-value <0.05) compared to the negative control were indicated with an asterisk (*).

3. Results

3.1. Imatinib and lapatinib increase the volume of the lysosomal compartment

As shown in Fig. 1A, imatinib increased the lysosomal volume in a concentration- and time-dependent manner showing the most pronounced effect at 6 h. After treatment for 0.5 and 6 h, imatinib started to increase the lysosomal volume at 5 μM, reaching significance at ≥10 μM. After treatment for 24 h, imatinib enlarged the lysosomal volume at ≥20 μM. Lapatinib significantly increased the lysosomal volume at concentrations ≥2 μM after ≥0.5 h-treatment with most pronounced effects after 6 h (Fig. 1B). In contrast to imatinib, the increase induced by lapatinib showed a plateau-like effect with increasing concentrations.

Fluorescence microscopy of HepG2 cells (Fig. 1C) and HuH-7 cells (Fig. S1) exposed for 24 h to 10 μM imatinib or 5 μM lapatinib showed that both TKIs strongly increased number and size of lysosomes compared to untreated control cells in both cell lines derived from human hepatomas.

3.2. Imatinib and lapatinib increase the lysosomal pH and perturb the lysosomal proteolytic activity

Next, we assessed the effect of imatinib and lapatinib on the lysosomal pH and membrane integrity by acridine orange (AO) staining. Imatinib redistributed AO into the cytosol at concentrations ≥20 μM after 6 h of treatment, leading to a significantly increased green-to-red AO ratio (Fig. 2A), while concentrations ≤10 μM had no effect on lysosomal pH at both 6 and 24 h. Like imatinib, lapatinib significantly elevated the green-to-red AO ratio at 10 and 20 μM at 6 h, while concentrations ≤5 μM had no effect (Fig. S2A). Thus, both imatinib and lapatinib perturbed the lysosomal pH and/or membrane stability in a concentration-dependent manner, with significant changes at the two highest concentrations tested.

Lysosomes contain more than 60 hydrolases (e.g., proteases), whose optimal activities are in an acidic environment (Xu and Ren, 2015). Since an increased lysosomal pH could impair protease activity, we investigated the effect of the TKIs on lysosomal protein degradation using fluorescent DQ-BSA. Bafilomycin A1, chloroquine, and amiodarone increased the percentage of cells with low (DQ-BSA^{neg} cells) lysosomal proteolytic activity, while the mTORC1 inhibitor rapamycin increased the percentage of cells with high (DQ-BSA^{high} cells) lysosomal

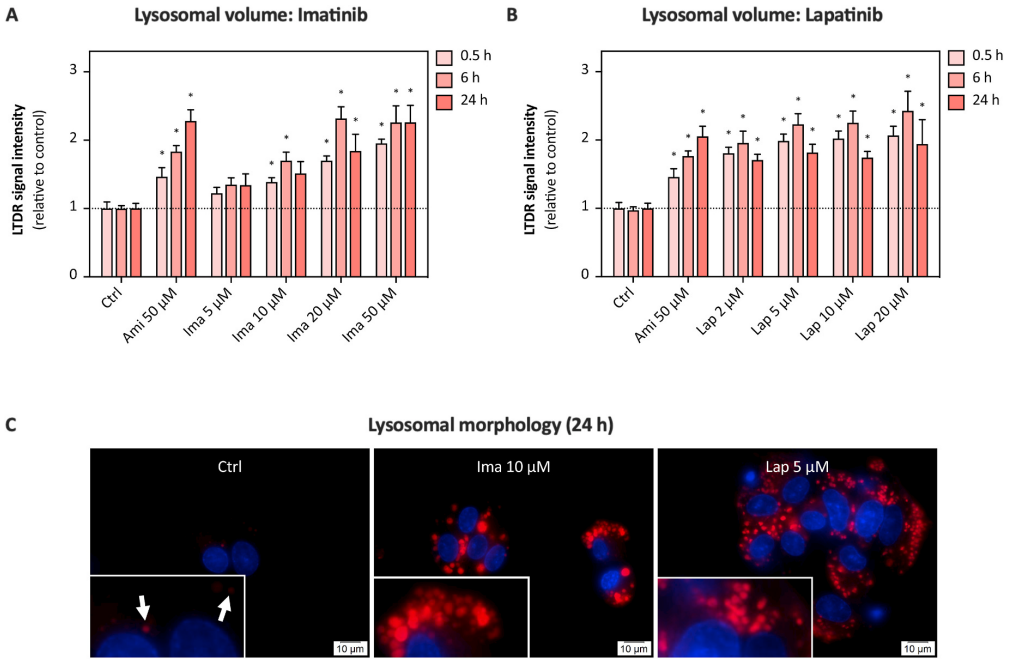

Fig. 1. Lysosomal volume and morphology. The volume of the lysosomal compartment was assessed by LysoTracker Deep Red (LTDR) staining in HepG2 cells treated with (**A**) imatinib (5–50 µM) and (**B**) lapatinib (2–20 µM) for 0.5 h, 6 h, and 24 h. Data are shown as fold increase relative to the negative control (ctrl) and are the mean ± SEM of at least five independent replicates. *$p < 0.05$ versus negative control. (**C**) Representative microscopic pictures of untreated HepG2 cells (ctrl) and HepG2 cells treated with 10 µM imatinib or 5 µM lapatinib for 24 h. Lysosomes (red) and nuclei (blue) were stained with LTDR and Hoechst 33342, respectively. Ima: Imatinib; Lap: lapatinib; Ami: amiodarone (positive control).

proteolytic activity (Figs. S3A and S3B). Imatinib significantly increased the percentage of DQ-BSA^{high} cells up to 20 µM at both 6 and 24 h, while 50 µM imatinib abolished the lysosomal proteolytic activity at both time points (Figs. S3A and S3B). Similarly, HepG2 cells exposed to lapatinib for 6 and 24 h showed a significantly increased lysosomal proteolytic activity up to 20 µM (Figs. S3A and S3B), while 24 h-treatment with 20 µM lapatinib resulted in a significant population of DQ-BSA^{neg} cells.

Since both imatinib and lapatinib increased the volume of the lysosomal compartment, we normalized the DQ-BSA signal intensity to the lysosomal volume. Upon normalization, 5 µM imatinib had no significant effect on lysosomal proteolytic activity, whereas 10 µM imatinib enhanced lysosomal proteolysis up to 6 h, but not up to 24 h (Fig. 2B). In comparison, 20 µM imatinib started to decrease lysosomal proteolytic activity at 24 h, and 50 µM imatinib after ≥6 h. For lapatinib, we observed a decreased lysosomal proteolytic activity starting at 20 µM (Fig. S2B). The decreased lysosomal protease activity at ≥20 µM imatinib and lapatinib corresponds to the observed increase in lysosomal pH at these concentrations. Since the effects of lapatinib on lysosomal morphology and function were less pronounced compared to imatinib, the following investigations were performed only for imatinib.

3.3. Imatinib interferes with cathepsin B activation

CTSB, one of the main lysosomal cysteine proteases, is synthetized as an inactive pro-enzyme in the endoplasmic reticulum and, while being transported to the lysosomes, processed to an active single chain form (Kominami et al., 1988). In the lysosome, the single chain (sc) is further processed to a two-chain form composed of a heavy (hc) and light chain. As shown in Fig. 2C and D, the expression of the sc-CTSB increased in a concentration-dependent manner up to 20 µM imatinib but dropped at 50 µM. In comparison, the expression of the hc-CTSB was significantly decreased at imatinib concentrations ≥5 µM. Total (sc- & hc-CTSB) CTSB was not affected up to 20 µM imatinib, while 50 µM caused a significant drop (Fig. S2C).

Accumulation of sc-CTSB and decreased formation of hc-CTSB indicated impairment of lysosomal proteolytic processing of CTSB by imatinib, confirming the results of the previous section.

3.4. Imatinib induces nuclear translocation of TFEB and upregulates the expression of lysosomal genes

Lysosomal dysfunction can activate the transcription factor TFEB, which stimulates lysosomal biogenesis (Puertollano et al., 2018). Under normal conditions, TFEB is phosphorylated and retained in the cytoplasm, while stressors such as starvation reduce phosphorylation and favor translocation into the nucleus (Puertollano et al., 2018). As shown in Fig. 3A and B, imatinib caused a decrease in cytoplasmic TFEB starting at 6 h and 5 µM, reaching statistical significance at ≥20 µM. In parallel, TFEB gradually accumulated in the nuclear fraction, reaching significance at ≥20 µM imatinib. In comparison, treatment for 0.5 h stimulated the import of TFEB into the nucleus only at the highest imatinib concentration (Fig. S4).

Nuclear TFEB binds to specific palindromic 10-base pair DNA sequences called coordinated lysosomal expression and regulation (i.e., CLEAR) elements (Sardiello et al., 2009), which are present in promotors of various genes encoding lysosomal proteins. Thus, we quantified the mRNA expression of the lysosomal associated membrane protein 1 (*LAMP1*), the ATPase H^+ transporting V1 subunit H (*ATP6V1H*), and

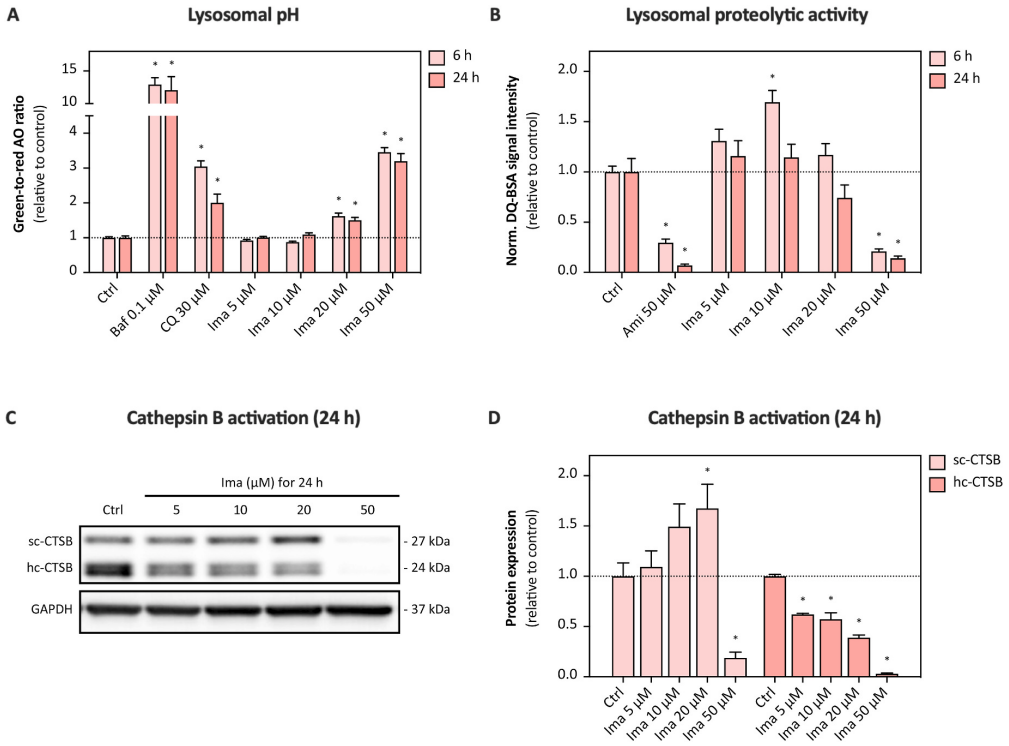

Fig. 2. Lysosomal pH and proteolytic activity. (**A**) Lysosomal pH assessed by acridine orange (AO) staining (ratio of green-to-red fluorescence) in HepG2 cells treated with imatinib (5–50 µM) for 6 h and 24 h. Bafilomycin A1 (Baf) and chloroquine (CQ) represent the positive controls. Data are shown as fold increase relative to the negative control (ctrl) and are the mean ± SEM of at least three independent replicates. *p < 0.05 versus negative control. (**B**) Lysosomal proteolytic activity assessed by DQ-BSA staining (normalized to the lysosomal volume) in HepG2 cells treated with imatinib (5–50 µM) for 6 h and 24 h. Amiodarone (Ami) represents the positive control. Data are shown as fold increase relative to the negative control (ctrl) and are the mean ± SEM of five independent replicates. *p < 0.05 versus negative control. (**C**) Representative Western blot and (**D**) quantification of cathepsin B (CTSB) in HepG2 cells treated with imatinib (5–50 µM) for 24 h. Single-chain (sc) CTSB and heavy-chain (hc) CTSB represent differently processed CTSB forms. GAPDH represents the loading control. Data are shown as fold increase relative to the negative control (ctrl) and are the mean ± SEM of four independent replicates. *p < 0.05 versus negative control. Ima: Imatinib.

cathepsin B (*CTSB*) in HepG2 cells exposed to imatinib for 6 h (Figs. 3C) and 24 h (Fig. 3D). Treatment with imatinib for 6 h did not affect mRNA expression of *LAMP1*, *ATP6V1H*, and *CTSB* (Fig. 3C), whereas their mRNA expression was increased at imatinib concentrations ≥10 µM after 24 h (Fig. 3D).

3.5. Imatinib reduces the activity of mTORC1

To investigate closer the mechanism of TFEB activation, we assessed the activity of the protein complex mTORC1 in imatinib-treated HepG2 cells. Among other kinases (i.e., AKT serine/threonine kinase 1 [AKT1], glycogen synthase kinase 3 beta [GSK3B], mitogen-activated protein kinase 1/3 [MAPK1/3]), mTORC1 is considered as the main negative regulator of TFEB activity (Roczniak-Ferguson et al., 2012). We evaluated the activity of mTORC1 in imatinib-treated HepG2 cells by assessing the phosphorylation state of Unc-51 like autophagy activating kinase 1 (ULK1), ribosomal protein S6 (RPS6), and eukaryotic translation initiation factor 4E binding protein 1 (EIF4EBP1), three well-established mTORC1 substrates (Kim et al., 2011; Sanvee et al., 2019). Upon treatment for 6 h, the phosphorylation of ULK1 (S757), RPS6 (S235/236), and EIF4EBP1 (S65) decreased in a concentration-dependent manner starting at 10 µM imatinib and reaching significance at ≥20 µM (Fig. 4A and B). The activity of mTORC1 further decreased with treatment for 24 h (Fig. 4C and D). After 0.5 h, the activity of mTORC1 was reduced at 50 µM imatinib (Fig. S5).

3.6. Imatinib does not impair the activity of activating kinases upstream of mTORC1

mTORC1 is activated on the lysosomal membrane by the GTPase RHEB, the activity of which is inhibited by the TSC complex (TSC1/2) (Sancak et al., 2010). Since TSC1/2 activity is regulated by AKT1, MAPK1/3, and PRKAA, a reduced activity of one of these kinases could impair mTORC1 activity (Kwiatkowski and Manning, 2005). AKT1 is activated by phosphorylation at T308 and S473 by the insulin signaling pathway and mTORC2, respectively (Sanvee et al., 2019). Imatinib treatment for 24 h increased the phosphorylation of AKT1 in a concentration-dependent manner starting at 5 µM for S473 and at 10 µM for T308 (Fig. 5A and B), while treatment for 6 h numerically enhanced the serine site phosphorylation at ≥20 µM (Figs. S6A and S6B). Beside TSC1/2, AKT1 phosphorylates GSK3B at S9, leading to GSK3B inactivation. Imatinib increased the phosphorylation of GSK3B (S9) in a concentration-dependent manner, reaching significance at ≥20 µM (Fig. 5A and B). Similar to AKT1, the phosphorylation of MAPK1/3 at T202 and Y204 increased, reaching the highest effects at 50 µM and 20 µM imatinib after 6 h (Fig. S6A and S6C) and 24 h (Fig. 5C and D), respectively. PRKAA, which is activated by phosphorylation at T172, showed no increase in T172 phosphorylation at both treatment times (Fig. 5C and D, Figs. S6A and S6C). While AKT1 and MAPK1/3 inhibit

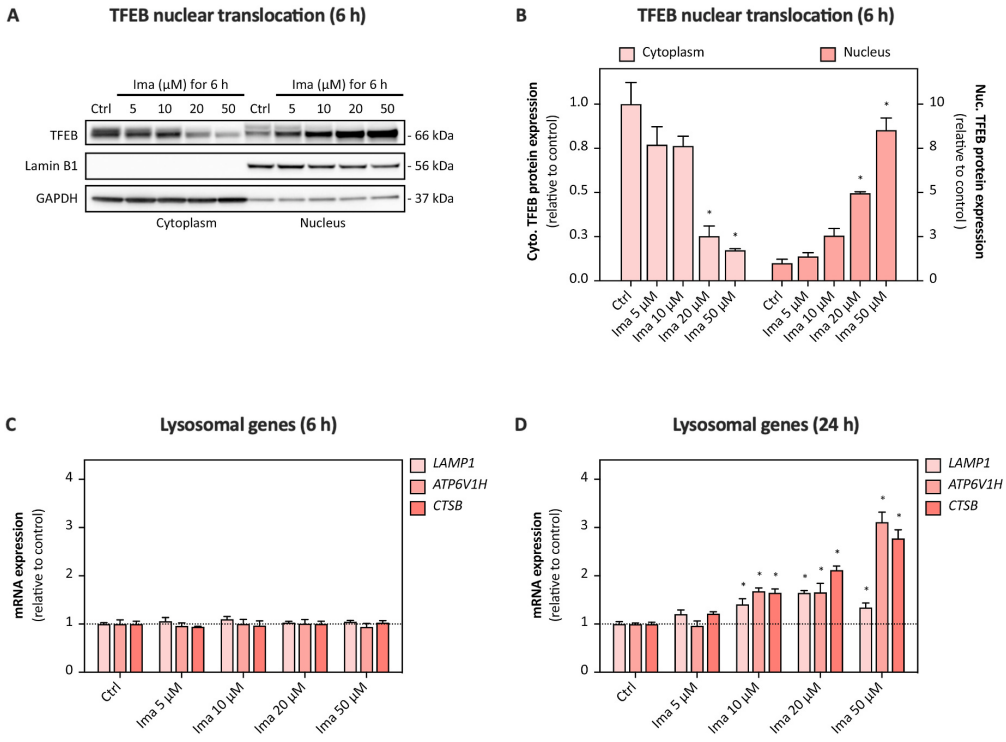

Fig. 3. Activation of transcription factor EB (TFEB). (**A**) Representative Western blot and (**B**) quantification of TFEB in cytoplasmic and nuclear fraction of HepG2 cells treated with imatinib (5–50 μM) for 6 h. Lamin B1 and GAPDH served as nuclear and cytoplasmic loading control, respectively. Data are shown as fold increase relative to the negative control (ctrl) and are the mean ± SEM of three independent replicates. *p < 0.05 versus negative control. Gene expression of lysosomal genes (*LAMP1*, *ATP6V1H*, *CTSB*) in HepG2 cells treated with imatinib (5–50 μM) for (**C**) 6 h and (**D**) 24 h. Data are shown as fold increase relative to the negative control (ctrl) and are the mean ± SEM of four independent replicates. *p < 0.05 versus negative control. Ima: Imatinib; *LAMP1*: Lysosomal associated membrane protein 1; *ATP6V1H*: ATPase H^+ transporting V1 subunit H; *CTSB*: Cathepsin B.

the activity of TSC1/2, PRKAA acts as an activator. Thus, inhibition of mTORC1 by imatinib did not result from AKT1 or MAPK1/3 inactivation or PRKAA activation. Moreover, a cell-free assay of the mTORC1 activity excluded a direct inhibition of mTORC1 by imatinib (Fig. 5E). This means that lysosomal dysfunction is the most probable explanation for impaired function of mTORC1 in HepG2 cells treated with imatinib.

3.7. Imatinib induces the transcription of autophagy genes and initiates autophagy

mTORC1 and TFEB connect lysosomal biogenesis to autophagy, a catabolic process by which unnecessary or dysfunctional cytoplasmic components are delivered to lysosomes for degradation (Settembre et al., 2011). To study the effect of imatinib on autophagy, we assessed the mRNA expression of beclin 1 (*BECN1*), sequestosome 1 (*SQSTM1*), microtubule associated protein 1 light chain 3 beta (*MAP1LC3B*), and UV radiation resistance associated gene (*UVRAG*), whose expression is controlled by TFEB. Upon treatment for 6 h, imatinib increased the expression of these genes at concentrations ≥20 μM (Fig. 6A), which is in line with TFEB nuclear translocation described above. After 24 h, the expression of *BECN1*, *SQSTM1*, *MAP1LC3B*, and *UVRAG* further increased, reaching significance ≥10 μM imatinib (Fig. 6B).

In mammalian cells, autophagy is initiated by a protein complex composed of ULK1, autophagy related protein 13 (ATG13), ATG101, and the focal adhesion kinase interacting protein of 200 kDa. Impaired activity of mTORC1 stimulates ULK1, which activates ATG13 by phosphorylation at S318 (Egan et al., 2015). Imatinib increased the phosphorylation of ATG13 (S318) starting at 5 μM, reaching significance at 10 and 20 μM upon 6 h of treatment (Fig. 7A and B). At 24 h, phosphorylation of ATG13 S318 was significantly increased at 5–20 μM imatinib and more pronounced than after 6 h (Fig. 7C and D).

Initiation of autophagy leads to the formation of new autophagosomes. The lipidated form of MAP1LC3A/B is integrated in the autophagosomal membranes and can be used as a marker for autophagosome accumulation (Klionsky et al., 2016). The 6 h-treatment with imatinib increased MAP1LC3A/B-II expression at 5 and 10 μM imatinib (Fig. 7A and B). After 24 h, the expression of MAP1LC3A/B-II was significantly increased at concentration between 5 and 20 μM imatinib and more pronounced than after 6 h (Fig. 7C and D), indicating accumulation of autophagosomes over time. The expression of the autophagy adaptor protein SQSTM1 significantly increased after 24 h imatinib exposure at ≥5 μM (Fig. 7C and D), while no increase was observable after 6 h (Fig. 7A and B).

To qualitatively assess the accumulation of autophagic vacuoles (e.g., autophagosomes, autolysosomes), we acquired electron micrographs of imatinib-treated HepG2 cells. A concentration of 10 μM imatinib applied for 24 h increased the number of autophagosomes (i.e., membrane-bound vacuoles containing morphologically intact cytoplasmic material) in HepG2 cells compared to the control cells (Fig. 7E). Among other materials, the autophagosomes of HepG2 cells treated with 10 μM imatinib contained electron-dense lysosomes. Chloroquine (30 μM) increased the size of lysosomes and prevented the degradation of autophagic cargo, which can be explained by the reduced lysosomal proteolytic activity (Fig. S3B). In contrast to control cells and HepG2

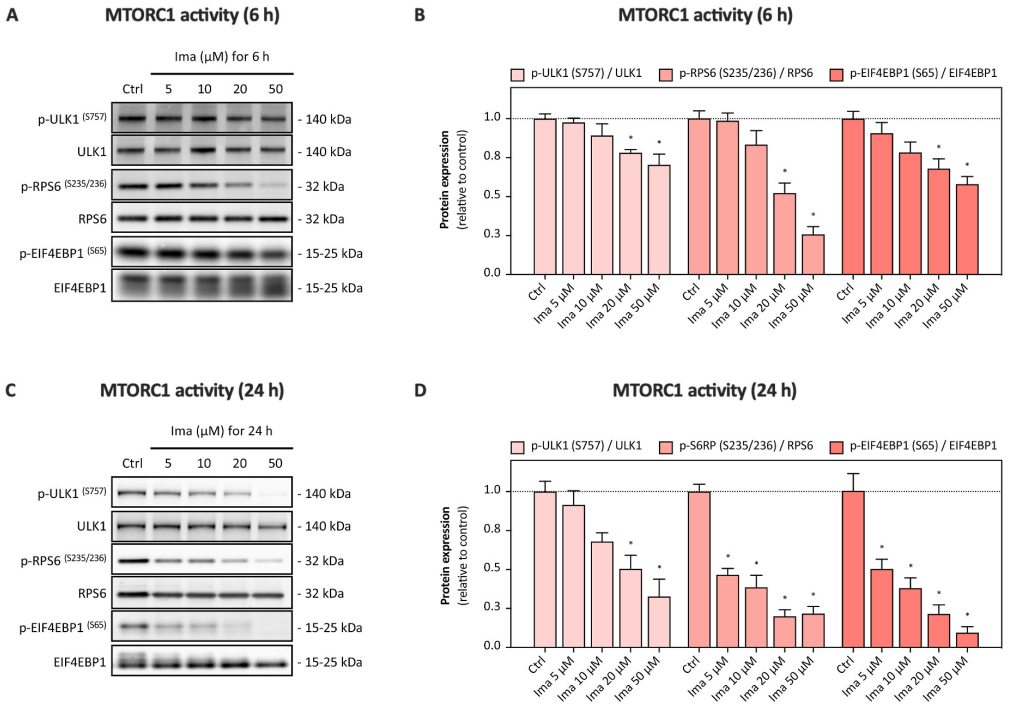

Fig. 4. Activity of mTOR complex 1 (mTORC1). (**A**, **C**) Representative Western blots and (**B**, **D**) quantification of phosphorylated mTORC1 substrates (ULK1, RPS6, and EIF4EBP1) in HepG2 cells treated with imatinib (5–50 μM) for (**A**, **B**) 6 h and (**C**, **D**) 24 h. The phosphorylation states of ULK1 (S7575), RPS6 (S235/236), and EIF4EBP1 (S65) were assessed using phospho-specific antibodies and normalized to the expressions of the total protein. Data are shown as fold increase relative to the negative control (ctrl) and are the mean ± SEM of at least three independent replicates. *p < 0.05 versus negative control. Ima: Imatinib; ULK1: Unc-51 like autophagy activating kinase 1; RPS6: Ribosomal protein S6; EIF4EBP1: Eukaryotic translation initiation factor 4E binding protein 1.

cells treated with chloroquine, imatinib-treated cells comprised also electron-translucent vacuoles containing cytoplasmic material at various stages of degradation, representing active autolysosomes.

3.8. Imatinib induces apoptosis in HepG2 cells in a concentration-dependent manner

Release of lysosomal hydrolases into the cytoplasm upon permeabilization of the lysosomal membrane and accumulation of undegraded material can induce apoptosis and necrosis (Boya and Kroemer, 2008). Having observed a disturbed lysosomal function, we finally assessed the effect of imatinib on cell death in HepG2 cells using the annexin V/PI staining. As expected, imatinib induced apoptosis in a concentration-dependent manner with a significant number of apoptotic cells at 50 μM after both 6 h and 24 h (Fig. 8A). Induction of apoptosis was by trend more pronounced at 6 than at 24 h, while necrosis was more pronounced after 24 h (Fig. 8B). Overall, the number of viable cells significantly decreased at imatinib concentrations ≥20 μM (Fig. 8C).

4. Discussion

The present study shows that the TKIs imatinib and lapatinib disturb lysosomal function and morphology in human hepatoma-derived cell lines, as demonstrated by an increase in the lysosomal volume fraction, perturbed lysosomal pH, and impaired proteolytic activity. Imatinib-induced lysosomal dysfunction was accompanied by activation of TFEB and impaired mTORC1 activity, which stimulated autophagy and apoptosis.

Imatinib is typically administered at doses of 400–800 mg daily, leading to steady state plasma concentrations in the range of 3.6–6.9 μM (Peng et al., 2005). Since imatinib is metabolized via cytochrome P450 3A4/5, inhibitors of these enzymes increase the plasma and probably also the hepatic concentrations of imatinib (Peng et al., 2005). For lapatinib, maximal plasma concentrations are between 4.1 and 7.4 μM and could also be higher when combined with cytochrome P450 3A4 inhibitors (Chu et al., 2007). In mice, the hepatic concentrations of imatinib and lapatinib have been reported to exceed the corresponding plasma concentrations by a factor of 5–10 (Gardner et al., 2009; Hudachek and Gustafson, 2013). Based on these considerations, most effects observed in the current investigations could therefore be relevant for patients treated with these drugs.

Lysosomotropic drugs are structurally diverse molecules of different drug classes including TKIs, which accumulate in acidic organelles (Nadanaciva et al., 2011). Lysosomes attract lipophilic, weakly basic drugs, which passively cross cell membranes in their neutral form and become trapped upon protonation, a phenomenon described as lysosomotropism (de Duve et al., 1974). Both imatinib and lapatinib are known to accumulate in lysosomes of several human cancer cell lines (Burger et al., 2015; Fu et al., 2014). For instance, in CML cells incubated for 1 h with 20 μM imatinib, the drug achieved lysosomal concentrations in the millimolar range (Fu et al., 2014). Similarly, Burger and co-workers found in several cell lines that after 0.5 h of incubation with imatinib the intracellular imatinib concentrations were 35- to >100-fold higher than in the incubation medium (Burger et al., 2015). The lysosomal accumulation occurred rapidly within 15 min and could be prevented by bafilomycin A1 (Burger et al., 2015), a proton pump V-ATPase

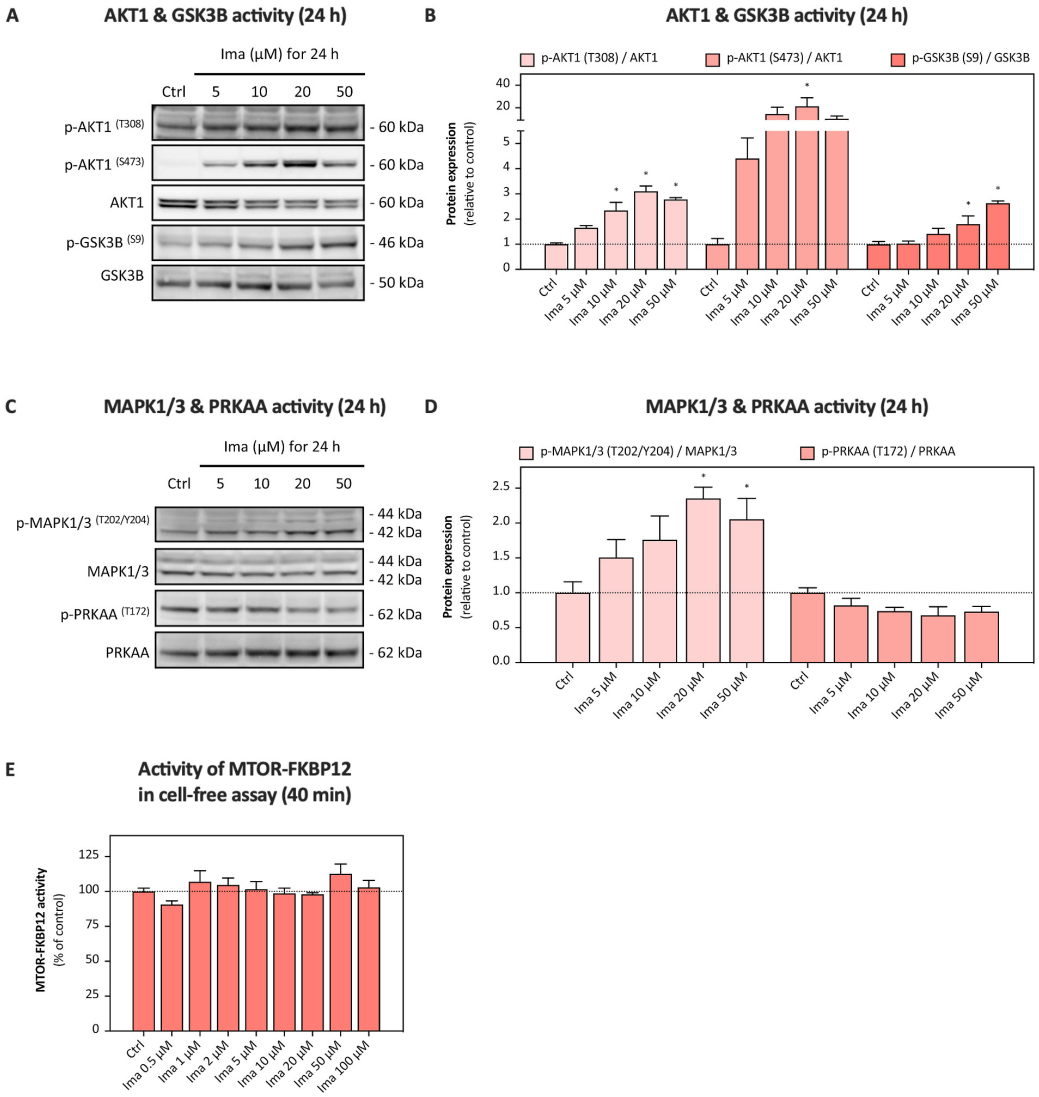

Fig. 5. Activity of kinases upstream of mTORC1 and mTORC1 activity in a cell-free assay. (**A**) Representative Western blots and (**B**) quantification of corresponding phosphorylation states of AKT1 and GSK3B in HepG2 cells treated with imatinib (1–50 µM) for 24 h. The phosphorylation of AKT1 (T308), AKT1 (S473), and GSK3B (S9) were assessed using phospho-specific antibodies and normalized to the expressions of the total protein. Data are shown as fold increase relative to the negative control (ctrl) and are the mean ± SEM of three to four independent replicates. *p < 0.05 versus negative control. (**C**) Representative Western blots and (**D**) quantification of corresponding phosphorylation states of MAPK1/3 and PRKAA1 in HepG2 cells exposed to imatinib (5–50 µM) for 24 h. The phosphorylation of MAPK1/3 (T202/Y204) and PRKAA (T172) were assessed using phospho-specific antibodies and normalized to the expressions of the total protein. Data are shown as fold increase relative to the negative control (ctrl) and are the mean ± SEM of three to four independent replicates. *p < 0.05 versus negative control. (**E**) Activity of mTOR-FKBP12 (assessed by the phosphorylation of the mTORC1 substrate p70S6K) in a cell-free, enzymatic assay upon incubation with imatinib for 40 min. Data are shown as percentage (%) of the negative control (ctrl) and are the mean ± SEM of three replicates. Ima: Imatinib; AKT1: AKT serine/threonine kinase 1; GSK3B: Glycogen synthase kinase 3 beta; MAPK1/3: Mitogen-activated protein kinase 1/3; PRKAA: Protein kinase AMP-activated catalytic subunit alpha 1 and 2; FKBP12: 12.6 kDa FK506-binding protein; p70S6K: 70 kDa ribosomal protein S6 kinase 1.

inhibitor, or by chloroquine (Fu et al., 2014), a stronger base than imatinib, confirming that the pH gradient is the driving force of this phenomenon.

Accumulation of lysosomotropic drugs in lysosomes is typically accompanied by an enlargement of the organelle (Funk and Krise, 2012; Lu et al., 2017), a cell type-independent effect already described for imatinib (Ertmer et al., 2007). We previously reported an increase in lysosomal volume in HepG2 cells by ponatinib, regorafenib, and sorafenib (Paech et al., 2018). In the present study, imatinib and lapatinib increased the lysosomal volume fraction after 0.5 h of incubation (Fig. 1A and C), a result in line with the reported rapid intracellular accumulation of imatinib (Burger et al., 2015). Fluorescence microscopy revealed that the size of lysosomes in cells exposed to imatinib or lapatinib largely exceeded the typical lysosomal size of 0.5–1 µm (Xu

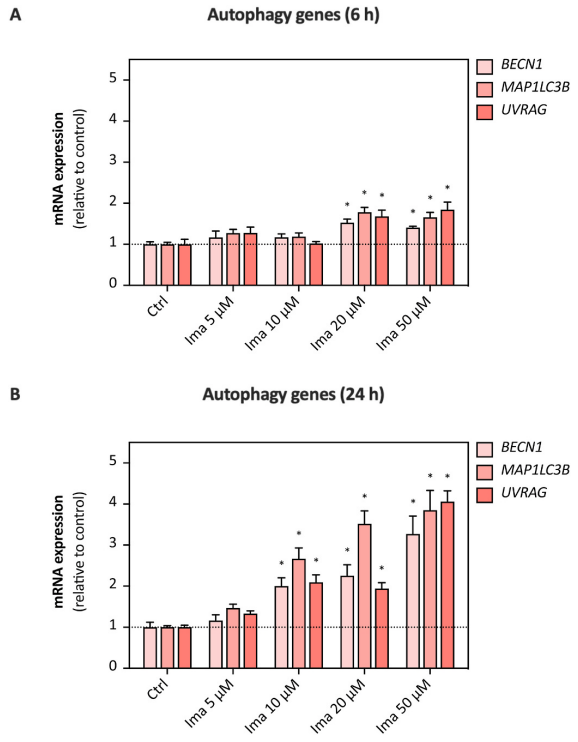

Fig. 6. Expression of autophagy genes. Gene expression of autophagic genes (*BECN1*, *SQSTM1*, *MAP1LC3B*, *UVRAG*) in HepG2 cells treated with imatinib (5–50 µM) for (**A**) 6 h and (**B**) 24 h. Data are shown as fold increase relative to the negative control (ctrl) and are the mean ± SEM of four independent replicates. *p < 0.05 versus negative control. Ima: Imatinib; *BECN1*: Beclin 1; *SQSTM1*: Sequestosome 1; *MAP1LC3B*: Microtubule associated protein 1 light chain 3 beta; *UVRAG*: UV radiation resistance associated gene protein.

and Ren, 2015). Osmotic water influx, impaired lysosomal vesicle trafficking, intercalation into the lysosomal membrane, and stimulated biogenesis are proposed mechanisms explaining an expansion of the lysosomal compartment (Morissette et al., 2008; Sardiello et al., 2009; Skoupa et al., 2020). In the current study, the rapid increase in lysosomal volume after exposure to imatinib or lapatinib is explained best by osmotic swelling, whereas intercalation into the lysosomal membrane and increased biogenesis may have contributed at later time points. As shown in the current and in a previous investigation (Paech et al., 2018), lysosomal accumulation of TKIs depends on the amphiphilic nature of these drugs, but not on the tyrosine kinase inhibited. The toxicity associated with lysosomal accumulation of TKIs may lead to adverse reactions such as hepatotoxicity and/or enhance the therapeutic efficacy of these drugs when tumor cells are affected.

Lysosomal biogenesis is regulated by mTORC1 and TFEB (Sardiello et al., 2009; Settembre et al., 2011). Since neither mTORC1 (Fig. S5) nor TFEB (Fig. S4) were affected after 0.5 h of exposure to imatinib, the early increase in the lysosomal volume cannot be explained by stimulation of biogenesis. However, after 6 h of exposure to imatinib, we observed impaired activity of mTORC1 and nuclear translocation of TFEB as well as increased transcription of lysosomal genes after 24 h, indicating stimulation of lysosomal biogenesis. At 24 h of exposure to imatinib and lapatinib, the lysosomal volume was generally numerically lower than at 6 h, which may be explained by the toxicity of these drugs. Similar to our findings, Skoupa and co-workers found that imatinib treatment for 6 h expanded the lysosomal volume in leukemia cells (Skoupa et al., 2020). However, they found no stimulation of lysosomal biogenesis and proposed Ca^{2+}-dependent lysosomal fusion as the principal mechanism. Furthermore, Lu and co-worker showed that chloroquine increased the protein expression of the lysosomal marker LAMP2 after 24 but not after 4 h, despite nuclear translocation of TFEB already after 1 h (Lu et al., 2017).

We not only observed an increase in lysosomal volume, but also an impairment of lysosomal function as evidenced by an elevation in the lysosomal pH and impaired proteolytic capacity. While the transiently increased degradation of DQ-BSA at low imatinib and lapatinib concentrations could be attributed to the raised lysosomal volume and proteolytic capacity, the decreased proteolytic activity at higher concentrations and longer exposure reflects a loss of lysosomal function. Lysosomes can degrade protein complexes and organelles through the autophagy-lysosome pathway (Klionsky et al., 2016). A dysfunction in this catabolic capacity has been associated with cell and organ damage, which can also affect the liver (Hara et al., 2006). Long-term treatment with imatinib and lapatinib could potentially decrease the hepatic degradation of long-lived proteins, as it has been observed for instance for siramesine (Ostenfeld et al., 2008).

As shown for concanamycin A and bafilomycin A1, a disturbed lysosomal function is associated with impaired activity of mTORC1 (Ostenfeld et al., 2008). When lysosomes function normally, mTOR is recruited to the lysosomal membrane in response to an increase in the amino acid concentration by four RRAG GTPases (RRAG A, B, C, and D) and LAMTOR, which is anchored in the lysosomal membrane through lipidation (Nada et al., 2009). Knock-down of RRAGC caused nuclear localization of TFEB, demonstrating that impaired docking of mTOR on the lysosomal surface is sufficient to stimulate TFEB nuclear translocation (Roczniak-Ferguson et al., 2012). Moreover, RHEB, the activator of mTORC1, is also attached to the lysosomal membrane (Sancak et al., 2010). Thus, damage of the lysosomal membrane, e.g., by fluidization, is a proposed mechanism of lysosomotropic drug-induced mTORC1 inhibition and TFEB activation (Zhitomirsky et al., 2018). Mechanistically, the hydrophobic ring-structure of imatinb could be incorporated into the lysosomal membrane, while the protonated amine group would face the lysosomal lumen. These detergent-like properties of lysosomotropic compounds could impair the integrity of the lysosomal membrane, as it has been shown for siramesine (Ostenfeld et al., 2008). Moreover, sequestration of lysosomes into autophagic vacuoles (Fig. 7E) diminishes the accessibility of this organelle for the recruitment of mTORC1. Since we have excluded impairment of the function of the main kinases responsible for mTORC1 phosphorylation and direct inhibition of mTORC1 by imatinib, disturbed lysosomal function appears to be most probable mechanism impairing the activation of mTORC1 by imatinib.

Beside by mTORC1, TFEB can be phosphorylated (and retained in the cytoplasm) by MAPK1, GSK3B, and AKT1 (Puertollano et al., 2018). The activities of AKT1 and MAPK1 were increased by imatinib (Fig. 5A–D, Fig. S6), excluding them as a cause for impaired TFEB phosphorylation. The phosphorylation of GSK3B was also increased in the presence of imatinib (Fig. 5A and B), inhibiting GSK3B activity. Impaired GSK3B activity could therefore have contributed to the imatinib-induced nuclear translocation of TFEB.

Inhibition of mTORC1, a well-established inhibitor of autophagy, and upregulation of the CLEAR gene network by TFEB are expected to stimulate autophagy in mammalian cells (Kim et al., 2011; Settembre et al., 2011). Accordingly, we observed activation of ULK1 (Fig. 4) and ATG13 (Fig. 7), upregulation of autophagic genes (Fig. 6) and increased levels of MAP1LC3A/B-II (Fig. 7) in HepG2 cells upon imatinib treatment. Our findings are in line with an earlier report that suggested stimulation of autophagy by imatinib in several mammalian cell types (Ertmer et al., 2007). However, the increased lysosomal pH and the impaired proteolysis suggest that the autophagic flux in the presence of imatinib is incomplete at a certain drug concentration. Several lysosomotropic drugs are known to be associated with ineffective autophagy

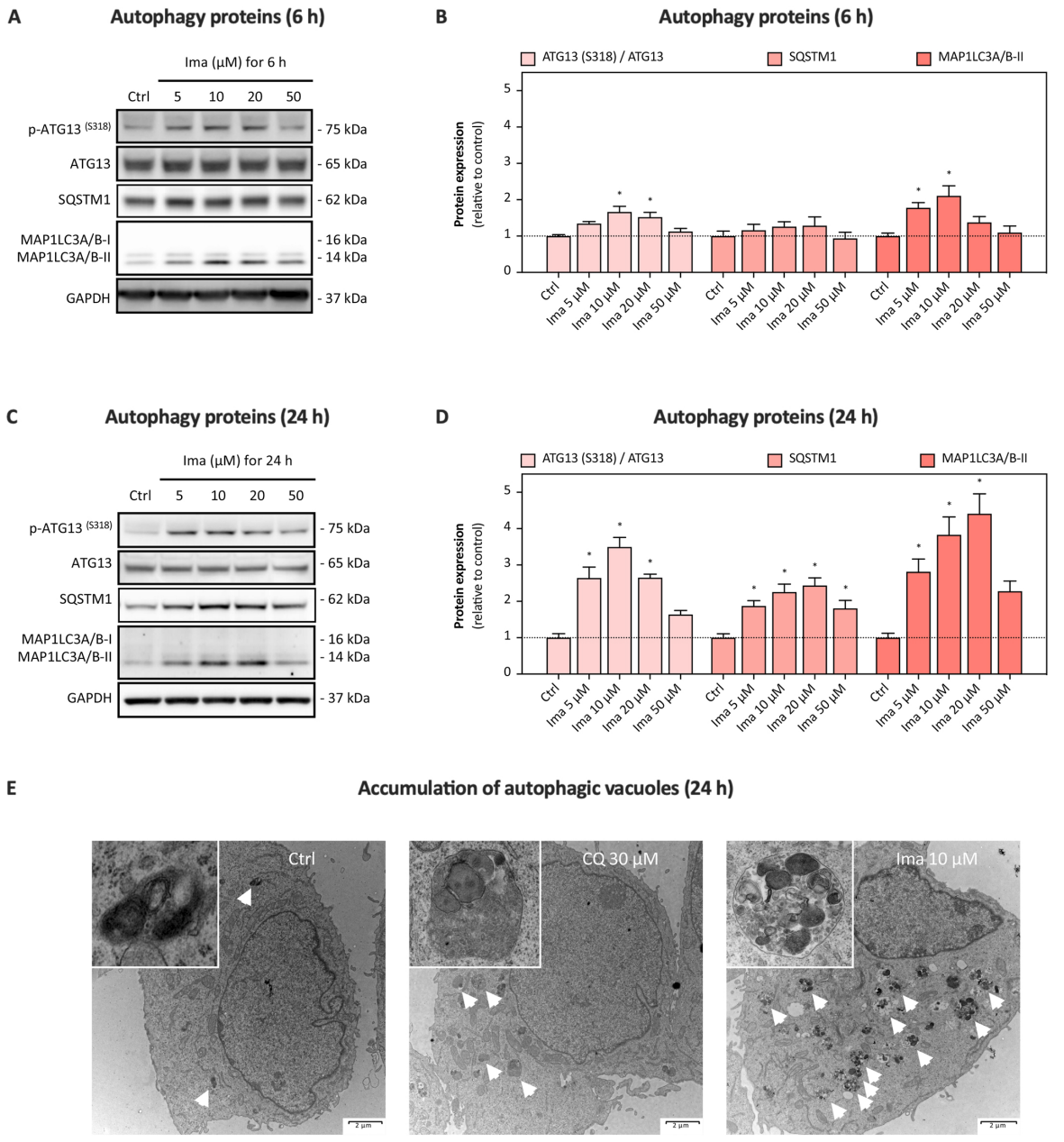

Fig. 7. Expression of autophagy proteins. (**A**) Representative Western blots and (**B**) quantification of phosphorylated ATG13 (S318), SQSTM1 and MAP1LC3A/B-I/II in HepG2 cells treated with imatinib (5–50 μM) for 6 h. The phosphorylation of ATG13 (S318) was assessed using a phospho-specific antibody and normalized to the expression of the total protein. Data are shown as fold increase relative to the negative control (ctrl) and are the mean ± SEM of three to four independent replicates. *p < 0.05 versus negative control. (**C**) Representative Western blots and (D) quantification of phosphorylated ATG13 (S318), SQSTM1 and MAP1LC3A/B-I/II in HepG2 cells treated with imatinib (5–50 μM) for 24 h. The phosphorylation of ATG13 (S318) was assessed using a phospho-specific antibody and normalized to the expression of the total protein. Data are shown as fold increase relative to the negative control (ctrl) and are the mean ± SEM of three to four independent replicates. *p < 0.05 versus negative control. (**E**) Representative electron microscopy micrographs of control (ctrl) HepG2 cells and cells exposed to chloroquine (30 μM) and imatinib (10 μM) for 24 h. The arrows indicate lysosomes (electron-dense, black vesicles) and autophagic vesicles (e.g., autophagosomes, autolysosomes). The scale bar represents a length of 2 μm. Ima: Imatinib; ATG13: Autophagy related protein 13; SQSTM1: Sequestosome 1; MAP1LC3A/B: Microtubule associated protein 1 light chain 3 alpha/beta, CQ: Chloroquine.

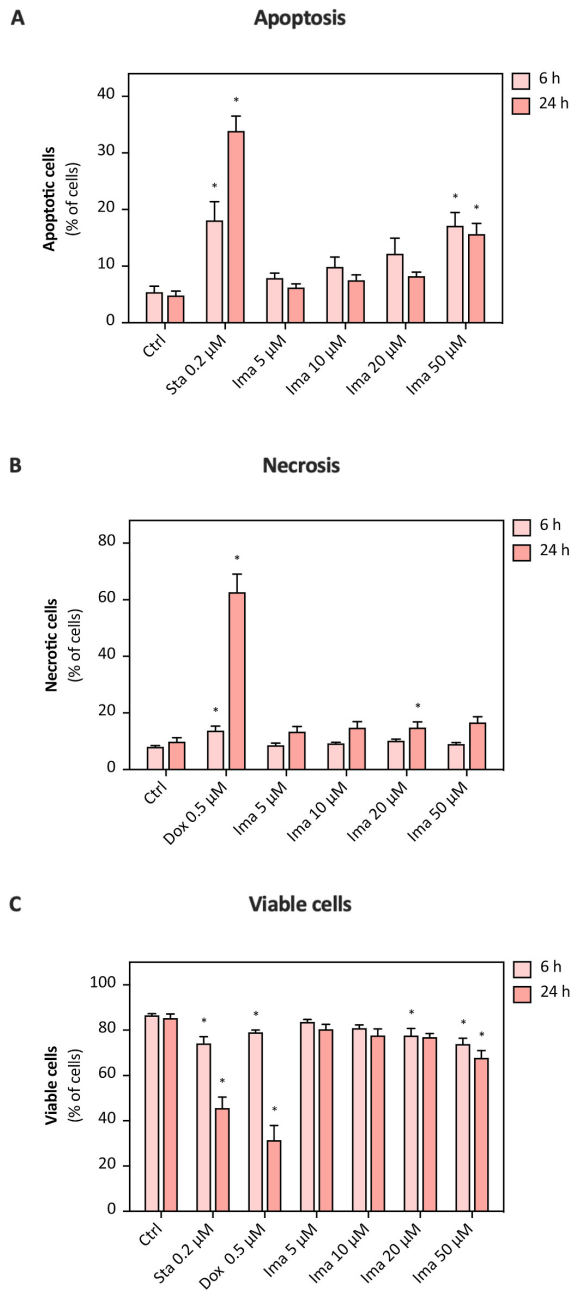

Fig. 8. Induction of apoptosis and necrosis. Percentage of (**A**) apoptotic, (**B**) necrotic and (**C**) viable HepG2 cells upon treatment with imatinib (5–50 µM) for 6 h and 24 h. Staurosporine (Sta) and doxorubicin (Dox) represent positive control for apoptosis and necrosis, respectively. The sum of apoptotic, necrotic, and viable cells was set as 100%. The percentage (%) of cells is shown as the mean ± SEM of four independent replicates. *$p < 0.05$ versus negative control. Ima: Imatinib.

(Morissette et al., 2009). Chloroquine, for instance, is a widely used late-stage inhibitor of autophagy (Klionsky et al., 2016). Ineffective autophagy can lead to lysosomal membrane permeabilization (LMP), which is associated with lysosome-dependent cell death (Galluzzi et al., 2018). LMP can induce both mitochondria-dependent and mitochondria-independent cell death through release of lysosomal proteases (i.e., cathepsins) into the cytoplasm (Aits and Jäättelä, 2013; Boya et al., 2003a). Cytosolic cathepsins that remain active at neutral pH (e.g., CTSB) can trigger mitochondrial membrane permeabilization, leading to cytochrome *c* release and induction of apoptosis (Aits and Jäättelä, 2013; Boya and Kroemer, 2008). In support of this notion, imatinib-induced LMP with subsequent activation and release of CTSB into the cytosol has been reported to contribute to the antileukemic effect of imatinib in CML cell models and CD34-positive cells from CML patients (Puissant et al., 2010).

We previously proposed mitochondrial dysfunction as a primary cause of imatinib-associated toxicity in HepG2 cells (Paech et al., 2017). Considering the results of the current study, lysosomal dysfunction appears to play at least an equally important role and may be the first step in the hepatotoxicity of imatinib and lapatinib. Lysosomal dysfunction impairs mitophagy, impeding the removal of damaged, potentially toxic mitochondria. Lysosomal dysfunction and ROS from damaged mitochondria can trigger LMP (Aits and Jäättelä, 2013), which stimulates apoptosis by causing mitochondrial membrane permeability transition and release of cytochrome *c* into the cytoplasm. The current study reveals the main toxicological mechanisms of lysosomotropic compounds and suggests a possible interplay with mitochondrial toxicity.

Conflict of interest

We declare that the research was conducted in the absence of any commercial or financial relationships that could be construed as a potential conflict of interest.

Funding

This research did not receive any specific grant from funding agencies in the public, commercial, or not-for-profit sectors.

CRediT authorship contribution statement

Noëmi Johanna Roos: conducted the experiments, interpreted data, prepared the figures, Writing – original draft. **Riccardo Vincenzo Mancuso:** conducted the experiments, interpreted data, prepared the figures, Writing – original draft. **Gerda Mawududzi Sanvee:** Methodology, interpreting data. **Jamal Bouitbir:** Methodology, interpreting data. **Stephan Krähenbühl:** Methodology, discussed and helped interpreting the data, Writing – original draft.

Declaration of competing interest

The authors declare that they have no known competing financial interests or personal relationships that could have appeared to influence the work reported in this paper.

Acknowledgement

We thank Cinzia Tiberi from the BioEM Lab of the Biozentrum, University of Basel, for her kind support with the transmission electron microscopy. We also thank Jens Casper from the Pharmaceutical Technology, University of Basel, for providing HuH-7 cells.

Appendix A. Supplementary data

Supplementary data to this article can be found online at https://doi.org/10.1016/j.fct.2022.112869.

References

Aits, S., Jäättelä, M., 2013. Lysosomal cell death at a glance. J. Cell Sci. 126, 1905–1912.

Azim Jr., H.A., et al., 2013. Pattern of rash, diarrhea, and hepatic toxicities secondary to lapatinib and their association with age and response to neoadjuvant therapy: analysis from the NeoALTTO trial. J. Clin. Oncol. 31, 4504–4511.

Boya, P., et al., 2003a. Lysosomal membrane permeabilization induces cell death in a mitochondrion-dependent fashion. J. Exp. Med. 197, 1323–1334.

Boya, P., et al., 2003b. Mitochondrial membrane permeabilization is a critical step of lysosome-initiated apoptosis induced by hydroxychloroquine. Oncogene 22, 3927–3936.

Boya, P., Kroemer, G., 2008. Lysosomal membrane permeabilization in cell death. Oncogene 27, 6434–6451.

Burger, H., et al., 2015. Lysosomal sequestration determines intracellular imatinib levels. Mol. Pharmacol. 88, 477–487.

Chu, Q.S., et al., 2007. Phase I and pharmacokinetic study of lapatinib in combination with capecitabine in patients with advanced solid malignancies. J. Clin. Oncol. 25, 3753–3758.

de Duve, C., et al., 1974. Commentary. Lysosomotropic agents. Biochem. Pharmacol. 23, 2495–2531.

Druker, B.J., et al., 2001. Efficacy and safety of a specific inhibitor of the BCR-ABL tyrosine kinase in chronic myeloid leukemia. N. Engl. J. Med. 344, 1031–1037.

Egan, D.F., et al., 2015. Small molecule inhibition of the autophagy kinase ULK1 and identification of ULK1 substrates. Mol. Cell 59, 285–297.

Ertmer, A., et al., 2007. The anticancer drug imatinib induces cellular autophagy. Leukemia 21, 936–942.

Fu, D., et al., 2014. Imaging the intracellular distribution of tyrosine kinase inhibitors in living cells with quantitative hyperspectral stimulated Raman scattering. Nat. Chem. 6, 614–622.

Funk, R.S., Krise, J.P., 2012. Cationic amphiphilic drugs cause a marked expansion of apparent lysosomal volume: implications for an intracellular distribution-based drug interaction. Mol. Pharm. 9, 1384–1395.

Galluzzi, L., et al., 2018. Molecular mechanisms of cell death: recommendations of the nomenclature committee on cell death 2018. Cell Death Differ. 25, 486–541.

Gardner, E.R., et al., 2009. Influence of the dual ABCB1 and ABCG2 inhibitor tariquidar on the disposition of oral imatinib in mice. J. Exp. Clin. Cancer Res. 28, 99.

Goldman, J.M., Melo, J.V., 2001. Targeting the BCR-ABL tyrosine kinase in chronic myeloid leukemia. N. Engl. J. Med. 344, 1084–1086.

Hara, T., et al., 2006. Suppression of basal autophagy in neural cells causes neurodegenerative disease in mice. Nature 441, 885–889.

Huang, L., et al., 2020. Tyrosine kinase inhibitors for solid tumors in the past 20 years (2001-2020). J. Hematol. Oncol. 13, 143.

Hudachek, S.F., Gustafson, D.L., 2013. Physiologically based pharmacokinetic model of lapatinib developed in mice and scaled to humans. J. Pharmacokinet. Pharmacodyn. 40, 157–176.

Kim, J., et al., 2011. AMPK and mTOR regulate autophagy through direct phosphorylation of Ulk1. Nat. Cell Biol. 13, 132–141.

Klionsky, D.J., et al., 2016. Guidelines for the use and interpretation of assays for monitoring autophagy. Autophagy 12, 1–222 third ed.

Kominami, E., et al., 1988. Biosyntheses and processing of lysosomal cysteine proteinases in rat macrophages. FEBS Lett. 231, 225–228.

Krause, D.S., Van Etten, R.A., 2005. Tyrosine kinases as targets for cancer therapy. N. Engl. J. Med. 353, 172–187.

Kwiatkowski, D.J., Manning, B.D., 2005. Tuberous sclerosis: a GAP at the crossroads of multiple signaling pathways. Hum. Mol. Genet. 14 (2), R251–R258.

Lin, N.U., et al., 2003. Fatal hepatic necrosis following imatinib mesylate therapy. Blood 102, 3455–3456.

Lu, S., et al., 2017. Lysosomal adaptation: how cells respond to lysosomotropic compounds. PLoS One 12, e0173771.

Morissette, G., et al., 2009. Intracellular sequestration of amiodarone: role of vacuolar ATPase and macroautophagic transition of the resulting vacuolar cytopathology. Br. J. Pharmacol. 157, 1531–1540.

Morissette, G., et al., 2008. Intense pseudotransport of a cationic drug mediated by vacuolar ATPase: procainamide-induced autophagic cell vacuolization. Toxicol. Appl. Pharmacol. 228, 364–377.

Moy, B., et al., 2007. Lapatinib. Nat. Rev. Drug Discov. 6, 431–432.

Nada, S., et al., 2009. The novel lipid raft adaptor p18 controls endosome dynamics by anchoring the MEK-ERK pathway to late endosomes. EMBO J. 28, 477–489.

Nadanaciva, S., et al., 2011. A high content screening assay for identifying lysosomotropic compounds. Toxicol. Vitro 25, 715–723.

Ostenfeld, M.S., et al., 2008. Anti-cancer agent siramesine is a lysosomotropic detergent that induces cytoprotective autophagosome accumulation. Autophagy 4, 487–499.

Paech, F., et al., 2017. Hepatocellular toxicity associated with tyrosine kinase inhibitors: mitochondrial damage and inhibition of glycolysis. Front. Pharmacol. 8, 367.

Paech, F., et al., 2018. Mechanisms of mitochondrial toxicity of the kinase inhibitors ponatinib, regorafenib and sorafenib in human hepatic HepG2 cells. Toxicology 395, 34–44.

Palmgren, M.G., 1991. Acridine orange as a probe for measuring pH gradients across membranes: mechanism and limitations. Anal. Biochem. 192, 316–321.

Peng, B., et al., 2005. Clinical pharmacokinetics of imatinib. Clin. Pharmacokinet. 44, 879–894.

Poole, B., Ohkuma, S., 1981. Effect of weak bases on the intralysosomal pH in mouse peritoneal macrophages. J. Cell Biol. 90, 665–669.

Puertollano, R., et al., 2018. The complex relationship between TFEB transcription factor phosphorylation and subcellular localization. EMBO J. 37.

Puissant, A., et al., 2010. Cathepsin B release after imatinib-mediated lysosomal membrane permeabilization triggers BCR-ABL cleavage and elimination of chronic myelogenous leukemia cells. Leukemia 24, 115–124.

Reis, R.C., et al., 1998. A novel methodology for the investigation of intracellular proteolytic processing in intact cells. Eur. J. Cell Biol. 75, 192–197.

Roczniak-Ferguson, A., et al., 2012. The transcription factor TFEB links mTORC1 signaling to transcriptional control of lysosome homeostasis. Sci. Signal. 5, ra42.

Roos, N.J., et al., 2020. The uricosuric benzbromarone disturbs the mitochondrial redox homeostasis and activates the NRF2 signaling pathway in HepG2 cells. Free Radic. Biol. Med. 152, 216–226.

Ryan, Q., et al., 2008. FDA drug approval summary: lapatinib in combination with capecitabine for previously treated metastatic breast cancer that overexpresses HER-2. Oncol. 13, 1114–1119.

Sancak, Y., et al., 2010. Ragulator-Rag complex targets mTORC1 to the lysosomal surface and is necessary for its activation by amino acids. Cell 141, 290–303.

Sanvee, G.M., et al., 2019. Insulin prevents and reverts simvastatin-induced toxicity in C2C12 skeletal muscle cells. Sci. Rep. 9, 7409.

Sardiello, M., et al., 2009. A gene network regulating lysosomal biogenesis and function. Science 325, 473–477.

Settembre, C., et al., 2011. TFEB links autophagy to lysosomal biogenesis. Science 332, 1429–1433.

Skoupa, N., et al., 2020. Lysosomal fusion: an efficient mechanism increasing their sequestration capacity for weak base drugs without apparent lysosomal biogenesis. Biomolecules 10.

Xu, H., Ren, D., 2015. Lysosomal physiology. Annu. Rev. Physiol. 77, 57–80.

Yoshimori, T., et al., 1991. Bafilomycin A1, a specific inhibitor of vacuolar-type H(+)-ATPase, inhibits acidification and protein degradation in lysosomes of cultured cells. J. Biol. Chem. 266, 17707–17712.

Zhitomirsky, B., et al., 2018. Lysosomotropic drugs activate TFEB via lysosomal membrane fluidization and consequent inhibition of mTORC1 activity. Cell Death Dis. 9, 1191.

General discussion

1 The NRF2-mediated oxidative stress response in DILI

After discovering NRF2's ability to induce cytoprotective phase II-detoxifying and antioxidant genes, researchers predicted its protective role against drug-induced toxicity (242). NRF2-deficient mice were subsequently used to investigate chemical carcinogenesis and drug resistance *in vivo*. Indeed, NRF2-deficient mice were more susceptible to acute organ toxicity including liver toxicity caused by diverse xenobiotics and environmental stresses (150). In the present thesis, the hepatotoxic drugs and mitochondrial toxicants benzbromarone and lapatinib activated the NRF2 pathway in HepG2 cells, suggesting a central role of NRF2 in DILI. Accordingly, I will discuss the protective role of NRF2 against DILI in a broader context and evaluate whether an impaired NRF2-mediated stress response represents a risk factor for DILI caused by mitochondrial damage and oxidative stress. Moreover, I will elaborate the potential of NRF2 activation in the prediction of DILI. Finally, a non-canonical mechanism of NRF2 activation as well as harmful aspects of constitutive NRF2 activation will be part of this general discussion.

1.1 The protective role of NRF2 in DILI

The cytoprotective role of NRF2 activation in a disease triggered by inflammation and oxidative stress was exemplary demonstrated by the approval of a NRF2-activator (dimethyl fumarate, Tecfidera®) for the treatment of multiple sclerosis (337). To study the relevance of NRF2 in the context of DILI, NRF2-null mutant mice were exposed to acetaminophen, a well-characterized hepatotoxin (338, 339). Acetaminophen concentrations that were non-toxic in wild-type mice caused fatal hepatocellular necrosis in NRF2-null mutant mice (338, 339). Moreover, acetaminophen-induced GSH depletion was restored in wild-type but not in NRF2-deficient mice (339). We similarly observed that GSH-biosynthetic genes and GSH biosynthesis were upregulated in lapatinib-treated NRF2 competent HepG2 cells. As anticipated, acetaminophen activated the KEAP1-NRF2 pathway both *in vitro* and *in vivo* in a dose-dependent manner as well as in a patient with acetaminophen overdose (340-342). In line with our results for benzbromarone, acetaminophen activated the KEAP1-NRF2 pathway already before hepatotoxicity occurred and provoked the strongest activation at hepatotoxic concentrations. In contrast to NRF2-deficient mice, hepatocyte-specific KEAP1-null mutant mice with constitutive hepatocyte-specific NRF2 activation were resistant to acetaminophen-induced hepatotoxicity (343). As expected, gene expression analysis of KEAP1-deficient liver revealed upregulation of numerous phase II-detoxifying and antioxidant genes (343). However, the expression of some prototypical NRF2-regulated genes (e.g., HO-1,

PRX1) were not increased. This observation indicated that the induction of AREs-containing genes might be more complex *in vivo* and depend on the tissue as well as mechanism of NRF2 activation (e.g., chemical vs. genetic activation). We similarly observed upregulation of well-characterized NRF2-regulated proteins in HepG2 cells exposed to benzbromarone (e.g., TRX, GPX), while others (e.g., NQO1, HO-1) were not increased (unpublished observation). Nevertheless, we could prevent benzbromarone-induced toxicity in KEAP1-deficient but not in wild-type HepG2 cells (344). Since acetaminophen hepatotoxicity is caused by similar mechanisms than benzbromarone- and lapatinib-induced hepatotoxicity (e.g., formation of reactive metabolites, mitochondrial dysfunction, oxidative stress), the protective role of NRF2 in acetaminophen-induced hepatotoxicity in mice may be translated to benzbromarone- and lapatinib-induced hepatotoxicity *in vivo* (345). This assumption is strengthened by the fact that NRF2 activation protects especially against xenobiotics that themselves activated NRF2 (346). Indeed, NRF2-deficient mice did not recover from lapatinib-induced liver damage after 5 days of lapatinib administration compared to wild-type mice (221). Consequently, impaired NRF2 activation in response to electrophilic and oxidative stress may represent a risk factor for lapatinib- and benzbromarone-induced liver toxicity.

1.2 Impaired NRF2-mediated oxidative stress response as a risk factor for DILI

Impaired NRF2 activation aggravates several oxidative stress-related liver diseases such as liver cirrhosis and alcoholic steatohepatitis (347). Thus, an impaired NRF2-mediated oxidative stress response could represent a risk factor for DILI caused by mitochondrial dysfunction and oxidative stress. Impaired NRF2 activation can result from genetic polymorphisms in the DNA binding sites (i.e., AREs) of NRF2-sMAF heterodimers located in the promotors of NRF2-regulated genes (348). Single nucleotide polymorphisms (SNPs) in AREs can both increases or decreases the DNA-binding affinity of NRF2-sMAF heterodimers and subsequently reduce or increase the expression of adjacent NRF2-target genes (349). Accordingly, SNPs in AREs can modulate the risk for oxidative stress-related diseases. For instance, a SNP in the ARE of the ferritin light chain gene promotor reduced the expression of L-ferritin, which can prevent the formation of oxidative $OH^{\bullet}$ through iron storage (350). Moreover, polymorphisms in the human NRF2 gene promotor increase the risk for oxidative-stress related diseases such as hyperoxia-induced pulmonary injury, chronic obstructive pulmonary disease, and oxidative-stress induced hearing loss (351-353). Since NRF2 regulates its own expression by a positive-feedback mechanism, SNPs in the promotor of the NRF2 gene could impair its own regulation (354). Nevertheless, functional SNPs in AREs are rare in the human genome due to negative selection (349). This fact corresponds to the low incidence of idiosyncratic

DILI, which occurs only in a few individuals. Indeed, polymorphisms in individual antioxidant genes such as GST and SOD2 (i.e., mutant C allele) increased the risk for hepatocellular DILI (355). For instance, patients with double-null genotype for GSTT1 and GSTM1 had a 2.7-fold increased DILI risk associated with certain drugs compared to GST-competent patients (34). Patients with the mutant SOD2 C allele contained more mitochondrial SOD2 and in turn generated more H_2O_2, which could explain the increased DILI risk observed in this cohort (356). In conclusion, polymorphisms in AREs and the NRF2 gene promotor could sensitize patients to oxidative-stress related diseases including drug-induced liver toxicity.

1.3 The NRF2-mediated oxidative stress response as a predictor for DILI

Due to its rarity and the lack of experimental models that reliably predict idiosyncratic reactions, idiosyncratic DILI is often missed during drug development. Accordingly, no alarming hepatotoxic event was observed for benzbromarone during clinical trials (186). Activation of the KEAP1-NRF2 pathway in liver by benzbromarone, lapatinib, acetaminophen, and numerous other well-characterized hepatotoxins such as bromobenzene, furosemide, and carbon tetrachloride raises the question whether hepatic NRF2 activation reflects a drug's hepatotoxic potential and could be used as a predictor for DILI (357). Most of these hepatotoxins activated NRF2 within the first hours of exposure, suggesting an intrinsic ability of these compounds or their metabolites to modify KEAP1. According to Copple and colleagues, the activation of the NRF2 transcriptional network in primary human hepatocytes (PHH) is a sensitive, specific, and accurate indicator with relatively high positive and negative predictive values for the intrinsic biochemical reactivity of a compound (358). However, the prediction of the clinical DILI risk was less sensitive with a relatively high false negative prediction. Nevertheless, the activity of NRF2 is a relevant biological response that should be considered in pre-clinical toxicological studies. Indeed, the ability of drug candidates to induce the expression of NRF2-related genes in hepatic parenchymal cells was assessed in drug development with the goal to predict hepatotoxicity at an early stage (359). Moreover, gene expression profiles can help elucidating mechanisms of toxicity. Nevertheless, distinguishing hepatotoxic changes in gene expression from changes that are well-tolerated is challenging, because cytoprotective stress responses often precede and prevent hepatic damage (360). Nonetheless, drugs that cause non-hepatotoxic gene expression changes might still trigger idiosyncratic DILI in individuals with underlying risk factors.

1.4 Non-canonical mechanism of NRF2 activation

In contrast to benzbromarone, which induced NRF2 activation within two hours of exposure, lapatinib activated the NRF2 pathway in HepG2 cells after 24 h. Moreover, activation of NRF2 by lapatinib could only be partially prevented by an antioxidant. Thus, we assume that beside oxidative stress, other mechanisms may be involved in the activation of NRF2 by lapatinib. A non-canonical way of NRF2 activation could occur through the selective autophagy receptor p62 (271). p62 inactivates KEAP1 through direct binding to KEAP1's NRF2 binding site and mediates degradation of KEAP1 by autophagy (361). We found increased levels of p62 and LC3-II in HepG2 cells exposed to lapatinib for 24 h (unpublished observation). Moreover, KEAP1 protein levels decreased in response to lapatinib. Both accumulation of p62 and LC3-II could result from an impaired autophagic flux, which might occur due to lysosomal dysfunction (313). Indeed, lapatinib disturbed the lysosomal homeostasis in HepG2 cells. Nonetheless, NRF2 stimulates the expression of p62 inducing a positive feedback mechanism (362). Thus, the increased protein levels of p62 caused by lapatinib could result from NRF2 activation. Assessing the gene expression of p62 and the autophagic flux at different time-points in lapatinib-treated HepG2 cells could clarify the cause-effect relationship. Finally, immunoprecipitation could reveal an interaction between KEAP1 and p62 (271).

1.5 The opposite side of the medal - hepatotoxic effect of constitutive NRF2 activation

We highlighted the cytoprotective effects of NRF2 activation against drug-induced toxicity and other oxidative stress related diseases. However, constitutive NRF2 activation has been shown to be harmful under certain conditions. For instance, KEAP1-null mutant mice with constitutive NRF2 activation developed hyperkeratosis in the esophagus and forestomach and died within three weeks after birth due to malnutrition (363). These findings demonstrate the importance of a tightly regulated NRF2 activity, especially in squamous cells that highly express NRF2. Moreover, constitutive NRF2 activation due to aberrant p62 accumulation was responsible for the liver injury in autophagy-deficient mice (361). In contrast to benzbromarone, which activated NRF2 at non-toxic concentrations, lapatinib stimulated the NRF2 pathway at hepatotoxic concentrations. Therefore, the contribution of NRF2 activation in lapatinib-induced hepatotoxicity is not entirely clear, although we found cytoprotective NRF2-mediated adaptations (e.g., increased GSH levels) in lapatinib-treated HepG2 cells. Knock-down of NRF2 or KEAP1 could help answer this ambiguity. Although the mechanism of NRF2-induced liver damage in autophagy-deficient mice is unclear, reductive stress and proteotoxicity have been proposed as adverse effects of constitutive NRF2 activation (150).

1.6 Limitations and further directions

We performed our experiments in HepG2 cells, a well-characterized human hepatoma cell line widely used for toxicological studies (58). HepG2 cells lack the expression of most drug-metabolizing CYPs with the exception of low levels of CYP3A4 and CYP2C19 (364). Thus, hepatotoxicity and activation of the NRF2-mediated oxidative stress response caused by reactive metabolites could have been missed in our cell system. A previous study performed in our research group revealed that lapatinib and imatinib were slightly more toxic in rifampicin-induced HepaRG cells, which are metabolically active, compared to non-induced HepaRG cells with minor metabolic activity (179). These findings suggested the formation of toxic lapatinib and imatinib metabolites. The increased toxicity of lapatinib in HepaRG cells with induced CYP3A4 activity was also observed in another study (365). Accordingly, CYP3A4 induction was identified as a risk factor for lapatinib-induced hepatotoxicity in patients (366, 367). The O-dealkylated lapatinib metabolite created by CYP3A4 is converted to an electrophilic quinone imine metabolite that can covalently bind to GSH and protein cysteine residues (211, 365). Similarly, formation of reactive benzbromarone metabolites that can bind to reactive cysteine residues have been identified both *in vitro* (189, 368) and *in vivo* (367, 369-371). Thus, NRF2 activation, which primarily results from modification of KEAP1's cysteine residues by reactive metabolites or ROS, should not only be assessed in HepG2 cells, but ideally also in metabolically more competent cells such as induced HepaRG cells or PHH (364). Indeed, HepG2 cells transfected with CYP2C9, the main CYP_{450} enzyme involved in benzbromarone metabolism, were more susceptible to benzbromarone when NRF2 was simultaneously down-regulated (372). This indicates that NRF2 protects against reactive benzbromarone metabolites, which contribute to benzbromarone-induced hepatotoxicity. Nevertheless, non-induced HepG2 cells showed low basal activities for CYP2C19 and CYP3A4, which are both involved in the metabolism of benzbromarone and lapatinib (364). Therefore, the formation of reactive benzbromarone and lapatinib metabolites as causes of NRF2 activation cannot be completely excluded in our cellular system, especially at supraphysiological drug concentrations.

The protective role of NRF2 against benzbromarone- and lapatinib-induced liver toxicity could be confirmed in NRF2-deficient mice, which might be more susceptible than wild-type mice. Moreover, the hepatotoxicity of benzbromarone and lapatinib should be assessed in mice with an impaired antioxidant defense such as $SOD2^{+/-}$ mice or y-glutamyl $transpeptidase^{-/-}$ mice with reduced hepatic GSH levels (373).

2 Lysosomotropism in DILI

Although lysosomes were called "suicide bags" by their discoverer Christian de Duve, lysosome-dependent cell death has been underrated for many years (374). One reason is the non-specificity of pan-caspase inhibitors (e.g., zVAD-fmk) used to prevent cell death. These inhibitors also block the activity of lysosomal cathepsin proteases, thereby masking their involvement in cell death (375). Lysosome-dependent cell death can be triggered by lipophilic weak basic molecules that accumulate in lysosomes, which is known as lysosomotropism. In our studies, the lysosomotropic and hepatotoxic TKIs lapatinib and imatinib disturbed the lysosomal homeostasis and related pathways in HepG2 cells, raising the questions whether the lysosomotropic properties of these drugs are responsible for their hepatotoxicity. Therefore, I will discuss the role of lysosomes in the development of diseases. Finally, since both lapatinib and imatinib are associate with mitochondrial damage, possible links between lysosomal and mitochondrial dysfunction will be elaborated.

2.1 The role of lysosomes in DILI

Even though numerous drugs with lysosomotropic properties accumulate in lysosomes of various organs including liver, lysosomal dysfunction is rarely considered as mechanisms of idiosyncratic DILI. The best characterized adverse reaction caused by lysosomotropic/cationic amphiphilic drugs (e.g., amiodarone) is phospholipidosis, a lysosomal storage disease (LSD) with excessive intracellular accumulation of lipids (376). However, phospholipidosis, which can also occur in liver, is not toxic per se and no cases of phospholipidosis have been reported for lapatinib and imatinib. In contrast, accumulation of undegraded intracellular material resulting from long-term lysosomal dysfunctions caused by congenital lysosomal enzyme defects can cause severe LSDs (377). The temporarily treatment with imatinib and lapatinib, which caused reversible lysosomal dysfunction, might not lead to such severe conditions. Nevertheless, inhibition of lysosome-related signaling pathways such the mTORC1 pathway by imatinib can compromise essential cellular functions such as protein synthesis or autophagy. Moreover, cellular toxicity caused by lysosomotropic drugs can result from destabilization of the lysosomal membrane, which can induce lysosome-dependent cell death (374). This type of cell death has been described for several drugs in clinical use including ciprofloxacin, norfloxacin (333), siramesine (378), and hydroxychloroquine (334). Lysosome-dependent cell death can be linked to mitochondria-dependent apoptosis through the induction of MOMP. This link could connect the findings of our third project to the previous observation of mitochondrial cytochrome *c* release induced by lapatinib and imatinib (179). However, LMP can occur both upstream (334) and

downstream of MOMP (379). Comparing the findings of our studies, lysosomal dysfunction induced by lapatinib and imatinib occurred earlier than mitochondrial dysfunction. This suggests that lysosomal impairment is a direct and fast effect on imatinib and lapatinib that precedes mitochondrial damage. Moreover, functional lysosomes might be essential to attenuate lapatinib- and imatinib-induced mitochondrial damage through mitophagy. Thus, lysosomal dysfunction could aggravate mitochondrial toxicity induced by lapatinib and imatinib, as it was reported for acetaminophen-induced hepatotoxicity (179). Moreover, ruptured lysosomes may aggravate drug-induced mitochondrial toxicity through release of iron, which can catalyze the formation of $HO^{\bullet}$ in the presence of ROS and induce mitochondrial permeability transition (380). Moreover, mitochondria-derived ROS can destabilized the lysosomal membrane through lipid peroxidation (297). Thus, the lysosomal-mitochondrial axis is a relevant cell death pathway that should be considered in DILI associated with lysosomotropic drugs. Nevertheless, lysosomal sequestration of lysosomotropic drugs such as imatinib and lapatinib could also act as an intracellular sink and reduce the cytotoxicity of these drugs. Indeed, sequestration of the TKI sunitinib in lysosomes enhanced the resistance of tumors cells towards this drug, demonstrating the controversial role of lysosomes in drug-induced toxicity (381).

2.2 Limitations and further directions

As common in toxicological studies, we exposed HepG2 cells also to supratherapeutic drug concentrations over a relatively short time period compared to the clinical situation. High drug concentrations can be justified by the fact that liver concentrations are often higher than the drug concentrations measured in the plasma. Indeed, the concentration of lapatinib in liver of lapatinib-treated mice was more than two orders of magnitude higher than the plasma concentrations (221). Our experimental settings might be useful to study the drug effects on the NRF2-mediated oxidative stress response. However, they do not reflect the situation in susceptible patients, which typically develop DILI over a longer time period under therapeutic concentrations. Thus, the effects of lapatinib and imatinib on lysosomal functions should be assessed over a longer time period with therapeutic concentrations.

Since an increased lysosomal volume induced by lysosomotropic drugs such as lapatinib and imatinib does not necessarily lead to LMP, the effect of lapatinib and imatinib on LMP should be assessed in more detail. A sensitive method to detect LMP is the lysosomal galectin puncta assay (382). Cytosolic galectins rapidly translocate to individual ruptured lysosomes, which allows the detection of early LMP. This assay could help clarifying the involvement of lysosomal damage in

imatinib- and lapatinib-induced hepatotoxicity. Subsequently, cathepsin inhibitors could be used to assess whether lysosomal cathepsins are involved in the induction of cell death induced by these TKIs. Since imatinib and lapatinib disturbed the lysosomal proteolytic function in HepG2 cells, the accumulation of long-lived proteins should be assessed (313). Imatinib increased the number of autophagosomes in HepG2 cells demonstrated by increased levels of LC3-II. However, we did not systematically distinguish between induction of autophagy and inhibition of autophagic flux, which could both lead to autophagosome accumulation (313). Thus, the proteins levels of LC3-II should be additionally assessed in the presence of a saturating lysosomal inhibitor such as chloroquine.

Conclusion

In the present thesis, I studied the role of the NRF2-mediated oxidative stress response in the context of DILI caused by mitochondrial damage and oxidative stress. Benzbromarone rapidly activated the NRF2 pathway in HepG2 cells with upregulation of cytosolic and mitochondrial antioxidant proteins. Moreover, NRF2 activation conferred protection against benzbromarone-induced hepatotoxicity. Lapatinib similarly activated the NRF2 pathway in this cell line, which was partially caused by ROS. Consequently, lapatinib upregulated the expression of mitochondrial antioxidant genes and proteins as well as GSH biosynthesis. Thus, an impaired NRF2-mediated oxidative stress response might be a risk factor for benzbromarone- and lapatinib-induced liver toxicity. Nevertheless, *in vivo* studies are required to further our knowledge about NRF2 activation in the protection against mitochondrial toxicants. In addition, we observed that the lysosomotropic TKIs lapatinib and especially imatinib impaired essential lysosomal functions and related pathways such as the mTORC1 signaling pathway and autophagy in HepG2 cells. Thus, we revealed principle toxicological mechanisms of lysosomotropic compounds. Since both lapatinib and imatinib are associated with mitochondrial dysfunction, the interplay between lysosomal and mitochondrial toxicity should be further elaborated. Overall, an improved understanding of the molecular mechanisms of drug-induced hepatotoxicity is essential to prevent idiosyncratic DILIs in patients.

References

1. Ostapowicz G, Fontana RJ, Schiødt FV, Larson A, Davern TJ, Han SH, McCashland TM, et al. Results of a prospective study of acute liver failure at 17 tertiary care centers in the United States. Ann Intern Med 2002;137:947-954.
2. Andrade RJ, Chalasani N, Björnsson ES, Suzuki A, Kullak-Ublick GA, Watkins PB, Devarbhavi H, et al. Drug-induced liver injury. Nat Rev Dis Primers 2019;5:58.
3. Olson H, Betton G, Robinson D, Thomas K, Monro A, Kolaja G, Lilly P, et al. Concordance of the toxicity of pharmaceuticals in humans and in animals. Regul Toxicol Pharmacol 2000;32:56-67.
4. Stevens JL, Baker TK. The future of drug safety testing: expanding the view and narrowing the focus. Drug Discov Today 2009;14:162-167.
5. Chalasani NP, Hayashi PH, Bonkovsky HL, Navarro VJ, Lee WM, Fontana RJ. ACG Clinical Guideline: the diagnosis and management of idiosyncratic drug-induced liver injury. Am J Gastroenterol 2014;109:950-966; quiz 967.
6. Gunawan B, Kaplowitz N. Clinical perspectives on xenobiotic-induced hepatotoxicity. Drug Metab Rev 2004;36:301-312.
7. Jaeschke H, Xie Y, McGill MR. Acetaminophen-induced Liver Injury: from Animal Models to Humans. J Clin Transl Hepatol 2014;2:153-161.
8. Mitchell JR, Jollow DJ, Potter WZ, Gillette JR, Brodie BB. Acetaminophen-induced hepatic necrosis. IV. Protective role of glutathione. J Pharmacol Exp Ther 1973;187:211-217.
9. Kaplowitz N. Idiosyncratic drug hepatotoxicity. Nat Rev Drug Discov 2005;4:489-499.
10. Stepan AF, Walker DP, Bauman J, Price DA, Baillie TA, Kalgutkar AS, Aleo MD. Structural alert/reactive metabolite concept as applied in medicinal chemistry to mitigate the risk of idiosyncratic drug toxicity: a perspective based on the critical examination of trends in the top 200 drugs marketed in the United States. Chem Res Toxicol 2011;24:1345-1410.
11. Teschke R, Danan G: Causality Assessment Methods in Drug-Induced Liver Injury. In: Chen M, Will Y, eds. Drug-Induced Liver Toxicity. New York, NY: Springer New York, 2018; 555-594.
12. Björnsson ES, Bergmann OM, Björnsson HK, Kvaran RB, Olafsson S. Incidence, presentation, and outcomes in patients with drug-induced liver injury in the general population of Iceland. Gastroenterology 2013;144:1419-1425, 1425.e1411-1413; quiz e1419-1420.
13. Sgro C, Clinard F, Ouazir K, Chanay H, Allard C, Guilleminet C, Lenoir C, et al. Incidence of drug-induced hepatic injuries: a French population-based study. Hepatology 2002;36:451-455.
14. Suk KT, Kim DJ, Kim CH, Park SH, Yoon JH, Kim YS, Baik GH, et al. A prospective nationwide study of drug-induced liver injury in Korea. Am J Gastroenterol 2012;107:1380-1387.
15. Krähenbühl S, Pichler WJ. Medikamentöse Hepatopathien. Ther Umsch 2017;74:123-130.
16. De Valle MB, Av Klinteberg V, Alem N, Olsson R, Björnsson E. Drug-induced liver injury in a Swedish University hospital out-patient hepatology clinic. Aliment Pharmacol Ther 2006;24:1187-1195.
17. de Abajo FJ, Montero D, Madurga M, García Rodríguez LA. Acute and clinically relevant drug-induced liver injury: a population based case-control study. Br J Clin Pharmacol 2004;58:71-80.
18. Vega M, Verma M, Beswick D, Bey S, Hossack J, Merriman N, Shah A, et al. The Incidence of Drug- and Herbal and Dietary Supplement-Induced Liver Injury: Preliminary Findings from Gastroenterologist-Based Surveillance in the Population of the State of Delaware. Drug Saf 2017;40:783-787.
19. Meier Y, Cavallaro M, Roos M, Pauli-Magnus C, Folkers G, Meier PJ, Fattinger K. Incidence of drug-induced liver injury in medical inpatients. Eur J Clin Pharmacol 2005;61:135-143.

20. Reuben A, Tillman H, Fontana RJ, Davern T, McGuire B, Stravitz RT, Durkalski V, et al. Outcomes in Adults With Acute Liver Failure Between 1998 and 2013: An Observational Cohort Study. Ann Intern Med 2016;164:724-732.
21. Russo MW, Galanko JA, Shrestha R, Fried MW, Watkins P. Liver transplantation for acute liver failure from drug induced liver injury in the United States. Liver Transpl 2004;10:1018-1023.
22. Weiler S, Merz M, Kullak-Ublick GA. Drug-induced liver injury: the dawn of biomarkers? F1000Prime Rep 2015;7:34.
23. Temple R. Hy's law: predicting serious hepatotoxicity. Pharmacoepidemiol Drug Saf 2006;15:241-243.
24. Danan G, Benichou C. Causality assessment of adverse reactions to drugs--I. A novel method based on the conclusions of international consensus meetings: application to drug-induced liver injuries. J Clin Epidemiol 1993;46:1323-1330.
25. Benichou C, Danan G, Flahault A. Causality assessment of adverse reactions to drugs--II. An original model for validation of drug causality assessment methods: case reports with positive rechallenge. J Clin Epidemiol 1993;46:1331-1336.
26. Björnsson ES. Epidemiology, Predisposing Factors, and Outcomes of Drug-Induced Liver Injury. Clin Liver Dis 2020;24:1-10.
27. Andrade RJ, Lucena MI, Fernández MC, Pelaez G, Pachkoria K, García-Ruiz E, García-Muñoz B, et al. Drug-induced liver injury: an analysis of 461 incidences submitted to the Spanish registry over a 10-year period. Gastroenterology 2005;129:512-521.
28. Lucena MI, Andrade RJ, Kaplowitz N, García-Cortes M, Fernández MC, Romero-Gomez M, Bruguera M, et al. Phenotypic characterization of idiosyncratic drug-induced liver injury: the influence of age and sex. Hepatology 2009;49:2001-2009.
29. Reuben A, Koch DG, Lee WM. Drug-induced acute liver failure: results of a U.S. multicenter, prospective study. Hepatology 2010;52:2065-2076.
30. Russmann S, Jetter A, Kullak-Ublick GA. Pharmacogenetics of drug-induced liver injury. Hepatology 2010;52:748-761.
31. Sun F, Chen Y, Xiang Y, Zhan S. Drug-metabolising enzyme polymorphisms and predisposition to anti-tuberculosis drug-induced liver injury: a meta-analysis. Int J Tuberc Lung Dis 2008;12:994-1002.
32. Daly AK, Aithal GP, Leathart JB, Swainsbury RA, Dang TS, Day CP. Genetic susceptibility to diclofenac-induced hepatotoxicity: contribution of UGT2B7, CYP2C8, and ABCC2 genotypes. Gastroenterology 2007;132:272-281.
33. Huang YS. Genetic polymorphisms of drug-metabolizing enzymes and the susceptibility to antituberculosis drug-induced liver injury. Expert Opin Drug Metab Toxicol 2007;3:1-8.
34. Lucena MI, Andrade RJ, Martínez C, Ulzurrun E, García-Martín E, Borraz Y, Fernández MC, et al. Glutathione S-transferase m1 and t1 null genotypes increase susceptibility to idiosyncratic drug-induced liver injury. Hepatology 2008;48:588-596.
35. Lang C, Meier Y, Stieger B, Beuers U, Lang T, Kerb R, Kullak-Ublick GA, et al. Mutations and polymorphisms in the bile salt export pump and the multidrug resistance protein 3 associated with drug-induced liver injury. Pharmacogenet Genomics 2007;17:47-60.
36. Stephens C, Andrade RJ. Genetic Predisposition to Drug-Induced Liver Injury. Clin Liver Dis 2020;24:11-23.
37. Andrade RJ, Lucena MI, Alonso A, García-Cortes M, García-Ruiz E, Benitez R, Fernández MC, et al. HLA class II genotype influences the type of liver injury in drug-induced idiosyncratic liver disease. Hepatology 2004;39:1603-1612.

38. Singer JB, Lewitzky S, Leroy E, Yang F, Zhao X, Klickstein L, Wright TM, et al. A genome-wide study identifies HLA alleles associated with lumiracoxib-related liver injury. Nat Genet 2010;42:711-714.
39. Kindmark A, Jawaid A, Harbron CG, Barratt BJ, Bengtsson OF, Andersson TB, Carlsson S, et al. Genome-wide pharmacogenetic investigation of a hepatic adverse event without clinical signs of immunopathology suggests an underlying immune pathogenesis. Pharmacogenomics J 2008;8:186-195.
40. Daly AK, Donaldson PT, Bhatnagar P, Shen Y, Pe'er I, Floratos A, Daly MJ, et al. HLA-B*5701 genotype is a major determinant of drug-induced liver injury due to flucloxacillin. Nat Genet 2009;41:816-819.
41. Mallal S, Phillips E, Carosi G, Molina JM, Workman C, Tomazic J, Jägel-Guedes E, et al. HLA-B*5701 screening for hypersensitivity to abacavir. N Engl J Med 2008;358:568-579.
42. Spraggs CF, Budde LR, Briley LP, Bing N, Cox CJ, King KS, Whittaker JC, et al. HLA-DQA1*02:01 is a major risk factor for lapatinib-induced hepatotoxicity in women with advanced breast cancer. J Clin Oncol 2011;29:667-673.
43. Thummel KE, Slattery JT, Ro H, Chien JY, Nelson SD, Lown KE, Watkins PB. Ethanol and production of the hepatotoxic metabolite of acetaminophen in healthy adults. Clin Pharmacol Ther 2000;67:591-599.
44. Lauterburg BH, Velez ME. Glutathione deficiency in alcoholics: risk factor for paracetamol hepatotoxicity. Gut 1988;29:1153-1157.
45. Zenger F, Russmann S, Junker E, Wüthrich C, Bui MH, Lauterburg BH. Decreased glutathione in patients with anorexia nervosa. Risk factor for toxic liver injury? Eur J Clin Nutr 2004;58:238-243.
46. Uberti-Foppa C, De Bona A, Morsica G, Galli L, Gallotta G, Boeri E, Lazzarin A. Pretreatment of chronic active hepatitis C in patients coinfected with HIV and hepatitis C virus reduces the hepatotoxicity associated with subsequent antiretroviral therapy. J Acquir Immune Defic Syndr 2003;33:146-152.
47. Boelsterli UA, Lim PL. Mitochondrial abnormalities--a link to idiosyncratic drug hepatotoxicity? Toxicol Appl Pharmacol 2007;220:92-107.
48. Krähenbühl S, Brandner S, Kleinle S, Liechti S, Straumann D. Mitochondrial diseases represent a risk factor for valproate-induced fulminant liver failure. Liver 2000;20:346-348.
49. Lammert C, Bjornsson E, Niklasson A, Chalasani N. Oral medications with significant hepatic metabolism at higher risk for hepatic adverse events. Hepatology 2010;51:615-620.
50. Chen M, Borlak J, Tong W. High lipophilicity and high daily dose of oral medications are associated with significant risk for drug-induced liver injury. Hepatology 2013;58:388-396.
51. Uetrecht J. Mechanisms of idiosyncratic drug-induced liver injury. Adv Pharmacol 2019;85:133-163.
52. Lee WM. Drug-induced hepatotoxicity. N Engl J Med 2003;349:474-485.
53. He K, Talaat RE, Pool WF, Reily MD, Reed JE, Bridges AJ, Woolf TF. Metabolic activation of troglitazone: identification of a reactive metabolite and mechanisms involved. Drug Metab Dispos 2004;32:639-646.
54. Almanza A, Carlesso A, Chintha C, Creedican S, Doultsinos D, Leuzzi B, Luís A, et al. Endoplasmic reticulum stress signalling - from basic mechanisms to clinical applications. Febs j 2019;286:241-278.
55. Séguin B, Uetrecht J. The danger hypothesis applied to idiosyncratic drug reactions. Curr Opin Allergy Clin Immunol 2003;3:235-242.
56. Matzinger P. Essay 1: the Danger model in its historical context. Scand J Immunol 2001;54:4-9.
57. Morgan RE, Trauner M, van Staden CJ, Lee PH, Ramachandran B, Eschenberg M, Afshari CA, et al. Interference with bile salt export pump function is a susceptibility factor for human liver injury in drug development. Toxicol Sci 2010;118:485-500.

58. Weaver RJ, Blomme EA, Chadwick AE, Copple IM, Gerets HHJ, Goldring CE, Guillouzo A, et al. Managing the challenge of drug-induced liver injury: a roadmap for the development and deployment of preclinical predictive models. Nat Rev Drug Discov 2020;19:131-148.
59. Fromenty B, Pessayre D. Inhibition of mitochondrial beta-oxidation as a mechanism of hepatotoxicity. Pharmacol Ther 1995;67:101-154.
60. Masubuchi Y, Kano S, Horie T. Mitochondrial permeability transition as a potential determinant of hepatotoxicity of antidiabetic thiazolidinediones. Toxicology 2006;222:233-239.
61. Zimorski V, Ku C, Martin WF, Gould SB. Endosymbiotic theory for organelle origins. Curr Opin Microbiol 2014;22:38-48.
62. Roger AJ, Muñoz-Gómez SA, Kamikawa R. The Origin and Diversification of Mitochondria. Curr Biol 2017;27:R1177-r1192.
63. Song J, Herrmann JM, Becker T. Quality control of the mitochondrial proteome. Nat Rev Mol Cell Biol 2021;22:54-70.
64. Giacomello M, Pyakurel A, Glytsou C, Scorrano L. The cell biology of mitochondrial membrane dynamics. Nat Rev Mol Cell Biol 2020;21:204-224.
65. Logan DC. The mitochondrial compartment. J Exp Bot 2006;57:1225-1243.
66. Vogel F, Bornhövd C, Neupert W, Reichert AS. Dynamic subcompartmentalization of the mitochondrial inner membrane. J Cell Biol 2006;175:237-247.
67. Herzig S, Shaw RJ. AMPK: guardian of metabolism and mitochondrial homeostasis. Nat Rev Mol Cell Biol 2018;19:121-135.
68. Bauer TM, Murphy E. Role of Mitochondrial Calcium and the Permeability Transition Pore in Regulating Cell Death. Circ Res 2020;126:280-293.
69. Crompton M. The mitochondrial permeability transition pore and its role in cell death. Biochem J 1999;341 (Pt 2):233-249.
70. Haworth RA, Hunter DR. The Ca2+-induced membrane transition in mitochondria. II. Nature of the Ca2+ trigger site. Arch Biochem Biophys 1979;195:460-467.
71. Assaly R, de Tassigny A, Paradis S, Jacquin S, Berdeaux A, Morin D. Oxidative stress, mitochondrial permeability transition pore opening and cell death during hypoxia-reoxygenation in adult cardiomyocytes. Eur J Pharmacol 2012;675:6-14.
72. Spinelli JB, Haigis MC. The multifaceted contributions of mitochondria to cellular metabolism. Nat Cell Biol 2018;20:745-754.
73. Martínez-Reyes I, Chandel NS. Mitochondrial TCA cycle metabolites control physiology and disease. Nat Commun 2020;11:102.
74. Anderson S, Bankier AT, Barrell BG, de Bruijn MH, Coulson AR, Drouin J, Eperon IC, et al. Sequence and organization of the human mitochondrial genome. Nature 1981;290:457-465.
75. Mishra P, Chan DC. Mitochondrial dynamics and inheritance during cell division, development and disease. Nat Rev Mol Cell Biol 2014;15:634-646.
76. Pfanner N, Warscheid B, Wiedemann N. Mitochondrial proteins: from biogenesis to functional networks. Nat Rev Mol Cell Biol 2019;20:267-284.
77. Rowland AA, Voeltz GK. Endoplasmic reticulum-mitochondria contacts: function of the junction. Nat Rev Mol Cell Biol 2012;13:607-625.
78. Bock FJ, Tait SWG. Mitochondria as multifaceted regulators of cell death. Nat Rev Mol Cell Biol 2020;21:85-100.

79. Sousa JS, D'Imprima E, Vonck J. Mitochondrial Respiratory Chain Complexes. Subcell Biochem 2018;87:167-227.
80. Letts JA, Sazanov LA. Clarifying the supercomplex: the higher-order organization of the mitochondrial electron transport chain. Nat Struct Mol Biol 2017;24:800-808.
81. Sazanov LA. A giant molecular proton pump: structure and mechanism of respiratory complex I. Nat Rev Mol Cell Biol 2015;16:375-388.
82. Berry BJ, Trewin AJ, Amitrano AM, Kim M, Wojtovich AP. Use the Protonmotive Force: Mitochondrial Uncoupling and Reactive Oxygen Species. J Mol Biol 2018;430:3873-3891.
83. Mitchell P. Coupling of phosphorylation to electron and hydrogen transfer by a chemi-osmotic type of mechanism. Nature 1961;191:144-148.
84. Fiedorczuk K, Letts JA, Degliesposti G, Kaszuba K, Skehel M, Sazanov LA. Atomic structure of the entire mammalian mitochondrial complex I. Nature 2016;538:406-410.
85. Sun F, Huo X, Zhai Y, Wang A, Xu J, Su D, Bartlam M, et al. Crystal structure of mitochondrial respiratory membrane protein complex II. Cell 2005;121:1043-1057.
86. Gao X, Wen X, Esser L, Quinn B, Yu L, Yu CA, Xia D. Structural basis for the quinone reduction in the bc1 complex: a comparative analysis of crystal structures of mitochondrial cytochrome bc1 with bound substrate and inhibitors at the Qi site. Biochemistry 2003;42:9067-9080.
87. Mitchell P. The protonmotive Q cycle: a general formulation. FEBS Lett 1975;59:137-139.
88. Brand MD. Mitochondrial generation of superoxide and hydrogen peroxide as the source of mitochondrial redox signaling. Free Radic Biol Med 2016;100:14-31.
89. Ott M, Zhivotovsky B, Orrenius S. Role of cardiolipin in cytochrome c release from mitochondria. Cell Death Differ 2007;14:1243-1247.
90. Tsukihara T, Aoyama H, Yamashita E, Tomizaki T, Yamaguchi H, Shinzawa-Itoh K, Nakashima R, et al. The whole structure of the 13-subunit oxidized cytochrome c oxidase at 2.8 A. Science 1996;272:1136-1144.
91. Wikström M, Verkhovsky MI. Towards the mechanism of proton pumping by the haem-copper oxidases. Biochim Biophys Acta 2006;1757:1047-1051.
92. Baker LA, Watt IN, Runswick MJ, Walker JE, Rubinstein JL. Arrangement of subunits in intact mammalian mitochondrial ATP synthase determined by cryo-EM. Proc Natl Acad Sci U S A 2012;109:11675-11680.
93. Watt IN, Montgomery MG, Runswick MJ, Leslie AG, Walker JE. Bioenergetic cost of making an adenosine triphosphate molecule in animal mitochondria. Proc Natl Acad Sci U S A 2010;107:16823-16827.
94. Ow YP, Green DR, Hao Z, Mak TW. Cytochrome c: functions beyond respiration. Nat Rev Mol Cell Biol 2008;9:532-542.
95. Alnemri ES, Livingston DJ, Nicholson DW, Salvesen G, Thornberry NA, Wong WW, Yuan J. Human ICE/CED-3 protease nomenclature. Cell 1996;87:171.
96. Riedl SJ, Shi Y. Molecular mechanisms of caspase regulation during apoptosis. Nat Rev Mol Cell Biol 2004;5:897-907.
97. Riedl SJ, Salvesen GS. The apoptosome: signalling platform of cell death. Nat Rev Mol Cell Biol 2007;8:405-413.
98. Wang X. The expanding role of mitochondria in apoptosis. Genes Dev 2001;15:2922-2933.
99. Singh R, Letai A, Sarosiek K. Regulation of apoptosis in health and disease: the balancing act of BCL-2 family proteins. Nat Rev Mol Cell Biol 2019;20:175-193.
100. Llambi F, Moldoveanu T, Tait SW, Bouchier-Hayes L, Temirov J, McCormick LL, Dillon CP, et al. A unified model of mammalian BCL-2 protein family interactions at the mitochondria. Mol Cell 2011;44:517-531.

101. Chipuk JE, Moldoveanu T, Llambi F, Parsons MJ, Green DR. The BCL-2 family reunion. Mol Cell 2010;37:299-310.
102. Große L, Wurm CA, Brüser C, Neumann D, Jans DC, Jakobs S. Bax assembles into large ring-like structures remodeling the mitochondrial outer membrane in apoptosis. Embo j 2016;35:402-413.
103. Salvador-Gallego R, Mund M, Cosentino K, Schneider J, Unsay J, Schraermeyer U, Engelhardt J, et al. Bax assembly into rings and arcs in apoptotic mitochondria is linked to membrane pores. Embo j 2016;35:389-401.
104. Acehan D, Jiang X, Morgan DG, Heuser JE, Wang X, Akey CW. Three-dimensional structure of the apoptosome: implications for assembly, procaspase-9 binding, and activation. Mol Cell 2002;9:423-432.
105. Liu X, Kim CN, Yang J, Jemmerson R, Wang X. Induction of apoptotic program in cell-free extracts: requirement for dATP and cytochrome c. Cell 1996;86:147-157.
106. Kim HE, Du F, Fang M, Wang X. Formation of apoptosome is initiated by cytochrome c-induced dATP hydrolysis and subsequent nucleotide exchange on Apaf-1. Proc Natl Acad Sci U S A 2005;102:17545-17550.
107. Hengartner MO. The biochemistry of apoptosis. Nature 2000;407:770-776.
108. Li H, Zhu H, Xu CJ, Yuan J. Cleavage of BID by caspase 8 mediates the mitochondrial damage in the Fas pathway of apoptosis. Cell 1998;94:491-501.
109. Kothakota S, Azuma T, Reinhard C, Klippel A, Tang J, Chu K, McGarry TJ, et al. Caspase-3-generated fragment of gelsolin: effector of morphological change in apoptosis. Science 1997;278:294-298.
110. Rudel T, Bokoch GM. Membrane and morphological changes in apoptotic cells regulated by caspase-mediated activation of PAK2. Science 1997;276:1571-1574.
111. Lüthi AU, Martin SJ. The CASBAH: a searchable database of caspase substrates. Cell Death Differ 2007;14:641-650.
112. Sies H, Berndt C, Jones DP. Oxidative Stress. Annu Rev Biochem 2017;86:715-748.
113. Sies H, Jones DP. Reactive oxygen species (ROS) as pleiotropic physiological signalling agents. Nat Rev Mol Cell Biol 2020;21:363-383.
114. Imlay JA. Pathways of oxidative damage. Annu Rev Microbiol 2003;57:395-418.
115. Loschen G, Azzi A, Richter C, Flohé L. Superoxide radicals as precursors of mitochondrial hydrogen peroxide. FEBS Lett 1974;42:68-72.
116. Ayala A, Muñoz MF, Argüelles S. Lipid Peroxidation: Production, Metabolism, and Signaling Mechanisms of Malondialdehyde and 4-Hydroxy-2-Nonenal. Oxidative Medicine and Cellular Longevity 2014;2014:360438.
117. Orrenius S, Gogvadze V, Zhivotovsky B. Mitochondrial oxidative stress: implications for cell death. Annu Rev Pharmacol Toxicol 2007;47:143-183.
118. Parvez S, Long MJC, Poganik JR, Aye Y. Redox Signaling by Reactive Electrophiles and Oxidants. Chem Rev 2018;118:8798-8888.
119. Szabó C, Ischiropoulos H, Radi R. Peroxynitrite: biochemistry, pathophysiology and development of therapeutics. Nat Rev Drug Discov 2007;6:662-680.
120. Winterbourn CC. The biological chemistry of hydrogen peroxide. Methods Enzymol 2013;528:3-25.
121. Koppenol WH, Hider RH. Iron and redox cycling. Do's and don'ts. Free Radic Biol Med 2019;133:3-10.
122. Wong HS, Dighe PA, Mezera V, Monternier PA, Brand MD. Production of superoxide and hydrogen peroxide from specific mitochondrial sites under different bioenergetic conditions. J Biol Chem 2017;292:16804-16809.
123. Fang J, Wong HS, Brand MD. Production of superoxide and hydrogen peroxide in the mitochondrial matrix is dominated by site I(Q) of complex I in diverse cell lines. Redox Biol 2020;37:101722.
124. Dröse S, Brandt U. Molecular mechanisms of superoxide production by the mitochondrial respiratory chain. Adv Exp Med Biol 2012;748:145-169.

125. Turrens JF, Alexandre A, Lehninger AL. Ubisemiquinone is the electron donor for superoxide formation by complex III of heart mitochondria. Arch Biochem Biophys 1985;237:408-414.
126. Miwa S, Brand MD. The topology of superoxide production by complex III and glycerol 3-phosphate dehydrogenase in Drosophila mitochondria. Biochim Biophys Acta 2005;1709:214-219.
127. Brand MD. The sites and topology of mitochondrial superoxide production. Exp Gerontol 2010;45:466-472.
128. Yeh JI, Chinte U, Du S. Structure of glycerol-3-phosphate dehydrogenase, an essential monotopic membrane enzyme involved in respiration and metabolism. Proc Natl Acad Sci U S A 2008;105:3280-3285.
129. St-Pierre J, Buckingham JA, Roebuck SJ, Brand MD. Topology of superoxide production from different sites in the mitochondrial electron transport chain. J Biol Chem 2002;277:44784-44790.
130. Fang J, Beattie DS. External alternative NADH dehydrogenase of Saccharomyces cerevisiae: a potential source of superoxide. Free Radic Biol Med 2003;34:478-488.
131. Logan R, Kong AC, Axcell E, Krise JP. Amine-containing molecules and the induction of an expanded lysosomal volume phenotype: a structure-activity relationship study. J Pharm Sci 2014;103:1572-1580.
132. Block K, Gorin Y, Abboud HE. Subcellular localization of Nox4 and regulation in diabetes. Proc Natl Acad Sci U S A 2009;106:14385-14390.
133. Shanmugasundaram K, Nayak BK, Friedrichs WE, Kaushik D, Rodriguez R, Block K. NOX4 functions as a mitochondrial energetic sensor coupling cancer metabolic reprogramming to drug resistance. Nat Commun 2017;8:997.
134. Panday A, Sahoo MK, Osorio D, Batra S. NADPH oxidases: an overview from structure to innate immunity-associated pathologies. Cell Mol Immunol 2015;12:5-23.
135. Holmes B, Quie PG, Windhorst DB, Good RA. Fatal granulomatous disease of childhood. An inborn abnormality of phagocytic function. Lancet 1966;1:1225-1228.
136. Kono H, Rusyn I, Yin M, Gäbele E, Yamashina S, Dikalova A, Kadiiska MB, et al. NADPH oxidase-derived free radicals are key oxidants in alcohol-induced liver disease. J Clin Invest 2000;106:867-872.
137. Gross E, Sevier CS, Heldman N, Vitu E, Bentzur M, Kaiser CA, Thorpe C, et al. Generating disulfides enzymatically: reaction products and electron acceptors of the endoplasmic reticulum thiol oxidase Ero1p. Proc Natl Acad Sci U S A 2006;103:299-304.
138. Antonenkov VD, Grunau S, Ohlmeier S, Hiltunen JK. Peroxisomes are oxidative organelles. Antioxid Redox Signal 2010;13:525-537.
139. Albertolle ME, Peter Guengerich F. The relationships between cytochromes P450 and H(2)O(2): Production, reaction, and inhibition. J Inorg Biochem 2018;186:228-234.
140. Battelli MG, Polito L, Bortolotti M, Bolognesi A. Xanthine Oxidoreductase-Derived Reactive Species: Physiological and Pathological Effects. Oxid Med Cell Longev 2016;2016:3527579.
141. Sena LA, Chandel NS. Physiological roles of mitochondrial reactive oxygen species. Mol Cell 2012;48:158-167.
142. Rhee SG, Bae YS, Lee SR, Kwon J. Hydrogen peroxide: a key messenger that modulates protein phosphorylation through cysteine oxidation. Sci STKE 2000;2000:pe1.
143. Finkel T. Signal transduction by reactive oxygen species. J Cell Biol 2011;194:7-15.
144. Finkel T. From sulfenylation to sulfhydration: what a thiolate needs to tolerate. Sci Signal 2012;5:pe10.
145. Chandel NS, Maltepe E, Goldwasser E, Mathieu CE, Simon MC, Schumacker PT. Mitochondrial reactive oxygen species trigger hypoxia-induced transcription. Proc Natl Acad Sci U S A 1998;95:11715-11720.

146. Bell EL, Klimova TA, Eisenbart J, Moraes CT, Murphy MP, Budinger GR, Chandel NS. The Qo site of the mitochondrial complex III is required for the transduction of hypoxic signaling via reactive oxygen species production. J Cell Biol 2007;177:1029-1036.

147. Chandel NS, McClintock DS, Feliciano CE, Wood TM, Melendez JA, Rodriguez AM, Schumacker PT. Reactive oxygen species generated at mitochondrial complex III stabilize hypoxia-inducible factor-1alpha during hypoxia: a mechanism of O2 sensing. J Biol Chem 2000;275:25130-25138.

148. Chandel NS, Vander Heiden MG, Thompson CB, Schumacker PT. Redox regulation of p53 during hypoxia. Oncogene 2000;19:3840-3848.

149. Chandel NS, Trzyna WC, McClintock DS, Schumacker PT. Role of oxidants in NF-kappa B activation and TNF-alpha gene transcription induced by hypoxia and endotoxin. J Immunol 2000;165:1013-1021.

150. Yamamoto M, Kensler TW, Motohashi H. The KEAP1-NRF2 System: a Thiol-Based Sensor-Effector Apparatus for Maintaining Redox Homeostasis. Physiol Rev 2018;98:1169-1203.

151. Eijkelenboom A, Burgering BM. FOXOs: signalling integrators for homeostasis maintenance. Nat Rev Mol Cell Biol 2013;14:83-97.

152. Scherz-Shouval R, Shvets E, Fass E, Shorer H, Gil L, Elazar Z. Reactive oxygen species are essential for autophagy and specifically regulate the activity of Atg4. Embo j 2007;26:1749-1760.

153. West AP, Brodsky IE, Rahner C, Woo DK, Erdjument-Bromage H, Tempst P, Walsh MC, et al. TLR signalling augments macrophage bactericidal activity through mitochondrial ROS. Nature 2011;472:476-480.

154. Emre Y, Hurtaud C, Nübel T, Criscuolo F, Ricquier D, Cassard-Doulcier AM. Mitochondria contribute to LPS-induced MAPK activation via uncoupling protein UCP2 in macrophages. Biochem J 2007;402:271-278.

155. Zhou R, Yazdi AS, Menu P, Tschopp J. A role for mitochondria in NLRP3 inflammasome activation. Nature 2011;469:221-225.

156. Zhang J, Khvorostov I, Hong JS, Oktay Y, Vergnes L, Nuebel E, Wahjudi PN, et al. UCP2 regulates energy metabolism and differentiation potential of human pluripotent stem cells. Embo j 2011;30:4860-4873.

157. Kowalska M, Piekut T, Prendecki M, Sodel A, Kozubski W, Dorszewska J. Mitochondrial and Nuclear DNA Oxidative Damage in Physiological and Pathological Aging. DNA Cell Biol 2020;39:1410-1420.

158. Yudkina AV, Shilkin ES, Endutkin AV, Makarova AV, Zharkov DO. Reading and Misreading 8-oxoguanine, a Paradigmatic Ambiguous Nucleobase. Crystals 2019;9:269.

159. Yasui M, Kanemaru Y, Kamoshita N, Suzuki T, Arakawa T, Honma M. Tracing the fates of site-specifically introduced DNA adducts in the human genome. DNA Repair (Amst) 2014;15:11-20.

160. Larsen NB, Rasmussen M, Rasmussen LJ. Nuclear and mitochondrial DNA repair: similar pathways? Mitochondrion 2005;5:89-108.

161. Nakamoto H, Kaneko T, Tahara S, Hayashi E, Naito H, Radak Z, Goto S. Regular exercise reduces 8-oxodG in the nuclear and mitochondrial DNA and modulates the DNA repair activity in the liver of old rats. Exp Gerontol 2007;42:287-295.

162. Jacob KD, Noren Hooten N, Trzeciak AR, Evans MK. Markers of oxidant stress that are clinically relevant in aging and age-related disease. Mech Ageing Dev 2013;134:139-157.

163. Kong Q, Lin CL. Oxidative damage to RNA: mechanisms, consequences, and diseases. Cell Mol Life Sci 2010;67:1817-1829.

164. Ott M, Gogvadze V, Orrenius S, Zhivotovsky B. Mitochondria, oxidative stress and cell death. Apoptosis 2007;12:913-922.

165. Conrad M, Pratt DA. The chemical basis of ferroptosis. Nat Chem Biol 2019;15:1137-1147.

166. Gęgotek A, Skrzydlewska E. Biological effect of protein modifications by lipid peroxidation products. Chem Phys Lipids 2019;221:46-52.

167. Stadtman ER. Protein oxidation and aging. Free Radic Res 2006;40:1250-1258.

168. Jiang X, Stockwell BR, Conrad M. Ferroptosis: mechanisms, biology and role in disease. Nat Rev Mol Cell Biol 2021.

169. Xiao M, Zhong H, Xia L, Tao Y, Yin H. Pathophysiology of mitochondrial lipid oxidation: Role of 4-hydroxynonenal (4-HNE) and other bioactive lipids in mitochondria. Free Radic Biol Med 2017;111:316-327.

170. Kagan VE, Tyurin VA, Jiang J, Tyurina YY, Ritov VB, Amoscato AA, Osipov AN, et al. Cytochrome c acts as a cardiolipin oxygenase required for release of proapoptotic factors. Nat Chem Biol 2005;1:223-232.

171. Esterbauer H, Eckl P, Ortner A. Possible mutagens derived from lipids and lipid precursors. Mutat Res 1990;238:223-233.

172. Ji C, Amarnath V, Pietenpol JA, Marnett LJ. 4-hydroxynonenal induces apoptosis via caspase-3 activation and cytochrome c release. Chem Res Toxicol 2001;14:1090-1096.

173. Hawkins CL, Davies MJ. Detection, identification, and quantification of oxidative protein modifications. J Biol Chem 2019;294:19683-19708.

174. Gardner PR. Aconitase: sensitive target and measure of superoxide. Methods Enzymol 2002;349:9-23.

175. Felser A, Blum K, Lindinger PW, Bouitbir J, Krahenbuhl S. Mechanisms of hepatocellular toxicity associated with dronedarone--a comparison to amiodarone. Toxicol Sci 2013;131:480-490.

176. Felser A, Stoller A, Morand R, Schnell D, Donzelli M, Terracciano L, Bouitbir J, et al. Hepatic toxicity of dronedarone in mice: role of mitochondrial β-oxidation. Toxicology 2014;323:1-9.

177. Felser A, Lindinger PW, Schnell D, Kratschmar DV, Odermatt A, Mies S, Jenö P, et al. Hepatocellular toxicity of benzbromarone: effects on mitochondrial function and structure. Toxicology 2014;324:136-146.

178. Paech F, Mingard C, Grünig D, Abegg VF, Bouitbir J, Krähenbühl S. Mechanisms of mitochondrial toxicity of the kinase inhibitors ponatinib, regorafenib and sorafenib in human hepatic HepG2 cells. Toxicology 2018;395:34-44.

179. Paech F, Bouitbir J, Krahenbuhl S. Hepatocellular Toxicity Associated with Tyrosine Kinase Inhibitors: Mitochondrial Damage and Inhibition of Glycolysis. Front Pharmacol 2017;8:367.

180. Mingard C, Paech F, Bouitbir J, Krähenbühl S. Mechanisms of toxicity associated with six tyrosine kinase inhibitors in human hepatocyte cell lines. J Appl Toxicol 2018;38:418-431.

181. Paech F, Abegg VF, Duthaler U, Terracciano L, Bouitbir J, Krähenbühl S. Sunitinib induces hepatocyte mitochondrial damage and apoptosis in mice. Toxicology 2018;409:13-23.

182. Heel RC, Brogden RN, Speight TM, Avery GS. Benzbromarone: a review of its pharmacological properties and therapeutic use in gout and hyperuricaemia. Drugs 1977;14:349-366.

183. Azevedo VF, Kos IA, Vargas-Santos AB, da Rocha Castelar Pinheiro G, Dos Santos Paiva E. Benzbromarone in the treatment of gout. Adv Rheumatol 2019;59:37.

184. Ichida K, Hosoyamada M, Kimura H, Takeda M, Utsunomiya Y, Hosoya T, Endou H. Urate transport via human PAH transporter hOAT1 and its gene structure. Kidney Int 2003;63:143-155.

185. Enomoto A, Kimura H, Chairoungdua A, Shigeta Y, Jutabha P, Cha SH, Hosoyamada M, et al. Molecular identification of a renal urate anion exchanger that regulates blood urate levels. Nature 2002;417:447-452.

186. Lee MH, Graham GG, Williams KM, Day RO. A benefit-risk assessment of benzbromarone in the treatment of gout. Was its withdrawal from the market in the best interest of patients? Drug Saf 2008;31:643-665.

187. Kitagawara Y, Ohe T, Tachibana K, Takahashi K, Nakamura S, Mashino T. Novel Bioactivation Pathway of Benzbromarone Mediated by Cytochrome P450. Drug Metab Dispos 2015;43:1303-1306.

188. Broekhuysen J, Pacco M, Sion R, Demeulenaere L, Van Hee M. Metabolism of benzbromarone in man. Eur J Clin Pharmacol 1972;4:125-130.

189. McDonald MG, Rettie AE. Sequential metabolism and bioactivation of the hepatotoxin benzbromarone: formation of glutathione adducts from a catechol intermediate. Chem Res Toxicol 2007;20:1833-1842.

190. Kobayashi K, Kajiwara E, Ishikawa M, Oka H, Chiba K. Identification of CYP isozymes involved in benzbromarone metabolism in human liver microsomes. Biopharm Drug Dispos 2012;33:466-473.

191. Uchida S, Shimada K, Misaka S, Imai H, Katoh Y, Inui N, Takeuchi K, et al. Benzbromarone pharmacokinetics and pharmacodynamics in different cytochrome P450 2C9 genotypes. Drug Metab Pharmacokinet 2010;25:605-610.

192. Ferber H, Vergin H, Hitzenberger G. Pharmacokinetics and biotransformation of benzbromarone in man. Eur J Clin Pharmacol 1981;19:431-435.

193. Walter-Sack I, de Vries JX, Ittensohn A, Weber E. Rapid and slow benzbromarone elimination phenotypes in man: benzbromarone and metabolite profiles. Eur J Clin Pharmacol 1990;39:577-581.

194. Yu TF. Pharmacokinetic and clinical studies of a new uricosuric agent - benzbromarone. J Rheumatol 1976;3:305-312.

195. Hosoya T, Sano T, Sasaki T, Fushimi M, Ohashi T. Dotinurad versus benzbromarone in Japanese hyperuricemic patient with or without gout: a randomized, double-blind, parallel-group, phase 3 study. Clin Exp Nephrol 2020;24:62-70.

196. Masbernard A, Giudicelli CP. Ten years' experience with benzbromarone in the management of gout and hyperuricaemia. S Afr Med J 1981;59:701-706.

197. Reinders MK, Haagsma C, Jansen TL, van Roon EN, Delsing J, van de Laar MA, Brouwers JR. A randomised controlled trial on the efficacy and tolerability with dose escalation of allopurinol 300-600 mg/day versus benzbromarone 100-200 mg/day in patients with gout. Ann Rheum Dis 2009;68:892-897.

198. van der Klauw MM, Houtman PM, Stricker BH, Spoelstra P. Hepatic injury caused by benzbromarone. J Hepatol 1994;20:376-379.

199. Wagayama H, Shiraki K, Sugimoto K, Fujikawa K, Shimizu A, Takase K, Nakano T, et al. Fatal fulminant hepatic failure associated with benzbromarone. J Hepatol 2000;32:874.

200. Arai M, Yokosuka O, Fujiwara K, Kojima H, Kanda T, Hirasawa H, Saisho H. Fulminant hepatic failure associated with benzbromarone treatment: a case report. J Gastroenterol Hepatol 2002;17:625-626.

201. Kumagai J, Kanda T, Yasui S, Haga Y, Sasaki R, Nakamura M, Wu S, et al. Autoimmune hepatitis following drug-induced liver injury in an elderly patient. Clin J Gastroenterol 2016;9:156-159.

202. Haring B, Kudlich T, Rauthe S, Melcher R, Geier A. Benzbromarone: a double-edged sword that cuts the liver? Eur J Gastroenterol Hepatol 2013;25:119-121.

203. Suzuki T, Suzuki T, Kimura M, Shinoda M, Fujita T, Miyake N, Yamamoto S, et al. [A case of fulminant hepatitis, possibly caused by benzbromarone]. Nihon Shokakibyo Gakkai Zasshi 2001;98:421-425.

204. Kaufmann P, Török M, Hänni A, Roberts P, Gasser R, Krähenbühl S. Mechanisms of benzarone and benzbromarone-induced hepatic toxicity. Hepatology 2005;41:925-935.

205. Spaniol M, Bracher R, Ha HR, Follath F, Krähenbühl S. Toxicity of amiodarone and amiodarone analogues on isolated rat liver mitochondria. J Hepatol 2001;35:628-636.

206. Moy B, Kirkpatrick P, Kar S, Goss P. Lapatinib. Nat Rev Drug Discov 2007;6:431-432.

207. Voigtlaender M, Schneider-Merck T, Trepel M. Lapatinib. Recent Results Cancer Res 2018;211:19-44.

208. Slamon DJ, Clark GM, Wong SG, Levin WJ, Ullrich A, McGuire WL. Human breast cancer: correlation of relapse and survival with amplification of the HER-2/neu oncogene. Science 1987;235:177-182.

209. Geyer CE, Forster J, Lindquist D, Chan S, Romieu CG, Pienkowski T, Jagiello-Gruszfeld A, et al. Lapatinib plus capecitabine for HER2-positive advanced breast cancer. N Engl J Med 2006;355:2733-2743.

210. Johnston S, Pippen J, Jr., Pivot X, Lichinitser M, Sadeghi S, Dieras V, Gomez HL, et al. Lapatinib combined with letrozole versus letrozole and placebo as first-line therapy for postmenopausal hormone receptor-positive metastatic breast cancer. J Clin Oncol 2009;27:5538-5546.

211. Teng WC, Oh JW, New LS, Wahlin MD, Nelson SD, Ho HK, Chan EC. Mechanism-based inactivation of cytochrome P450 3A4 by lapatinib. Mol Pharmacol 2010;78:693-703.

212. Towles JK, Clark RN, Wahlin MD, Uttamsingh V, Rettie AE, Jackson KD. Cytochrome P450 3A4 and CYP3A5-Catalyzed Bioactivation of Lapatinib. Drug Metab Dispos 2016;44:1584-1597.

213. Castellino S, O'Mara M, Koch K, Borts DJ, Bowers GD, MacLauchlin C. Human metabolism of lapatinib, a dual kinase inhibitor: implications for hepatotoxicity. Drug Metab Dispos 2012;40:139-150.

214. Chu QS, Schwartz G, de Bono J, Smith DA, Koch KM, Versola MJ, Pandite L, et al. Phase I and pharmacokinetic study of lapatinib in combination with capecitabine in patients with advanced solid malignancies. J Clin Oncol 2007;25:3753-3758.

215. Burris HA, 3rd, Hurwitz HI, Dees EC, Dowlati A, Blackwell KL, O'Neil B, Marcom PK, et al. Phase I safety, pharmacokinetics, and clinical activity study of lapatinib (GW572016), a reversible dual inhibitor of epidermal growth factor receptor tyrosine kinases, in heavily pretreated patients with metastatic carcinomas. J Clin Oncol 2005;23:5305-5313.

216. Moy B, Goss PE. Lapatinib-associated toxicity and practical management recommendations. Oncologist 2007;12:756-765.

217. Shah RR, Morganroth J, Shah DR. Hepatotoxicity of tyrosine kinase inhibitors: clinical and regulatory perspectives. Drug Saf 2013;36:491-503.

218. Moy B, Rappold E, Williams L, Kelly T, Nicolodi L, Maltzman JD, Goss PE. Hepatobiliary abnormalities in patients with metastatic cancer treated with lapatinib. Journal of Clinical Oncology 2009;27:1043-1043.

219. Peroukides S, Makatsoris T, Koutras A, Tsamandas A, Onyenadum A, Labropoulou-Karatza C, Kalofonos H. Lapatinib-induced hepatitis: a case report. World J Gastroenterol 2011;17:2349-2352.

220. Gomez HL, Doval DC, Chavez MA, Ang PC, Aziz Z, Nag S, Ng C, et al. Efficacy and safety of lapatinib as first-line therapy for ErbB2-amplified locally advanced or metastatic breast cancer. J Clin Oncol 2008;26:2999-3005.

221. Eno MR, El-Gendy Bel D, Cameron MD. P450 3A-Catalyzed O-Dealkylation of Lapatinib Induces Mitochondrial Stress and Activates Nrf2. Chem Res Toxicol 2016;29:784-796.

222. Schaid DJ, Spraggs CF, McDonnell SK, Parham LR, Cox CJ, Ejlertsen B, Finkelstein DM, et al. Prospective validation of HLA-DRB1*07:01 allele carriage as a predictive risk factor for lapatinib-induced liver injury. J Clin Oncol 2014;32:2296-2303.

223. Cohen MH, Williams G, Johnson JR, Duan J, Gobburu J, Rahman A, Benson K, et al. Approval summary for imatinib mesylate capsules in the treatment of chronic myelogenous leukemia. Clin Cancer Res 2002;8:935-942.

224. Dagher R, Cohen M, Williams G, Rothmann M, Gobburu J, Robbie G, Rahman A, et al. Approval summary: imatinib mesylate in the treatment of metastatic and/or unresectable malignant gastrointestinal stromal tumors. Clin Cancer Res 2002;8:3034-3038.

225. Faderl S, Talpaz M, Estrov Z, O'Brien S, Kurzrock R, Kantarjian HM. The biology of chronic myeloid leukemia. N Engl J Med 1999;341:164-172.

226. Goldman JM, Melo JV. Targeting the BCR-ABL tyrosine kinase in chronic myeloid leukemia. N Engl J Med 2001;344:1084-1086.

227. Druker BJ, Lydon NB. Lessons learned from the development of an abl tyrosine kinase inhibitor for chronic myelogenous leukemia. J Clin Invest 2000;105:3-7.

228. Flynn JP, Gerriets V: Imatinib. In: StatPearls. Treasure Island (FL): StatPearls Publishing

229. Cohen MH, Johnson JR, Justice R, Pazdur R. Approval summary: imatinib mesylate for one or three years in the adjuvant treatment of gastrointestinal stromal tumors. Oncologist 2012;17:992-997.

230. Zhuang W, Qiu HB, Chen XM, Yuan XH, Yang LF, Sun XW, Zhou XJ, et al. Simultaneous quantification of imatinib and its main metabolite N-demethyl-imatinib in human plasma by liquid chromatography-tandem mass spectrometry and its application to therapeutic drug monitoring in patients with gastrointestinal stromal tumor. Biomed Chromatogr 2017;31.

231. Peng B, Lloyd P, Schran H. Clinical pharmacokinetics of imatinib. Clin Pharmacokinet 2005;44:879-894.

232. Ridruejo E, Cacchione R, Villamil AG, Marciano S, Gadano AC, Mandó OG. Imatinib-induced fatal acute liver failure. World J Gastroenterol 2007;13:6608-6111.

233. Talpaz M, Silver RT, Druker BJ, Goldman JM, Gambacorti-Passerini C, Guilhot F, Schiffer CA, et al. Imatinib induces durable hematologic and cytogenetic responses in patients with accelerated phase chronic myeloid leukemia: results of a phase 2 study. Blood 2002;99:1928-1937.

234. Cross TJ, Bagot C, Portmann B, Wendon J, Gillett D. Imatinib mesylate as a cause of acute liver failure. Am J Hematol 2006;81:189-192.

235. Pariente A, Etcharry F, Cales V, Laborde Y, Ferrari S, Biour M. Imatinib mesylate-induced acute hepatitis in a patient treated for gastrointestinal stromal tumour. Eur J Gastroenterol Hepatol 2006;18:785-787.

236. Ishii T, Itoh K, Takahashi S, Sato H, Yanagawa T, Katoh Y, Bannai S, et al. Transcription factor Nrf2 coordinately regulates a group of oxidative stress-inducible genes in macrophages. J Biol Chem 2000;275:16023-16029.

237. Moi P, Chan K, Asunis I, Cao A, Kan YW. Isolation of NF-E2-related factor 2 (Nrf2), a NF-E2-like basic leucine zipper transcriptional activator that binds to the tandem NF-E2/AP1 repeat of the beta-globin locus control region. Proc Natl Acad Sci U S A 1994;91:9926-9930.

238. McMahon M, Itoh K, Yamamoto M, Chanas SA, Henderson CJ, McLellan LI, Wolf CR, et al. The Cap'n'Collar basic leucine zipper transcription factor Nrf2 (NF-E2 p45-related factor 2) controls both constitutive and inducible expression of intestinal detoxification and glutathione biosynthetic enzymes. Cancer Res 2001;61:3299-3307.

239. Romeo PH, Prandini MH, Joulin V, Mignotte V, Prenant M, Vainchenker W, Marguerie G, et al. Megakaryocytic and erythrocytic lineages share specific transcription factors. Nature 1990;344:447-449.

240. Mignotte V, Wall L, deBoer E, Grosveld F, Romeo PH. Two tissue-specific factors bind the erythroid promoter of the human porphobilinogen deaminase gene. Nucleic Acids Res 1989;17:37-54.

241. Pitoniak A, Bohmann D. Mechanisms and functions of Nrf2 signaling in Drosophila. Free Radic Biol Med 2015;88:302-313.

242. Itoh K, Chiba T, Takahashi S, Ishii T, Igarashi K, Katoh Y, Oyake T, et al. An Nrf2/small Maf heterodimer mediates the induction of phase II detoxifying enzyme genes through antioxidant response elements. Biochem Biophys Res Commun 1997;236:313-322.

243. Itoh K, Wakabayashi N, Katoh Y, Ishii T, Igarashi K, Engel JD, Yamamoto M. Keap1 represses nuclear activation of antioxidant responsive elements by Nrf2 through binding to the amino-terminal Neh2 domain. Genes Dev 1999;13:76-86.

244. Itoh K, Igarashi K, Hayashi N, Nishizawa M, Yamamoto M. Cloning and characterization of a novel erythroid cell-derived CNC family transcription factor heterodimerizing with the small Maf family proteins. Mol Cell Biol 1995;15:4184-4193.

245. Mohler J, Vani K, Leung S, Epstein A. Segmentally restricted, cephalic expression of a leucine zipper gene during Drosophila embryogenesis. Mech Dev 1991;34:3-9.

246. Igarashi K, Kataoka K, Itoh K, Hayashi N, Nishizawa M, Yamamoto M. Regulation of transcription by dimerization of erythroid factor NF-E2 p45 with small Maf proteins. Nature 1994;367:568-572.

247. Katsuoka F, Yamamoto M. Small Maf proteins (MafF, MafG, MafK): History, structure and function. Gene 2016;586:197-205.

248. Yamazaki H, Katsuoka F, Motohashi H, Engel JD, Yamamoto M. Embryonic lethality and fetal liver apoptosis in mice lacking all three small Maf proteins. Mol Cell Biol 2012;32:808-816.

249. Tong KI, Katoh Y, Kusunoki H, Itoh K, Tanaka T, Yamamoto M. Keap1 recruits Neh2 through binding to ETGE and DLG motifs: characterization of the two-site molecular recognition model. Mol Cell Biol 2006;26:2887-2900.

250. Tong KI, Padmanabhan B, Kobayashi A, Shang C, Hirotsu Y, Yokoyama S, Yamamoto M. Different electrostatic potentials define ETGE and DLG motifs as hinge and latch in oxidative stress response. Mol Cell Biol 2007;27:7511-7521.

251. Chowdhry S, Zhang Y, McMahon M, Sutherland C, Cuadrado A, Hayes JD. Nrf2 is controlled by two distinct β-TrCP recognition motifs in its Neh6 domain, one of which can be modulated by GSK-3 activity. Oncogene 2013;32:3765-3781.

252. Rushmore TH, Morton MR, Pickett CB. The antioxidant responsive element. Activation by oxidative stress and identification of the DNA consensus sequence required for functional activity. J Biol Chem 1991;266:11632-11639.

253. Friling RS, Bensimon A, Tichauer Y, Daniel V. Xenobiotic-inducible expression of murine glutathione S-transferase Ya subunit gene is controlled by an electrophile-responsive element. Proc Natl Acad Sci U S A 1990;87:6258-6262.

254. Watai Y, Kobayashi A, Nagase H, Mizukami M, McEvoy J, Singer JD, Itoh K, et al. Subcellular localization and cytoplasmic complex status of endogenous Keap1. Genes Cells 2007;12:1163-1178.

255. Xue F, Cooley L. kelch encodes a component of intercellular bridges in Drosophila egg chambers. Cell 1993;72:681-693.

256. Kang MI, Kobayashi A, Wakabayashi N, Kim SG, Yamamoto M. Scaffolding of Keap1 to the actin cytoskeleton controls the function of Nrf2 as key regulator of cytoprotective phase 2 genes. Proc Natl Acad Sci U S A 2004;101:2046-2051.

257. Zollman S, Godt D, Privé GG, Couderc JL, Laski FA. The BTB domain, found primarily in zinc finger proteins, defines an evolutionarily conserved family that includes several developmentally regulated genes in Drosophila. Proc Natl Acad Sci U S A 1994;91:10717-10721.

258. Zipper LM, Mulcahy RT. The Keap1 BTB/POZ dimerization function is required to sequester Nrf2 in cytoplasm. J Biol Chem 2002;277:36544-36552.

259. Kobayashi A, Kang MI, Okawa H, Ohtsuji M, Zenke Y, Chiba T, Igarashi K, et al. Oxidative stress sensor Keap1 functions as an adaptor for Cul3-based E3 ligase to regulate proteasomal degradation of Nrf2. Mol Cell Biol 2004;24:7130-7139.

260. Cullinan SB, Gordan JD, Jin J, Harper JW, Diehl JA. The Keap1-BTB protein is an adaptor that bridges Nrf2 to a Cul3-based E3 ligase: oxidative stress sensing by a Cul3-Keap1 ligase. Mol Cell Biol 2004;24:8477-8486.

261. Canning P, Cooper CD, Krojer T, Murray JW, Pike AC, Chaikuad A, Keates T, et al. Structural basis for Cul3 protein assembly with the BTB-Kelch family of E3 ubiquitin ligases. J Biol Chem 2013;288:7803-7814.

262. Itoh K, Wakabayashi N, Katoh Y, Ishii T, O'Connor T, Yamamoto M. Keap1 regulates both cytoplasmic-nuclear shuttling and degradation of Nrf2 in response to electrophiles. Genes Cells 2003;8:379-391.

263. Tong KI, Kobayashi A, Katsuoka F, Yamamoto M. Two-site substrate recognition model for the Keap1-Nrf2 system: a hinge and latch mechanism. Biol Chem 2006;387:1311-1320.

264. Baird L, Yamamoto M. The Molecular Mechanisms Regulating the KEAP1-NRF2 Pathway. Mol Cell Biol 2020;40.

265. Baird L, Llères D, Swift S, Dinkova-Kostova AT. Regulatory flexibility in the Nrf2-mediated stress response is conferred by conformational cycling of the Keap1-Nrf2 protein complex. Proc Natl Acad Sci U S A 2013;110:15259-15264.

266. Yamamoto T, Suzuki T, Kobayashi A, Wakabayashi J, Maher J, Motohashi H, Yamamoto M. Physiological significance of reactive cysteine residues of Keap1 in determining Nrf2 activity. Mol Cell Biol 2008;28:2758-2770.

267. Saito R, Suzuki T, Hiramoto K, Asami S, Naganuma E, Suda H, Iso T, et al. Characterizations of Three Major Cysteine Sensors of Keap1 in Stress Response. Mol Cell Biol 2016;36:271-284.

268. Suzuki T, Muramatsu A, Saito R, Iso T, Shibata T, Kuwata K, Kawaguchi SI, et al. Molecular Mechanism of Cellular Oxidative Stress Sensing by Keap1. Cell Rep 2019;28:746-758 e744.

269. Kobayashi A, Kang MI, Watai Y, Tong KI, Shibata T, Uchida K, Yamamoto M. Oxidative and electrophilic stresses activate Nrf2 through inhibition of ubiquitination activity of Keap1. Mol Cell Biol 2006;26:221-229.

270. Kobayashi M, Li L, Iwamoto N, Nakajima-Takagi Y, Kaneko H, Nakayama Y, Eguchi M, et al. The antioxidant defense system Keap1-Nrf2 comprises a multiple sensing mechanism for responding to a wide range of chemical compounds. Mol Cell Biol 2009;29:493-502.

271. Komatsu M, Kurokawa H, Waguri S, Taguchi K, Kobayashi A, Ichimura Y, Sou YS, et al. The selective autophagy substrate p62 activates the stress responsive transcription factor Nrf2 through inactivation of Keap1. Nat Cell Biol 2010;12:213-223.

272. Thimmulappa RK, Mai KH, Srisuma S, Kensler TW, Yamamoto M, Biswal S. Identification of Nrf2-regulated genes induced by the chemopreventive agent sulforaphane by oligonucleotide microarray. Cancer Res 2002;62:5196-5203.

273. Lu SC. Regulation of hepatic glutathione synthesis. Semin Liver Dis 1998;18:331-343.

274. Wickham S, West MB, Cook PF, Hanigan MH. Gamma-glutamyl compounds: substrate specificity of gamma-glutamyl transpeptidase enzymes. Anal Biochem 2011;414:208-214.

275. Griffith OW, Meister A. Origin and turnover of mitochondrial glutathione. Proc Natl Acad Sci U S A 1985;82:4668-4672.

276. Ketterer B. A bird's eye view of the glutathione transferase field. Chem Biol Interact 2001;138:27-42.

277. Brigelius-Flohé R, Maiorino M. Glutathione peroxidases. Biochim Biophys Acta 2013;1830:3289-3303.

278. Lubos E, Loscalzo J, Handy DE. Glutathione peroxidase-1 in health and disease: from molecular mechanisms to therapeutic opportunities. Antioxid Redox Signal 2011;15:1957-1997.

279. Ran Q, Liang H, Gu M, Qi W, Walter CA, Roberts LJ, 2nd, Herman B, et al. Transgenic mice overexpressing glutathione peroxidase 4 are protected against oxidative stress-induced apoptosis. J Biol Chem 2004;279:55137-55146.

280. Han D, Hanawa N, Saberi B, Kaplowitz N. Mechanisms of liver injury. III. Role of glutathione redox status in liver injury. Am J Physiol Gastrointest Liver Physiol 2006;291:G1-7.

281. Karlenius TC, Tonissen KF. Thioredoxin and Cancer: A Role for Thioredoxin in all States of Tumor Oxygenation. Cancers (Basel) 2010;2:209-232.

282. Kwak MK, Wakabayashi N, Itoh K, Motohashi H, Yamamoto M, Kensler TW. Modulation of gene expression by cancer chemopreventive dithiolethiones through the Keap1-Nrf2 pathway. Identification of novel gene clusters for cell survival. J Biol Chem 2003;278:8135-8145.

283. Rhee SG, Woo HA, Kang D. The Role of Peroxiredoxins in the Transduction of H2O2 Signals. Antioxid Redox Signal 2018;28:537-557.

284. Rhee SG, Kang SW, Chang TS, Jeong W, Kim K. Peroxiredoxin, a novel family of peroxidases. IUBMB Life 2001;52:35-41.

285. Rhee SG. Overview on Peroxiredoxin. Mol Cells 2016;39:1-5.

286. Cao Z, Lindsay JG, Isaacs NW. Mitochondrial peroxiredoxins. Subcell Biochem 2007;44:295-315.

287. Lu J, Holmgren A. The thioredoxin antioxidant system. Free Radic Biol Med 2014;66:75-87.

288. Holmgren A. Thioredoxin. Annu Rev Biochem 1985;54:237-271.

289. Miranda-Vizuete A, Damdimopoulos AE, Spyrou G. The mitochondrial thioredoxin system. Antioxid Redox Signal 2000;2:801-810.

290. Poss KD, Tonegawa S. Reduced stress defense in heme oxygenase 1-deficient cells. Proc Natl Acad Sci U S A 1997;94:10925-10930.

291. Zhu H, Itoh K, Yamamoto M, Zweier JL, Li Y. Role of Nrf2 signaling in regulation of antioxidants and phase 2 enzymes in cardiac fibroblasts: protection against reactive oxygen and nitrogen species-induced cell injury. FEBS Lett 2005;579:3029-3036.

292. Kwak MK, Itoh K, Yamamoto M, Sutter TR, Kensler TW. Role of transcription factor Nrf2 in the induction of hepatic phase 2 and antioxidative enzymes in vivo by the cancer chemoprotective agent, 3H-1, 2-dimethiole-3-thione. Mol Med 2001;7:135-145.

293. Okado-Matsumoto A, Fridovich I. Subcellular distribution of superoxide dismutases (SOD) in rat liver: Cu,Zn-SOD in mitochondria. J Biol Chem 2001;276:38388-38393.

294. Radi R, Turrens JF, Chang LY, Bush KM, Crapo JD, Freeman BA. Detection of catalase in rat heart mitochondria. J Biol Chem 1991;266:22028-22034.

295. Ma Q. Role of nrf2 in oxidative stress and toxicity. Annu Rev Pharmacol Toxicol 2013;53:401-426.

296. Ballabio A, Bonifacino JS. Lysosomes as dynamic regulators of cell and organismal homeostasis. Nat Rev Mol Cell Biol 2020;21:101-118.

297. Wang F, Gómez-Sintes R, Boya P. Lysosomal membrane permeabilization and cell death. Traffic 2018;19:918-931.

298. de Duve C, de Barsy T, Poole B, Trouet A, Tulkens P, Van Hoof F. Commentary. Lysosomotropic agents. Biochem Pharmacol 1974;23:2495-2531.

299. Fu D, Zhou J, Zhu WS, Manley PW, Wang YK, Hood T, Wylie A, et al. Imaging the intracellular distribution of tyrosine kinase inhibitors in living cells with quantitative hyperspectral stimulated Raman scattering. Nat Chem 2014;6:614-622.

300. De Duve C, Pressman BC, Gianetto R, Wattiaux R, Appelmans F. Tissue fractionation studies. 6. Intracellular distribution patterns of enzymes in rat-liver tissue. Biochem J 1955;60:604-617.

301. de Duve C. The lysosome turns fifty. Nat Cell Biol 2005;7:847-849.

302. Schröder BA, Wrocklage C, Hasilik A, Saftig P. The proteome of lysosomes. Proteomics 2010;10:4053-4076.

303. Ohkuma S, Moriyama Y, Takano T. Identification and characterization of a proton pump on lysosomes by fluorescein-isothiocyanate-dextran fluorescence. Proc Natl Acad Sci U S A 1982;79:2758-2762.

304. Forgac M. Vacuolar ATPases: rotary proton pumps in physiology and pathophysiology. Nat Rev Mol Cell Biol 2007;8:917-929.

305. Mindell JA. Lysosomal acidification mechanisms. Annu Rev Physiol 2012;74:69-86.

306. Settembre C, Fraldi A, Medina DL, Ballabio A. Signals from the lysosome: a control centre for cellular clearance and energy metabolism. Nat Rev Mol Cell Biol 2013;14:283-296.

307. Peters C, von Figura K. Biogenesis of lysosomal membranes. FEBS Lett 1994;346:108-114.

308. Schulze H, Kolter T, Sandhoff K. Principles of lysosomal membrane degradation: Cellular topology and biochemistry of lysosomal lipid degradation. Biochim Biophys Acta 2009;1793:674-683.

309. Saftig P, Klumperman J. Lysosome biogenesis and lysosomal membrane proteins: trafficking meets function. Nat Rev Mol Cell Biol 2009;10:623-635.

310. Brix K: Lysosomal Proteases. In: Lysosomes. Boston, MA: Springer US, 2005; 50-59.

311. Patel S, Homaei A, El-Seedi HR, Akhtar N. Cathepsins: Proteases that are vital for survival but can also be fatal. Biomed Pharmacother 2018;105:526-532.

312. Luzio JP, Parkinson MD, Gray SR, Bright NA. The delivery of endocytosed cargo to lysosomes. Biochem Soc Trans 2009;37:1019-1021.

313. Klionsky DJ, Abdelmohsen K, Abe A, Abedin MJ, Abeliovich H, Acevedo Arozena A, Adachi H, et al. Guidelines for the use and interpretation of assays for monitoring autophagy (3rd edition). Autophagy 2016;12:1-222.

314. Ueno T, Komatsu M. Autophagy in the liver: functions in health and disease. Nat Rev Gastroenterol Hepatol 2017;14:170-184.

315. Long X, Lin Y, Ortiz-Vega S, Yonezawa K, Avruch J. Rheb binds and regulates the mTOR kinase. Curr Biol 2005;15:702-713.

316. Sancak Y, Peterson TR, Shaul YD, Lindquist RA, Thoreen CC, Bar-Peled L, Sabatini DM. The Rag GTPases bind raptor and mediate amino acid signaling to mTORC1. Science 2008;320:1496-1501.

317. Rebsamen M, Pochini L, Stasyk T, de Araújo ME, Galluccio M, Kandasamy RK, Snijder B, et al. SLC38A9 is a component of the lysosomal amino acid sensing machinery that controls mTORC1. Nature 2015;519:477-481.

318. Sancak Y, Bar-Peled L, Zoncu R, Markhard AL, Nada S, Sabatini DM. Ragulator-Rag complex targets mTORC1 to the lysosomal surface and is necessary for its activation by amino acids. Cell 2010;141:290-303.

319. Zoncu R, Bar-Peled L, Efeyan A, Wang S, Sancak Y, Sabatini DM. mTORC1 senses lysosomal amino acids through an inside-out mechanism that requires the vacuolar H(+)-ATPase. Science 2011;334:678-683.

320. Menon S, Dibble CC, Talbott G, Hoxhaj G, Valvezan AJ, Takahashi H, Cantley LC, et al. Spatial control of the TSC complex integrates insulin and nutrient regulation of mTORC1 at the lysosome. Cell 2014;156:771-785.

321. Saxton RA, Sabatini DM. mTOR Signaling in Growth, Metabolism, and Disease. Cell 2017;169:361-371.

322. Martina JA, Chen Y, Gucek M, Puertollano R. MTORC1 functions as a transcriptional regulator of autophagy by preventing nuclear transport of TFEB. Autophagy 2012;8:903-914.

323. Settembre C, Di Malta C, Polito VA, Garcia Arencibia M, Vetrini F, Erdin S, Erdin SU, et al. TFEB links autophagy to lysosomal biogenesis. Science 2011;332:1429-1433.

324. Sardiello M, Palmieri M, di Ronza A, Medina DL, Valenza M, Gennarino VA, Di Malta C, et al. A gene network regulating lysosomal biogenesis and function. Science 2009;325:473-477.

325. Roczniak-Ferguson A, Petit CS, Froehlich F, Qian S, Ky J, Angarola B, Walther TC, et al. The transcription factor TFEB links mTORC1 signaling to transcriptional control of lysosome homeostasis. Sci Signal 2012;5:ra42.

326. Puertollano R, Ferguson SM, Brugarolas J, Ballabio A. The complex relationship between TFEB transcription factor phosphorylation and subcellular localization. EMBO J 2018;37.

327. Palmieri M, Impey S, Kang H, di Ronza A, Pelz C, Sardiello M, Ballabio A. Characterization of the CLEAR network reveals an integrated control of cellular clearance pathways. Hum Mol Genet 2011;20:3852-3866.

328. Corrotte M, Castro-Gomes T. Lysosomes and plasma membrane repair. Curr Top Membr 2019;84:1-16.

329. Wang F, Salvati A, Boya P. Lysosome-dependent cell death and deregulated autophagy induced by amine-modified polystyrene nanoparticles. Open Biol 2018;8.

330. Boya P, Kroemer G. Lysosomal membrane permeabilization in cell death. Oncogene 2008;27:6434-6451.

331. Terman A, Kurz T, Gustafsson B, Brunk UT. Lysosomal labilization. IUBMB Life 2006;58:531-539.

332. Xu M, Yang L, Rong JG, Ni Y, Gu WW, Luo Y, Ishidoh K, et al. Inhibition of cysteine cathepsin B and L activation in astrocytes contributes to neuroprotection against cerebral ischemia via blocking the tBid-mitochondrial apoptotic signaling pathway. Glia 2014;62:855-880.

333. Boya P, Andreau K, Poncet D, Zamzami N, Perfettini JL, Metivier D, Ojcius DM, et al. Lysosomal membrane permeabilization induces cell death in a mitochondrion-dependent fashion. J Exp Med 2003;197:1323-1334.

334. Boya P, Gonzalez-Polo RA, Poncet D, Andreau K, Vieira HL, Roumier T, Perfettini JL, et al. Mitochondrial membrane permeabilization is a critical step of lysosome-initiated apoptosis induced by hydroxychloroquine. Oncogene 2003;22:3927-3936.

335. Bidère N, Lorenzo HK, Carmona S, Laforge M, Harper F, Dumont C, Senik A. Cathepsin D triggers Bax activation, resulting in selective apoptosis-inducing factor (AIF) relocation in T lymphocytes entering the early commitment phase to apoptosis. J Biol Chem 2003;278:31401-31411.

336. Papadopoulos C, Kravic B, Meyer H. Repair or Lysophagy: Dealing with Damaged Lysosomes. J Mol Biol 2020;432:231-239.

337. Gold R, Kappos L, Arnold DL, Bar-Or A, Giovannoni G, Selmaj K, Tornatore C, et al. Placebo-controlled phase 3 study of oral BG-12 for relapsing multiple sclerosis. N Engl J Med 2012;367:1098-1107.

338. Enomoto A, Itoh K, Nagayoshi E, Haruta J, Kimura T, O'Connor T, Harada T, et al. High sensitivity of Nrf2 knockout mice to acetaminophen hepatotoxicity associated with decreased expression of ARE-regulated drug metabolizing enzymes and antioxidant genes. Toxicol Sci 2001;59:169-177.

339. Chan K, Han XD, Kan YW. An important function of Nrf2 in combating oxidative stress: detoxification of acetaminophen. Proc Natl Acad Sci U S A 2001;98:4611-4616.

340. Aleksunes LM, Goedken M, Manautou JE. Up-regulation of NAD(P)H quinone oxidoreductase 1 during human liver injury. World J Gastroenterol 2006;12:1937-1940.

341. Goldring CE, Kitteringham NR, Elsby R, Randle LE, Clement YN, Williams DP, McMahon M, et al. Activation of hepatic Nrf2 in vivo by acetaminophen in CD-1 mice. Hepatology 2004;39:1267-1276.

342. Copple IM, Goldring CE, Jenkins RE, Chia AJ, Randle LE, Hayes JD, Kitteringham NR, et al. The hepatotoxic metabolite of acetaminophen directly activates the Keap1-Nrf2 cell defense system. Hepatology 2008;48:1292-1301.

343. Okawa H, Motohashi H, Kobayashi A, Aburatani H, Kensler TW, Yamamoto M. Hepatocyte-specific deletion of the keap1 gene activates Nrf2 and confers potent resistance against acute drug toxicity. Biochem Biophys Res Commun 2006;339:79-88.

344. Roos NJ, Duthaler U, Bouitbir J, Krähenbühl S. The uricosuric benzbromarone disturbs the mitochondrial redox homeostasis and activates the NRF2 signaling pathway in HepG2 cells. Free Radic Biol Med 2020;152:216-226.

345. Ramachandran A, Jaeschke H. A mitochondrial journey through acetaminophen hepatotoxicity. Food Chem Toxicol 2020;140:111282.

346. Cao TT, Ma L, Kandpal G, Warren L, Hess JF, Seabrook GR. Increased nuclear factor-erythroid 2 p45-related factor 2 activity protects SH-SY5Y cells against oxidative damage. J Neurochem 2005;95:406-417.

347. Shin SM, Yang JH, Ki SH. Role of the Nrf2-ARE pathway in liver diseases. Oxid Med Cell Longev 2013;2013:763257.

348. Otsuki A, Yamamoto M. Cis-element architecture of Nrf2-sMaf heterodimer binding sites and its relation to diseases. Arch Pharm Res 2020;43:275-285.

349. Wang X, Campbell MR, Lacher SE, Cho HY, Wan M, Crowl CL, Chorley BN, et al. A Polymorphic Antioxidant Response Element Links NRF2/sMAF Binding to Enhanced MAPT Expression and Reduced Risk of Parkinsonian Disorders. Cell Rep 2016;15:830-842.

350. Kuosmanen SM, Viitala S, Laitinen T, Peräkylä M, Pölönen P, Kansanen E, Leinonen H, et al. The Effects of Sequence Variation on Genome-wide NRF2 Binding--New Target Genes and Regulatory SNPs. Nucleic Acids Res 2016;44:1760-1775.

351. Cho HY, Jedlicka AE, Reddy SP, Zhang LY, Kensler TW, Kleeberger SR. Linkage analysis of susceptibility to hyperoxia. Nrf2 is a candidate gene. Am J Respir Cell Mol Biol 2002;26:42-51.

352. Masuko H, Sakamoto T, Kaneko Y, Iijima H, Naito T, Noguchi E, Hirota T, et al. An interaction between Nrf2 polymorphisms and smoking status affects annual decline in FEV1: a longitudinal retrospective cohort study. BMC Med Genet 2011;12:97.

353. Honkura Y, Matsuo H, Murakami S, Sakiyama M, Mizutari K, Shiotani A, Yamamoto M, et al. NRF2 Is a Key Target for Prevention of Noise-Induced Hearing Loss by Reducing Oxidative Damage of Cochlea. Sci Rep 2016;6:19329.

354. Suzuki T, Shibata T, Takaya K, Shiraishi K, Kohno T, Kunitoh H, Tsuta K, et al. Regulatory nexus of synthesis and degradation deciphers cellular Nrf2 expression levels. Mol Cell Biol 2013;33:2402-2412.

355. Huang YS, Su WJ, Huang YH, Chen CY, Chang FY, Lin HC, Lee SD. Genetic polymorphisms of manganese superoxide dismutase, NAD(P)H:quinone oxidoreductase, glutathione S-transferase M1 and T1, and the susceptibility to drug-induced liver injury. J Hepatol 2007;47:128-134.

356. Degoul F, Sutton A, Mansouri A, Cepanec C, Degott C, Fromenty B, Beaugrand M, et al. Homozygosity for alanine in the mitochondrial targeting sequence of superoxide dismutase and risk for severe alcoholic liver disease. Gastroenterology 2001;120:1468-1474.

357. Randle LE, Goldring CE, Benson CA, Metcalfe PN, Kitteringham NR, Park BK, Williams DP. Investigation of the effect of a panel of model hepatotoxins on the Nrf2-Keap1 defence response pathway in CD-1 mice. Toxicology 2008;243:249-260.

358. Copple IM, den Hollander W, Callegaro G, Mutter FE, Maggs JL, Schofield AL, Rainbow L, et al. Characterisation of the NRF2 transcriptional network and its response to chemical insult in primary human hepatocytes: implications for prediction of drug-induced liver injury. Arch Toxicol 2019;93:385-399.

359. McMillian M, Nie A, Parker JB, Leone A, Kemmerer M, Bryant S, Herlich J, et al. Drug-induced oxidative stress in rat liver from a toxicogenomics perspective. Toxicol Appl Pharmacol 2005;207:171-178.

360. McMillian M, Nie AY, Parker JB, Leone A, Bryant S, Kemmerer M, Herlich J, et al. A gene expression signature for oxidant stress/reactive metabolites in rat liver. Biochem Pharmacol 2004;68:2249-2261.

361. Taguchi K, Fujikawa N, Komatsu M, Ishii T, Unno M, Akaike T, Motohashi H, et al. Keap1 degradation by autophagy for the maintenance of redox homeostasis. Proc Natl Acad Sci U S A 2012;109:13561-13566.

362. Jain A, Lamark T, Sjøttem E, Larsen KB, Awuh JA, Øvervatn A, McMahon M, et al. p62/SQSTM1 is a target gene for transcription factor NRF2 and creates a positive feedback loop by inducing antioxidant response element-driven gene transcription. J Biol Chem 2010;285:22576-22591.

363. Wakabayashi N, Itoh K, Wakabayashi J, Motohashi H, Noda S, Takahashi S, Imakado S, et al. Keap1-null mutation leads to postnatal lethality due to constitutive Nrf2 activation. Nat Genet 2003;35:238-245.

364. Berger B, Donzelli M, Maseneni S, Boess F, Roth A, Krähenbühl S, Haschke M. Comparison of Liver Cell Models Using the Basel Phenotyping Cocktail. Front Pharmacol 2016;7:443.

365. Hardy KD, Wahlin MD, Papageorgiou I, Unadkat JD, Rettie AE, Nelson SD. Studies on the role of metabolic activation in tyrosine kinase inhibitor-dependent hepatotoxicity: induction of CYP3A4 enhances the cytotoxicity of lapatinib in HepaRG cells. Drug Metab Dispos 2014;42:162-171.

366. Moon JY, Han JM, Seo I, Gwak HS. Risk factors associated with the incidence and time to onset of lapatinib-induced hepatotoxicity. Breast Cancer Res Treat 2019;178:239-244.

367. Teo YL, Saetaew M, Chanthawong S, Yap YS, Chan EC, Ho HK, Chan A. Effect of CYP3A4 inducer dexamethasone on hepatotoxicity of lapatinib: clinical and in vitro evidence. Breast Cancer Res Treat 2012;133:703-711.

368. Cho N, Kobayashi K, Yoshida M, Kogure N, Takayama H, Chiba K. Identification of novel glutathione adducts of benzbromarone in human liver microsomes. Drug Metab Pharmacokinet 2017;32:46-52.

369. Yoshida M, Cho N, Akita H, Kobayashi K. Association of a reactive intermediate derived from 1',6-dihydroxy metabolite with benzbromarone-induced hepatotoxicity. J Biochem Mol Toxicol 2017;31.

370. Wang H, Peng Y, Zhang T, Lan Q, Zhao H, Wang W, Zhao Y, et al. Metabolic Epoxidation Is a Critical Step for the Development of Benzbromarone-Induced Hepatotoxicity. Drug Metab Dispos 2017;45:1354-1363.

371. Wang H, Feng Y, Wang Q, Guo X, Huang W, Peng Y, Zheng J. Cysteine-Based Protein Adduction by Epoxide-Derived Metabolite(s) of Benzbromarone. Chem Res Toxicol 2016;29:2145-2152.

372. Iwamura A, Fukami T, Hosomi H, Nakajima M, Yokoi T. CYP2C9-mediated metabolic activation of losartan detected by a highly sensitive cell-based screening assay. Drug Metab Dispos 2011;39:838-846.

373. Habib GM, Shi ZZ, Ou CN, Kala G, Kala SV, Lieberman MW. Altered gene expression in the liver of gamma-glutamyl transpeptidase-deficient mice. Hepatology 2000;32:556-562.

374. Aits S, Jäättelä M. Lysosomal cell death at a glance. J Cell Sci 2013;126:1905-1912.

375. Schotte P, Declercq W, Van Huffel S, Vandenabeele P, Beyaert R. Non-specific effects of methyl ketone peptide inhibitors of caspases. FEBS Lett 1999;442:117-121.

376. Breiden B, Sandhoff K. Emerging mechanisms of drug-induced phospholipidosis. Biol Chem 2019;401:31-46.

377. Platt FM, d'Azzo A, Davidson BL, Neufeld EF, Tifft CJ. Lysosomal storage diseases. Nat Rev Dis Primers 2018;4:27.

378. Ostenfeld MS, Høyer-Hansen M, Bastholm L, Fehrenbacher N, Olsen OD, Groth-Pedersen L, Puustinen P, et al. Anti-cancer agent siramesine is a lysosomotropic detergent that induces cytoprotective autophagosome accumulation. Autophagy 2008;4:487-499.

379. Oberle C, Huai J, Reinheckel T, Tacke M, Rassner M, Ekert PG, Buellesbach J, et al. Lysosomal membrane permeabilization and cathepsin release is a Bax/Bak-dependent, amplifying event of apoptosis in fibroblasts and monocytes. Cell Death Differ 2010;17:1167-1178.

380. Kon K, Kim JS, Uchiyama A, Jaeschke H, Lemasters JJ. Lysosomal iron mobilization and induction of the mitochondrial permeability transition in acetaminophen-induced toxicity to mouse hepatocytes. Toxicol Sci 2010;117:101-108.

381. Giuliano S, Cormerais Y, Dufies M, Grepin R, Colosetti P, Belaid A, Parola J, et al. Resistance to sunitinib in renal clear cell carcinoma results from sequestration in lysosomes and inhibition of the autophagic flux. Autophagy 2015;11:1891-1904.

382. Aits S, Kricker J, Liu B, Ellegaard AM, Hämälistö S, Tvingsholm S, Corcelle-Termeau E, et al. Sensitive detection of lysosomal membrane permeabilization by lysosomal galectin puncta assay. Autophagy 2015;11:1408-1424.